THEORY AND APPLICATIONS OF ARYL CH HYDROGEN BONDS IN

ARYLYETHYNYL RECEPTORS

by

BLAKELY W. TRESCA

A DISSERTATION

Presented to the Department of Chemistry and Biochemistry
and the Graduate School of the University of Oregon
in partial fulfillment of the requirements
for the degree of
Doctor of Philosophy

September 2016

DISSERTATION APPROVAL PAGE

Student: Blakely W. Tresca

Title: Theory and Applications of Aryl CH Hydrogen Bonds in Arylethynyl Receptors

This dissertation has been accepted and approved in partial fulfillment of the requirements for the Doctor of Philosophy degree in the Department of Chemistry and Biochemistry by:

Michael D. Pluth	Chairperson
Darren W. Johnson	Advisor
Michael M. Haley	Advisor
David R. Tyler	Core Member
S. James Remington	Institutional Representative

and

Scott L. Pratt   Dean of the Graduate School

Original approval signatures are on file with the University of Oregon Graduate School.

Degree awarded September 2016

DISSERTATION ABSTRACT

Blakely W. Tresca

Doctor of Philosophy

Department of Chemistry and Biochemistry

September 2016

Title: Theory and Applications of Aryl CH Hydrogen Bonds in Arylethynyl Receptors

Design of selective non-covalent binding systems for chemical and biological recognition requires an intimate understanding of the factors that control the strength of each interaction. Weak interactions such as anion-π, π-π, and CH-π are understood to be important contributors to the overall binding of ligands, however, these interactions are almost purely electrostatic. Aryl CH hydrogen bond donors are a recent addition to the field and provide new possibilities by introducing a partial covalent character, which imparts greater directionality and acceptor preference. CH hydrogen bonds, and other similar weakly polarized donors, are an exciting development in supramolecular chemistry because of their ubiquity, stability and structural diversity. The use of experimental and computational techniques in this dissertation has provided us with a new understanding of the energetic factors that control CH hydrogen bond strength and selectivity for anion binding.

2,6-bis(2-anilinoethynyl) receptors with an aryl CH donor as the central arene act as anion receptors with one CH hydrogen bond and four supporting NH hydrogen bonds around a semi-preorganized pocket. The scaffold provides an efficient route to substitution *para* to the donor, which allows for tuning of optoelectronic properties and the measurement of linear free energy relationships (LFERs) on anion binding. Association constants with anions, Cl^-, Br^-, I^-, NO_3^-, were measured by ^1H NMR and UV-vis spectroscopy in water saturated chloroform. The solution data was combined with calculated and empirical

measurements to provide LFERs and identify an anion dependent substituent character. The importance of substituent resonance or inductive character has been further probed by measuring the isotope effect of selective monodeuteration. Solution measurement of a normal equilibrium isotope effect points to the role of covalency in this non-traditional hydrogen bond. The application of this new understanding to developing fluorescent probes for biological and environmental anions is demonstrated with a small receptor array.

This dissertation includes both previously published and unpublished co-authored material.

CURRICULUM VITAE

NAME OF AUTHOR: Blakely W. Tresca

GRADUATE AND UNDERGRADUATE SCHOOLS ATTENDED:

University of Oregon, Eugene
Trinity University, San Antonio

DEGREES AWARDED:

Doctor of Philosophy, Chemistry, 2016, University of Oregon
Master of Science, Chemistry, 2012, University of Oregon
Bachelor of Science, Biochemistry, 2010, Trinity University

AREAS OF SPECIAL INTEREST:

Organic Synthesis
Physical Organic Chemistry
Computational Modeling
Supramolecular Systems

PROFESSIONAL EXPERIENCE:

Graduate Research Assistant, Department of Chemistry and Biochemistry,
    University of Oregon, Eugene, Oregon, 2011-2016

Graduate Teaching Assistant, Department of Chemistry and Biochemistry,
    University of Oregon, Eugene, Oregon, 2011-2016

Graduate Intern, SupraSensor Technologies, Eugene, Oregon, 2015

Production Intern, VIRxSYS LLC, Gaithersburg, MD, 2011

Undergraduate Teaching Assistant, Department of Chemistry, Trinity University,
    2010

GRANTS, AWARDS, AND HONORS:

Graduate Student Award for Excellence in the Teaching of Chemistry, Department
    of Chemistry and Biochemistry, University of Oregon, 2016

National Meeting Travel Award, American Chemical Society, Division of Organic Chemistry, 2014

Graduate Travel Award, Department of Chemistry and Biochemistry, University of Oregon, 2013

PUBLICATIONS:

B. W. Tresca, R. J. Hansen, C. V. Chau, B. P. Hay, L. N. Zakharov, M. M. Haley, D. W. Johnson, "Substituent Effects in CH Hydrogen Bond Interactions: Linear Free Energy Relationships and Influence of Anions" *J. Am. Chem. Soc.* **2015**, *137*, 14959-14967.

B. W. Tresca, O. B. Berryman, L. N. Zakharov, D. W. Johnson, M. M. Haley, "Anion-directed self-assembly of a 2,6-bis(2-anilinoethynyl)pyridine bis(amide) scaffold" *Supramol. Chem.* **2015**, *28*, 37-44, invited for special issue in honor of Jonathan L. Sessler.

C. L. Vonnegut, B. W. Tresca, D. W. Johnson, M. M. Haley, "Ion and Molecular Recognition Using Aryl-Ethynyl Scaffolding" *Chem. Asian J.* **2015**, *10*, 522-535, invited Focus Review and cover article.

B. W. Tresca, L. N. Zakharov, C. N. Carroll, D. W. Johnson, M. M. Haley, "Aryl C–H•••Cl⁻ hydrogen bonding in a fluorescent anion sensor" *Chem. Commun.* **2013**, *49*, 7240–7242.

B. Tresca, M. Higbee, N. S. Mills, "Reduction of Benzylidene Dibenzo[a,d]cycloheptenes: Over-Reduction of Antiaromatic Dianions to Aromatic Tetraanions" *J. Org. Chem.* **2011**, *76*, 5539–5546.

ACKNOWLEDGMENTS

The completion of my dissertation would not have been possible without the support of my amazing friends and family. The encouragement from my parents to pursue my dream and their continually offered love and guidance along the winding path to becoming a full-fledged scientist was instrumental in reaching this point. As well, my brother Clayton has always been there to provide technical support in my hour of greatest need.

The influence of the people that I have met while in graduate school is present throughout this work. The graduate students and undergraduates whom I have worked with at Oregon will forever shape my work, especially Anna Oliveri, Mary Collins, Calvin Chau, and Ryan Hansen. In particular, I have had the honor to share an office and a committee with Kara Nell for the past five years. My advisors, Darren and Mike, along with the people they have attracted to their groups are what made graduate school not just bearable but exciting every day.

Finally, I would like to thank my amazing fiancé, Julia Matsuno. She has been there to offer support through these tough years, which has helped us to grow closer as we look forward to the future.

This dissertation is dedicated to Annie Tresca and Jane Clay,
who were inspirations in the art of persistence.

TABLE OF CONTENTS

Chapter   Page

LIST OF FIGURES

Figure   Page

LIST OF TABLES

LIST OF SCHEMES

CHAPTER I

ION AND MOLECULAR RECOGNITION USING ARYL–ETHYNYL

SCAFFOLDING

Chapter I is primarily composed from a focus review written for *Chemistry – An Asian Journal* and published in Volume 10, 2015. The review was co-written by Dr. Chrisgen Lee Vonnegut and myself with editing by Profs. Darren W. Johnson and Michael M. Haley. The work in Chapter II includes published co-authored material with contributions by Dr. Calden Carroll, Dr. Lev Zakharov, Profs. Darren Johnson, and Michael Haley. The original article appears in Volume 49, 2013 of *Chem. Commun.* Chapter III has been published in the *Journal of the American Chemical Society*, Volume 137 for 2015. The work was co-authored with Ryan Hansen, Calvin Chau, Dr. Benjamin Hay, Dr. Lev Zakharov, Prof. Michael Haley, and Prof. Darren Johnson. Chapter IV is entirely unpublished work which was co-authored with Alex Breuckner, Maduka Ogba, Prof. Paul Cheong, Prof. Darren Johnson, and Prof. Michael Haley and will be submitted to *Journal of Organic Chemistry* later this year. The work for Chapter V was co-authored with Prof. Orion Berryman, and Dr. Lev N. Zakahrov. Profs. Michael Haley and Darren Johnson provided editorial assistance for the publication in *Supramolecular Chemistry*, Volume 28, in 2016. Chapter VI is entirely unpublished work with contributions by undergraduates Leif Winstead and Anne-Lisa Emig, as well as editing by Profs. Darren Johnson and Michael Haley. The proposed new directions in Chapter VII were conceptualized by me and preliminary work was performed by Calvin Chau under my direction.

General Introduction

The focus of this dissertation is the study of aryl CH hydrogen bonds for their use in the design of supramolecular anion receptors. The design of an effective receptor depends upon optimizing two principles, affinity and selectivity. In order to incorporate receptors as part of a functioning sensor, the method for signal generation must also be considered. A series of coordinated studies have been undertaken to obtain a complete understanding pertaining to the function of aryl CH hydrogen bonds in supramolecular anion receptors. CH hydrogen bonds are emerging across all facets of chemistry and biology as an important interaction for both structure and function. The impact these studies have upon broader fields, e.g. catalysis, enzyme functions, and supramolecular chemistry, will be discussed throughout this dissertation. The first chapter will serve as an introduction to the general concepts of ion and molecular recognition, some mechanisms for sensing, and specifically how aryl–ethynyl scaffolds have been applied in this area.

Introduction to Ion and Molecular Recognition

The use of defined, preorganized scaffolds for host–guest chemistry originates in the discovery of cyclodextrins, and the recognition of their rich intermolecular interactions in the earlier half of the 20th century.[1] Quickly thereafter, the field of inclusion chemistry exploded with the advent of crown ethers, cryptands, and cavitands, which defined the discipline of supramolecular chemistry.[2] Since their inception, synthetic molecular hosts have utilized a variety of linkers to elaborate their binding cavities. Oftentimes, structural rigidity must be considered as a design principle in host construction. For example, a large segment of macrocyclic receptors use the rigidity inherent in aryl–aryl linkages to create the appropriate geometries for suitable guest inclusion.[3] Alternatively, inclusion of an alkyne linkage between

2

aryl groups has been utilized within synthetic molecular hosts, both for its ability to directly connect two units by an essentially inflexible spacer, and for the electronic conjugation it enables between the two aryl units.[4]

Alkynes are installed synthetically via a variety of well-proven techniques. Classically, the alkyne functionality can be formed through dehydrohalogenation reactions or via nucleophilic attack of an acetylide anion. There are also a number of routes to access the alkyne unit from carbonyls, via the Corey–Fuchs reaction, the Colvin rearrangement, or the Seyferth–Gilbert homologation.[5] These methods all suffer from harsh reaction conditions, typically requiring a strong base and thus precluding the use of more functionally diverse starting materials. Some work has been done to extend the scope of these reactions to gentler conditions, such as the modified Bestmann–Ohira homologation, though this route is still limited to the formation of terminal alkynes.[6] For the preparation of aryl–ethynyl linkages, however, few reactions can match the robustness and versatility of the Sonogashira cross-coupling reaction.[7–9] A large variety of aryl–ethynyl scaffolds are now easily accessible because of the gentle conditions, high yields, and wide functional group tolerance of this reaction.

As the supramolecular chemistry field has grown and the need for new receptors has increased, the alkyne linkage has emerged as a useful rigid unit for construction of receptors with designed cavities. In addition, this motif allows spatial separation of the binding site and a spectroscopic handle, yet still confers the electronic effects of the binding event. In this way, the binding event and the spectroscopic changes can act independently, with the alkyne acting as a wire to convey the electronic perturbations of the binding event to the spectroscopic site.

In this chapter, we explore recent advances in the use of aryl–ethynyl receptors in the host–guest chemistry of analyte sensing. The major families of analytes are covered, from cationic metal species to anionic or neutral species prevalent in biological systems. As well, we will cover host use in the development of sensor molecules for a variety of applications, such as detection of chemical weapons. This is not intended to be a comprehensive review, but rather a survey of recent literature exemplifying the utility and versatility of the aryl–ethynyl unit as a structural and/or sensing motif in the construction of molecular receptors. This review focuses mostly on the use of small-molecule synthetic hosts. Except for a few specific examples, the vast, well-studied area of arylene–ethynylene polymers in such sensing applications will not be covered as it has already garnered multiple reviews.[10]

Sensing Strategies

Numerous strategies for the detection of analytes have been employed in recent years. The classic observable changes utilized are either colorimetric or fluorometric, although sensors based upon a gelation response[11] or other physical state changes have also been developed.[12,13] Chiroptical changes measured by circular dichroism (CD) enhancement is emerging as a new method for analyte detection.[14] Fluorescence remains the most commonly utilized spectroscopic change because of the enhanced sensitivity compared to colorimetric changes.[15] Fluorescence also lends itself well to sensing within biological microenvironments, such as those inside cells, as native fluorescence of cells can be filtered out by selecting a fluorophore possessing non-competitive emission or excitation.[16,17] As well, the variety of fluorescence mechanisms aids in the design of sensor molecules.

The more common and more widely understood mechanisms are photo-induced electron transfer (PET), intramolecular charge transfer (ICT), metal-ligand charge transfer

(MLCT), twisted intramolecular charge transfer (TICT),[18] electronic energy transfer (EET), fluorescence resonance energy transfer (FRET), and excimer/exciplex formation. Some of the more recently developed fluorescent mechanisms are aggregation-induced emission (AIE)[19] and excited-state intramolecular proton transfer (ESIPT). All of these methods have been utilized for detection of analytes, with particular attention paid to AIE and ESIPT in recent years.[20,21]

The aryl–ethynyl scaffold can readily participate in many of these mechanisms toward sensing strategies, as it provides a rigid structural unit for the formation of an appropriate binding cavity, allows for conjugative communication between aryl units for appropriate fluorescent responses, and has fewer degrees of freedom than an alkyl chain, disfavoring non-radiative decay. While free rotation around an alkyne–arene C–C single bond can lead to detrimental non-radiative decay, this conformational flexibility provides a useful handle for sensing purposes utilizing AIE or TICT (Figure 1), where inclusion of an appropriate guest can restrict rotation and yield a spectroscopic response through either twisted relaxation of the excited state, or aggregation of the now-hindered fluorophore to initiate an AIE process.[22]
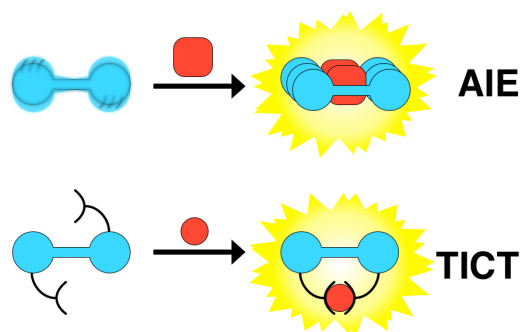
Figure 1. Two common fluorescence mechanisms used in sensing: AIE, where hindrance of internal rotation via aggregation reduces non-radiative relaxation, and TICT, where interaction of a suitable guest causes the TICT state to no longer inhibit fluorescence.

Classically, sensor molecules were built utilizing principles outlined in de Silva's seminal review of fluorescent recognition events.[15] For a PET-based response (Figure 2), the common method of sensor design utilizes an electron-rich donor site (D) as the recognition element tethered to a fluorophore (F). Until the binding event occurs, PET from the donor to the fluorophore quenches fluorescence; however, upon coordination of a cationic or suitably electron-poor guest (G), electron donation ceases and fluorescence turns on. This technique has been utilized since the early 1970s to build sensor molecules, and can be related conceptually to the original complexone sensors first described in the 1950s.[23]
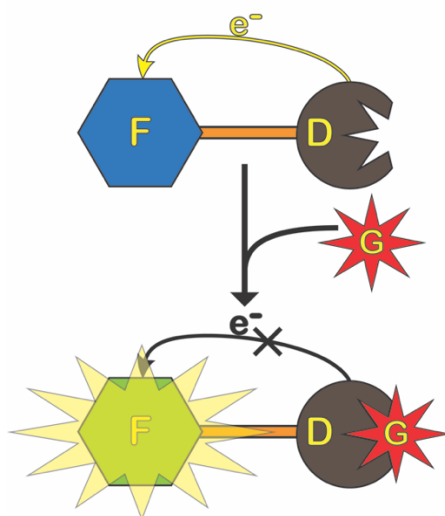
Figure 2. Illustration of PET mechanism for sensing. Coordination of a guest (G) diminishes the electron-donation of the chelating group/electron donor (D), thus stopping quenching and enabling native fluorescence of the fluorophore (F).

For many fluorescent sensing mechanisms, the aryl–ethynyl functionality confers the three concepts of the so-called 'magic triangle' of sensor design: rigidification, to confer a large quantum yield; preorganization, to build a binding site already tailored to the intended guest; and electronic decoupling, where the binding subunit and fluorophore are spatially

separated enough to inhibit direct interaction of the guest.[24] To control the signaling response of the host molecule, modification of electron-withdrawing/donating groups attached to a fluorophore significantly affects the spectroscopic changes of the binding event. For example, in our studies, changing the appended groups alters the electron density within an anion sensor and thus the nature of the fluorescent response from different anionic guests (see Anions section).[25,26]

Conformational changes upon a binding event can also play a large role in spectroscopic sensing responses. Alkyne linkers provide an axle about which the host molecule can rotate, affording differing conformations upon inclusion of diverse guests. Within our group we have found that an aryl–ethynyl scaffold can adopt varying conformations in the solid state or in solution when influenced by a guest (see below).[27–29] These conformational changes have a direct effect on the conjugation throughout the system, giving rise to differences in the emission spectra.

<u>**Charged Species**</u>

Cations

Sensing and quantification of metal cations in solution and complex media are needed due to their environmental prevalence and human health relevance (both beneficial and detrimental). In humans the three most common metal cations are Fe, Zn, and Cu.[30] Since disruption of homeostasis by these metal ions is causative in many diseases, a more complete understanding of their roles in the body would be beneficial to the medical field.[30,31] In addition, the detection of heavy metal cations such as Cd, Hg, Cr, and Pb is an integral research area due to their presence in waste streams and their detrimental effects on living organisms. Molecules selective for these metal ions are thus essential for both

environmental and biological sciences. To this end, many sensors based upon aryl–ethynyl scaffolding have been developed to detect metal ions in recent years, with some key examples outlined below. While there are many mechanisms to sense metal cations based upon the variety of interactions with the host molecule, that subject is not broached here as a number of comprehensive reviews are available in the literature.[30–37]

A tris-phenanthrolyl oligomer connected via ethynyl linkers was used to selectively sense Cr^{III} over other metal cations.[38] Upon full occupation of the three phenanthroline units, the emission spectrum was shifted by 100 nm, allowing quantification across a range of concentrations. An OFF–ON assay to determine the concentration of Cr^{III} in solution was realized through the Cu^{II} complex with quenched fluorescence; in the presence of Cr^{III} the emission was restored. In addition, a ratiometric assay of Cr^{II} and Cr^{III} was possible through the use of monomeric **1** (Figure 3).
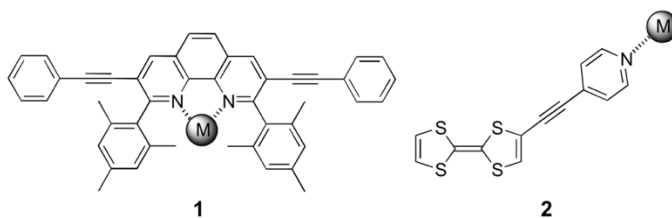
Figure 3. Two examples of metal coordination by nitrogen lone pairs in conjugated fluorophores: an alkyne-substituted phenanthroline monomer (**1**) for fluorescent detection of Cr^{II} and a donor–acceptor (D–A) fluorophore with a 4-pyridyl receptor (**2**).

Similar utilization of an acetylene unit as a conjugative linker was realized by Tung, who employed a D-A dyad connected via an alkyne bridge to detect Pb^{II} in solution (**2**, Figure 3).[39] The 4-pyridyl unit coordinated to Pb^{II} ions and changed the nature of the D-A interaction to give a measurable UV/Vis spectral response, with a binding constant of

log(K_a)=3.76 in acetonitrile. Interaction between Pb^{II} and the donor tetrathiafulvalene (TTF) led to no spectroscopic change, as demonstrated with a phenyl analogue.

TTFs are widely used as donors in sensing scaffolds. In one example, a crown-ether-fused π-expanded tetrathiafulvalene (**3**, exTTF) attached to ethynyl anthracenes experienced PET quenching of the anthracene fluorophores (Figure 4),[40] similar to classical complexone-type sensors.[41] Upon binding a cation, the donor ability decreases and disables PET to yield an OFF–ON fluorescent sensor for cations. Receptor **3** displayed a selective spectroscopic response for large, soft cations such as Ba^{2+}, with a log(K_a) of 4.11 in THF.
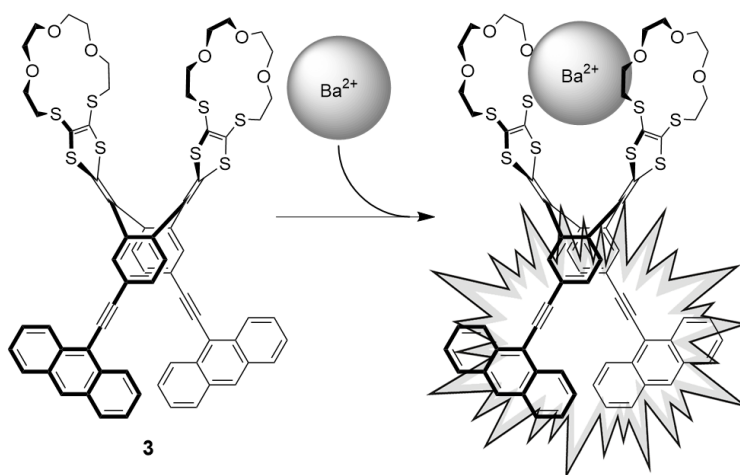
Figure 4. Structure of a crown-ether functionalized π-expanded fluorophore for the detection of large, soft metal cations. Inclusion of a cation within the crown-ether pincer limits PET between the exTTF donor and anthracene fluorophore, recovering the anthracene fluorescence of **3**.

Alkynes define the binding pocket with naphthalene walls in cation sensor **4** (Figure 5), allowing selective fluorometric detection of Fe^{III} ions over a variety of other metal cations.[42] The alkyne linker provided facile synthetic access to the target sensor molecules (through Sonogashira methodologies) and rigidified the binding site.

4, R = CO₂Et
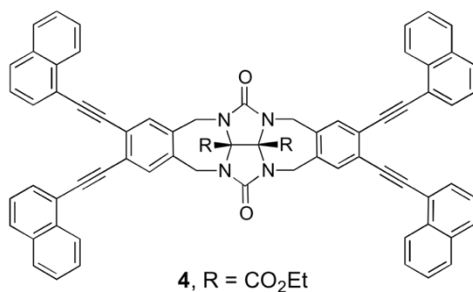
Figure 5. Pincer-like molecule **4** with conjugated aromatic walls selectively senses Fe[III] via an ON–OFF quenching response.

Cruciform-shaped molecules have been extensively employed as sensors for metal cations as well as for neutral molecules. Bunz et al. found that a series of structures such as **5** and **6** (Figure 6),[43] when utilized in a differential sensing array, could discriminate between a variety of metal cations and amines via both colorimetric and fluorometric responses and solvatochromic behaviors.[44–46] Variants with non-conjugated amine substituents selectively interacted with Zn cations over other metals, while those with conjugated coordinating groups had differing responses.[47] These structurally simple systems provide superior HOMO–LUMO separation along the X and Y axes, yielding distinctive solvatochromic and analyte-sensitive spectroscopic changes.

5   **6**
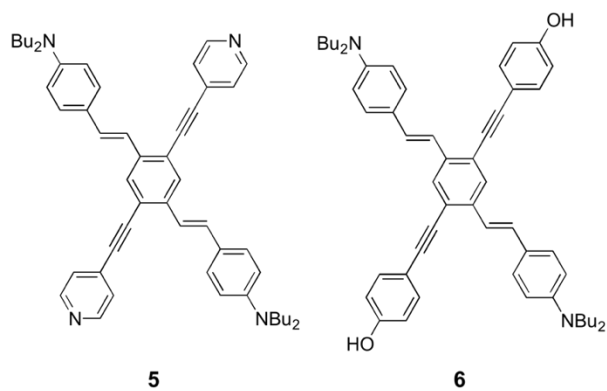
Figure 6. Cruciform molecules **5** and **6** with donor and acceptor groups or differing coordination groups.

Another class of cruciform sensors based on 1,2,4,5-tetrakis-(arylethynyl)benzenes is exemplified by the work of Haley et al.,[48] where the molecules were found to have selective responses to a variety of metal ions. This class of aryl–ethynyl cruciforms has seen extensive exploration in the literature from fundamental structure–property studies as substructures of larger dehydrobenzannulene derivatives,[49,50] as well as by the group of Baxter in their work on strained- and oligo-cruciform aryl–alkynyl systems.[51,52]

Anions

Anion Sensing Mechanisms. In recent years, anion recognition has begun to compete with cation sensing in the literature as a major research thrust. Cation sensor development was spurred in the mid-1960s by the advent of crown ethers and continues to be quite thoroughly explored.[31,53] Anion recognition has been slower to progress because of the difficulties of sensing anions over other analytes, with numerous books and reviews citing poorly-defined solvation geometries, low basicity, and high hydration energies among the limitations in coordinating anionic species.[54–58] A wide variety of mechanisms have been employed to produce a sensing response for an anion over competing analytes.[59]

Fluorophore collisional quenching is the most easily accessed mechanism for anion sensing, with a variety of neutral and cationic fluorophores having been developed based on this mechanism. Fluorescent polymers are able to maximize the resulting fluorogenic response by providing multiple binding sites. Bringing the anion closer to the fluorophore, as in guanidinium probe **7a,** can also increase the quenching effect (Figure 7).[60] The increased proximity produced a four-fold increase in response compared to a similar ammonium probe (**7b**).

11
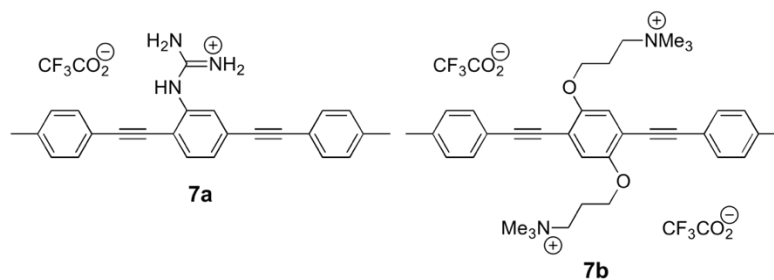
Figure 7. Examples of collisional quenching in anion receptor design. Guanidinium-appended fluorophore **7a** provides hydrogen bonding and ion pairing in close proximity to the fluorophore for a high fluorescent response versus ammonium probe **7b**.

The second method for designing fluorogenic sensors relies on the ability of the aryl–ethynyl unit to relay electrons in a PET sensor. Unlike the turn-on response commonly encountered with cations, anions typically produce a turn-off fluorescence response when the mechanism is PET-based. This mechanism has been used extensively to produce sensors for the common water contaminant fluoride.[61] In the BODIPY probe **8** (Figure 8), the terminal boronyl sites are able to selectively coordinate F^- in the presence of competing anions. The additional electron density of $-BMes_2F^-$ is transferred through the ethynyl linker and quenches the BODIPY dye upon excitation.[62]

PET anion sensors also utilize protons as messengers to detect anions, especially more basic anions such as F^-. A solution of hemi-cruciform **9** (Figure 9) exhibits a large bathochromic shift and quenching upon addition of excess of TBA^+F^-, which is likely due to deprotonation of the benzimidazole core.[63] A similar response to acids, bases, and anions was observed with cruciform **10**.[64] Gratifyingly, a combination of PET and solvatochromism allowed the absolute identification of numerous amines, boronic acids, and anions.[65] As with all cruciform structures, their interesting fluorescent behavior is attributed to the excellent orbital separation of the HOMO and LUMO, which facilitates energy transfer during fluorescence, and is easily perturbed by analytes.
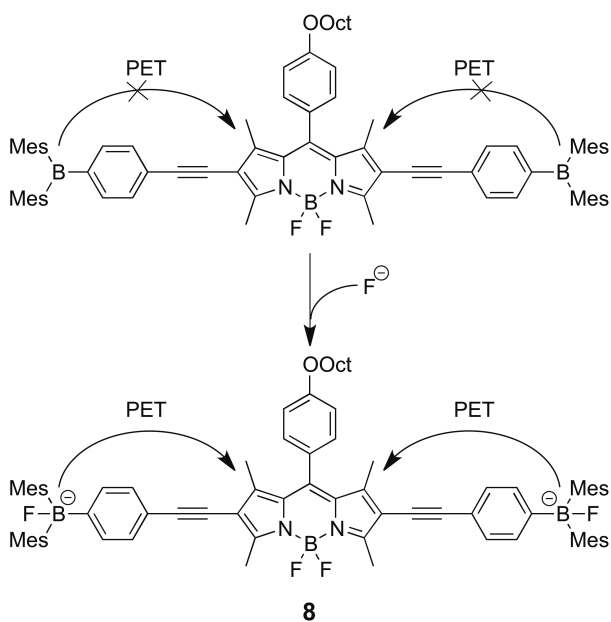
Figure 8. Addition of fluoride to aryl–ethynyl BODIPY fluorophore **8** quenches the fluorescence via a PET mechanism.
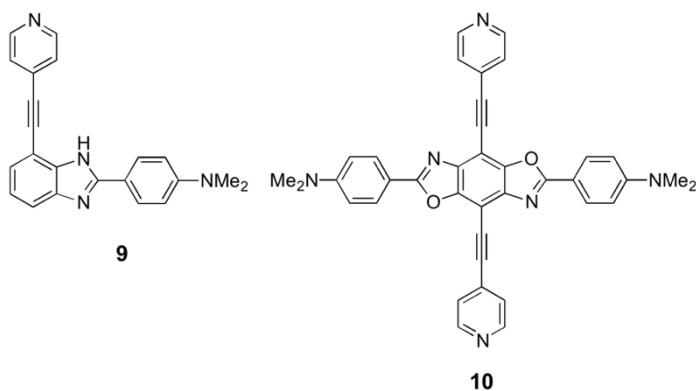
Figure 9. Cruciform architectures **9** and **10** used for the identification of whole structural families by differential analysis.

Altering the angle or freedom of rotation about the alkyne can also cause a change in fluorescence upon anion binding.[22] The first examples of such a system were bis-ureas **11** and **12** with mono- or dialkyne linker (Figure 10).[66] A low barrier to rotation provides easy access to the desired *syn* binding conformation from the stable unbound *anti* conformer. In addition, enforced planarity by anion binding causes the energy for non-emissive internal

conversion to increase, and the result is a 'turn-on' fluorescent response to Cl⁻. The effect of

induced planarity is reinforced by titrating in AcO⁻, which binds 1:2 to a solution of **12**·Cl⁻,

and observing a decreased quantum yield as the AcO⁻ displaces Cl⁻. Whereas both PET and

collisional quenching mechanisms result in 'turn-off' fluorescent responses, the alkyne rotor

mechanism is able to generate a turn-on response, which is much easier to detect, and

warrants further investigation.

11, n = 1
12, n = 2
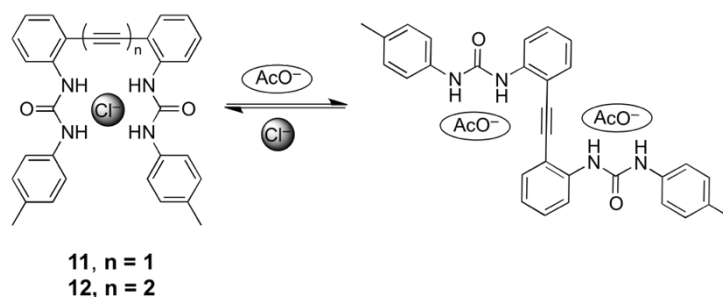
Figure 10. The ability of aryl–ethynyl receptors to provide a desirable turn-on response to anions was discovered using bis-ureas **11** and **12**. Cl⁻ binds 1:1 and turns on fluorescence, while AcO⁻ binds 1:2 and turns off fluorescence.

Insight into the turn-on response can be found in the parallel field of molecular

switches. The lowest energy conformation of molecular rotors **13** and **14** is 'closed' in the

unbound state with two intramolecular hydrogen bonds (Figure 11).[67] The alkyne can be

switched to a second 'closed' state by introducing Cl⁻, and the rotor now forms a stable

complex with two intermolecular and one intramolecular hydrogen bond. A new Na⁺

complex has been observed by cryogenic ion vibrational predissociation spectroscopy that is

analogous to the rotational transition state between the two 'closed' states.[68] The 'open' state

can also be considered similar to the unbound state of an alkyne anion host that lacks

preorganization.
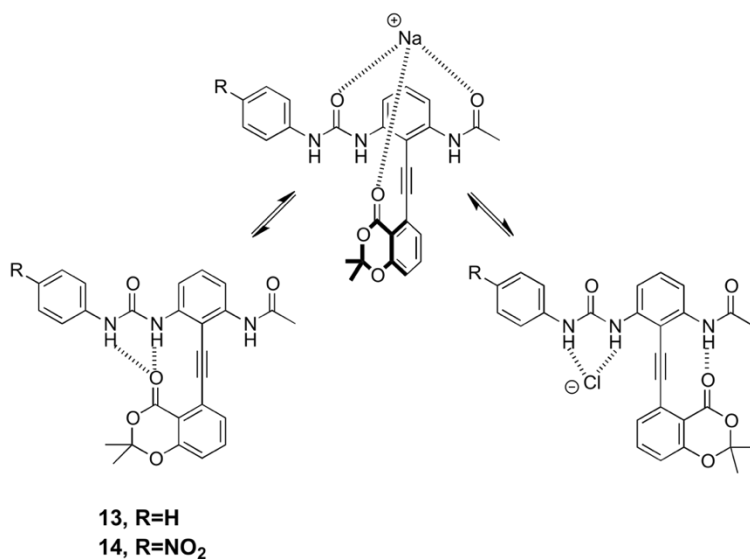
Figure 11. Cryogenic ion vibrational predissociation experiments reveal three distinct states of aryl–ethynyl molecular switches **13** and **14**.

AIE is another promising mechanism for designing turn-on fluorescent sensors. The close packing of fluorophores into aggregates blocks non-emissive conformers, similar to the alkyne rotors. The Allen group's synthesis of a series of fluorescent lipid mimics incorporating both an anion coordination site and the zwitterionic phosphocholine group (**15,** Figure 12) is an example of AIE in sensors.[69] The complimentary urea and phosphate groups form head-to-tail dimers in non-coordinating solvents. Fluorescence studies revealed that weakly basic anions (Cl⁻ or NO_3^-) do not disrupt the dimers, but that more basic anions ($H_2PO_4^-$ or HCO_3^-) cause dissociation and quenching. This offers the possibility of using an anion to template the assembly of non-emissive aryl–ethynyls into emissive dimers or oligomers for a turn-on response.
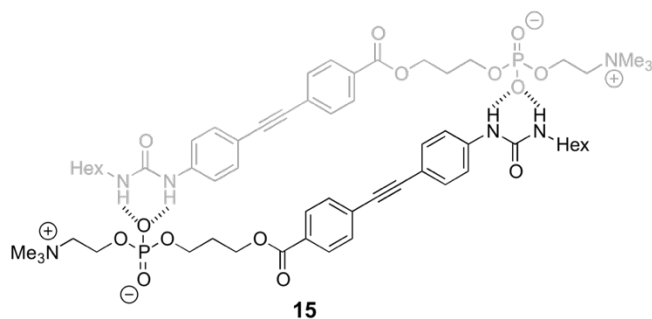
Figure 12. Phospholipid mimic **15** forms head-to-tail dimers that are emissive through an AIE mechanism.

Selectivity. Considerable effort has gone into the design of reporting mechanisms for anion sensing. The next necessary step is to provide these sensors with not just strong anion binding but selectivity as well. To accomplish this, a variety of methods have been used to develop catalogues of discriminating hosts by altering the selectivity within a single structural family. The most direct method is to alter the size or shape of a rigid binding pocket. For example, the constrictive binding pocket in bisindolocarbazole macrocycle **16** forces N_3^- to bind upright, or perpendicular to the plane of the host (Figure 13).[70] The N_3^- can rotate 90° to bind parallel to the plane of the host simply by expanding the pocket to 1,3-diyne **17**.
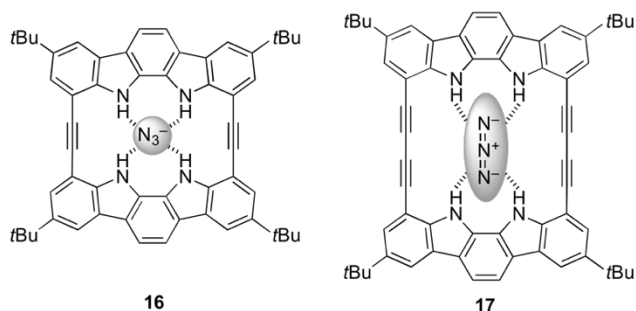
Figure 13. Ethynyl-linked bisindolyl host **16** binds N_3^- in an upright fashion, perpendicular to the host plane. Extended diethynyl-linked bisindolyl host **17** is able to accommodate linear N_3^- inside the binding pocket, parallel to the host plane.

Selectivity through bottom-up design can nonetheless be time-consuming. As a result, several groups have developed methods for quickly modifying existing hosts to equip a trusted scaffold with new selectivity, for instance, molecular self-assembly, post-synthetic modification, and photoswitching. A particularly ambitious method for quickly building a library of hosts is through the anion-templated assembly of coordination complexes. Two $[M_2L_4]^{4+}$ monomers, with M=Pd^{2+} and L=**18** (Figure 14), assemble around a single BF$_4^-$ into an interlocked structure, $[M_2L_4]_2^{8+}$, with two additional binding pockets.[71] The interlocked structure encapsulates BF$_4^-$, as observed in ^{19}F NMR and ESI-MS data. The $[M_2L_4]_2^{8+}$ complex also exhibited strong allosteric Cl$^-$ binding, where the first equivalent of Cl$^-$ caused a collapse of the outer cavities and facilitated the binding of a second Cl$^-$.
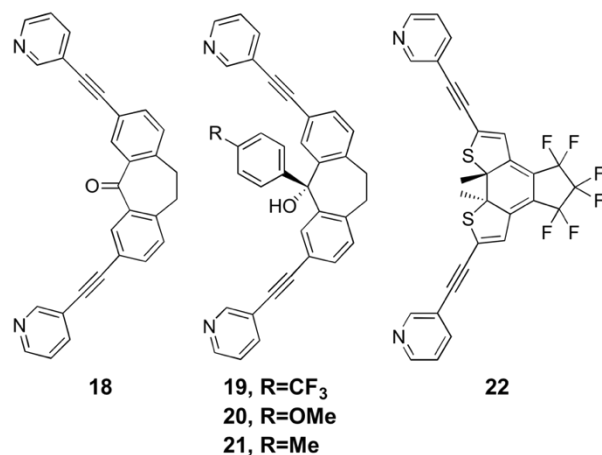
Figure 14. A variety of acetylene-linked pyridine ligands employed for constructing $[M^2L_4]^{2+}$ and $[M^2L_4]_2^{4+}$ cages for anion recognition.

A single step modification of **18** led to more sterically bulky ligands **19–21** (Figure 14), which formed stable $[M_2L_4]^{4+}$ complexes with BF$_4^-$ templates. Adding Cl$^-$ drove formation of a $[M_2L_4]_2^{8+}$ interlocked cage with Cl$^-$ trapped inside the smaller central cavity.[72] The smaller central cavity leaves more space in the outer cavities, and the weakly bound BF$_4^-$

undergoes ion exchange with ReO_4^-, to give the final structure $[Pd_2L_4]_2[Cl][ReO_4]_2^{5+}$.

Photoswitchable ligand **22** forms a stable $[M_2L_4]^{4+}$ cage upon addition of Pd^{2+}.[73] This

structure is intriguing because it reversibly switches between open and closed conformations

upon irradiation with UV (open➜closed) or visible light (closed➜open). The open cage has

a 47-fold higher affinity for $B_{12}F_{12}^{2-}$ than the closed cage, likely due to increased rigidity

preventing Pd^{2+} to $B_{12}F_{12}^{2-}$ close contacts. The ability to control anion binding or selectivity

through light stimulus is an exciting opportunity for controlling anion concentration or

removing harmful anions with a reusable ligand.

Not surprisingly, the complex host–guest interactions that are important for efficient

anion coordination can also be used to quickly change anion selectivity. In systems large

enough to bind multiple guests, such as ditopic receptors, the first guest can be used to tune

selectivity. The 1,3-diyne macrocyclic host **23** (Figure 15) is capable of exhibiting two

binding modes.[74] First, two independent binding sites coordinate anions inside through

hydrogen bonds with one cation external and a second found between the anions. Enclosing

a cation inside the binding pocket leads Cl^- to be favored over linear anions and a large

cooperativity factor for binding Cl^-. Interestingly, host **23** also assembles into a

pseudorotaxane by hydrogen bonding with 3,5-pyridinecarboxamide-*N*-oxide.[75] The smaller

binding pocket still provides six hydrogen bond donors and is selective for the linear anions

cyanate and azide. In this case, three distinct binding modes have been demonstrated with a

single rigid host molecule.
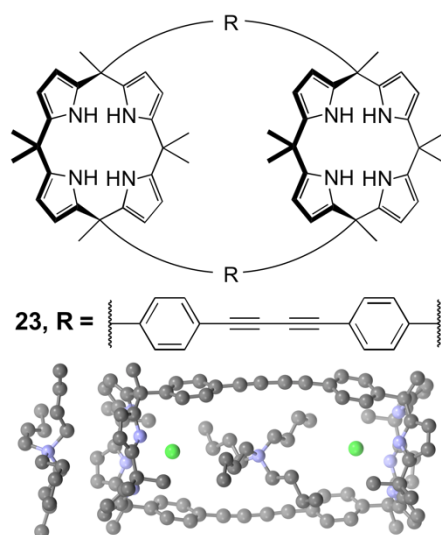
Figure 15. A tricyclic calix[4]pyrrole macrocyclic host (top) and the X-ray crystal structure of tricyclic host **23** (bottom) reveals the supramolecular assembly of a [1:2:2] ditopic receptor with TBA^+Cl^-. Hydrogen atoms have been omitted.

Rigid host molecules provide the greatest degree of control over the size and shape of the anion binding pocket. While they can be tuned through synthetic modification and secondary guest–guest interactions, sometimes the best method is to provide the host with a certain degree of flexibility to choose its own best guest. Bis-indolocarbazole host **24** (Figure 16) binds SO_4^{2-} ($K_a=25000m^{-1}$) with a 2500-fold selectivity over other anions in 10% (v/v) MeOH/acetone. Conformationally free hosts can exhibit weaker anion binding than their rigid counterparts; however, this can be overcome by using noncovalent interactions to favor a preorganized binding pocket. Internal hydrogen bonds organize **24** into a pocket too large for halides, but one that embraces SO_4^{2-} comfortably through eight hydrogen bonds.[76]

Non-rigid hosts can also be tuned for a desired anion by changing the size and shape of the binding pocket. We have developed a research program that utilizes a modular approach to synthesize highly conjugated aryl–ethynyl receptors for anion recognition. Unlike many fluorescent anion sensors, these sensors contain an inherently fluorescent

24
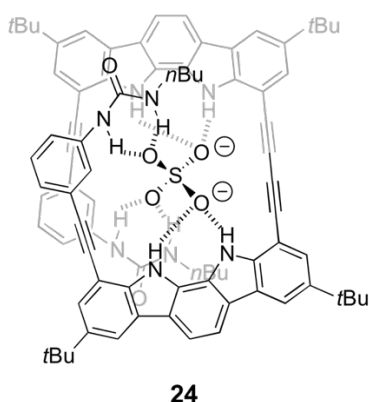
Figure 16. Urea-appended indolocarbazole **24** forms an internal hydrogen-bond supported helix, which binds SO_4^{2-} selectively over other common anions.

backbone that features an aryl–ethynyl core as opposed to a pendant fluorophore unit. We have previously described a series of both bis(sulfonamido)- and bis(urea)ethynylpyridines that exhibit positive fluorescent responses to anions with the right combination of electron-donating and/or electron-withdrawing substituents on the pendant phenyl rings.[4,25–29,77] The bis-ureas (e.g., **25–28**, Figure 17) exhibit a rich solvent-based conformational dependence, showing in the solid state that "S"-, "U"- and "W"-type conformations are all possible depending on solvent guests (for instance, "S" shown in **28**, "U" shown in **25–27**).[27]

25, Y = N
26, Y = +NH
27, Y = CH

28

29, X = H
30, X = F
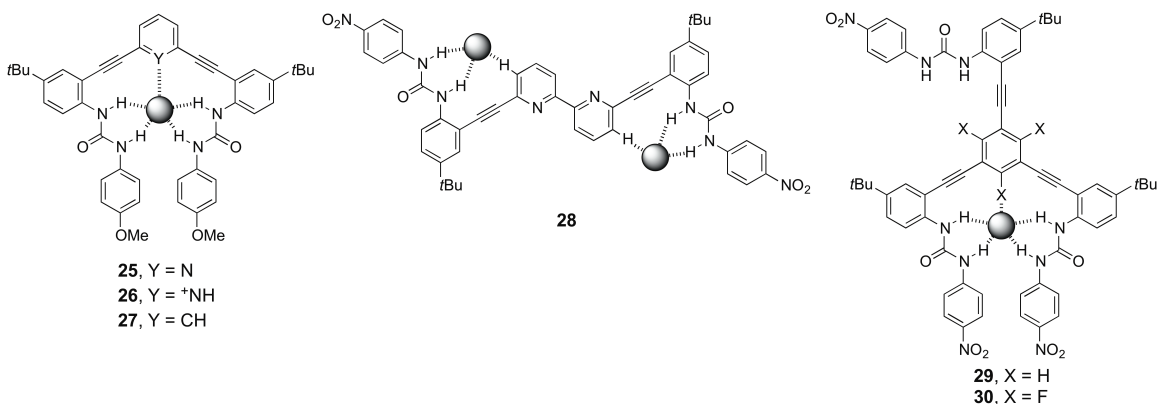
Figure 17. A family of aryl–ethynyl-urea receptors **25–30** for selective anion recognition.

More recently we discovered a NO_3^- selective probe, realized by modification of bis-urea scaffold to add an additional binding site that forms an idealized pocket for trigonal planar anions (e.g., **29–30**).[78] The desired selectivity of **29** for NO_3^- over halides was supported by ^{1}H NMR titrations in 10% DMSO/CDCl$_3$. The X-ray crystal structure favors an uncommon explanation for selectivity, namely an anion–π type interaction between NO_3^- and the alkyne attached to the central arene, where the anion rests offset from the center of a tripodal binding pocket. Whereas the anion–π interaction is engendered by electron-poor receptor **29**, it is not observed in non-fluorinated receptor **30**, which also loses NO_3^- selectivity over the halogens. ^{1}H NMR spectroscopy titrations reveal a large shift in the central arene protons of **30** upon complexation to Cl$^-$, suggesting a C–H···X$^-$ hydrogen bonding interaction (as depicted in Figure 17) that is not observed in the presence of NO_3^-.

The formation of a C–H···halide hydrogen bond is not unique to the tripodal ligand. Two-armed host **27** (Figure 17) also forms strong C–H···X$^-$ hydrogen bonds, both in solution and in the solid state.[89] X-ray crystal structure determination of the **27**·Cl$^-$ complex showed a short and nearly linear C–H···Cl$^-$ contact. The hydrogen bonding interaction was also evident in solution by a large downfield shift of the core proton upon addition of anions. The additional hydrogen bond resulted in a 10-fold increase of the association constant over the free-base parent pyridine host **25**.

Another example of C–H···X$^-$ binding in one of our bis-urea hosts surprisingly led to an anion controlled, three-way molecular switch. Bipy-based ligand **28** (Figure 17) was designed as a selective probe for the complexation of $H_2PO_4^-$ over halides and other oxoanions.[29,80] Including hydrogen bond acceptors and donors in the binding pocket improved the selectivity by matching the two-donor, two-acceptor architecture of $H_2PO_4^-$ and allowed the host to bind this ideal guest in a "U" conformation. Titrations and X-ray

21

crystal structures revealed an alternative "S" binding mode for the halides, wherein a urea arm rotates about the alkyne linkage to form a C–H⋯X⁻ hydrogen bond at the 3-position of the bipy subunit. The two distinct binding modes can be accessed sequentially, making the bipy ligand a three-way switchable probe.

An extreme case of a conformationally flexible anion host not only requires internal organization but also relies on two or more host molecules to assemble around a guest. A family of bis-diketodipyrrole receptors (Figure 18) was synthesized to study anion-templated assemblies;[81] diyne **31** formed a [2+2] double helix as a major species under controlled conditions (1×10^{-3}m [**7**], low [Cl⁻], $-50°$C). Appending additional arenes stabilized the dimeric complex and facilitated observation in solution at room temperature. A *cis*-Pt linked ligand was also of a suitable geometry to form [2+2] complexes with Cl⁻ under specific conditions.
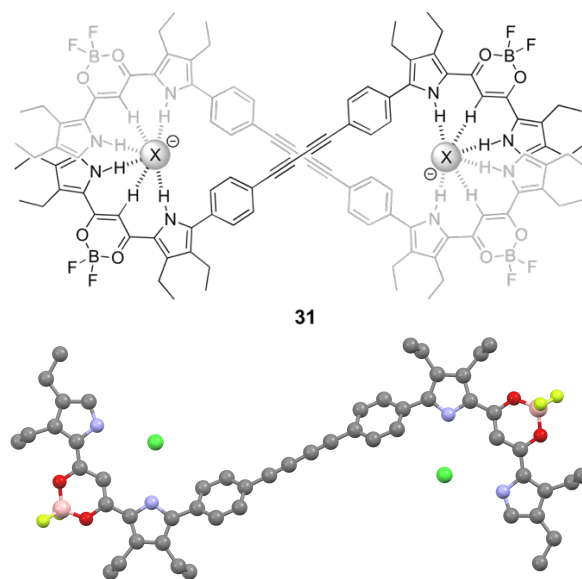
Figure 18. Dipyrrole-diketo anion receptor **31** designed to have two anion binding pockets (top); X-ray crystal structure of **31** complexed with Cl⁻ (bottom). TBA⁺ and hydrogen atoms have been omitted.

Despite the numerous hurdles set up by anions to hinder efforts in designing potent and selective hosts, complex coordination events that were previously only possible with metals have been achieved. The ability of aryl–ethynyl hosts to act as building blocks or foldamers is not restricted to anions as templates. Methods for using the aryl–ethynyl for chiral sensing and even more complex architectures have also been achieved.

Emerging Areas

Chirality

Chirality sensing is the basis of many biological processes and an emerging field for synthetic receptor design. Novel aryl–ethynyl sensors have been synthesized which report the absolute chirality of analytes. Sensors have also been developed that use circular dichroism spectroscopy as a mechanism for selective reporting of non-chiral analytes. Polymeric receptors in the burgeoning field of chiral detection have intriguing prospects for the assembly of supramolecular architectures to mimic natural structures such as proteins and enzymes. Though a detailed discussion on the use of polymeric receptors is beyond this review, a few notable examples will be highlighted in the context of chirality sensing.

Fluorescent aryl–ethynyl polymers have been modified for chiral detection by incorporating chiral binding sites. The Zhu group used a binaphthalene derivative with axial chirality, in conjunction with a Schiff base binding site, to give sensor **32**, which has selectivity for (*D*)-phenylalaninol (Figure 19).[82]
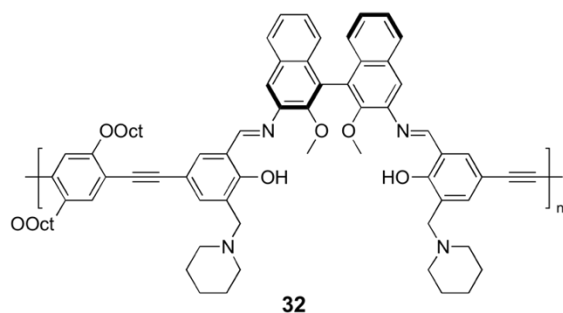
Figure 19. Aryl–ethynyl polymer **32** with an integrated chiral receptor unit.

Another interesting area of research for aryl–ethynyl oligomers and polymers is reproducing the double-stranded helix of DNA with synthetic precursors, which can then be used as induced chiral reporters. In solution and in the solid state, *m*-terphenyl polymers and oligomers such as **33** were found to form an achiral mixture of double helices through carboxylate salt bridges (Figure 20).[83] The addition of chiral secondary amines induced the dimers to refold into chiral double helices, held together via a salt bridge. The handedness is dependent on the chirality of the amine and could be measured both in solution by CD and in the solid state by AFM. Further studies elucidated a large "sergeant and soldiers" effect, as well as a "majority rules" effect on the chirality.

An oligomeric double-helix was prepared by ring-closing metathesis of salt-bridged *m*-terphenyl monomeric derivatives of **33** appended with alkenes.[84] The dimeric helix produced a large CD response with little solvent dependence, compared to a model dimer that displayed a small CD signal. The addition of TFA or Zn^{2+} caused a near complete loss of the observed chirality in the helix due to disruption of the salt bridges. In addition, Zn^{2+} produced a turn-on fluorescence response. The chirality could be returned by addition of sequestering agents for the initial stimuli, addition of DIPEA for acid or [2.2.1] cryptand for Zn^{2+}.
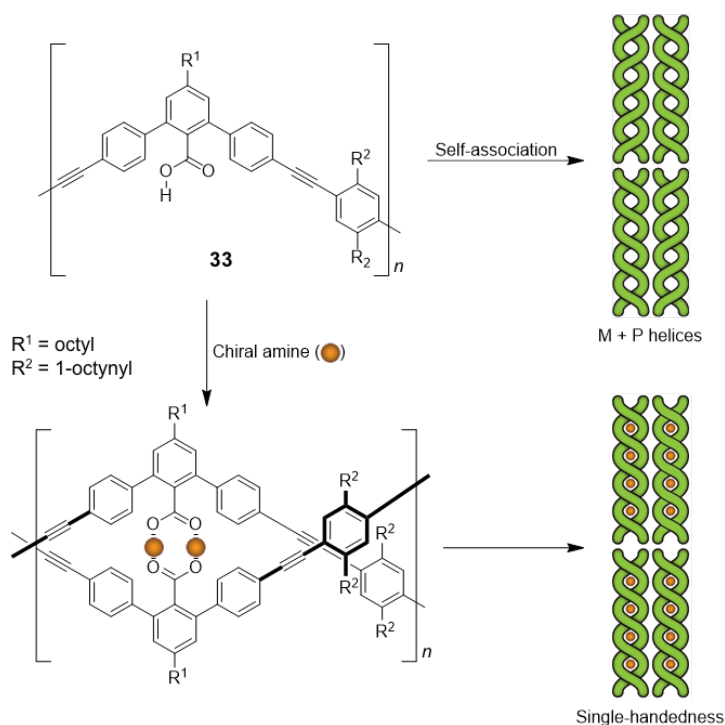
Figure 20. Foldamer **33** acts as a chiral reporter in the presence of chiral amines, generating helices of a single handedness due to the amine's chirality.

The design strategy of combining a fluorescent molecule with a probe group has also been used for modular, fluorescent chirality sensors. A phenothiazine fluorophore linked with both a chiral amine and boronic acid binding sites furnished **34** (Figure 21).[85] The resulting aryl–ethynyl sensor provided enantioselective determination of a variety of sugars and organic acids.

The Wolf group has developed a chirality sensing scaffold by appending aryl–amines or aldehydes to a central aryl–ethynyl rod, giving sensors with the general scaffold of **35–36** (Figure 21).[86–88] The functionalized aryl–ethynyl rotors form imines upon reaction with amine or aldehyde analytes. Chiral diamines or dialdehydes lock the probe in a single chiral conformer, which leads to a large Cotton effect, and quantitative determination of *ee* is

possible. Further studies with mono-substituted chiral analytes revealed similar large Cotton effects and linear calibration curves for *ee* determination via CD analysis.
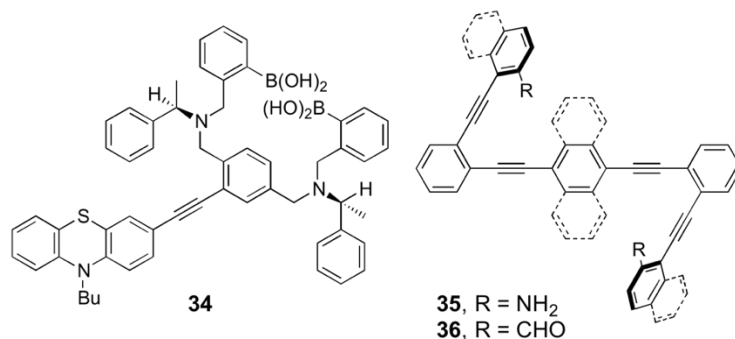
Figure 21. Examples of probes for determining chirality. **34**, a fluorescent sensor with chiral binding sites, shows chirally-selective recognition of chiral analytes. An achiral rotor within **35** and **36** can be induced to chiral conformations via imine formation.

The ethynyl-indolocarbazole anion sensors of Jeong have also been reengineered to act as both a chiral reporter for achiral analytes and a enantiomer-selective sensor for chiral analytes (Figure 22).[89] The addition of chiral methylene groups to a known indolocarbazole anion probe produced foldamer **37** with a strong helicity preference measured by CD in non-polar solvents. The chiral response of this probe is affected by both the solvent polarity and the presence of anions in solution. For instance, changing the solvent from toluene to CH_2Cl_2 or $CHCl_3$ resulted in a decrease of the CD signal by half; further increasing the polarity to DMSO or CH_3CN caused a near complete loss of the chirality. Notably, the switchable chirality could also be used to detect anions by noting the CD signal inversion in the presence of Cl⁻, Br⁻, or AcO⁻.
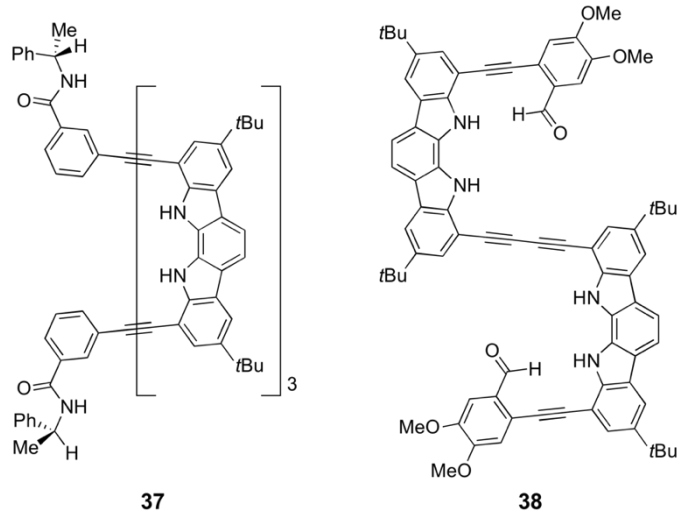
Figure 22. Foldamers **37** and **38** have been engineered to act as hosts for chiral guests using the aryl–ethynyl scaffolding.

The absolute configuration and *ee* of amino acids can also be determined using indolocarbazole foldamers.[90,91] Bis(ethynyl-indolocarbazole)s with appended aryl–aldehydes such as **38** form chiral helices in the presence of *N*-Boc protected amino acids; these helices can subsequently be locked in place by imine formation with ethylene-1,2-diamine. The resulting chiral macrocycles produce a large CD response, and calibration with mixtures of isomers permits rapid determination of *ee* for a given sample. Analysis of X-ray crystal structures and computational models revealed that this stereoselectivity is likely due to steric interactions between amino acid side chains and the bis-alkyne. The development of novel chirality sensors brings supramolecular chemistry closer to its roots in biology and biomolecules.

Biological Species

One of the primary purposes for synthesizing anion-selective fluorescent probes is to provide biologists and biochemists with better tools for studying anion-regulated cellular processes. A corollary to this purpose is the synthesis of small molecule-based anion

27

transporters or anion channel mimics. These mimics are useful for studying the mechanisms of cellular anion transport and as possible treatments for anion transport protein deficiencies. The Jeong group was successfully able to design a synthetic chloride channel to mimic the *S. typhimurium* protein.[92] The combination of four hydrogen-bond donors in an anion-binding pocket with judicious side-chain selection produced a potent anion binder and anion transporter. The presence of both a greasy side-chain and activated alcohols was necessary for efficient anion transport.

Ion transport across cell membranes has also been achieved by designing synthetic molecules to form porous channels.[93] Oligomers with alternating regions of hydrophilic and hydrophobic chains interpenetrate the lipid bilayer and form supramolecular assemblies. The timescale of the ion transport, measured by time-dependent conductance, indicates a pore formation mechanism, not flip-flopping. Transport rates with various alkali metals allowed for rough determination of the pore size as 0.53 nm.

The work of Moore et al. has gone a long way in proving the viability of designing artificial protein mimics from aryl–ethynyl scaffolds.[94] Oligomers of phenylacetylene form a helical structure with a well-defined hydrophobic cavity that is able to bind guests in water. Replacement of a single phenyl with a pyridine in the chain provides a reactive site for guest modification either by protonation or methylation reactions. Aryl–ethynyl foldamers have also been used to selectively bind saccharides.[95–97] A pyridineacetylene foldamer offers multiple hydrogen bond acceptors and provides good shape complimentarity. Covalent linkage of the foldamer with a coherent saccharide allows for the synthesis of stable, chiral aryl–ethynyl foldamers (Figure 23). This method of covalent linkage also allows for the possibility of a displacement assay for other guests.
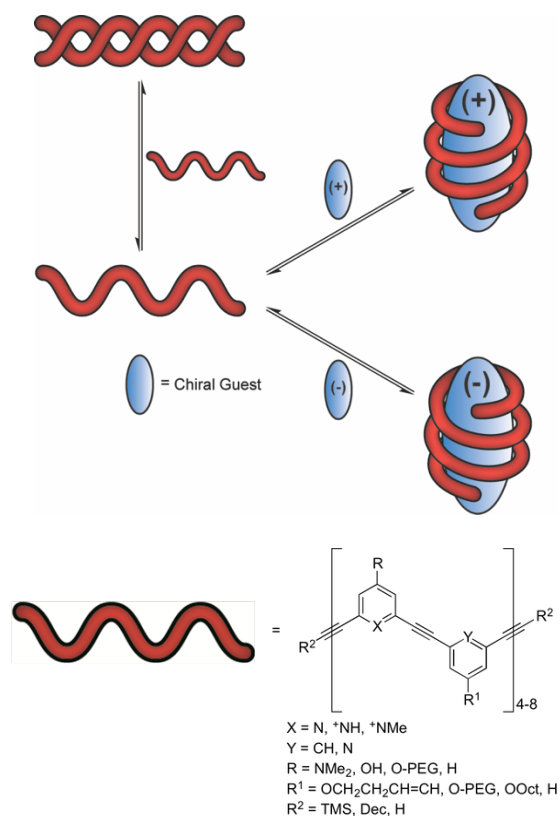
Figure 23. Aryl–ethynyl foldamers form complimentary binding pockets to provide guest selectivity, in conjunction with specific binding motifs.

Water-soluble aryl–ethynyl probes have also been applied as selective binders and stabilizers for G-quadruplex DNA structures. A series of bisamide (**39**) and trisamide (**40**) functionalized aryl–ethynylpyridines were studied for the effects of structural modifications on G-quadruplex stabilization and sequence selectivity (Figure 24).[98] The trisamide was found to be the most potent ligand at stabilizing a range of G-quadruplex sequences with a 2-fold increase in ΔT_m over the parent bisamide ligand. Addition of a triazole to the bisamide by click chemistry improved the ΔT_m, albeit less than the trisamide. Surface plasmon resonance (SPR) was used to elucidate the kinetics and equilibrium binding constants, K_d, for each ligand. The triazole ligand was found to have good selectivity for one G-quadruplex

sequence over others; however, the trisamide was found to have lower sequence selectivity, and both ligands displayed non-specific or multiple binding at high [L].
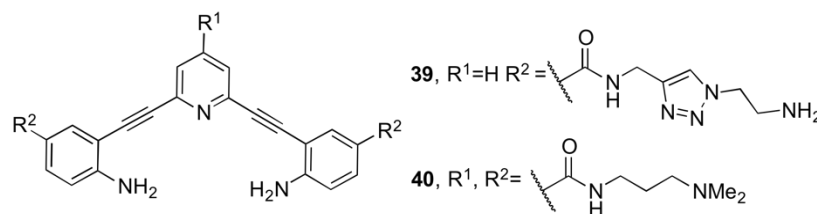
Figure 24. Side-chain engineering provides both water solubility and G-quadruplex selectivity for bisethynylanilinopyridines.

Chemical Warfare Agents

Another targeted application where aryl–ethynyls have proven their utility is the sensing of chemical warfare agents and high-energy organic compounds. Recent events have reemphasized these compounds as an important area for sensor development. The principles of aryl–ethynyl sensor design pioneered with simple metals and halides, and including structure design, π-conjugation, π-stacking, and metal coordination have been invaluable when applied to more dangerous compounds.

Stang et al. and Mukherjee et al. have developed a series of cages utilizing alkyne linkers and various metal centers whose native fluorescence is quenched in the presence of nitro-aromatics.[99,100] The quenching response of cages such as **41–43** (Figure 25) was selective for nitrated aromatics typical to explosives manufacture over other electron-poor aromatic molecules. A similar quenching response was found in a series of alkyne-linked dendrimers, based upon a silole core. These fully conjugated dendrimers exhibited a fluorescence emission which was selectively quenched in the presence of nitrated aromatics.[101]
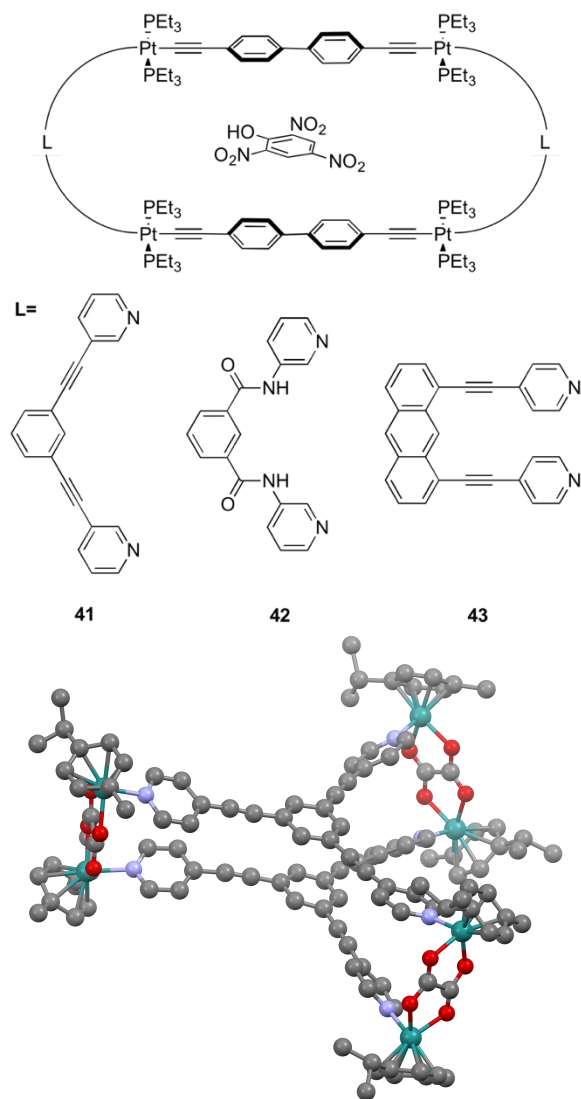
Figure 25. A family of macrocyclic hosts based on Pt (top) and X-ray crystal structure of another macrocyclic host based on Ru (bottom) for the detection of nitrated aromatics.

In addition to sensing mechanisms utilizing the quenching abilities of nitrated aromatics, Wild et al. developed a series of alkyne-linked terpyridine Zn complexes such as **44** (Figure 26).[102] These complexes responded selectively to organophosphate model compounds that are representative of the G-series of nerve agents. These sensor compounds were loaded on a solid support to create a test strip for nerve agents in the gaseous phase.
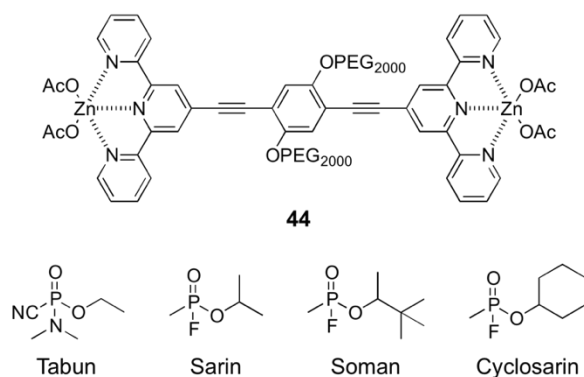
Figure 26. Zn complex (top) utilized in the detection of common nerve agents (bottom).

Gas Storage

In addition to their use in sensing nitrated aromatics, macrocyclic cage structures assembled from aryl–ethynyl linkages have been used for the selective storage and subsequent release of gases such as CO_2 over other atmospheric gases. The Zhang group has developed a family of organic molecular cages assembled with aryl–ethynyl linkages (Figure 27). These cages demonstrate selective adsorption of CO_2 in the presence of N_2, which shows promise in carbon capture applications; the ability to filter out and separate CO_2 in the presence of N_2 carrier gas is a potent method for the reduction of carbon emissions from industrial processes.[103] By assembly through dynamic covalent chemistry, formation of the cages **45** and **46** proceeded with exceedingly good yields. Comparison of alkyne-based **46** against previously developed anthracene-based cage **45** showed over a twofold increase in CO_2 selectivity versus N_2 in the solid phase (138/1 for **46** vs. 62/1 for **45**).[104,105] Crosslinking **46** via Sonogashira cross-coupling with *p*-diethynylbenzene formed an all-organic framework which demonstrated lower CO_2 selectivity (63/1) over N_2, but higher absorption of CO_2 by weight than all other cages studied (8.01 cm^3/g vs. 5.58-3.32 cm^3/g).
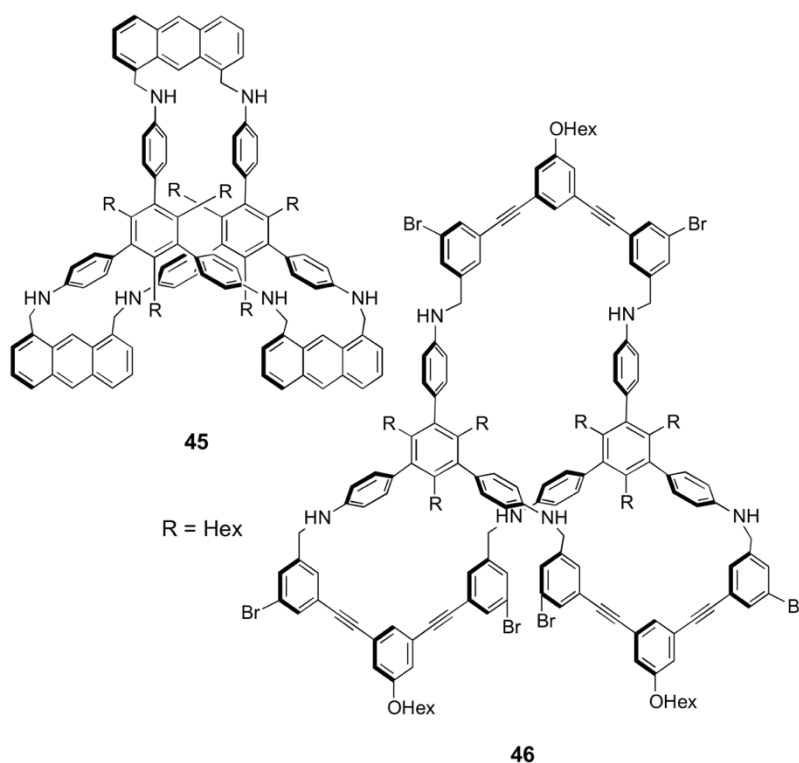
Figure 27. Large molecular cages **45** and **46** demonstrate selective adsorption of CO_2 over other atmospheric gases.

Conclusion

In summary, a variety of methods for incorporating aryl–ethynyl groups into recognition scaffolds, and their unique roles as both rigid structural units and conjugative linkers have been summarized. The methods covered utilize the unique characteristics of the ethynyl group to provide selectivity and responsiveness to designed sensors. The simplest usage relies only on acetylenes as rigid, conjugated linkers for reporter and recognition units. However, the complexity of possible aryl–ethynyl-based systems is limited only by the designer's imagination. This has been demonstrated by such a variety of uses as multi-analyte responsiveness from a single probe and analyte-responsive mimics of large biomolecules, proteins, and DNA, in addition to the classical guests such as the inorganic anions and cations.

The future directions of aryl–ethynyl compounds in sensing and recognition purposes shows a strong potential for artificial protein mimics, where the alkyne-linked foldamers can construct a chiral structure with a hydrophobic central cavity for stereoselective supramolecular catalysis. When appended with water-solubilizing groups, this can yield a powerful methodology for water-based supramolecular chemistry. As the field of supramolecular chemistry grows, the aryl–ethynyl linkage is showing itself to be a privileged scaffold for the construction of both molecular machines and supramolecular architectures.

Bridge to Chapter II

This chapter provided an introduction to the vast applications of aryl–ethynyl scaffolds for molecular recognition and for the sensing of anions in particular. Chapter II will provide an example of the combination of an aryl–ethynyl with a CH hydrogen bond donor for anion detection. In particular, benzene is shown to act as an isostructural replacement for pyridinium in an aryl–ethynyl bisurea scaffold. The work in Chapter II will offer an estimate of the energy for a single C–H$\cdots$X$^-$ hydrogen bond in solution by comparison to N: and N$^+$–H.

CHAPTER II

ARYL C–H···CL⁻ HYDROGEN BONDING IN A FLUORESCENT ANION SENSOR

This chapter was published as a *Chemical Communication* in issue 65 of volume 49. The synthesis of the pyridine receptor and preliminary titrations related to that molecule were performed by Dr. Calden N. Carroll. The X-ray diffraction data for **5** was collected and solved by Dr. Lev N. Zakharov. Synthesis of new compounds and titrations in triplicate were performed by me, along with preparation of the manuscript. My advisors, Prof. Darren W. Johnson and Prof. Michael M. Haley, provided editorial assistance and were the principal investigators for this work.

Introduction

Numerous supramolecular hosts for anionic guests have been developed, including polymers, macrocycles and cryptands.[1] Neutral hosts frequently combine a complementary geometry and strong hydrogen bond donors to selectively bind anionic guests.[2] A range of hydrogen bond donors that exhibit drastically different pK_as are found in supramolecular hosts. Some examples are amides (p$K_a^{DMSO} \approx$ 23-25), sulfonamides (p$K_a^{DMSO} \approx$ 13-18), phenols (p$K_a^{DMSO} \approx$ 12-20), pyrroles (p$K_a^{DMSO} \approx$ 23.0), and ureas (p$K_a^{DMSO} \approx$ 20-27).[3,4] These examples of hydrogen bond donors all rely on protic N- or O-groups. Highly electronegative elements are favored, but are not the only hydrogen bond donors extant. Of the donors employed in molecular sensors, the phenyl C–H (p$K_a^{H2O} \approx$ 37)[4,i] donor is relatively underappreciated by supramolecular chemists.

The C–H donor was recognized early on by molecular biologists as an important component in the secondary structures of biomolecules.[5,6] Carbonaceous hydrogen bond donors have experienced a renaissance in recent years with the introduction of new functional groups, including imidazolium,[7] triazole,[8] diketopropylene-BF$_2$,[9-11] and benzene.[12] The 1,2,3-triazole functionality is a promising anion binding moiety in neutral receptors,[13] since the C–H hydrogen bond donor is activated by a strong dipole oriented through the nitrogen atoms.[14] As previously observed in other selective hosts, the anion binding ability of 1,2,3-triazoles is optimized when the receptor is preorganized in an appropriately sized macrocycle.[15]

Aryl groups are used as the rigid linkers in supramolecular hosts to provide the desired anion receptor geometry. As a result, phenyl protons are a frequent feature in anion binding pockets.[1] Despite their ubiquity, aryl protons play only a small role in the anion binding of most hosts. Contrary to this, calculations suggest phenyl protons can bind anions with association energies (ΔG) approaching –9.0 kcal mol^{-1} and volumes of crystallographic data exist for the general C–H···anion interaction.[12,16] Recent solution studies have demonstrated the action of C–H hydrogen bonds in supramolecular hosts, yet crystal structures of these complexes are still rare.[17-19]

2,6-Bis(2-anilinoethynyl)pyridine (**1**, Figure 1) is an easily functionalized fluorescent core. Addition of sulfonamides or ureas (e.g., **2**) has illustrated the versatility of this scaffold for the construction of fluorescent sensors.[20,21] Judicious modification of the substituents allows control of the fluorescent and coordinating properties.[22,23] Previous work in our labs has demonstrated the increased anion binding ability by the pyridine-protonated receptors (**3**), showing an almost two order of magnitude increase in anion binding.[24] The greater anion binding ability of the pyridinium host is limited by its pK_a. While the exact pK_a of **3** is

not known, the pK_as for a series of similar ethynylpyridines have been measured in acetonitrile; the electron-withdrawing alkynes shift the pK_a of 2,6-bis(ethynyl)pyridinium to 8.9[25] from 12.5 for pyridinium (MeCN).[26] This complicates any attempts to apply a pyridinium-based anion sensor in an environment such as cells where a low pH cannot be maintained.[ii] Replacement of the pyridine with a phenyl moiety in the ethynyl core (e.g., **4**, **5**) will maintain the same geometry, while altering the electronic and anion binding properties. The phenyl C–H hydrogen bond offers an opportunity to expand the working conditions of this sensor and explore the nature of C–H hydrogen bonds. Herein, we introduce an aryl hydrogen bond donor in place of the pyridine-pyridinium moiety and report the anion binding characteristics of this new receptor.
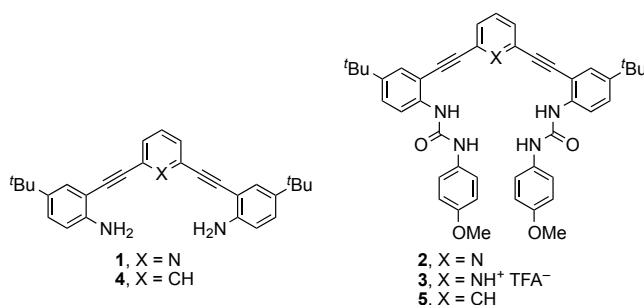
Figure 1. Structures of 2,6-bis(2-anilinoethynyl)arene cores **1** and **4** and anion receptors **2**, **3** and **5**.

Results and Discussion

Phenyl core **4** was obtained by deprotection and subsequent Sonogashira cross-coupling of ethynylaniline **6** with 1,3-diiodobenzene in 47% yield (Scheme 1). Reaction of **4** with 4-methoxyphenyl isocyanate gave bisurea receptor **5** in 94% yield. The anion binding properties of **5** were analyzed using ¹H NMR and UV-Vis spectroscopy. Titrations were performed in water-saturated chloroform with anions added as tetra-*n*-butylammonium

(TBA) salts. A representative ^{1}H NMR titration experiment with **5** and Cl⁻ is shown in Figure 2. The Δδ of urea proton H_g was fit using non-linear regression in MatLab to determine association constants (K_a).[27] A 1:1 host:guest binding model was used to fit the data as this agrees with previous binding studies on similar systems.[24] In addition, the model is supported by UV-Vis spectroscopic evidence and solid-state structures. Association constants for **5** and comparison with data for structurally similar hosts **2** and **3** are reported in Table 1.
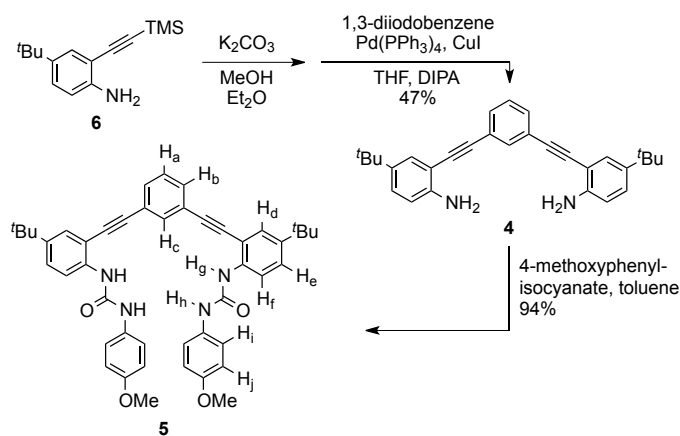
Scheme 1. Synthesis of receptor **5**. Proton assignments determined via ^{1}H-^{13}C HSQC and ^{1}H-^{1}H ROESY NMR spectroscopy.
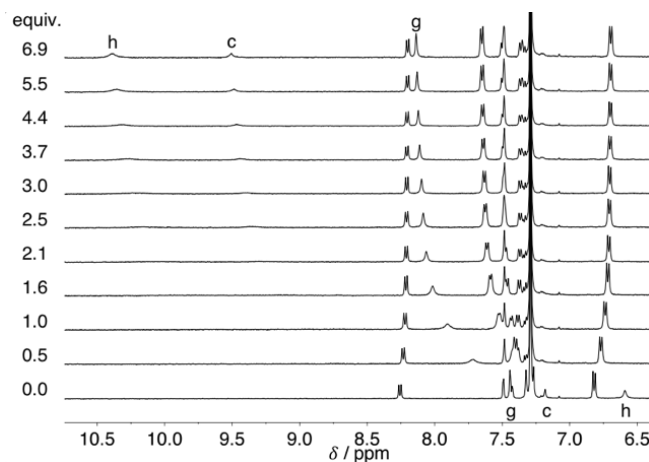
Figure 2. ^{1}H NMR titration of **5** with TBA⁺Cl⁻ at 298 K; [**5**] = 0.69 mM in water saturated CDCl₃. Peak assignments refer to Scheme 1.

Table 1 Anion association constants (K_a) obtained by fitting titration data using MatLab for ^{1}H NMR data or Hyperquad for UV-Vis data.[a]

Host	Cl^-/M^{-1}	$Cl^- \Delta G/kcal\ mol^{-1}$	Br^-/M^{-1}	I^-/M^{-1}
2	700[b]	–3.88	—	—
5	6700[c]	–5.21	1600[b]	150[b]
3	40700[c]	–6.28	—	—

[a] Anions added as tetrabutylammonium salts in water-saturated $CHCl_3$ or $CDCl_3$ at 298 K. Error is *ca.* ±10% and the values represent an average of three titrations. [b] Titrations performed using ^{1}H NMR. [c] Titrations performed using UV-Vis.

Pyridine host **2**, with only four hydrogen bond donors, has the lowest K_a for the tested anions. As previously reported, protonation of this class of receptor activates anion binding, increasing the K_a from 700 M^{-1} to 40700 M^{-1} for **3**•Cl$^-$.[24] The difference in K_a between **2** and **3** can be separated into three influencing factors: (1) the repulsive effect of the nitrogen lone pair on **2**, (2) the additional hydrogen bond in **3**, and (3) the electrostatic interaction of Cl$^-$ with **3**. For the three hosts, receptor **2** has the lowest energy interaction due to the repulsion between the pyridine lone pair. The inclusion of an aryl C–H hydrogen bond donor in **5** increases the K_a by an order of magnitude for Cl$^-$ (Table 1). The difference in energy ($\Delta\Delta G = \Delta G$ **2**•Cl$^-$ – ΔG **5**•Cl$^-$) is 1.33 kcal mol^{-1}. This $\Delta\Delta G$ is very close to the value (1.44 kcal mol^{-1}) reported by Sessler *et al.* for strapped pyrroles containing benzene or furan.[28] The additional electrostatic attraction in protonated receptor **3** leads to 1.07 kcal mol^{-1} added stabilization ($\Delta\Delta G$). This value is perhaps smaller due to competition from the trifluoroacetate counter ion.

2-D HSQC and ROESY NMR spectroscopy were used to assign the urea and aryl peaks in the proton NMR spectrum of **5** (see Figure 20-22 in Appendix A). The urea protons (H_h and H_g) shift downfield upon addition of Cl$^-$. A close examination of the aryl peak H_c reveals a large downfield shift, $\Delta\delta$ >2 ppm. The magnitude of $\Delta\delta$ suggests a strong aryl hydrogen bond, but may also be influenced by structural changes induced by anion

binding. The other aromatic peaks shift very little or slightly upfield likely as a result of weak CH–π interactions. The lack of a significant Δδ for H_a or H_b contraindicates the influence of alternative binding conformations, although multiple conformations have been previously observed in **2** and **3** by rotation about the ethynyl linkers.[22,24,29] The stronger urea hydrogen bond to Cl⁻ is formed with the more distant proton from the core, H_h, which is apparent in the large shift (Δδ 3.8 ppm) as compared to the interior urea H_g. Similar shifts are observed upon titration with Br⁻ and I⁻ (Figure 4 and 7 in Appendix A).

Evidence of hydrogen bonding was also observed in the X-ray crystal structure of **5•Cl⁻**, which is shown in Figure 3. The chloride resides within a binding pocket created by the aryl proton and the urea arms with a TBA⁺ cation in close proximity. The central phenylacetylene carbons (C_1-C_9, C_{27}-C_{29}) form a plane (± 0.033 Å), which the chloride sits slightly above (0.257(4) Å). The urea arms are twisted with one slightly above the plane and the other slightly below the plane. The C(H_c)···Cl distance is 3.579(3) Å and the C(H_c)···Cl angle is 169°. The N(H)···Cl distances vary greatly with the shortest distance at 3.212(3) Å and the longest distance measuring 3.732(3) Å. The N(H)···Cl angles vary from 146° to 170°. The C(H)···Cl total distance is less than the sum of the van der Waals radii for the component elements and is shorter than previously reported examples of arene C(H)···Cl contacts in anion hosts (3.538–3.793 Å).[17-19] The large angle and short distance fall well within previously defined criteria for an aryl hydrogen bond ($\theta > 140°$, $d < 3.86$ Å)[5,30-32] and add credence for the importance of this C–H hydrogen bond in anion binding.
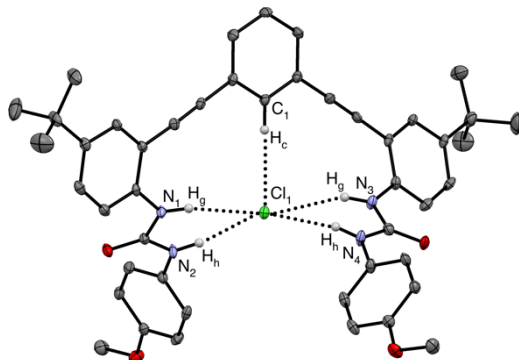
Figure 3. X-ray crystal structure of **5**•Cl⁻ shown as ORTEP representation. Hydrogen bond interactions are shown as dashed lines. Non-coordinating hydrogens, TBA^+ counter cation and solvent have been omitted for clarity. Ellipsoids drawn at 50% probability level.

The urea hydrogen bond distances provide further evidence for the binding conformation observed in solid-state studies to exist in solution. The urea hydrogen bonds are divided into two asymmetric groups, where N_2/N_4 are on average 0.41 Å closer to Cl than N_1/N_3 (H_h and H_g, respectively). The average distance for $N(H_g)\cdots Cl$ is 3.637 Å and the average distance for $N(H_h)\cdots Cl$ is 3.213 Å. A longer $N(H_g)\cdots Cl$ distance would account for the smaller downfield shift observed by ^1H NMR spectroscopy. The solution and solid state experiments provide a relative rank of the hydrogen bond lengths to Cl⁻, and perhaps strengths as follows: $N(H_h) > C(H_c) > N(H_g)$.

UV-Vis and fluorescence spectroscopy experiments were performed to evaluate the sensing ability of compound **5** (see Figure 11 and 15 in Appendix A). The color change of **5** was modest but allowed for the determination of binding constants. Cl⁻ titrations of **5** have an isosbestic point at 312 nm indicating a clean transition from free host and guest to the final host:guest complex, which lends credence to the 1:1 host:guest model used for K_a determination. Crystallographic evidence points to a higher order complex (1:2 or 2:1 host:guest) being unlikely and these larger complexes would require an intermediate complex, which is not evident in solution. Receptors **2** and **3** were previously shown to be

good fluorescent sensors[22,23], and the conjugated core of **5** should also lend itself to this application. Excitation at 320 nm produced a fluorescence emission at 381 nm with a Stoke's shift of 5000 cm^{-1}. Addition of one equivalent TBACl caused a marked decrease in the fluorescence. The turn-off fluorescent response for chloride is the same as previously observed with receptor **3**. The fluorescence response of this class of sensors can be controlled by substitution at the *para* position of the phenylureas. In the pyridine sensors **2** and **3**, an electron donating group (OMe) produced an "on-off" response; however, electron withdrawing groups (NO$_2$) led to an "off-on" response.[22,23]

In summary, replacement of a pyridyl unit with a phenyl moiety in the bis(anilinoethynyl)arene class of anion receptors has provided a new avenue of inquiry into aryl C–H hydrogen bonding. The importance of the phenyl hydrogen bond donor has been demonstrated with solution and solid-state evidence for a strong C–H to Cl$^-$ contact. In addition, the structural modification has not negatively affected the selectivity or electronic properties of the host. Related computational modeling has shown that substitution with electron withdrawing groups can increase the hydrogen bond energy of benzene closer to that of pyrrole.[12] Further experiments with the phenyl core may help to elucidate the mechanism of fluorescence in this class of sensor, especially the influence of the pyridine ring in the parent receptor. Work is underway to explore substituted phenyl cores with the goal of achieving K_as on the same order or greater than found for **3**.

Experimental

General Procedures

^{1}H and ^{13}C NMR spectra were obtained on a Varian 300 MHz spectrometer (^{1}H 299.95 MHz, ^{13}C 75.43 MHz), 500 MHz spectrometer (^{1}H 500.10 MHz, ^{13}C 125.75 MHz) or

600 MHz spectrometer (^{1}H 599.98 MHz, ^{13}C 150.87 MHz). Chemical shifts (δ) are expressed in ppm relative to tetramethylsilane (TMS) using residual non-deuterated solvent (CDCl$_3$: ^{1}H 7.26 ppm, ^{13}C 77.0 ppm; CD$_2$Cl$_2$: ^{1}H 5.32 ppm, ^{13}C 54.0 ppm; DMSO–d_6: ^{1}H 2.50 ppm, ^{13}C 39.51 ppm). UV-Vis spectra were recorded on an HP 8453 UV-Vis spectrophotometer. Unless otherwise specified, all reagents were purchased and used as received. Dry solvents were obtained from distillation using published literature procedures directly before use. Fluorescence data was acquired with a Horiba Jobin-Yvon FluoroMax-4 fluorescence spectrophotometer in CHCl$_3$ prepared in the same manner as for UV-Vis; slit widths (ex/em) were 3 nm/3 nm. Compounds **1, 2, 3** and **6** were synthesized using previously reported procedures.[23,24] Crystallographic data for **5** can be found as CCDC 929532.

Synthesis

Dianiline 4. A suspension of ethynylaniline **6** (2.262 g, 9.22 mmol) and K$_2$CO$_3$ (6.37 g, 46.1 mmol) in Et$_2$O (15 mL) and MeOH (30 mL) was stirred at room temperature and monitored by TLC until completion (30 min). The solution was diluted with DCM and washed three times with water and brine. The organic layer was dried over MgSO$_4$ and concentrated *in vacuo*. The residue was dissolved in minimal THF and added to an N$_2$ purged solution of 1,3-diiodobenzene (1.39 g, 4.20 mmol), Pd(PPh$_3$)$_4$ (0.49 g, 0.42 mmol) and CuI (0.16 g, 0.84 mmol) in dry THF (45 mL) and *i*-Pr$_2$NH (45 mL). The solution was stirred at 50 °C for 8 h. The reaction was concentrated *in vacuo* and the residue was taken up into DCM. The solution was filtered through a 3 cm silica gel plug and washed with additional DCM. The combined organics were concentrated *in vacuo* and the product was purified by column chromatography (2:1 hexanes/CH$_2$Cl$_2$) to afford **4** (1.01 g, 57%) as a pale brown solid. Mp: 132.1-133.0 °C; ^{1}H NMR (600 MHz, CD$_2$Cl$_2$): δ 1.28 (s, 18H), 4.22 (br s, 4H), 6.69 (d, *J* = 8.5 Hz, 2H), 7.21 (dd, *J* = 8.5, 2.4 Hz, 2H), 7.34-7.40 (m, 3H), 7.50 (dd, *J* = 7.7,

1.7 Hz, 2H), 7.71 (t, J = 1.7 Hz, 1H); ^{13}C NMR (151 MHz, CD$_2$Cl$_2$) δ 146.37, 141.29, 134.56, 131.37, 129.26, 129.22, 128.00, 124.40, 114.73, 107.30, 93.69, 87.78, 34.35, 31.68; HRMS (ESI) for C$_{30}$H$_{33}$N$_2$ [M+H]$^+$: calcd 421.2625, found 421.2644.

Bisurea 5. All glassware was dried in a 150 °C oven for at least 1 h. Dianiline **4** (200 mg, 0.5 mmol) and *p*-methoxyphenyl isocyanate (177 mg, 1.2 mmol) in toluene (50 mL) were stirred at 50 °C for 8 h. The reaction became cloudy upon completion and acetone was added until the turbidity was removed. Hexanes were added until a slight turbidity returned, and the suspension was left to precipitate overnight in the refrigerator. Filtration afforded **5** (320 mg, 93%) as a fine white powder. Mp: 158.5-160.0 °C; ^{1}H NMR (600 MHz, DMSO-*d$_6$*): δ 1.29 (s, 18H), 3.70 (s, 6H), 6.86 (d, J = 8.9 Hz, 4H), 7.37 (d, J = 8.9 Hz, 3H), 7.42 (dd, J = 8.8, 2.4 Hz, 2H), 7.50 (d, J = 2.4 Hz, 2H), 7.55 (t, J = 7.8 Hz, 1H), 7.72 (dd, J = 7.6, 1.7 Hz, 2H), 7.99 (t, J = 1.7 Hz, 1H), 8.02 (d, J = 8.8 Hz, 2H), 8.11 (s, 2H), 9.28 (s, 2H); ^{13}C NMR (151 MHz, DMSO-*d$_6$*): δ 154.61, 152.40, 144.38, 138.04, 134.33, 132.43, 131.77, 129.16, 128.69, 126.96, 122.94, 120.22, 119.64, 114.03, 110.73, 93.69, 86.75, 55.13, 33.94, 31.02; HRMS (ESI) for C$_{46}$H$_{47}$N$_4$O$_4$ [M+H]$^+$: calcd 719.3563, found 719.3597.

Titrations

General Titration Procedures. Receptor concentration was kept constant by preparing a stock solution of receptor and preparing a guest serial dilution with the stock receptor solution. A constant receptor concentration was maintained during the titration to avoid concentration effects on the proton chemical shifts and provide clean isosbestic points in the UV spectra. Tetrabutylammonium salts were purchased from TCI America or Fluka and dried by heating to 70 °C *in vacuo* before use. Hamilton gas-tight syringes were used for all titrations and additions were made through septa when available. The reported binding

constants represent the average of the fits from titrations performed in triplicate. Representative data are provided for each halide anion in Appendix A.

¹H NMR Titration Conditions. ¹H NMR titrations were carried out on an Inova 500 MHz spectrometer (¹H 500.10 MHz). Chemical shifts (δ) are expressed in ppm relative to tetramethylsilane (TMS) using residual non-deuterated solvent (CDCl₃: ¹H 7.26 ppm, ¹³C 77.0 ppm). CDCl₃ was prepared by passing over activated alumina. 1:1 v/v CDCl₃ and deionized water was mixed in a separatory funnel and the organic layer was collected. Association constants were determined using non-linear regression fitting in MatLab.[27]

UV–Vis Titration Conditions. UV-Vis titrations were carried out on an HP 8453 UV-Vis spectrometer. Water saturated CHCl₃ was prepared in the same manner as for ¹H NMR titrations. Association constants were determined by non-linear regression using HYPerquad.[33]

X-Ray Crystallography

Diffraction intensities were collected at 100(2) K on a Bruker Apex2 CCD diffractometer using MoKα radiation λ = 0.71073 Å. The systematic absences allow the space group to be *Pnma* or *Pna*2₁; *Pna*2₁ was chosen and confirmed by the analysis. Absorption corrections were applied by SADABS.[34] Structure was solved by direct methods and Fourier techniques and refined on F^2 using full matrix least-squares procedures. All non-H atoms were refined with anisotropic thermal parameters. All H atoms were treated in calculated positions in a rigid group model. PLATON checks show that there is an 80% fit to a structure in space group *Pccn*. In this *Pccn* system, molecule **5** would have crystallographically-imposed twofold symmetry with disordered t-butyl groups; in addition, two of the n-butyl moieties in the tetrabutylammonium cation would be disordered, as would be the chloroform of solvation. As the *Pna*2₁ structure shows no anomalous

anisotropic displacement parameters, the obvious conclusion is that the reported nicely-ordered $Pna2_1$ structure is correct. All calculations were performed by the Bruker SHELXTL (v. 6.10) package.[35]

Crystallographic data for **5**: $C_{63}H_{83}Cl_4N_5O_4$, M_r = 1116.14, crystal size 0.25 x 0.19 x 0.13 mm³, orthorhombic, space group $Pna2_1$, a = 24.2423(16), b = 25.3429(17), c = 9.7891(7) Å, V = 6014.1(17) Å³, Z = 4, ϱ_{calc} = 1.233 g cm⁻³, μ = 0.247 mm⁻¹, F(000)=2384, MoKα radiation λ= 0.71073 Å, T = 100(2) K, $2\Theta_{max}$ = 54.00°, 90937 reflections measured [R_{int}=0.0396], 10521 reflections observed, 686 refined parameters, R1 = 0.0614, $wR2$ = 0.1674, and GOF = 1.054 for reflections with $I > 2\sigma(I)$, R1 = 0.0670, $wR2$ = 0.1737, and GOF = 1.054 for all data, max/min residual electron density +1.026/-1.258 e Å⁻³, the Flack = 0.47(7). CCDC 929532 contains the supplementary crystallographic data for these compounds. These data can be obtained free of charge from The Cambridge Crystallographic Data Centre via www.ccdc.cam.ac.uk/data_request/cif.

<u>Bridge to Chapter III</u>

The work presented in Chapter II offers an example of the general utility provided by aryl C–H hydrogen bonds in designing supramolecular receptors. Importantly, it has been demonstrated that an aryl C–H may be substituted for an aryl N or N–H⁺ with little effect on the ability to bind anions. In point of fact, a ubiquitous C–H donor is shown to act as a strong hydrogen bond donor in both the solid state and solution. In Chapter III, new evidence will be reported to quantify the strength of this hydrogen bond in anion binding. As well, we will show that this aryl C–H can be tuned for selective anion interactions by a systematic structure-property relationship. Linear free energy relationships will be used to

probe the role of substituents on the strength and selectivity of a single C–H hydrogen

bond.

---

i There appears to be discrepancy for the pK_a of benzene in water, with values of 37 and 43 appearing most commonly. We chose to use the value reported by E. V. Anslyn and D. A. Dougherty.[4]

ii It should be noted that this value is determined in CH_3CN; in water the bis(ethynyl)pyridiniums should still be more acidic than pyridinium and thus have pK_as < 5.

CHAPTER III

SUBSTITUENT EFFECTS IN CH HYDROGEN BOND INTERACTIONS:

LINEAR FREE ENERGY RELATIONSHIPS AND INFLUENCE OF ANIONS

This work was published in volume 147 of the *Journal of the American Chemical Society*. Ryan Hansen synthesized half of the receptors and performed ^{1}H NMR titrations for that set of compounds. Undergraduate student Calvin Chau performed analytical titrations by UV-vis under my direct supervision. Dr. Lev N. Zakharov collected and solved the X-ray diffraction data for **1b**. Dr. Benjamin Hay performed computational modelling and assisted with editing, along with Profs. Darren Johnson and Michael Haley.

Introduction

CH hydrogen bonds (HBs) are now understood to be a ubiquitous structural feature in chemistry and biology.[1,2] CH donors play important and previously unrecognized roles in the multidisciplinary fields of molecular biology, supramolecular chemistry[3-5] and catalysis.[1,6] CH$\cdots$O hydrogen bonds are common in protein folding and are found in the minor groove of DNA.[7,8] Catalysts have also been found to include CH$\cdots$O hydrogen bonds as an important factor in stereoselectivity.[6] Chemists are now widely using CH groups as HB donors in designed systems for anion capture[1,9-11] and catalysis.[12,13]

New CH donors have been developed to maximize the strength of a CH hydrogen bond, including triazoles, bisketo-boronates, and pyridinium ions (Figure 1a).[14] These strong, acidic CH donors, when incorporated within heterocycles with electron-poor atoms, are aligned to maximize the C$\leftarrow$H dipole. The development of such new CH donors has increased the utility of these non-classical HBs in structural design.
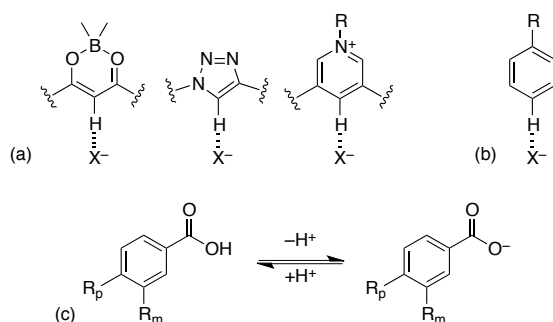
Figure 1. (a) Prototypical examples of polarized, strong CH donors. (b) Preferred benzene hydrogen bond geometries. (c) Equilibrium of benzoic acids for derivation of Hammett parameters.

Despite the numerous computational studies on strong CH hydrogen bond donors, experimental studies that quantify the energetic components of CH HBs, especially for weaker donors like benzene, have proven very difficult to obtain. As such, explanations and descriptions for CH HB strengths have been overwhelmingly dominated by the electrostatic component. Notable computational and experimental studies by Flood et al. have sought to dissect the strength of an arene CH vs. an alkyl CH.[15] A similar structure was used by Garcia Mancheño and co-workers to examine the influence of structure and electronics on catalysis;[12,13] however, neither of these investigations measured the direct effects of substituents or anions on the CH donor energy or the CH component of the total Gibbs free energy of association for these HBs. The lack of studies on these aspects of CH HBs has led to some confusion on the characteristics, i.e. strength and selectivity, compared to traditional HB donors.

Conversely, the related interactions between anions and electron-deficient aromatic rings have been the subject of extensive computational and experimental studies that have resulted in the complete dissection of the energetic components and substituent effects.[16,17] It has also been recognized that an anion can interact with the face of an arene via anion-π

or weak-σ interactions, leading to differentiation in both substituent and anion effects.[18-20] Computational studies indicate this type of dual anion and substituent dependence is important in CH HBs as well, although this has not been reduced to practice experimentally.[21] As a standard and classical physical organic tool, the use of linear free energy relationships (LFER), particularly the Hammett equation, for probing dynamic interactions is increasingly popular.[22-25]

Hay et al. performed an initial study to quantify the binding energy of benzene CH HBs, wherein they described both quite strong HBs to anions in the gas phase and a linear dependence of the binding energy with substituent electron withdrawing ability as measured by different substituent effects.[26,27] The substituent effects in their model (Figure 1b) could be described by a Hammett σ_m or electrostatic potential (ESP).[27] The use of a Hammett σ_m parameter to describe an interaction at the *para* position is typically assumed to indicate a mostly electrostatic interaction, due to the lack of conjugation at the *meta* position in the prototypical Hammett reaction, namely, the ionization of benzoic acid (Figure 1c).[28]

The assumption of electrostatic dominance is supported by the additional correlation with ESP. A more recent analysis by Scheiner et al.[21] of HBs to trifluoromethane revealed subtler energetic parameters. As included in the definition of a hydrogen bond, there exists a bond critical point between the H and X^- (anion), as well as a shift in the vibrational frequency of the CH stretch.[29] These effects are driven by the partial covalency of the HB and can be accentuated by examining the changes across a series of anions.

In the course of designing selective, fluorescent anion receptors, our group recently introduced the benzene CH HB donor into our existing bisarylethynyl urea scaffold to produce **1a** (Figure 2a).[30] In this report we have sought to better understand the parameters for controlling aryl CH HB acidity with anions by substitution *para* to the CH donor, **1b-g**.

50

The modularity of our scaffold allows us the unique chance to study a single CH···X⁻ HB by easily accessible solution techniques: ^{1}H NMR and UV-vis spectroscopic titrations with multiple anions (Cl⁻, Br⁻, I⁻ and NO$_3^-$). Association constants, K_a, are reported for seven receptors (**1a-g**) in water-saturated CHCl$_3$. Combined solution experiments, crystallography, and computations provide new insight into the preferred CH binding geometry and electronic control. Linear free energy relationships using Hammett parameters and ESP reveal ϱ dependence on the anion being titrated. Multivariate analysis with Swain-Lupton field (*F*) and resonance (*R*) parameters provides a deeper understanding of the percent resonance contribution to aryl CH acidity.[31,32] Our combined experimental and computational approach for understanding CH hydrogen bonds provides renewed support for the role of resonance in CH HBs. In addition, consideration of the anion in a supramolecular structure activity relationship identifies a new avenue for understanding and predicting anion binding selectivity.
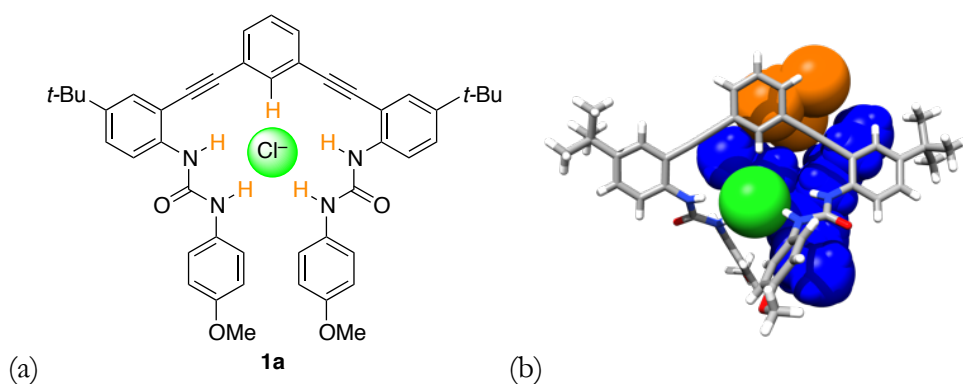
Figure 2. (a) Urea anion receptor **1a** shown in optimal binding geometry for Cl⁻. (b) X-ray crystal structure of **1a**⊂Cl⁻ with solvent (CHCl$_3$, orange) and counter-ion (TBA⁺, blue) included as space filling models. CCDC 929532.

Results and Discussion

Synthesis and Characterization

The substituted receptors used for this study are part of the bis(2-anilino-ethynyl)arene family of conjugated, fluorescent receptors we have reported previously.[33-39] In this case, pendant methoxy substituted phenylureas act as additional HB donors to direct the anion binding into a single site, as illustrated in Figure 2b.[19,35,38] The synthesis of **1a** has been previously reported and forms the parent scaffold for our study of substituent effects.[30] These receptors are highly modular and easily broken into three key units for stepwise synthesis—a core arene, an alkynyl aniline, and an isocyanate.[39] For the current investigation, the core arene can be any 3,5-dibromo- or 3,5-diiodobenzene suitable for Sonogashira cross-coupling possessing either an electron-withdrawing or electron-donating substituent in the 1-position. The *t*-Bu group on the alkynyl aniline was used to provide solubility in non-competitive organic solvents (i.e., CHCl$_3$). The 4-methoxy unit was chosen for the pendant phenylurea due to its simpler monomeric speciation in solution and to modulate the strength of the competing urea HBs. Such electron-rich ureas provide less competition with the CH$\cdots$X$^-$ hydrogen bond and have proven to be less prone towards self-aggregation.

Dianilines **2a-g** were synthesized by Sonogashira cross-coupling of 2-ethynyl-4-*t*-butylaniline (desilylated **3**) with the corresponding dihaloarenes **4a-g** (Scheme 1). Reaction of the resulting dianilines with 4-methoxyphenyl isocyanate afforded the bisureas **1a-g**. In most cases, the bisurea could be purified by trituration with EtOH to provide analytically pure samples. Receptors **1a-g** were characterized by ^{1}H and ^{13}C NMR spectroscopy and high-resolution mass spectrometry (complete spectra in Appendix B).
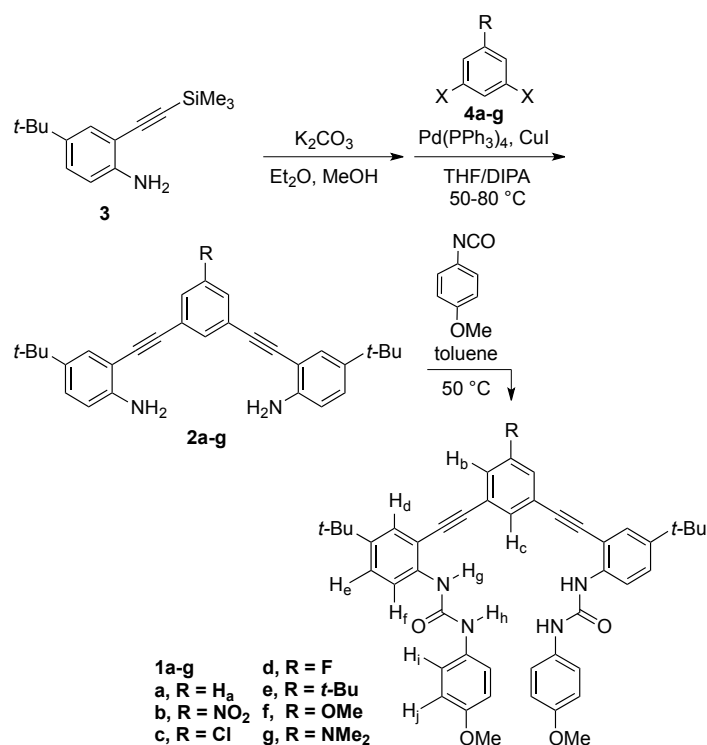
Scheme 1. Synthesis of Bisarylethynyl Urea Receptors 1a-g.

The pendent ureas on our receptors are necessary to boost the overall binding energy high enough to observe in solution by ^{1}H NMR and UV-vis spectroscopy.[40] Previous efforts to study substituent effects in noncovalent interactions have been complicated by substituents altering peripheral hydrogen bonds.[16,41] Gratifyingly, the ^{1}H NMR spectra of these receptors in DMSO show a small shift in the urea protons (H_h and H_g, Figure 3), suggesting substitution is far enough away to minimize, but not completely mitigate, the substituent effects on the ureas while still modulating the core CH HB donor acidity.[i] The closest aromatic proton to the central ring, H_d, shifts less than 0.01 ppm between the $-NO_2$ (**1b**) and $-NMe_2$ (**1g**) substituted receptors. The central ring protons, however, show a strong substitution dependence with H_b ranging from 6.8 (**1f**) to 8.0 ppm (**1b**). The isolation of substituent effects on the $\Delta\delta$ to just the central ring is necessary to measure only the effects

on the CH$\cdots$X$^-$ interactions without complicating secondary effects. ^{1}H NMR chemical shifts are subject to conformational changes and are insufficient evidence alone, however, calculations of Mulliken charge and ESP also support a small influence on the urea HB donors.
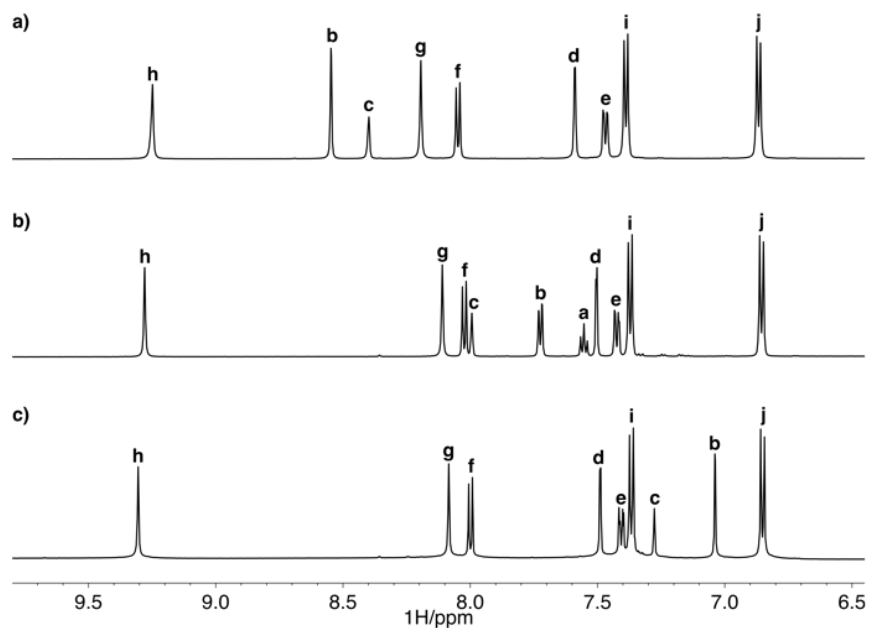
Figure 3. Stacked NMR spectra of (a) **1b**, (b) **1a** and (c) **1g** in DMSO-d_6. Proton assignments refer to Scheme 1.

The solid-state structure determined by single crystal X-ray diffraction is consistent with our structural characterization and solution behavior as studied previously by NMR, including 2D ^{1}H-^{13}C HSQC.[30] A single crystal of **1a•Cl$^-$** was obtained by slow evaporation of CHCl$_3$ containing a 2-fold excess of TBACl. The previously reported structure of **1a•Cl$^-$** has a short, linear C(H)$\cdots$Cl contact of 3.579(3) Å and 169° ($\angle$C–H$\cdots$Cl). The asymmetric unit is a 1:1 receptor:anion complex with a co-crystallized tetrabutylammonium (TBA) cation and solvent molecule (Figure 2b). The presence of a 1:1 complex is encouraging for binding in solution and is consistent with other examples of this scaffold.[35,37,39,42,43] The packing of this

54

structure is dominated by ion pairing between Cl⁻ and TBA⁺ with dispersion interactions playing a secondary role. The lack of inter-host hydrogen bonds or π–π stacking interactions also suggested a decreased likelihood of aggregation in solution.

The structure of bisurea **1b** was determined from a single crystal grown by vapor diffusion of n-hexane into CH₃CN. Host **1b**, in the absence of a guest anion, forms long columnar stacks with urea hydrogen bonds and π–π interactions stitching the layers together (Figure 4a). Columns are held together by dispersion forces between alkyl groups (*t*-Bu and Me) and arrange into a herringbone pattern (Figure 4b). The propensity for **1b** to form hydrogen-bonded aggregates is embodied by poor solubility and aggregation at high concentrations in solution limiting the maximum concentration during ¹H NMR titration experiments.
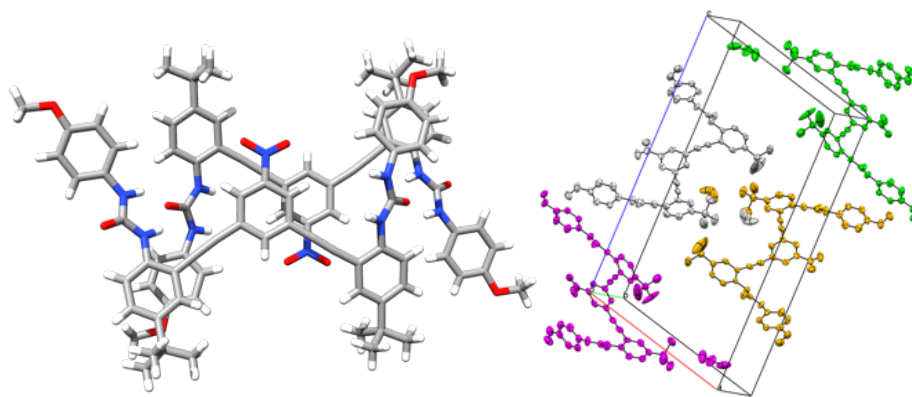
Figure 4. (a) X-ray crystal structure (left) of **1b** showing hydrogen bonded stacks. (b) Packing of **1b**.

NMR Titrations

¹H NMR titrations were performed to study the substituent effects in solution on the anion binding conformation and CH chemical shift. The magnitude and direction of the change in chemical shift are additional parameters set out in the HB definition for the

presence and strength of a HB (instead of an alternative attractive force, such as dispersion).[29] Consistent with previous studies on anion-π interactions,[17] water-saturated CHCl$_3$ was used as the solvent and anions were added as their TBA salts. Titrations were performed keeping the host concentrations constant (starting at 0.5–1.5 mM) during an experiment and titrating in a solution of concentrated anion in a solution of the host. Urea proton chemical shift changes between hosts are similar to the small changes observed in DMSO (see Appendix B).

A representative titration is shown in Figure 5. This example of unsubstituted receptor **1a** follows the trends for all of the receptors. The alkyl protons (*t*-Bu and OMe) remain unchanged throughout the course of anion addition (see Appendix B for complete titration data). The urea proton (H$_h$) and the CH proton (H$_c$) are unresolved during most of the titration, which may be due to the large shifts ($\Delta\delta = 4.0$ and 2.5 ppm) between the free host and the saturated host:Cl$^-$ complex. Although the broadening prevents fitting these peaks for an association constant (K_a), the large, downfield shifts indicate strong hydrogen bonds with H$_h$ and H$_c$. Fortunately, the other aromatic and urea protons remain well resolved throughout the titration, except for brief periods of overlap for some peaks. Urea H$_g$ shifts downfield with anion binding, while the aromatic protons remain stationary or move up field slightly. The decreased broadening and smaller $\Delta\delta$ for H$_g$, observed for the halides with all hosts, is evidence for an overall weaker hydrogen bond to this urea proton.

The chemical shift change of urea NH$_g$ was fit using non-linear regression analysis in MatLab to a 1:1 host:guest model.[44] This model was selected based on the crystallographic evidence for 1:1 binding and quality of fit compared to higher order models. The trend for association constants follows the general electron withdrawing ability of the substituents and the expected Hoffmeister bias (Cl$^-$ > NO$_3^-$ > Br$^-$ >> I$^-$).[45,47] The large association constants

measured for Cl⁻ (>10^5 M⁻¹ in some cases) indicates NMR spectroscopy is not the ideal

technique for determining high quality association constants. Strong EWG hosts (**1b**) with

Cl⁻ are at the upper limit for measuring K_as by NMR titrations and the fit is based on a single

proton shift. We can make a qualitative analysis of the bound geometry and trends, but the

further quantitative analysis is based on UV-vis titrations.
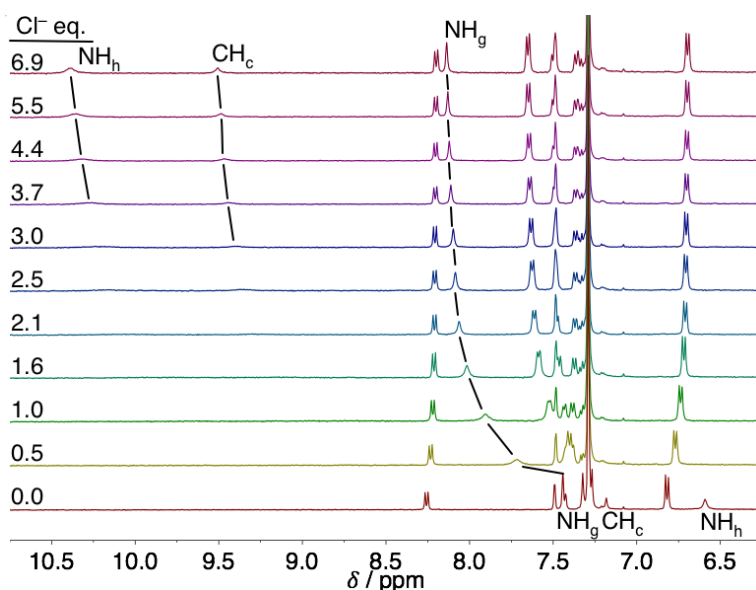
Figure 5. Representative stacked plot for a Cl⁻ titration with host **1a** in water saturated
CHCl₃ using a TBA salt.

The ¹H NMR spectra of the bound receptors are remarkably similar considering the

variety of substituents used (Figure 6). As with the free receptors, the largest variation of Δδ

is seen for two equivalent phenyl H$_b$ resonances. The final δ for the urea protons, H$_g$ and H$_h$,

changes less than 0.1 ppm for all of the receptors. The only peak that shows a large change is

the aromatic core CH$_c$, where there is a difference of 1.2 ppm between **1b•Cl⁻** and **1g•Cl⁻**.

Subtracting the difference before anion binding (Figure 3) leaves Δδ = 0.2 ppm due to a

change in the HB strength. Also of note, the final position follows the trend of EWG

strength. A similar trend is observed for Br⁻ and I⁻ binding, albeit with smaller Δδ for H_h and H_c. The chemical shift of the internal urea proton H_g changes minimally when bound to Br⁻, I⁻, or Cl⁻, consistent with it being mostly peripheral to halide binding.
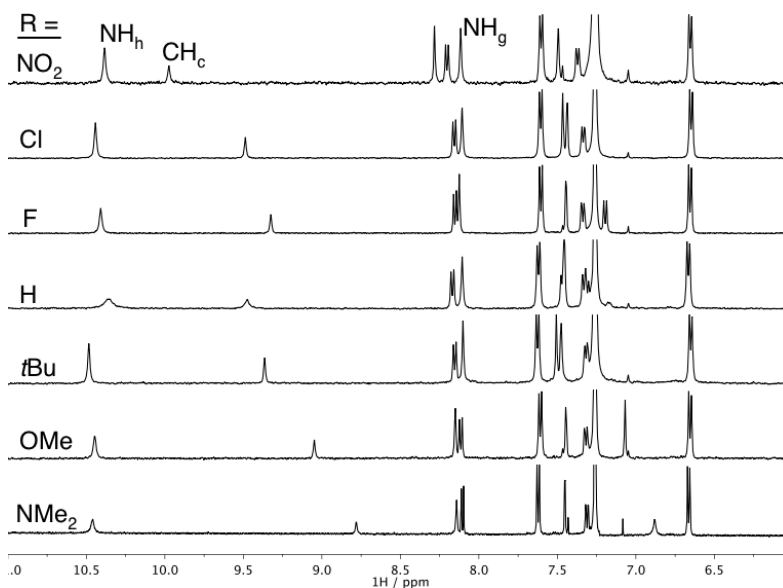
Figure 6. ¹H NMR spectra of receptors **1a-g** near the saturation point with Cl⁻. The peak showing the largest shift between 8.5-10.0 ppm is aryl proton H_c. Peak assignment refers to Scheme 1.

In addition to the halides, titrations were also performed with nitrate to consider shape as a variable in the binding studies (Figure 7, top). While the halides are spherical and have very small preference for hydrogen bond arrangements, nitrate is trigonal planar and prefers a bifurcated, O···(C)H···O structure (Figure 7, bottom).[21] In this case, the hydrogen bonding protons NH_h and CH_c shifted less than observed with the halides and urea NH_g ends up slightly farther downfield. Considering the likely geometries for nitrate binding, the relative chemical shifts point to a geometry where two oxygens are bound by NH_g and bifurcated by CH_c; the third oxygen only weakly interacts with NH_h. Modelling of the nitrate complex in Figure 7 supports this hypothesis with two local minima, from divergent starting

structures, found with nitrate parallel to the CH bond. With confirmation that the anions were bound in a similar manner by all of the receptors in solution, we sought to obtain quantitative association constants by performing UV-vis titrations.
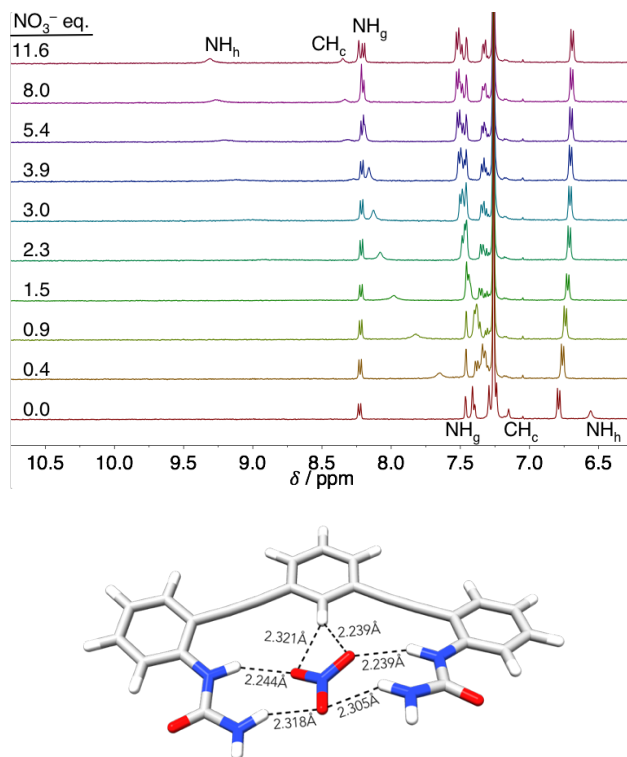
Figure 7. (top) Stacked plots showing the NO_3^- titration of **1a**. (bottom) A local minimum of truncated **5a·NO$_3^-$** with distances showing the preference of NO_3^- for maximized urea contacts and a bifurcated CH hydrogen bond. B3LYP/6-31g(d).

UV-vis Titrations and Association Constants

The rigid, conjugated arylethynyl backbone used in these receptors has the added benefit of providing a convenient absorbance for performing UV-vis titrations.[39] Although they do not provide as much structural information as NMR, UV-vis titrations are more accurate in determining K_as for our system because the required receptor concentrations are lowered (limiting aggregation), and problems with disappearing or overlapping peaks present in [1]H

NMR studies cease. The conditions for UV-vis titrations were chosen to most closely match the ^{1}H NMR binding experiments: water-saturated CHCl$_3$ was used as solvent and anions as their TBA salts were monitored at 298 K. Association constants were determined using the HYPERquad 2006 package to fit the complete spectral window with non-linear regression.[45] Consistent with the ^{1}H NMR experiments, all titrations were fit to a 1:1 binding isotherm. Job's plot analysis also confirms the best fit model for selected host and anion combinations (see Appendix B).

Table 1 contains the compiled association constants for receptors **1a-g** with Cl$^-$, Br$^-$, I$^-$, and NO$_3^-$. The selectivity of these receptors follows this preference, with the trend of Cl$^-$ > NO$_3^-$ > Br$^-$ >> I$^-$ holding for all hosts. The chloride association constants are typically 3-fold higher than the bromide K_a. Interestingly, nitrate is not able to outcompete Cl$^-$ despite nitrate's ability to maximize NH hydrogen bonds. The extremely low association for iodide prevented the accurate determination of binding constant by UV-vis spectrophotometry and necessitated the use of ^{1}H NMR binding data for further analysis.

The range of association constants for Cl$^-$ alone spans an order of magnitude, with just altering a single arene substituent. Consistent with the changes in chemical shift, the association constants for a given anion can be ranked according to the relative electron withdrawing ability of the substituent. Surprisingly, fluorine is an outlier for the trend in electronegativity of the substituent. Fluorine typically acts as an electron withdrawing group for electrostatic interactions, except when resonance is a contributor. Fluorine acts as both a strong electron withdrawing group due to induction and an electron donating group by resonance with one of its lone pairs. Other groups in this table (OMe, NMe$_2$, Cl) share this dual function and are important for differentiating between induction and resonance effects. The association constants have also been converted to ΔG (kcal mol^{-1}) for comparison to

Table 1. Complete Association Constants and Binding Energy for Receptors **1a-g** at 298K

Host (R)	Cl^{-a}		Br^{-a}		I^{-b}		NO_3^{-a}	
	K_a (M^{-1})	ΔG (kcal mol^{-1})	K_a (M^{-1})	ΔG (kcal mol^{-1})	K_a (M^{-1})	ΔG (kcal mol^{-1})	K_a (M^{-1})	ΔG (kcal mol^{-1})
1a (H)	6750±600[c]	–5.22±0.05	1630±120[c]	–4.38±0.04	150±10[c]	–2.97±0.03	3310±170	–4.80±0.03
1b (NO$_2$)	24600±3500	–5.99±0.09	5830±510	–5.13±0.05	580±30	–3.76±0.03	10600±800	–5.49±0.04
1c (Cl)	7900±1300	–5.32±0.09	2680±230	–4.67±0.05	290±10	–3.36±0.03	5520±640	–5.10±0.07
1d (F)	6760±620	–5.22±0.05	2340±180	–4.59±0.05	240±10	–3.25±0.03	4810±320	–5.02±0.04
1e (*t*Bu)	4560±720	–4.99±0.09	1370±100	–4.28±0.03	150±10	–2.98±0.04	2700±420	–4.68±0.09
1f (OMe)	4730±240	–5.01±0.03	1000±70	–4.09±0.04	170±10	–3.02±0.03	3060±360	–4.75±0.07
1g (NMe$_2$)	2660±320	–4.67±0.07	800±40	–3.96±0.03	100±10	–2.74±0.07	1720±160	–4.41±0.05

[a]Determined using UV-vis titrations in H$_2$O sat. CHCl$_3$; error is the std. dev. of at least three titrations. [b]Determined using ^{1}H NMR titrations in H$_2$O sat. CDCl$_3$; error is the std. dev. of at least two titrations. The minimum error is assumed to be 5% in cases where the std. dev. is < 5%. [c]Previously reported (ref. 30).

other supramolecular receptors. The total binding energy can be tuned by substituent effects by 1.02-1.32 kcal mol^{-1} depending on the anion being titrated, i.e., Cl$^-$ is bound more strongly than I$^-$ by 1.92-2.23 kcal mol^{-1} throughout this class of receptors.

Computations

Prior computations on model structures of chloride and nitrate with benzene showed C–H hydrogen bond strength (ΔH) follows linearly with the Hammett σ parameters and ESP.[26,27] We have expanded upon these prior computations by calculating the electrostatic potential surfaces for the model systems **5** and **6** (Figure 8) to measure electrostatic contributions in the bisurea receptors. The primary metric from these calculations is the ESP of **6a-g** (Table 2) at the point where the C–H axis intercepts the 0.002Å isoelectronic surface. The ESP at this point trends with the electron withdrawing ability of the substituents. Hammett plots of the ESP (**6a-g**, Table 2, and Figure 52 in Appendix B) and σ parameters favor σ$_p$ over σ$_m$ with R^2 = 0.97 and 0.88, respectively. This is a first indication that interactions with the CH are dependent on both field/inductive and resonance contributions of the substituents.
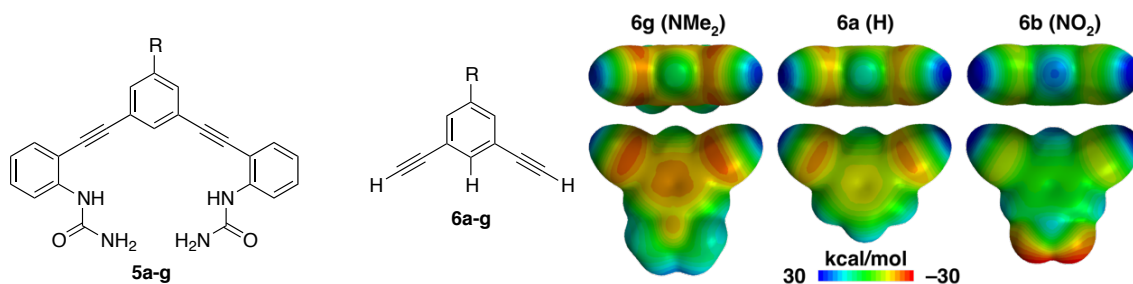
Figure 8. (left) Structures of the truncated model compounds **5** and **6** used for computational studies. (right) MESP maps showing effects of substituent on ESP at a 0.002Å isoelectric surface, calculated using B3LYP/6-31+g(d) in Spartan '10.

Table 2. Computational and Empirical Values for LFER Analysis

Host (R)	ESP[a]	σ_m[28]	σ_p[28]	F[32]	R[32]
1b (NO$_2$)	28.9	0.71	0.78	1.00	1.00
1c (Cl)	22.1	0.37	0.23	0.72	–0.24
1d (F)	21.4	0.34	0.06	0.74	–0.39
1a (H)	17.9	0.00	0.00	0.00	0.00
1e (*t*Bu)	16.3	–0.10	–0.20	–0.11	–0.29
1f (OMe)	16.3	0.12	–0.27	0.54	–1.68
1g (NMe$_2$)	12.0	–0.15	–0.83	0.69	–3.81

[a]ESP (kcal mol^{-1}) at the point where the CH bond intersects a 0.002Å isoelectric surface, calculated using B3LYP/6-31+g(d) in Spartan '10.

The bisurea model system **5a-g** is also useful to measure whether substitution at the central arene affects the urea group. A change in the Mulliken charge on the hydrogen bond donating carbon and nitrogens is representative of the effects at each of these positions. The Hammett plot of Mulliken charge at the HB donating carbon in **5** is linear with σ_p, $R^2 = 0.90$ and $\rho = -0.10 \pm 0.02$. Mulliken charges on the urea nitrogens produce Hammett plots, for σ_p and σ_m, with very poor fits, $R^2 \leq 0.70$, $\rho \sim 0.007 \pm 0.002$ (Table 43 in Appendix B). Substitution on the central arene has very weak through-bond effect on the ureas in this system. The through-space effect is better estimated by the ESP near the urea hydrogens. In this case, Hammett plots reveal the change at the urea is < 50% of the change at the CH donor. This model, however, does not account for the electron donating pendant phenyls in the full receptor, **1a-g**, which would further diminish the influence of the ureas.

Linear Free Energy Relationships

Linear free energy plots of the ESP and association constants are one way of comparing computational and experimental results, bridging the gap between gas phase and solution.[48] Non-normalized plots in kcal mol^{-1} are linear with R^2 greater than 0.95 for all four

anions (Figure 9). A break in the trend of the fitted slopes appears between the harder

anions (Cl⁻ and Br⁻) and soft anions (I⁻ and NO_3^-). The hardness of anions has been used to

explain the selectivity of Cl⁻ transport in micelles, although alternative explanations have not

been conclusively ruled out.[49]
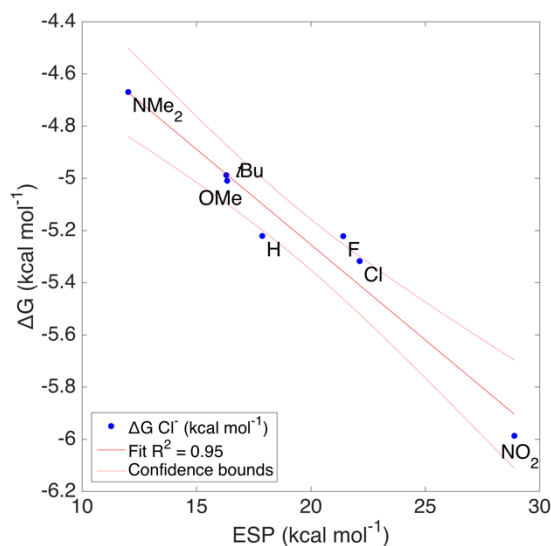
Figure 9. Linear free energy relationship of the solution Gibbs free energy (ΔG) of binding for Cl⁻ with the ESP at the CH bond. Intercept predicts a hypothetical system where electrostatic potential is zero.

Another interesting implication falls out of the intercept in these plots. When the

ESP is reduced to zero at the intercept, the remaining binding energy is due to the non-CH

interactions. This is based on an assumption that the electrostatics model completely or

mostly describes the CH···X interaction. As would be expected the intercept follows the

same trend in energies (kcal mol⁻¹), Cl⁻ = –3.79, NO_3^- = –3.67, Br⁻ = –3.06, I⁻ = –1.98. The

remaining "CH hydrogen bond energies" after subtracting the intercept from the solution

ΔG for **1b** are –2.20, –1.82, –2.07, and –1.78 kcal mol⁻¹ for each anion, respectively. Previous

studies with this system compared **1a** to a pyridine receptor and estimated the CH HB

energy at –1.33 kcal mol^{-1} to Cl$^-$.[30] In this case, the estimated energy for **1a** with Cl$^-$ is quite close at –1.43 kcal mol^{-1}. Nitrate is a clear outlier in this series based on its preference for a bifurcated HB. The CH HB is less important for nitrate; however, using this model 47% of the total binding energy for iodide originates from the CH HB solely.

Since the substitution is only on the central arene and appears to only affect the C–H$_c$ proton, we hypothesized that trends in our association constants should, also, be well-described by the σ parameter for substituents. The Hammett plots for Cl$^-$, Br$^-$, I$^-$, and NO$_3^-$ were prepared for both σ$_m$ and σ$_p$ constants. Figure 10 compares the fit for σ$_p$ with K_a (Cl$^-$) and K_a (I$^-$). Association constants and substituent parameters were fit using the Hammett equation (eq. 1 and eq. 2) in MatLab. The intercept acts as another measure for the quality of fit. In this case, the large intercept for I$^-$, a poor fit for σ$_p$, places **1a** outside of the confidence bounds (Figure 10 right). Table 3 contains the complete results for fitting all four anions to σ$_p$ and σ$_m$.[ii]
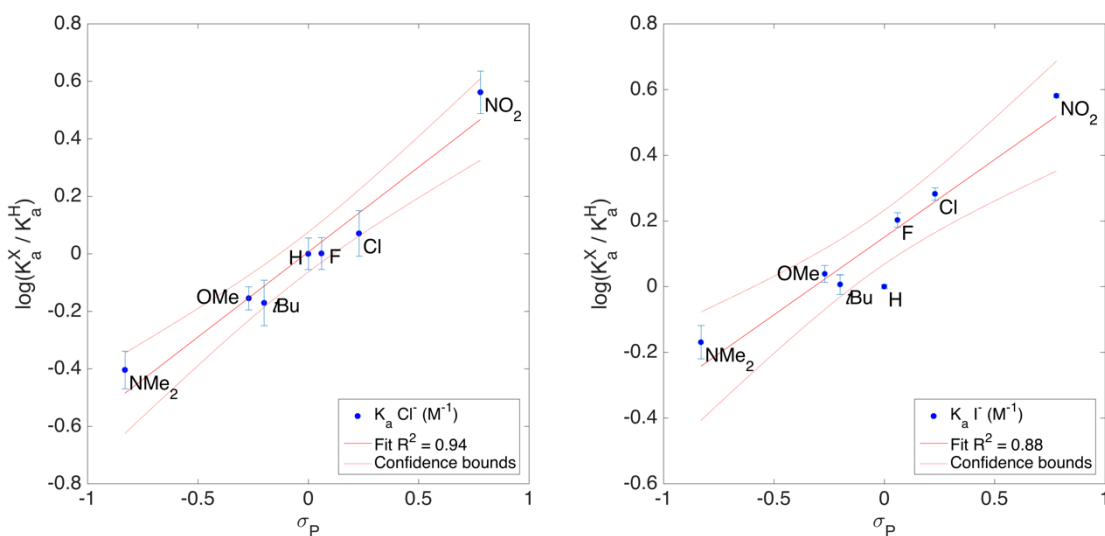
Figure 10. Hammett plots of K_a (Cl$^-$) (left) and K_a (I$^-$) (right) with σ$_p$ (Table 2). Goodness of fit (R^2) indicates Cl$^-$ is well described by σ$_p$, while I$^-$ is weaker.

$$\log(K_R/K_H) = \rho\sigma_p + i \tag{1}$$

$$(K_a \text{ Cl}^-) \log(K_R/K_H) = 0.59(\pm0.06)\sigma_p + 0.01(\pm0.03), N = 7, R^2 = 0.95, R_{adj}^2 = 0.94,$$

$$\text{RMSE} = 0.07, F = 100 \tag{2}$$

The ρ values for all combinations of σ and anion are < 1, an average of 0.54 for σ_p and 0.85 for σ_m. Reactions with ρ values > 1 are considered more sensitive than benzoic acid and ρ values < 1 are less sensitive to ionization by substituent effects. If $CH\cdots X^-$ is a hydrogen bond and incorporates some covalent character, then it follows that there is a small proton transfer event contributing to the binding energy.[29] The method of fitting anion association to a Hammett σ_p is also applicable to other CH HB anion receptors. For instance, it is interesting to note, at least preliminarily, that a Hammett plot of Cl$^-$ association to a CH HB-donating rotaxane host has a ρ of 0.53.[50] The similarity of this relationship to a very different host in a different solvent is encouraging, and suggests this understanding is extendable to other such systems.

The question remains, has the influence of the urea HB donors been sufficiently accounted for? The ρ for Hammett plots of Mulliken charge and ESP at the ureas is consistently < 0.06. The change in association constant due to the ureas is estimated to be < 10% based on this and is insufficient to explain the effects on the binding event.

The small ρ value is consistent with the CH bond being much less acidic than benzoic acid. Also consistent with a traditional hydrogen bond definition, the σ_p parameter has a better fit for Cl$^-$ than σ_m (R^2 (σ_p) = 0.95 vs. (σ_m) = 0.83). σ_p is often thought to represent a greater resonance contribution; however, two points conflict with this observation: (1) DFT calculations favored σ_m for Cl$^-$,[27] and (2) the results for I$^-$ do not match Cl$^-$, where Hammett plots for I$^-$ are a better fit using σ_m. Further confounding the issue, NO$_3^-$ is well described by both σ_p and σ_m.

Table 3. Coefficients and Fitting Statistics for Hammett Plots for Each Anion Studied

K_a (X⁻)	ρ	I^a	N^b	$R^{2\,c}$	F^d
Cl⁻ (σ_p)	0.59(±0.06)	0.01(±0.03)	7	0.95	100
Br⁻ (σ_p)	0.57(±0.07)	0.07(±0.03)	7	0.93	68
I⁻ (σ_p)	0.47(±0.07)	0.15(±0.03)	7	0.90	46
NO₃⁻ (σ_p)	0.50(±0.05)	0.09(±0.02)	7	0.95	98
Cl⁻ (σ_m)	0.89(±0.18)	−0.18(±0.06)	7	0.83	25
Br⁻ (σ_m)	0.87(±0.16)	−0.11(±0.06)	7	0.85	28
I⁻ (σ_m)	0.78(±0.08)	−0.01(±0.03)	7	0.95	102
NO₃⁻ (σ_m)	0.80(±0.09)	−0.08(±0.03)	7	0.94	83

[a]Intercept obtained from the linear fit. [b]Number of points used for fitting. [c]Coefficient of determination for quality of fit determination. [d]F-value for comparison of models.

The unusual results for NO_3^- can be described by the geometry and altered binding mode in this case. The oxoanion is trigonal planar and can maximize contacts to the NH donors, as discussed above; however, the CH donor is still important to the overall binding energy. The CH proton still shifts downfield by nearly the same magnitude as the NH protons. The observed ρ values are the result of both inductive and resonant contributions. The degree of resonance contribution is a key difference between the σ_m and σ_p parameters. A more accurate method for determining resonance contribution is to perform multivariable fitting with field (*F*) and resonance (*R*) parameters, such as those derived by Swain and Lupton.[31,32] While many methods for determining field and resonance contribution have been proposed, the *F* and *R* parameters (Table 4) developed by Swain-Lupton most closely match Hammett's σ parameters in their derivation (eq. 3). MatLab is capable of handling large, multivariable linear regressions and can easily handle fitting values for *F* and *R* from the data presented above. The method was applied to the experimental K_a values and the

results for Cl^- are plotted in Figure 11. A figure of merit for simultaneous F and R fitting is the percent resonance contribution, %R (eq. 4).

$$\log(K_X/K_H) = \rho_f F + \rho_r R + i \qquad (3)$$

$$\%R = \rho_r \, / \, (\rho_f + \rho_r) * 100 \qquad (4)$$

This reports the resonance contribution observed in the reaction and is the percent of R from the combined ρ_f and ρ_r coefficients. Of note, the resonance contribution for Cl^- and Br^- is higher, but the values drop off for I^- and NO_3^-. The error values in %R exceed 10% in most cases, which is due to the small sample size to variable ratios. As a result of the increasing number of variables, the difference in the %R contribution among the various anions studied is well below the 95% confidence interval by t test. A similar trend, however, in anion effects was observed by Scheiner et al. using computation to study anion binding to trifluoromethane.[21] By their computations, the overall binding energy and charge transfer from the anion were correlated, consistent with the effect of resonance contribution we have observed. As in the extreme hydrogen bond example, increased charge on the carbon can be dissipated by resonance and contribute additional hydrogen bond energy beyond inductive effects alone.

Table 4. Field and Resonance Fitting Parameters

	ρ_f	ρ_r	R^2	%R^a
Cl^-	0.36(±0.09)	0.17(±0.02)	0.937	32 ± 7
Br^-	0.37(±0.03)	0.15(±0.01)	0.995	30 ± 6
I^-	0.40(±0.05)	0.14(±0.01)	0.977	25 ± 3
NO_3^-	0.37(±0.02)	0.14(±0.01)	0.996	28 ± 1

^{a}Calculated from eq. (4) for percent resonance.
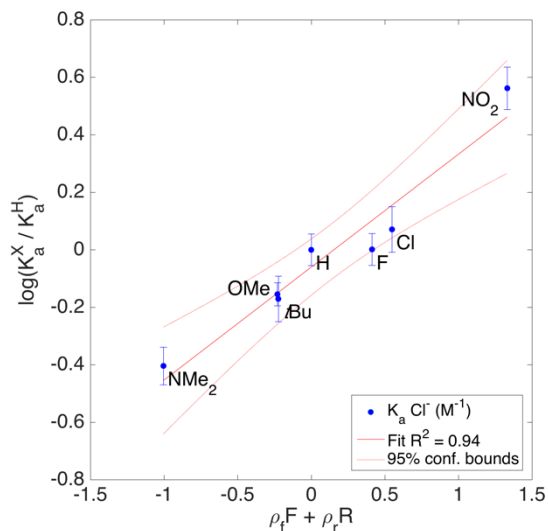
Figure 11. LFER plot of K_a (Cl$^-$) and $\rho_f F + \rho_r R$ to determine resonance contribution from Swain-Lupton field and resonance parameters.

Conclusions

The resonance contribution of a substituent clearly plays a role in dictating hydrogen

bond strength, even for CH donors. We have observed a weak dependence of σ_p and σ_m

contribution on the anion being bound. Hammett parameters remain a powerful tool for

predicting changes in CH hydrogen bond strength. It is important to also consider the

hydrogen bond acceptor, not only its charge but also size, shape, and polarizability. The

change in resonance contributions as a result of substituent effects as calculated by Swain-

Lupton parameters is too small to differentiate between the anions studied, suggesting that

emerging hypotheses offering hard-soft acid-base theory as a model for understanding anion

binding specificity are overly simplistic. Anion effects on resonance contribution are also

supported by calculations of the charge transfer energy and bond stretching in model

$CH \cdots X^-$ systems.

Computationally determined binding energies are a valuable tool for understanding solution binding events, especially in the case of weak interactions. Remarkably, venerable empirical substituent constants such as σ, F and R can also effectively describe substituent effects in CH hydrogen bonds, which are increasingly appreciated as rivals to more well-studied highly polar hydrogen bond donors (e.g., N–H, O–H). We have found through experimental results that the strength of a single CH HB is tuneable across a range of 1.02–1.23 kcal mol^{-1} by modifying substituents on the receptor and that these interactions vary up to 0.42 kcal mol^{-1} by changing the anion accepting the CH HBs. Although these values are small, they represent a 10-fold and 3-fold change in anion binding, respectively, and hint at the nature of anion binding selectivity in such receptors. Considering multivalent effects in the largest HB donating receptors that bring to bear many such interactions in targeting a single anion, the combined effect can be used to dramatically alter the binding event in selectivity and strength. While hard-soft acid-base theory remains a useful tool in understanding coordination chemistry, the present studies add to the evidence that this theory is too simplistic to describe accurately the nature of selectivity in anion binding using hydrogen bonding receptors; ESPs and other empirical substituent constants appear to provide a more robust understanding.

Aryl CH hydrogen bonds have seen increasing study in numerous fields, including anion transport, organocatalysis, molecular/ion recognition, and biological ligand/receptor binding. New methods for understanding and controlling the strength and selectivity of these interactions are vital for continued progress in these fields. For instance, ligand and/or drug binding to proteins can be improved by studying and optimizing important CH hydrogen bonding interactions, and enhancing such interactions in organocatalysis and receptor design may enable improved stereo- and regioselectivity. Although the CH donor

cannot be easily categorized as hard or soft, we have made the more important discovery that the possibility exists to influence the preference of this interaction for different anions. A concerted effort to maximize both the resonance withdrawing ability of substituents and the number of CH hydrogen bond donors should lead to an increased affinity for hard anions. Conversely, the same should be possible by maximizing the inductive substituents to bind soft anions. The results from this study provide important insights to aid chemists and biologists in accomplishing such CH HB optimization.

Experimental

General Comments

^{1}H and ^{13}C NMR spectra were obtained on a Varian 300 MHz (^{1}H 299.95 MHz, ^{13}C 75.43 MHz), Inova 500 MHz (^{1}H 500.10 MHz, ^{13}C 125.75 MHz) or Bruker Avance-III-HD 600 MHz (^{1}H 599.98 MHz, ^{13}C 150.87 MHz) spectrometer with a Prodigy multinuclear broadband BBO CryoProbe. Chemical shifts (δ) are expressed in ppm relative to tetramethylsilane (TMS) using residual non-deuterated solvent (CDCl$_3$: ^{1}H 7.26 ppm, ^{13}C 77.0 ppm; CD$_2$Cl$_2$: ^{1}H 5.32 ppm, ^{13}C 54.0 ppm; DMSO–d_6: ^{1}H 2.50 ppm, ^{13}C 39.51 ppm). UV-vis spectra were recorded on an HP 8453 UV-vis spectrophotometer using a 265 nm high-pass filter. Dry solvents were obtained from distillation using published literature procedures directly before use. 2-(Trimethylsilyl)ethynyl-4-t-butylaniline (**3**),[18,51] 1,3-dibromo-5-nitrobenzene (**4b**),[52] 1-t-butyl-3,5-diiodobenzene (**4e**),[53,54] and *N,N*-dimethyl-3,5-diiodoaniline (**4g**)[55,56] were synthesized as previously reported. All other reagents were purchased and used as received.

Synthesis

Dianiline 2a (R=H). A suspension of ethynylaniline **3** (2.262 g, 9.22 mmol) and

K$_2$CO$_3$ (6.37 g, 46.1 mmol) in Et$_2$O (15 mL) and MeOH (30 mL) was stirred at 25 °C and

monitored by TLC until completion (30 min). The solution was diluted with CH$_2$Cl$_2$ and

washed three times with water and brine. The organic layer was dried (MgSO$_4$) and

concentrated *in vacuo*. The residue was dissolved in minimal THF and added to an N$_2$-purged

solution of 1,3-diiodobenzene (**4a**, 1.39 g, 4.20 mmol), Pd(PPh$_3$)$_4$ (0.49 g, 0.42 mmol) and

CuI (0.16 g, 0.84 mmol) in dry THF (45 mL) and *i*-Pr$_2$NH (45 mL). After stirring at 50 °C

for 8 h, the cooled reaction was concentrated *in vacuo* and the residue was taken up into

CH$_2$Cl$_2$. The solution was filtered through a 3 cm silica gel plug and washed with additional

CH$_2$Cl$_2$. The combined organics were concentrated *in vacuo* and the product was purified by

column chromatography (2:1 hexanes/CH$_2$Cl$_2$) to afford **2a** (1.01 g, 57%) as a pale brown

solid. ^{1}H NMR (600 MHz, CD$_2$Cl$_2$): δ 7.71 (t, J = 1.7 Hz, 1H), 7.50 (dd, J = 7.7, 1.7 Hz, 2H),

7.34-7.40 (m, 3H), 7.21 (dd, J = 8.5, 2.4 Hz, 2H), 6.69 (d, J = 8.5 Hz, 2H), 4.22 (br s, 4H),

1.28 (s, 18H). ^{13}C NMR (151 MHz, CD$_2$Cl$_2$) δ 146.37, 141.29, 134.56, 131.37, 129.26, 129.22,

128.00, 124.40, 114.73, 107.30, 93.69, 87.78, 34.35, 31.68. HRMS (ESI) for C$_{30}$H$_{33}$N$_2$

[M+H]$^+$: calcd 421.2625, found 421.2644.

Dianiline 2b (R=NO$_2$). A suspension of ethynylaniline **3** (2.07 g, 8.43 mmol) and

K$_2$CO$_3$ (5.3 g, 38.3 mmol) in Et$_2$O (15 mL) and MeOH (30 mL) was stirred at 25 °C and

monitored by TLC until completion (30 min). The solution was diluted with CH$_2$Cl$_2$ and

washed three times with water and brine. The organic layer was dried (MgSO$_4$) and

concentrated *in vacuo*. The residue was dissolved in minimal THF and added to an N$_2$-purged

solution of 1-nitro-1,3-dibromo-5-nitrobenzene[52] (**4b**, 1.067 g, 3.8 mmol), Pd(PPh$_3$)$_4$ (0.22 g,

0.19 mmol) and CuI (0.156 g, 0.82 mmol) in dry THF (40 mL) and *i*-Pr$_2$NH (40 mL). After

stirring at 50 °C for 24 h, the cooled reaction was concentrated *in vacuo* and the residue was taken up into CH_2Cl_2. The solution was filtered through a 3 cm silica gel plug and washed with additional CH_2Cl_2. The combined organics were concentrated *in vacuo* and the product was purified by column chromatography (2:1 hexanes:CH_2Cl_2) to afford **2b** (1.7 g, 95%) as an orange solid. ^{1}H NMR (600 MHz, DMSO-d_6) δ 8.46 (d, J = 1.5 Hz, 2H), 8.32 (t, J = 1.4 Hz, 1H), 7.27 (d, J = 2.4 Hz, 2H), 7.19 (dd, J = 8.6, 2.4 Hz, 2H), 6.69 (d, J = 8.6 Hz, 2H), 5.61 (s, 4H), 1.23 (s, 18H). ^{13}C NMR (151 MHz, DMSO-d_6) δ 148.16 (overlapping peaks), 138.94, 137.86, 128.29, 128.07, 125.21, 124.46, 114.06, 103.56, 90.86, 90.84, 33.47, 31.23. HRMS (ESI) for $C_{30}H_{32}N_3O_2$ [M+H]$^+$: calcd 466.2495, found 466.2515.

Dianiline 2c (R=Cl). A suspension of ethynylaniline **5** (2.701 g, 10.98 mmol) and K_2CO_3 (7.554 g, 54.7 mmol) in Et_2O (20 mL) and MeOH (40 mL) was stirred at 25 °C and monitored by TLC until completion (30 min). The solution was diluted with CH_2Cl_2 and washed three times with water and brine. The organic layer was dried ($MgSO_4$) and concentrated *in vacuo*. The residue was dissolved in minimal THF and added to an N_2-purged solution of 1,3-dibromo-5-chlorobenzene (**4c**, 1.615 g, 5.97 mmol), Pd(PPh$_3$)$_4$ (0.245 g, 0.21 mmol) and CuI (0.025 g, 0.13 mmol) in dry THF (50 mL) and *i*-Pr$_2$NH (50 mL). After stirring at 50 °C for 8 h, the cooled reaction was concentrated *in vacuo* and the residue was taken up into CH_2Cl_2. The solution was filtered through a 3 cm silica gel plug and washed with additional CH_2Cl_2. The combined organics were concentrated *in vacuo* and the product was purified by column chromatography (2:1 hexanes/CH_2Cl_2) to afford **2c** (1.440 g, 53%) as a brown oil. ^{1}H NMR (500 MHz, CDCl$_3$) δ 7.58 (s, 1H), 7.46 (d, J = 1.5 Hz, 2H), 7.37 (d, J = 2.0 Hz, 2H), 7.22 (dd, J = 8.5, 2.1 Hz, 2H), 6.69 (d, J = 8.5 Hz, 2H), 4.16 (s, 4H), 1.29 (s, 18H). ^{13}C NMR (126 MHz, DMSO-d_6) δ 147.85, 137.89, 133.26, 132.04, 129.83, 128.08,

127.75, 125.36, 114.02, 103.96, 91.35, 89.78, 33.44, 31.22. HRMS (ESI) for $C_{30}H_{32}N_2Cl$ [M+H]$^+$: calcd 455.2254, found 455.2242.

Dianiline 2d (R=F). A suspension of ethynylaniline **3** (1.231 g, 5.018 mmol) and K_2CO_3 (3.468 g, 25.09 mmol) in Et_2O (15 mL) and MeOH (30 mL) was stirred at 25 °C and monitored by TLC until completion (30 min). The solution was diluted with CH_2Cl_2 and washed three times with water and brine. The organic layer was dried (MgSO$_4$) and concentrated *in vacuo*. The residue was dissolved in minimal THF and added to an N_2-purged solution of 1,3-dibromo-5-fluorobenzene (**4d**, 0.637 g, 2.509 mmol), Pd(PPh$_3$)$_4$ (0.100 g, 0.0865 mmol) and CuI (0.014 g, 0.735 mmol) in dry THF (20 mL) and *i*-Pr$_2$NH (20 mL). After stirring at 50 °C for 8 h the cooled reaction was concentrated *in vacuo* and the residue was taken up into CH_2Cl_2. The solution was filtered through a 3 cm silica gel plug and washed with additional CH_2Cl_2. The combined organics were concentrated *in vacuo* and the product was purified by column chromatography (2:1 hexanes/CH_2Cl_2) to afford **2d** (0.715 g, 65%) as a brown oil. ^{1}H NMR (500 MHz, CDCl$_3$) δ 7.49 (t, *J* = 1.4 Hz, 1H), 7.38 (d, *J* = 2.3 Hz, 2H), 7.22 (dd, *J* = 8.5, 2.3 Hz, 2H), 7.19 (dd, *J* = 9.1, 1.4 Hz, 2H), 6.70 (d, *J* = 8.5 Hz, 2H), 4.16 (s, 4H), 1.30 (s, 18H). ^{13}C NMR (151 MHz, CDCl$_3$) δ 163.05 (d, *J* = 244 Hz), 145.76, 141.13, 130.49, 130.47, 128.98, 127.85, 125.61 (d, *J* = 10.5 Hz), 118.05 (d, *J* = 22.9 Hz), 114.57, 106.79, 92.44 (d, *J* = 3.5 Hz), 88.33, 34.09, 31.53. HRMS (ESI) for $C_{30}H_{32}N_2F$ [M+H]$^+$: calcd 439.2550, found 439.2531.

Dianiline 2e (R=*t*-Bu). A suspension of ethynylaniline **3** (2.0 g, 8.15 mmol) and K_2CO_3 (5.63 g, 40.74 mmol) in Et_2O (20 mL) and MeOH (40 mL) was stirred at 25 °C and monitored by TLC until completion (30 min). The solution was diluted with CH_2Cl_2 and washed three times with water and brine. The organic layer was dried (MgSO$_4$) and concentrated *in vacuo*. The residue was dissolved in minimal THF and added to an N_2-purged

solution of 1-*t*-butyl-3,5-diiodobenzene[53] (1.19 g, 3.08 mmol), Pd(PPh$_3$)$_4$ (0.178 g, 0.15 mmol) and CuI (0.12 g, 0.62 mmol) in dry THF (10 mL) and *i*-Pr$_2$NH (10 mL). After stirring at 50 °C for 23 h, the cooled reaction was concentrated *in vacuo* and the residue was taken up into CH$_2$Cl$_2$. The solution was filtered through a 3 cm silica gel plug and washed with additional CH$_2$Cl$_2$. The combined organics were concentrated *in vacuo* and the product was purified by column chromatography (3:2 hexanes/EtOAc) to afford **2e** (0.903 g, 61%) as a pale brown solid. ^{1}H NMR (500 MHz, CD$_2$Cl$_2$) δ 7.63–7.52 (m, 3H), 7.39 (d, *J* = 2.3 Hz, 2H), 7.21 (dd, *J* = 8.5, 2.3 Hz, 2H), 6.70 (d, *J* = 8.5 Hz, 2H), 4.23 (s, 4H), 1.37 (s, 9H), 1.29 (s, 18H). ^{13}C NMR (126 MHz, CD$_2$Cl$_2$) δ 152.51, 146.34, 141.29, 131.77, 129.27, 128.90, 127.89, 123.96, 114.73, 107.47, 94.26, 87.10, 35.24, 34.36, 31.71, 31.45. HRMS (ESI) for C$_{34}$H$_{41}$N$_2$ [M+H]$^+$: calcd 477.3270, found 477.3263.

Dianiline 2f (R=OMe). A suspension of ethynylaniline **3** (0.808 g, 4.27 mmol) and K$_2$CO$_3$ (2.95 g, 21.33 mmol) in Et$_2$O (15 mL) and MeOH (30 mL) was stirred at 25 °C and monitored by TLC until completion (30 min). The solution was diluted with CH$_2$Cl$_2$ and washed three times with water and brine. The organic layer was dried over MgSO$_4$ and concentrated *in vacuo*. The residue was dissolved in minimal THF and added to an N$_2$-purged solution of 3,5-dibromoanisole (0.250 g, 0.940 mmol), Pd(PPh$_3$)$_4$ (0.100 g, 0.0865 mmol) and CuI (0.010 g, 0.0525 mmol) in dry THF (50 mL) and *i*-Pr$_2$NH (50 mL). After stirring at 50 °C for 8 h, the cooled reaction was concentrated *in vacuo* and the residue was taken up into CH$_2$Cl$_2$. The solution was filtered through a 3 cm silica gel plug and washed with additional CH$_2$Cl$_2$. The combined organics were concentrated *in vacuo* and the product was purified by column chromatography (CH$_2$Cl$_2$) to afford **2f** (0.182 g, 43%) as a brown oil. ^{1}H NMR (300 MHz, CDCl$_3$) δ 7.38 (d, *J* = 1.9 Hz, 2H), 7.33 (s, 1H), 7.20 (dd, *J* = 8.4, 2.1 Hz, 2H), 7.04 (s, 2H), 6.69 (d, *J* = 8.5 Hz, 2H), 4.17 (s, 4H), 3.85 (s, 3H), 1.29 (s, 18H). ^{13}C NMR (126 MHz,

CDCl$_3$) δ 159.45, 145.68, 141.07, 128.92, 127.50, 127.24, 124.82, 116.92, 114.50, 107.25, 93.50, 87.10, 55.66, 34.07, 31.54. HRMS (ESI) for C$_{31}$H$_{35}$N$_2$O [M+H]$^+$: calcd 451.2749, found 451.2729.

Dianiline 2g (R=NMe$_2$). A suspension of ethynylaniline **3** (0.312 g, 1.24 mmol) and K$_2$CO$_3$ (0.856 g, 6.195 mmol) in Et$_2$O (10 mL) and MeOH (20 mL) was stirred at 25 °C and monitored by TLC until completion (30 min). The solution was diluted with CH$_2$Cl$_2$ and washed three times with water and brine. The organic layer was dried (MgSO$_4$) and concentrated *in vacuo*. The residue was dissolved in minimal THF and added to an N$_2$-purged solution of *N,N*-dimethyl-3,5-diiodoaniline[55,56] (0.20 g, 0.59 mmol), Pd(PPh$_3$)$_4$ (0.014 g, 0.012 mmol) and CuI (0.005 g, 0.02 mmol) in dry THF (15 mL) and *i*-Pr$_2$NH (5 mL). After stirring at 50 °C for 8 h, the cooled reaction was concentrated *in vacuo* and the residue was taken up into CH$_2$Cl$_2$. The solution was filtered through a 3 cm silica gel plug and washed with additional CH$_2$Cl$_2$. The combined organics were concentrated *in vacuo* and the product was purified by column chromatography (3:1 hexanes/EtOAc followed by 100% EtOAc) to afford **2g** (0.111 g, 41%) as a pale brown solid. ^{1}H NMR (600 MHz, CD$_2$Cl$_2$) δ 7.37 (d, *J* = 2.4 Hz, 2H), 7.19 (dd, *J* = 8.5, 2.4 Hz, 2H), 7.05 (t, *J* = 1.3 Hz, 1H), 6.86 (d, *J* = 1.3 Hz, 2H), 6.69 (d, *J*=8.5, 2H), 4.22 (s, 4H), 3.00 (s, 4H), 1.28 (s, 18H). ^{13}C NMR (151 MHz, CD$_2$Cl$_2$) δ 150.94, 146.30, 141.24, 129.23, 127.76, 124.60, 122.69, 115.30, 114.67, 107.57, 94.74, 86.39, 40.78, 34.34, 31.69. HRMS (ESI) for C$_{32}$H$_{38}$N$_3$ [M+H]$^+$: calcd 464.3066, found 464.3055.

Bisurea 1a (R=H). All glassware was dried in a 150 °C oven for at least 1 h. Dianiline **2a** (200 mg, 0.5 mmol) and *p*-methoxyphenyl isocyanate (177 mg, 1.2 mmol) in toluene (50 mL) were stirred at 50 °C for 8 h. The reaction became cloudy upon completion and acetone was added until the turbidity was removed. Hexanes was added until a slight turbidity returned and the suspension was left to precipitate overnight in the refrigerator.

Filtration afforded **1a** (320 mg, 93%) as a fine white powder. ^{1}H NMR (600 MHz, DMSO-d_6)

δ 9.28 (s, 2H), 8.11 (s, 2H), 8.02 (d, J = 8.8 Hz, 2H), 7.99 (t, J = 1.7 Hz, 1H), 7.72 (dd, J =

7.6, 1.7 Hz, 2H), 7.55 (t, J = 7.8 Hz, 1H), 7.50 (d, J = 2.4 Hz, 2H), 7.42 (dd, J = 8.8, 2.4 Hz,

2H), 7.37 (d, J = 8.9 Hz, 4H), 6.86 (d, J = 8.9 Hz, 4H), 3.70 (s, 6H), 1.29 (s, 18H). ^{13}C NMR

(151 MHz, DMSO-d_6): δ 154.61, 152.40, 144.38, 138.04, 134.33, 132.43, 131.77, 129.16,

128.69, 126.96, 122.94, 120.22, 119.64, 114.03, 110.73, 93.69, 86.75, 55.13, 33.94, 31.02.

HRMS (ESI) for $C_{46}H_{47}N_4O_4$ [M+H]$^+$: calcd 719.3563, found 719.3597.

Bisurea 1b (R=NO$_2$). All glassware was dried in a 150 °C oven for at least 1 h.

Dianiline **1b** (0.100 g, 0.215 mmol) and *p*-methoxyphenyl isocyanate (0.08 mg, 0.536 mmol)

in toluene (50 mL) were stirred at 80 °C for 8 h. The reaction became cloudy upon

completion and filtration afforded **1b** (100 mg, 47%) as a fine yellow powder. ^{1}H NMR (600

MHz, DMSO-d_6) δ 9.25 (s, 2H), 8.55 (s, 2H), 8.40 (s, 1H), 8.19 (s, 2H), 8.05 (d, J = 8.8 Hz,

2H), 7.59 (d, J = 2.3 Hz, 2H), 7.47 (dd, J = 8.8, 2.4 Hz, 2H), 7.39 (d, J = 8.7 Hz, 4H), 6.87

(d, J = 8.7 Hz, 4H), 3.70 (s, 6H), 1.30 (s, 18H). ^{13}C NMR (151 MHz, DMSO-d_6) δ 154.65,

152.36, 148.18, 144.47, 139.77, 138.41, 132.35, 129.03, 127.63, 125.72, 124.55, 120.25,

119.71, 114.06, 110.03, 91.79, 89.11, 55.14, 33.99, 31.01. HRMS (ESI) for $C_{46}H_{46}N_5O_6$

[M+H]$^+$: calcd 764.3448, found 764.3412.

Bisurea 1c (R=Cl). All glassware was dried in a 150 °C oven for at least 1 h.

Dianiline **2c** (125 mg, 0.274 mmol) and *p*-methoxyphenyl isocyanate (94 mg, 0.632 mmol) in

toluene (50 mL) were stirred at 50 °C for 8 h. The reaction became cloudy upon completion

and filtration afforded **1c** (186 mg, 90%) as a fine white powder. ^{1}H NMR (500 MHz,

DMSO-d_6) δ 9.25 (s, 2H), 8.11 (s, 2H), 8.04 (d, J = 8.6 Hz, 2H), 7.95 (s, 1H), 7.84 (s, 2H),

7.53 (s, 2H), 7.44 (d, J = 8.8 Hz, 2H), 7.39 (d, J = 8.3 Hz, 4H), 6.86 (d, J = 8.3 Hz, 4H), 3.71

(s, 6H), 1.29 (s, 18H). ^{13}C NMR (126 MHz, DMSO-d_6) δ 154.64, 152.36, 144.41, 138.25,

133.52, 132.85, 132.38, 131.07, 128.83, 127.34, 124.77, 120.26, 119.67, 114.04, 110.29, 92.34, 88.16, 55.13, 33.95, 30.99. HRMS (ESI) for $C_{46}H_{46}N_4O_4Cl$ $[M+H]^+$: calcd 753.3208, found 753.3215.

Bisurea 1d (R=F). All glassware was dried in a 150 °C oven for at least 1 h. Dianiline **2d** (250 mg, 0.570 mmol) and *p*-methoxyphenyl isocyanate (177 mg, 1.2 mmol) in toluene (50 mL) were stirred at 50 °C for 8 h. The reaction became cloudy upon completion and filtration afforded **1d** (400 mg, 95%) as a fine white powder. ^{1}H NMR (500 MHz, DMSO-d_6) δ 9.25 (s, 2H), 8.11 (s, 2H), 8.03 (d, *J* = 9.0 Hz, 2H), 7.85 (s, 1H), 7.63 (d, *J* = 9.2 Hz, 2H), 7.52 (s, 2H), 7.44 (d, *J* = 7.2 Hz, 2H), 7.38 (d, *J* = 8.8 Hz, 4H), 6.86 (d, *J* = 8.8 Hz, 4H), 3.70 (s, 6H), 1.29 (s, 18H). ^{13}C NMR (126 MHz, DMSO-d_6) δ 161.6 (d, *J* = 245.2), 155.12, 152.85, 144.90, 138.71, 132.86, 131.34, 129.26, 127.80, 124.83 (d, *J* = 11.0 Hz), 120.75, 120.17, 119.00, 114.51, 110.78, 92.55 (d, *J* = 3.8 Hz), 88.32, 55.61, 34.43, 31.48. HRMS (ESI) for $C_{46}H_{46}N_4O_4F$ $[M+H]^+$: calcd 737.3503, found 737.3487.

Bisurea 1e (R=*t*-Bu). Dianiline **2e** (300 mg, 0.63 mmol) and *p*-methoxyphenyl isocyanate (235 mg, 1.57 mmol) in dry toluene (50 mL) were stirred at 50 °C for 48 h. The reaction was evaporated to dryness in vacuo and purified by column chromatography (3:2 hexanes:EtOAc, 410 mg, 84%). Trituration with EtOH afforded analytically pure **1e** (40 mg, 10%) as a fine white powder. ^{1}H NMR (500 MHz, DMSO-d_6) δ 9.29 (s, 2H), 8.13 (s, 2H), 8.02 (d, *J* = 8.8 Hz, 2H), 7.84 (t, *J* = 1.4 Hz, 1H), 7.73 (d, *J* = 1.5 Hz, 2H), 7.52 (d, *J* = 2.3 Hz, 2H), 7.42 (dd, *J* = 8.9, 2.4 Hz, 2H), 7.38 (d, *J* = 8.7 Hz, 4H), 6.86 (d, *J* = 8.6 Hz, 4H), 3.70 (s, 6H), 1.35 (s, 9H), 1.29 (s, 18H). ^{13}C NMR (126 MHz, DMSO-d_6) δ 155.06, 152.90, 152.24, 144.89, 138.49, 132.97, 132.21, 129.37, 129.18, 127.32, 123.18, 120.58, 120.23, 114.52, 111.48, 94.64, 86.76, 55.60, 35.11, 34.42, 31.50, 31.29. HRMS (ESI) for $C_{50}H_{55}N_4O_4$ $[M+H]^+$: calcd 775.4223, found 775.4191.

Bisurea 1f (R=OMe). Dianiline **2f** (150 mg, 0.33 mmol) and *p*-methoxyphenyl isocyanate (105 mg, 0.70 mmol) in dry toluene (40 mL) were stirred at 50 °C for 8 h. The reaction became cloudy upon completion and acetone was added until the turbidity was removed. Hexanes was added until a slight turbidity returned and the suspension was left to precipitate overnight in the refrigerator. Filtration afforded **1f** (215 mg, 87%) as a fine white powder. ^{1}H NMR (500 MHz, DMSO-d_6) δ 9.28 (s, 2H), 8.09 (s, 2H), 8.02 (d, J = 8.8 Hz, 2H), 7.59 (s, 1H), 7.50 (d, J = 2.4 Hz, 2H), 7.42 (dd, J = 8.7, 2.4 Hz, 2H), 7.37 (d, J = 8.9 Hz, 4H), 7.32 (s, 2H), 6.85 (d, J = 8.9 Hz, 4H), 3.86 (s, 3H), 3.70 (s, 6H), 1.29 (s, 18H). ^{13}C NMR (126 MHz, DMSO-d_6) δ 159.19, 154.60, 152.39, 144.37, 138.06, 132.44, 128.87, 128.70, 126.97, 123.94, 120.19, 119.68, 117.45, 114.02, 110.71, 93.68, 86.56, 55.64, 55.12, 33.93, 31.01. HRMS (ESI) for $C_{46}H_{46}N_4O_4F$ [M+H]$^+$: calcd 737.3503, found 737.3487.

Bisurea 1g (R=NMe$_2$). Dianiline **2g** (50 mg, 0.11 mmol) and *p*-methoxyphenyl isocyanate (37 mg, 0.25 mmol) in toluene (20 mL) were stirred at 50 °C for 48 h. The reaction became cloudy upon completion and was cooled overnight at –20 °C. Filtration afforded **1g** (47 mg, 57%) as a fine white powder. ^{1}H NMR (600 MHz, DMSO-d_6) δ 9.30 (s, 2H), 8.08 (s, 2H), 8.00 (d, J = 8.8 Hz, 2H), 7.49 (d, J = 2.4 Hz, 2H), 7.41 (dd, J = 8.8, 2.4 Hz, 2H), 7.37 (d, J = 9.0 Hz, 4H), 7.28 (s, 1H), 7.04 (d, J = 1.3 Hz, 2H), 6.85 (d, J = 9.0 Hz, 4H), 3.70 (s, 6H), 2.98 (s, 6H), 1.29 (s, 18H). ^{13}C NMR (151 MHz, DMSO) δ 154.57, 152.43, 150.20, 144.40, 137.93, 132.50, 128.67, 126.72, 123.25, 122.16, 120.12, 119.73, 115.28, 114.04, 111.13, 94.82, 85.46, 55.14, 39.97, 33.95, 31.04. HRMS (ESI) for $C_{48}H_{52}N_5O_4$ [M+H]$^+$: calcd 762.4019, found 762.3986.

X-Ray Crystallography

Diffraction intensities were collected at 173(2) K on a Bruker Apex2 CCD diffractometer using CuKα radiation λ= 1.54178 Å. The space group was determined based

on systematic absences. Absorption corrections were applied by SADABS.[5] The structure was solved by direct methods and Fourier techniques and refined on F^2 using full matrix least-squares procedures. All non-H atoms were refined with anisotropic thermal parameters. All H atoms were treated in calculated positions, except those at the N atoms involved in H-bonds, which were found from the residual density map and refined with restrictions on their N-H distances; the value of 1 Å was used in the refinement as a target for the corresponding N-H bonds. In addition to **1b** the crystal structure includes solvent acetonitrile molecules. The refinement showed that position of the acetonitrile is not fully occupied; in the structure there is a half of acetonitrile molecule per one main molecule. Crystals of the investigated compound were very small needles and diffraction at high angles was very weak. Even using a strong *Incoatec IµS* Cu source we could collect visible diffraction data only up to $\theta_{max} = 100.0°$. While the final structure is not very precise, it clearly represents all chemical results. All calculations were performed by the Bruker SHELXTL (v. 6.10)[58] and SHELXL-2013 packages.[59] The crystal structure of TBA$^+$ (**1a•Cl$^-$**) has been reported previously[30] and the data deposited with the CCDC as structure 929532.

Crystallographic data for **1b**: $C_{46}H_{46.5}N_{5.5}O_6$ [$C_{46}H_{45}N_5O_6$.0.5(CH_3CN)], M = 784.39, 0.14 x 0.04 x 0.03 mm, T = 173(2) K, Monoclinic, space group $P2/c$, a = 16.7165(16) Å, b = 9.0824(8) Å, c = 29.495(3) Å, β = 101.756(7)°, V = 4384.2(8) Å^3, Z = 4, D_c = 1.188 Mg/m^3, μ = 0.642 mm^{-1}, $F(000)$ = 1660, $2\theta_{max}$ = 100.0°, 15027 reflections, 4362 independent reflections [R_{int} = 0.0699], R_1 = 0.1023, wR_2 = 0.2840 and GOF = 1.083 for 4362 reflections (557 parameters) with I>2σ(I), R_1 = 0.1270, wR_2 = 0.3018 and GOF = 1.083 for all reflections, max/min residual electron density +0.432/−0.298 eÅ^3.

Titrations

^{1}H NMR Titration Conditions. ^{1}H NMR titrations were carried out on an Inova 500 MHz spectrometer ([1]H 500.10 MHz). Chemical shifts (δ) are expressed in ppm relative to tetramethylsilane (TMS) using residual non-deuterated solvent (CDCl$_3$: [1]H 7.26 ppm, [13]C 77.0 ppm). CDCl$_3$ was prepared by passing over activated alumina. 1:1 v/v CDCl$_3$ and deionized water was mixed in a separatory funnel and the organic layer was collected. Association constants were determined using non-linear regression fitting in MatLab.[42] Titration data for **1a** with halides has been previously reported.[30]

A stock solution of **1a-g** in CDCl$_3$ (3 mL) was prepared and used in the preparation of a TBA salt solution (2.4 mL). The remaining stock solution (0.6 mL) was used as the starting volume in an NMR tube. Spectra were recorded after each addition of TBA salt on a 500 MHz spectrometer and the $\Delta\delta$ of urea proton H$_g$ was used to follow the progress of the titration.

UV-vis Titration Conditions. UV-vis titrations were carried out on an HP 8453 UV-vis spectrometer equipped with a 265 nm high-pass filter. Water-saturated CHCl$_3$ was prepared in the same manner as for ^{1}H NMR titrations. Association constants were determined by non-linear regression in HYPERquad fitting the complete spectrum simultaneously.[60] Hamilton gas-tight micro-syringes were used during serial dilutions and titrations. The reported association constants and errors were obtained from the average and standard deviation of three repeated titrations. Single representative titrations for each host/anion pair are included in Appendix B. Titration data for **1a** with halides has been previously reported.[30]

A stock solution of **1a-g** was prepared by serial dilution from 1 mL to a final volume of 5 mL in CHCl$_3$. An aliquot (2.0 mL) of the stock host solution was transferred to a quartz

cuvette with septum cap as the starting volume. Guest solutions were prepared by taking a

TBA salt up in the host stock solution (1 mL) then serial diluting to the final concentration

(2.0 mL) using the host stock solution. Aliquots of guest solution were added to the cuvette

and a spectrum recorded after each addition.

Bridge to Chapter IV

Chapter III presented an in depth study of the substituent effects on aryl CH anion

hydrogen bonds. The ability to control association constants across a large range by altering

a single CH hydrogen bond was demonstrated. A key outcome from this study was the

identification of a possible method for tuning the selectivity of anion receptors by variable

substitution. Chapter IV further explores the underlying factors for this tunability through

studies of the equilibrium isotope effect and the partial covalent nature of the hydrogen

bond.

---

[i] DMSO was chosen in this case because it is a highly competitive solvent and allows for high receptor concentration without fear of aggregation or saturation. The DMSO also acts to bind to the ureas, as indicated by their downfield shifts, decreasing the anion binding strength and making it a poor solvent for titrations. As well, the hydroscopic nature of DMSO hinders attempts to accurately control the water content between experiments.

[ii] Hammett analysis was also performed using the alternative parameters σ^+ and σ^- to better represent the buildup or depletion of charge, however, in all cases the fit was worse (Table 44 in Appendix B). The buildup of charge is small in this case.

CHAPTER IV

EQUILIBRIUM DEUTERIUM ISOTOPE EFFECTS OF ARYL CH HYDROGEN BONDS

The quantum chemical calculations for this chapter were performed by Alex Brueckner and Dr. Maduka Ogba at Oregon State University. I performed proton and deuterium labeled receptor synthesis and NMR experiments. The computational results and discussion were contributed by Dr. Maduka Ogba and Alex Brueckner. Prof. Darren Johnson and Prof. Michael Haley provided editorial assistance, along with Prof. Paul Cheong at Oregon State University.

Introduction

The ability of isotopes to alter the strength and selectivity of binding in non-covalent interactions is well-documented for biological and non-biological systems.[1,2] As well, numerous methods have been developed to utilize selective labeling experiments to differentiate the importance of individual interactions on the complete symphony of binding, including relative chromatographic retention times,[3] binding studies by mass spectrometry and spectroscopic titrations,[4] and enzyme kinetic studies.[5,6] The numerous examples of deuterium isotope effects (DIE) in biological systems highlights the complex effects of deuterium labeling on non-covalent interactions.[5] Current predictive descriptions of DIEs are related to the properties of whole molecules, e.g., lipophilicity, polarizability, and hydrophobicity, and often do not apply to single interactions, as desired for *ab initio* drug or sensor design. To advance this field, models are now being developed to understand isotope effects in both simple and complex supramolecular systems.[4,7-13]

Lewis and Schramm have extensively studied the equilibrium isotope effect (EIE) of glucose binding to human brain hexokinase (HBH) and the pre-binding equilibrium of glucose.[14,15] The tritium EIE for binding to HBH ranged from 1.027 to 0.927 depending on the site of CH substitution. The normal EIEs were consistently explained by proximal hydrogen bonding groups in the protein binding site. The large inverse effect could be explained by a steric interaction between the CH and neighboring OH groups. In addition, measurements of the α/β–glucose equilibrium with deuterium labeling were shown to be insufficient to explain the EIE of HBH binding. Salient to the current study, the α/β–glucose EIE was the result of perturbations to the anomeric effect in orbital interactions upon deuterium labeling and conformational equilibrium.

One example of a less complex system with a single interaction is the position-specific secondary DIEs on the pK_a of pyridine, which have been measured for deuterium-labeled pyridines and lutidines with exceptional precision.[11] The development of competitive titrations using ^{13}C NMR spectroscopy of the ~1:1 mixed H/D systems allows for the direct measurement of K_a^H/K_a^D as small as 10^{-4} from linear eq. **1**. The DIEs always favor d_x-pyridine protonation (K_a^H/K_a^D range from 1.0139 to 1.0828), and positional isomer effects highlight the variable nature of DIEs, switching from sterics/electronics in 2,6-lutidine, to zero-point energy (ZPE) vibration driven in most other cases. A similar method was applied to the supramolecular complex of benzyltrimethylphosphonium with tetrahedral cage **1**, Figure 1. The ^{31}P NMR resonance was tracked to measure small normal DIEs for the association to the exterior and interior of the cage.[8,9] In this second case, the association of non-deuterated phosphonium is favored over the various isotopologues. As in the pK_a of pyridines, the measured DIEs are the result of nonspecific interactions with the deuterium

labels and the deuterium EIE arises from changes in the vibrational ZPE of the labeled

compounds according to eq. 2.

$$(\delta_H^f - \delta_H)(\delta_D - \delta_D^o) = (K_a^H/K_a^D)(\delta_H - \delta_H^o)(\delta_H^f - \delta_H) \tag{1}$$

$$\text{EIE} = (K_a^H/K_a^D) = (\text{ZPE}(H \bullet G) - \text{ZPE}(H)) / (\text{ZPE}(D \bullet G) - \text{ZPE}(D)) \tag{2}$$
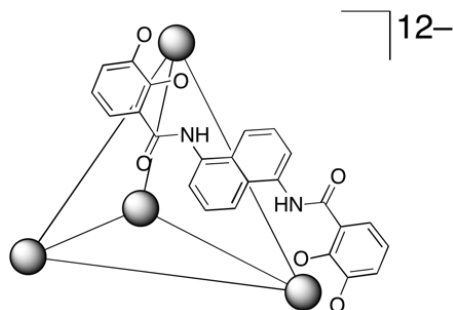
Figure 1. Tetrahedral $[L_6Ga_4]^{12-}$ cage **1** used for measurement of DIE with benzyltrimethylphosphonium cations.

The precise measurement of relative association constants by this method is broadly

applicable and requires only a fast exchanging system with resolved resonances for two

systems to be compared. Herein, we report measurement of the deuterium EIE on C–

H···Cl⁻ hydrogen bonding by both solution measurement and computation. The synthesis

of a selectively deuterated arylethynyl bisurea anion receptor **2D** (Scheme 1) facilitates the

measurement by competitive titration of the DIE in DMSO-d_6. Extensive quantum chemical

calculations on **2D** and similar compounds validate the solution measurements and

demonstrate the importance of vibrational changes on the observed DIE. As well, the large

DIE of a single deuteration corroborates previous studies on the importance of this

hydrogen bond to the overall binding energy while the vibrational mechanism supports the

covalent nature of this interaction.[16]
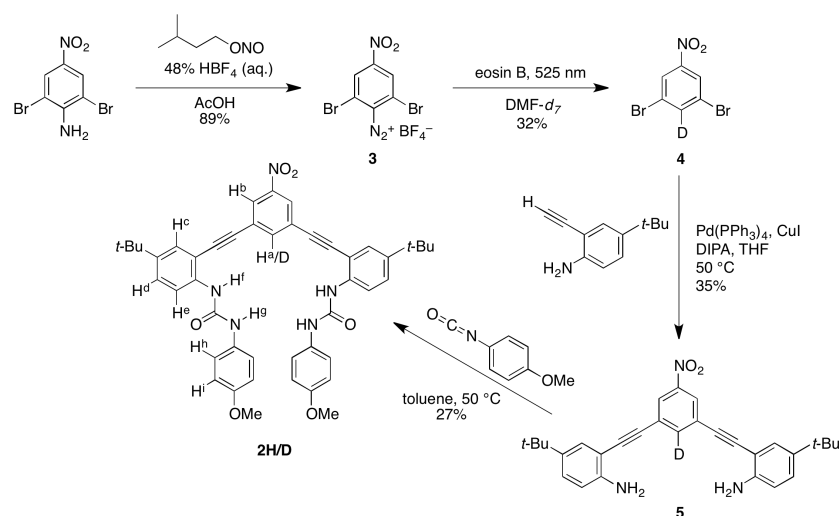
Scheme 1. Synthesis of selectively deuterated receptor **2D**.

Results and Discussion

Synthesis

The receptor **2H** has been previously shown to act as a strong CH donor with $\log K_a$ for Cl⁻ of 4.39 ± 0.62 in chloroform.[16] Isotopologue **2D** is prepared by similar methods starting from **4**, obtained by the selective deutero-deamination reaction of **3**. The monodeuterated arene **4** was synthesized by photo-catalyzed Sandmeyer deamination of the diazonium tetrafluoroborate salt **3**. The use of eosin B as a photo-catalyst under mild conditions (r.t. and 3W 525 nm LEDs) provides unmatched selectivity and labeling efficiency (>99% based on ^{1}H, ^{2}H, ^{13}C NMR spectroscopy and GC-MS) when the reaction is performed in DMF-d_7.[17] Unfortunately, the desired product was produced as an inseparable 2:1 mixture of **4** and 1,2,3-tribromo-5-nitrobenzene (identified by GC-MS).[i] This mixture was moved on to the subsequent Sonogashira cross-coupling with 2-ethynyl-4-*t*-butylaniline[18,19] and dianiline **5** was easily separated at this stage. The final receptor **2D** and key intermediates were characterized by ^{1}H, ^{2}H, and ^{13}C NMR spectroscopy, and high-resolution mass spectrometry of **2D** for purity and labeling efficiency (see Appendix C for

supplementary spectra). The ^{1}H and ^{13}C NMR peaks were assigned by ^{1}H–^{13}C HSQC NMR and assignments in Figure 2 refer to Scheme 1.
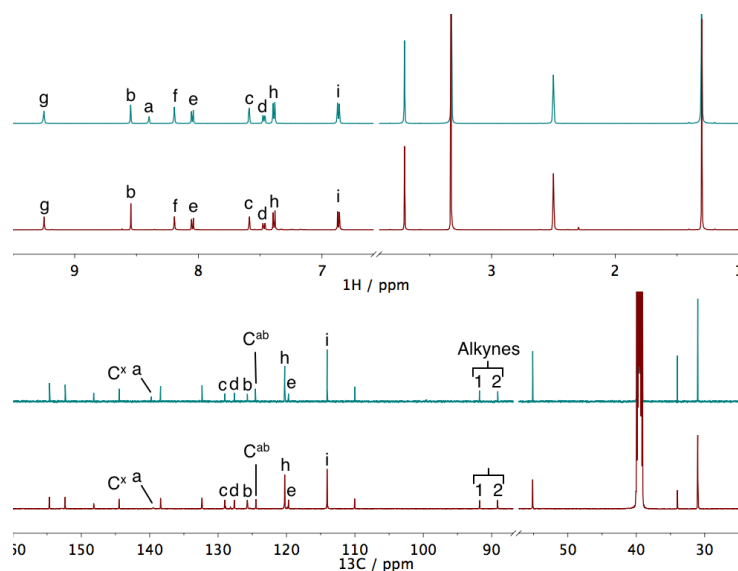
Figure 2. ^{1}H (top) and ^{13}C (bottom) NMR spectra of **2H** (blue) and **2D** (red) in DMSO-d_6; assignments refer to Scheme 1. C^{ab} is the aryl carbon between H^a and H^b.

NMR Titrations

Exemplified by the methods of Perrin et al., ^{13}C NMR spectroscopy is exceptionally sensitive to chemical shifts from isotopic labeling.[11,20] The ^{1}H and ^{13}C NMR spectra of **2H** and **2D** are shown in Figure 2 to illustrate the similarities and key differences in these compounds. To obtain a sufficient S/N for ^{13}C NMR in a reasonable integration time, competitive titrations were performed in DMSO-d_6 with ~1:1 mixture of the H and D receptors at a combined concentration of 6.1 mM, and TBACl was added in 5 μL aliquots as a 1.8 M solution.[ii] Although many ^{1}H and ^{13}C signals shift over the course of the titration, only four ^{13}C peaks are sufficiently resolved for **2H** and **2D** to be used for fitting to measure

the EIE. Of the four peaks differentiated by labeling, the ^{13}C signal directly labeled with D is too weak for accurate measurement of δ during the course of a titration.

The binding isotherm for mixed **2H:2D** is plotted in Figure 3 for both ^{1}H and ^{13}C NMR spectroscopy from the same competitive titration. C^{ab} is the next closest carbon to the labeled CH hydrogen bond donor and is well resolved between **2H** and **2D** with greater intensity than the labeled peak. The ^{13}C peak presents a large downfield shift and the isotherm for this carbon approximates a binding curve for a 1:1 association. The alkyne peaks, also differentiated for **2H** and **2D**, are complex curves indicative of possible multistep equilibria. A large shift in the alkyne carbons is surprising due to the large distance from the nearest hydrogen bonding site. One explanation is the through space effect of an approaching anion which shields the alkyne. An alternative effect is rotation about the alkyne upon binding of the anion, a conformational change that has also been observed in similar alkyne receptors.[21,22]
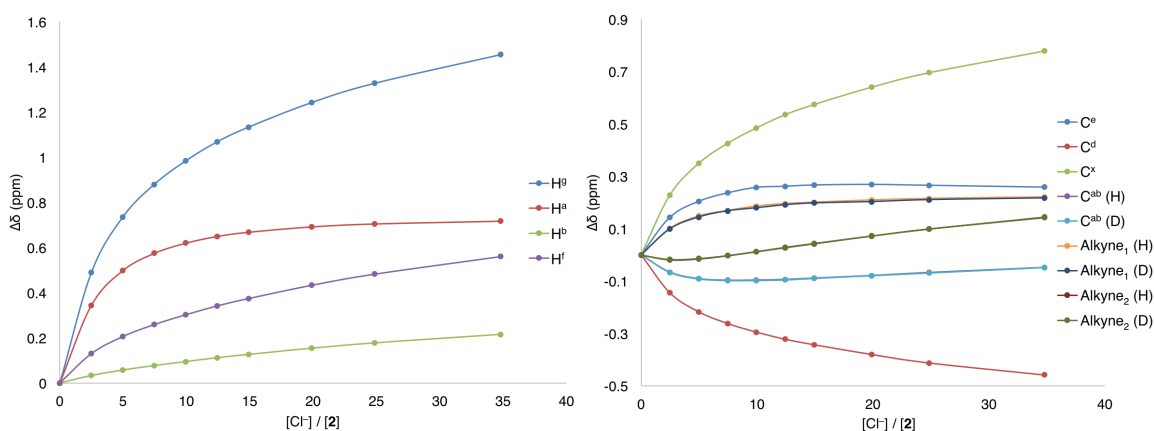
Figure 3. Binding isotherm for 1:1 **2H:2D** in DMSO-d_6 by [1]H (*left*) and ^{13}C (*right*) NMR spectroscopy, lines added as a guide for the eye. Isotherm shape is consistent with weak 1:2 binding where $K_a^{1:1} \gg K_a^{1:2}$. (H) and (D) ^{13}C NMR peaks are used for linear EIE fitting, the isotherms overlap although the peaks are resolved.

The remaining ^{1}H and ^{13}C NMR peaks produce simpler and consistent binding curves, which can be split into two categories. First, several peaks reach a saturation point near 15 equiv. Cl$^-$ and remain mostly flat for the remainder of the titration, H^a, C^e, and C^{ab}. The second category includes peaks that never appear to reach saturation in the range studied but continue to increase linearly after 15 equiv., H^g, H^f, C^x, and C^d. The second case is consistent with a weak 1:2 complex, whereas the first case is more indicative of a 1:1 binding event. An estimated value for the overall K_a (log β) is obtained from the fitting of the ^{1}H resonances and C^{ab} to a 1:2 **2**:Cl$^-$ model using the combined [**2H** + **2D**]. The binding in DMSO-d_6 is significantly weaker (log β ~ 1.8) than in CHCl$_3$ (log K_a = 4.4 ± 0.62), which is expected for a solvent system with high polarity and strong hydrogen bond acceptors. As well, the second Cl$^-$ association is likely very weak with $K_a^{1:2}$ < 5. Based on the curve shape and position on **2** of atoms for the two binding isotherm categories, it is clear that the first Cl$^-$ binds in the expected pocket to CH^a with both ureas, and then a second Cl$^-$ weakly binds to one of the ureas at high [Cl$^-$], forcing the alkyne to rotate open to accommodate it.[21,22] The complex binding isotherm, however, does not prevent the use of a linearized plot to determine the relative K_as for **2H** and **2D** with greater precision than possible by direct analytical titration and non-linear regression.

The linearized plot of K_a^H/K_a^D provides an accurate measure of the DIE from a competitive titration with minimal dependence on the receptor concentrations and no need to accurately determine the Cl$^-$ concentration. The method only requires that free and bound species be in fast equilibrium with resolved peaks but is otherwise a robust method for relative K_a determination. Least squares linear regression of the ^{13}C NMR chemical shifts of **2H** and **2D** according to eq. **1** provides the relative K_a^H/K_a^D. The chemical shifts for three ^{13}C peaks were fit simultaneously with an R^2 = 0.996 and K_a^H/K_a^D = 1.0142 ± 0.0104, shown

in Figure 4. This value is comparable to the isotope effects observed for glucose binding to human brain hexokinase (tritium EIEs of 1.027 – 1.065 for hydrogen bond sites and 0.927 – 0.988 for other sites), specifically a normal EIE that is strongly correlated to a hydrogen bonding interaction.[14,15] The EIE was also measured for each peak individually and used to calculate the error in the overall EIE, data found in Table 1. The normal EIE favors association of Cl$^-$ with the unlabeled receptor **2H**. In this case, several alternative explanations for the mechanism of this EIE can be eliminated. Both steric and inductive mechanisms based on the shorter CD bond would result in an inverse EIE with association to **2D** favored. Here we observe a case where the only explanations are based upon the vibrational changes of the ZPE, which are partially driven by the covalent nature of a hydrogen bond. The mechanism is further elucidated by quantum chemical calculations to measure the EIE of **2D** along with additional model compounds.
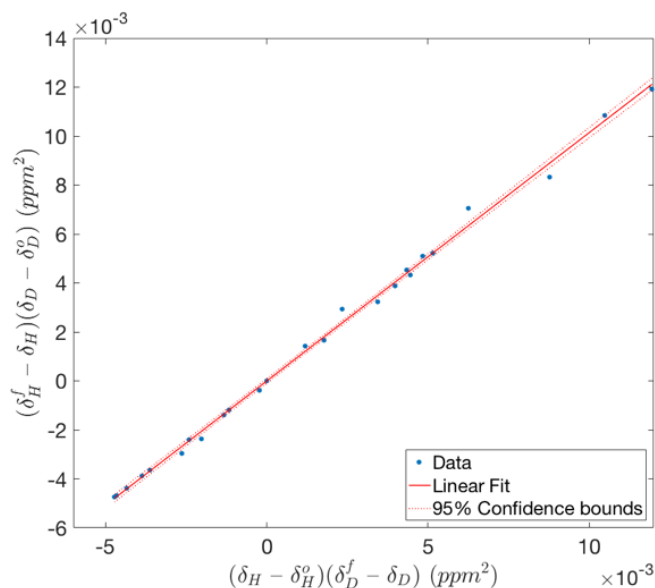
Figure 4. Linearized plot of K_a^H/K_a^D from differences in **2H:2D** ^{13}C NMR spectroscopy.

Table 1. Equilibrium Isotope Effects Measured Overall and for Individual ^{13}C NMR Peaks

	K_a^H/K_a^D	R^2
C^{ab}	1.0045	0.99992
Alkyne$_1$	1.0164	0.990
Alkyne$_2$	1.0145	0.996
Overall	1.0142	0.997

Computations

Quantum chemical calculations are particularly effective at predicting the deuterium isotope effects for both reactions and equilibria.[10,11,23] The EIE for Cl$^-$ binding was calculated in the gas phase and in solvent polarization fields using B3LYP/6-31G* and B3LYP/6-31G*/PCM(chloroform) respectively in Gaussian 09.[24-26] Complex **[2D•Cl$^-$][TBA$^+$]** was found to have an EIE of 1.026 in the gas phase, which was a slight overestimation but within error of the experimental value. There is little difference between EIEs in the gas phase and in a solvent polarization field, and this limits the contribution polarization of the CD bond may have on the total EIE. Several alternative deuteration and substitution patterns were also explored, which were not practical to assess synthetically (Figure 5). Interestingly, the substitution on both ureas for D in **2D$_5$** increases the overall EIE to 1.124. Labeling the interior urea alone, H^f in Scheme 1, leads to an inverse isotope effect, 0.969. The large isotope effect for **2D$_5$** is expected based on the strength of an N–H$\cdots$Cl$^-$ hydrogen bond and represents an EIE of 1.05 per NH^g (after subtracting the contribution from CH^a and NH^f).
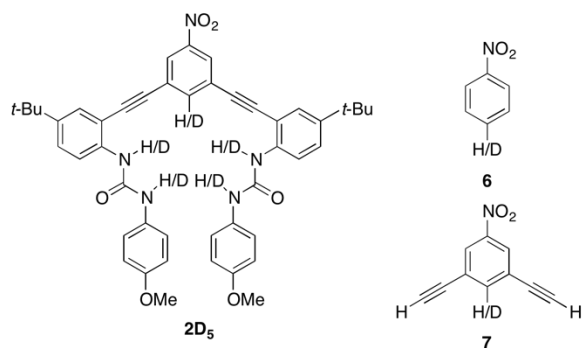
Figure 5. Structures of model compounds used for EIE estimates by quantum chemical calculations.

To address a possible steric mechanism, the EIE was also calculated for the model compounds **6** and **7** that remove the directing urea groups and were previously shown to be an excellent predictor of trends in the overall binding energy.[16] The simplified bisalkyne **7** was able to reproduce the isotope effect calculated for **2** and match closely the value measured experimentally (EIE **7** = 1.021, **6** = 1.011). This is an important test case because it eliminates the interference of the supporting ureas and allows the Cl^- to find the most stable $CH\cdots Cl^-$ hydrogen bond. The calculated distance from the optimized geometries between $C\cdots Cl^-$ for **2H** is 3.599 Å, while the $C\cdots Cl^-$ distance for **7H** is 3.757 Å, engendering a bond length difference of 0.158 Å. A steric mechanism for the EIE with **2D•Cl⁻** would arise from the shorter CD bond providing a larger binding pocket for Cl^-. The ability of **7•Cl⁻** to reproduce this same EIE with a much longer $C–H\cdots Cl^-$ contact is strong evidence against the steric argument.

Conclusion

The synthesis of a selectively labeled receptor has allowed for the first accurate measurement of an EIE in an aryl $C–H\cdots X^-$ hydrogen bond. The deuterium EIE from competitive titrations and computational measurements agree on a small, normal EIE that

92

facors the formation of a CH hydrogen bond over a CD hydrogen bond. The measured EIE is consistent with a ZPE mechanism and this mechanism is supported by additional deuterated compounds accessible through computations. Alternative mechanisms using inductive or steric effects are refuted by both the computational and experimental results. The tritium EIE for glucose binding to HBH was also the result of vibrational ZPE changes with the anomeric effect playing a role. There is a clear comparison between the $\sigma \rightarrow \sigma^*$ interaction observed for the anomeric effect in glucose and the $lp \rightarrow \sigma^*$ interaction of a C–H$\cdots$X$^-$ hydrogen bond.

The measurement of the DIE for anion binding in a selectively labeled receptor has highlighted the importance of vibrational change in the C–H$\cdots$X$^-$ hydrogen bond, which reveals covalency as a major contributor to these interactions. In addition, we have shown that deuterium labeling of hydrogen bonds leads to a decreased association energy even if the donor is the relatively weak CH; this serves as a guide to assist with interpreting steric effects[4,7] versus attractive interactions[8,10] for past and future supramolecular isotope effect studies. The aryl CH donor has now been unambiguously assigned the category of hydrogen bond donor. These results will facilitate the design and modeling of novel biological and chemical supramolecular systems using CH hydrogen bonds.

Experimental

General Procedures

^{1}H, ^{2}H, and ^{13}C NMR spectra were obtained on an Inova 500 MHz (^{1}H 500.10 MHz, ^{2}H 76.75 MHz, ^{13}C 125.75 MHz) spectrometer. ^{1}H and ^{13}C NMR titrations were performed on a Bruker Avance-III-HD 600 MHz (^{1}H 599.98 MHz, ^{13}C 150.87 MHz) spectrometer with a Prodigy multinuclear broadband BBO CryoProbe. Chemical shifts (δ) are expressed in

ppm relative to tetramethylsilane (TMS) using residual solvent signals(CDCl$_3$: ^{1}H 7.26 ppm, ^{13}C 77.0 ppm; CD$_3$CN: ^{1}H 1.94 ppm, ^{13}C 118.26; CD$_2$Cl$_2$: ^{1}H 5.32 ppm, ^{13}C 54.0 ppm; CH$_2$Cl$_2$: ^{2}H 5.32 ppm; DMSO-d_6: ^{1}H 2.50 ppm, ^{13}C 39.51 ppm; (CH$_3$)$_2$CO: ^{2}H 2.05). Dry toluene was prepared by distillation from CaH$_2$ immediately before use. Tetrabutylammonium salts were dried by heating at 60 °C under high vacuum for 24 h. Deuterated solvents were purchased from Cambridge Isotope Labs. All other reagents were purchased and used as received. The synthesis of **2H** has been reported previously.[16]

Synthesis

Synthesis of 3. 2,6-Dibromo-4-nitroaniline (1.32g, 4.5 mmol) was taken up in a mixture of glacial AcOH (3 mL) and 48% aqueous HBF$_4$ (1.3 mL) and subsequently isoamylnitrite (1 mL) in glacial AcOH (2 mL) was added dropwise over 5 min at room temperature. The diazonium salt was crystallized by adding Et$_2$O (3.3 mL) and cooling in a freezer at –30 °C. After filtration and washing with additional Et$_2$O (3 x 5 mL), salt **3** was collected as a grey powder (1.57 g, 89%). ^{1}H NMR (500 MHz, CD$_3$CN) δ 8.88 (s, 2H). ^{13}C NMR (126 MHz, CD$_3$CN) δ 154.39, 130.70, 129.78, 126.84.

Synthesis of 4. Diazonium salt **3** (0.788 mg, 2.0 mmol) was added to an oven-dried, septum cap vial and taken up in DMF-d_7 (16 mL). Working in a darkroom, the solution was sparged with N$_2$ for 30 min before adding the photo-catalyst Eosin-B (0.024 mg, 0.04 mmol). After sparging an additional 30 min, the reaction was irradiated with 525 nm light (two 3w green LEDs at 520-530 nm) for 4 h or until gas evolution had ceased. Et$_2$O (30 mL) was added and the organic layer was washed with aq. 5% NH$_4$Cl soln. (3 x 10 mL), then H$_2$O (3 x 10 mL), and finally with brine (3 x 10 mL). The organic layer was dried (MgSO$_4$) and concentrated in vacuo. The crude powder was purified by flash chromatography on silica (4:1 hexanes:EtOAc) to obtain a 2:1 mixture of **4** (0.16 g, 32% NMR yield) and 1,2,3-

tribromo-5-nitrobenzene. ^{1}H NMR (600 MHz, CD_2Cl_2) δ = 8.45 (s, 2H), 8.34 (s, 2H, **4**). ^{2}H NMR (76.75 MHz, CH_2Cl_2) δ = 8.08 (s, 1H). ^{13}C NMR (151 MHz, CD_2Cl_2) δ 140.37 (t, J = 26.9 Hz), 136.15, 127.62, 127.20, 126.17, 123.79.

Synthesis of 5. 2-Ethynyl-4-*t*-butylaniline (0.26 g, 1.56 mmol) was dissolved in minimal THF and added to an N_2-purged solution of 3,5-dibromo-4-[2]H-nitrobenzene (**4**, 0.133 g, 0.47 mmol), $Pd(PPh_3)_4$ (0.042 g, 0.035 mmol), and CuI (0.026 g, 0.142 mmol) in dry THF (20 mL) and *i*-Pr_2NH (20 mL). The reaction was stirred at 50 °C for 24 h before concentrating *in vacuo,* and the residue was taken up into CH_2Cl_2. The solution was filtered through a 3 cm silica gel plug and washed with additional CH_2Cl_2. The combined organics were concentrated *in vacuo,* and the product was purified by column chromatography (15% EtOAc in hexanes) to afford **5** (0.078 g, 35%) as an orange solid. ^{1}H NMR (600 MHz, $CDCl_3$) δ 8.28 (s, 2H), 7.39 (d, J = 2.3 Hz, 2H), 7.25 (dd, J = 8.5, 2.5 Hz, 2H), 6.71 (d, J = 8.5 Hz, 2H), 4.19 (s, 4H), 1.30 (s, 18H); ^{2}H NMR (76.75 MHz, $(CH_3)_2CO$) δ = 8.21 (s, 1H); ^{13}C NMR (151 MHz, $CDCl_3$) δ 148.38, 145.98, 141.25, 129.12, 128.36, 125.64, 125.13, 114.72, 106.18, 91.35, 90.22, 34.11, 31.51.

Synthesis of 2D. The labeled receptor **2D** was prepared following the procedure for **2H** as previously reported[13] to obtain the final product as a pale yellow powder (0.026 g, 27%). ^{1}H NMR (600 MHz, DMSO-d_6): δ 9.25 (s, 2H), 8.55 (s, 2H), 8.19 (s, 2H), 8.05 (d, J = 8.8 Hz, 2H), 7.59 (d, J = 2.4 Hz, 2H), 7.47 (dd, J = 8.8, 2.4 Hz, 2H), 7.39 (d, J = 9.0 Hz, 4H), 6.87 (d, J = 9.0 Hz, 4H), 3.70 (s, 6H), 1.30 (s, 18H). ^{2}H NMR (76.75 MHz, $(CH_3)_2CO$) δ = 8.23 (s, 1H). ^{13}C NMR (151 MHz, DMSO-d_6) δ 154.66, 152.36, 148.18, 144.48, 139.47 (d, J = 13.8 Hz), 138.41, 132.35, 129.03, 128.90, 128.20, 127.63, 125.73, 124.46, 120.26, 119.71, 114.07, 110.04, 91.76, 89.14, 55.15, 33.99, 31.01. HRMS (ESI) for $C_{46}{}^1H_{45}{}^2HN_5O_6$ [M+H]$^+$: calcd 765.3511, found 765.3541.

Competitive Titration of 2H:2D

Mixed samples of **2H:2D** were prepared from approximately equal masses in 600 μL DMSO-d_6 at a combined [**2H + 2D**] of 6.1 mM, and a 1.8 M solution of Cl⁻ was prepared from the TBA salt in DMSO-d_6. The Cl⁻ solution was titrated as 5 μL aliquots followed by collection of ¹H and ¹³C NMR spectra after each addition. Two additional 10 μL aliquots and a final 20 μL aliquot were added to assure complete complexation and accurate determination of the final δ. All samples were regulated at 298 K and ¹³C NMR spectra were collected for 548-1107 scans. The peaks for **2H** and **2D** in this mixed solution were assigned by relative intensity and confirmed by the ¹³C NMR spectra of pure samples.

Bridge to Chapter V

Chapter IV established the ability to synthesize a selectively deuterium labeled receptor and measure the equilibrium isotope effect with high precision. The normal EIE demonstrates the vibrational contributions to this hydrogen bond and highlights the importance of covalent character in this hydrogen bond interaction. Chapter V will explore the importance of binding pocket geometry and pre-organization provided by the urea hydrogen bond donors. The anion binding and self-assembly properties of a bis-amide pyridine receptor will be reported. The propensity to form anion-templated dimers in the solid state but not in solution elucidates the role each urea hydrogen bond donor and the importance of binding pocket design.

---

[i] The side product is the result of a kinetic isotope effect where radicals in DMF-d_7 persist with much longer half-life than when the reaction is performed in reagent-grade DMF.

[ii] Titrations with pure **2D** were also performed by UV-vis and ¹H NMR spectroscopy; however, these results offer limited information because differences in the raw data and determined K_as are not significant enough to distinguish **2H** and **2D**.

CHAPTER V

ANION-DIRECTED SELF-ASSEMBLY OF A
2,6-BIS(2-ANILINOETHYNYL)PYRIDINE BIS(AMIDE) SCAFFOLD

Chapter V was published in the journal *Supramolecular Chemistry* as part of a special issue to honor Prof. J. Sessler. The bis(amide) was synthesized by Dr. Orion Berryman, who also performed the data collection for the single crystal X-ray diffraction experiments. The crystal structure was solved by Dr. Berryman and Dr. Lev N. Zakharov. I performed the solution characterization and wrote the manuscript. Prof. Darren Johnson and Prof. Michael Haley assisted with the editing of this chapter as my advisors.

Introduction

Self-assembly plays an important role in the design of supramolecular materials and host-guest complexes.[1] Macromolecules resulting from self-assembly provide unique properties such as conductivity,[2,3] metal capture,[4] sensing,[5,6] motion[7,8] or logic gates.[9] Self-assembled receptors or sensors are also capable of selecting guests by an 'induced fit' model,[10,11] not just the restrictive lock and key method. The self-assembly of many such complexes has been effected using metal ions,[12,13] small molecules,[14] and anions.[15,16] Advancing the use of anions as directing elements and/or templates in self-assembling systems requires an improved understanding of conformational preferences of the flexible receptors comprising these assemblies.[5,8]

Alkynes offer many characteristics that are useful to designing self-assembled receptors: linear rigidity, rotational freedom, π-electron conjugation, and easy functionalization.[17] We have previously reported on a family of modular arylethynyl

receptors for anion binding and fluorescent sensing using 2,6-bis(2-anilinoethynyl)pyridine,[18-25] -bipyridine,[24,26-28] -phenanthroline,[28] -benzene,[29-30] and -thiophene[24] scaffolds. The anilines are further functionalized with amide,[20] sulfonamide,[18,24] or urea[19,21-23,25-30] groups to provide capabilities such as anion selectivity for nitrate[30] and $H_2PO_4^-$,[26] water solubility[25] or metal coordination.[27] An example of a pyridine receptor with sulfonamide arms (e.g., **1**) is shown in Figure 1. The sulfonamide receptors exhibited an exceptional capacity to bind water by self-assembling into 2+2 dimers.[18,24] The water molecules can be substituted by halides to form a 2+2 homodimer and even a 2+1+1 heterodimer (H_2O/Cl), as all three configurations have been observed in the solid-state. Unfortunately, the persistence of these dimers in solution made characterization of binding equilibria difficult except for determination of the dimerization constants (K_{dim}).
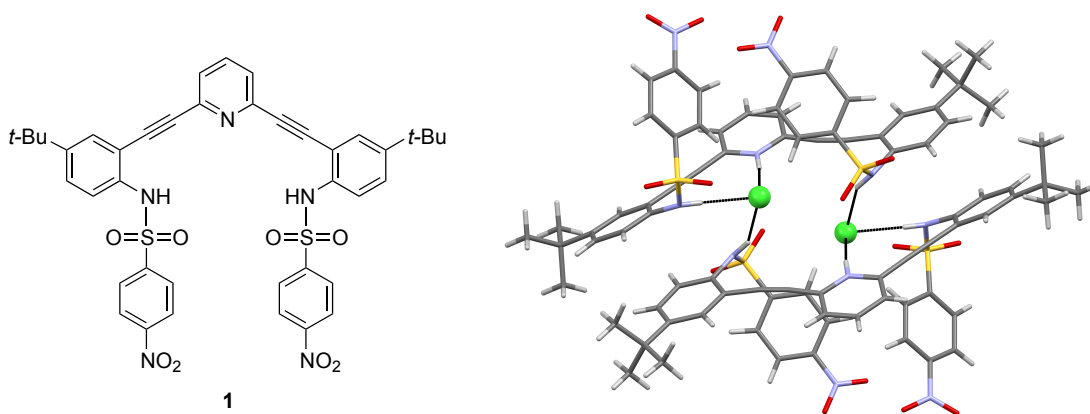
Figure 1. Sulfonamide **1** (left) and X-ray crystal structure of (**H1$^+$•Cl$^-$**)$_2$ (right). Three hydrogen bonds to each Cl$^-$ are shown. Nitroarenes are tilted up by the sulfonyl oxygens and a 2+2 dimer forms with Cl$^-$ (or H_2O).

In addition to hydrogen bonds, anion-π interactions are underutilized[31-33] and have the potential to improve selectivity for soft anions, such as iodide[34] and nitrate.[30,35] We previously reported some of the first examples of hydrogen bond assisted[31] and unassisted[36]

anion-π halide receptors. Aromatic interactions featuring anions have the added benefit of sometimes producing a unique color change due to charge transfer, which offers additional sensing opportunities. Inspired by our previous work with anion-π interactions and the self-assembly of sulfonamides such as **1**, we sought to design a new receptor that would combine these properties for new selectivity and increased fluorescent response. Herein we report the synthesis and binding properties of bis(amide) receptor **2** derived from 2,6-bis(2-anilinoethynyl)pyridine and electron-poor 3,5-dinitrobenzoyl chloride, the latter unit intended to promote anion-π interactions.

Results and Discussion

Synthesis

Precursor **3** has been previously reported as a versatile building block for selective, fluorescent receptors. The large family of compounds cited above, along with **3**, are accessible by Sonogashira cross-coupling a suitable 2-ethynylaniline to a haloarene core.[18-25] Amide condensation of **3** with the commercially available 3,5-dinitrobenzoyl chloride furnishes bis(amide) **2** in moderate yield (Scheme 1) after recrystallization from hot EtOAc.
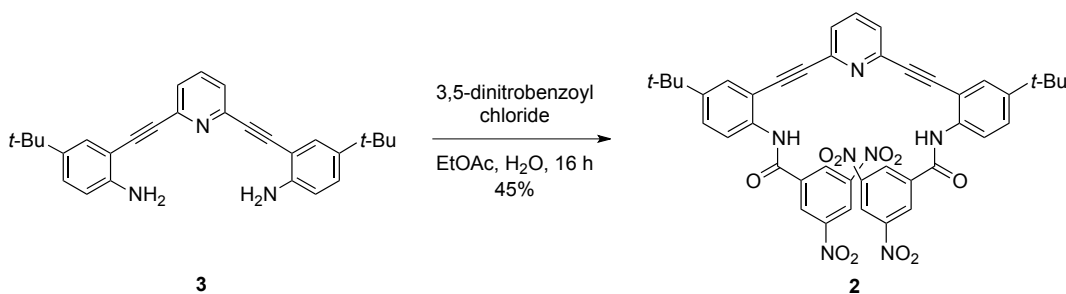
Scheme 1. Synthesis of bis(amide) **2**.

Absorbance and Fluorescence

The electronic absorption spectrum of **2** (Figure 2, left) is characteristic of the 2,6-bis(2-anilinoethynyl)pyridine backbone. The freebase receptor has a broad absorbance with shoulders at 290 and 315 nm. Protonation with trifluoroacetic acid (TFA) or HCl results in a yellow solution. In the absorbance spectrum of **H2$^+$Cl$^-$**, a new peak appears at 395 nm with a slight decrease in absorbance below 340 nm. The TFA$^-$ salt has a shoulder at 380 nm and an increased absorbance at 308 nm.
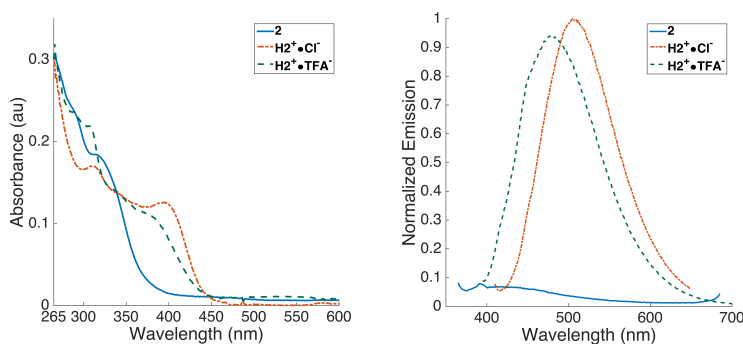
Figure 2. Absorbance (left) and emission (right) spectra of **2** and **H2$^+$** as Cl$^-$ and TFA$^-$ salt ([**2**] = 10 μM, **2** and **H2$^+$•TFA$^-$** Ex = 380 nm, **H2$^+$•Cl$^-$** Ex = 395; in wet, O$_2$-containing CHCl$_3$).

Electron-poor receptor **1** is non-emissive as the free-base and the additional nitro groups on **2** should further quench fluorescence. Prior studies in our lab showed that electron-poor receptors like **1** exhibit a highly desirable 'OFF-ON' fluorescence response to acids such as HCl and TFA.[21] Whereas receptor **2** has no appreciable fluorescence in O$_2$-containing CHCl$_3$ (Figure 2, right), the addition of HCl affords a yellow solution that possesses a yellow emission when irradiated with a handheld UV lamp. When exciting at 395 nm, the fluorescence maximum of **H2$^+$•Cl$^-$** is 505 nm, which matches with the λ_{max} of **H1$^+$•Cl$^-$**. The fluorescence emission of **H2$^+$•TFA$^-$** was unexpectedly similar in intensity to

H2⁺•Cl⁻, although the λ_{max} was hypsochromically shifted to 477 nm. In comparison, sulfonamide **1** exhibited the same λ_{max} for Cl⁻ and TFA⁻, but the TFA⁻ salt had less than 50% the emission intensity of the Cl⁻ salt. The increased response from **H2⁺•TFA⁻** is unusual because of the weak binding of TFA and breaks from the normally observed quenching. The fluorescence mechanism for this family of receptors is expected to include significant rigidification of the alkyne backbone due to anion binding. We next sought to examine whether a change in the anion binding structure could explain this anomaly.

X-Ray crystallography

Single crystals of **H2⁺•Cl⁻** suitable for X-ray diffraction analysis were grown by slow evaporation of an HCl-saturated CH_2Cl_2 solution. **H2⁺•Cl⁻** crystallized as a dimeric structure in the triclinic space group *P*-1 with two CH_2Cl_2 molecules. Figure 3 shows the ORTEP representation of a single protonated receptor bound to one chloride. The asymmetric bis(amide) **2** adopts an '**S**' conformation with only one arm appearing to bind a Cl⁻ ion, as the other arm is rotated away from the binding pocket. Interestingly, this result is in contrast to our earlier studies that showed that the sulfonamides[18,24] and ureas[19] derived from pyridine scaffold **3** both bind halides in a '**U**'-shaped conformation.
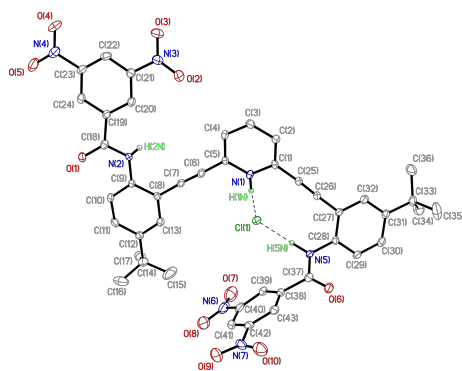
Figure 3. Top view of the X-ray crystal structure of **H2⁺•Cl⁻** showing the asymmetric unit with atom labels. Hydrogens not involved in hydrogen bonds and two CH_2Cl_2 molecules have been omitted for clarity.

Figure 4 shows the (**H2$^+$•Cl$^-$**)$_2$ dimer. Consistent with the *P*-1 space group, the monomers are aligned with opposite axes and are centrosymmetric with an inversion centre between the monomers. The bridging Cl$^-$ atoms in (**H2$^+$•Cl$^-$**)$_2$ are held by three hydrogen bonds: a N$_{pyr}$–H$^+$ contact, one N$_{amide}$–H H-bond from one receptor, and another N$_{amide}$–H contact from the second receptor. The hydrogen bond distances are (N$_{pyr}$···Cl) 3.024(4) Å, (N$_{amide}$···Cl) 3.276(4) Å, and (N$_{amide}$···Cl$_b$) 3.426(5) Å. The closest face-to-face arene-arene contacts are 4.004 Å between the pyridine and an opposing benzene ring. A long π–π interaction (3.705 Å) and long bridging hydrogen bond in the Cl$^-$-centred dimer are indicative of weak dimerization. The packing also reveals a lone pair-π interaction (3.203 Å) between –NO$_2$ on one receptor and the 3,5-dinitroarene on another.

Figure 4. Dimeric structure of (**H2$^+$•Cl$^-$**)$_2$ which is stitched together by three hydrogen bonds to each Cl atom.

We have previously observed that **1** adopts unusual conformations to accommodate larger guests that do not fit in the idealized binding pocket. In addition, the sulfonamide receptors form strong dimers with water or halide anions providing seven or six bridging hydrogen bonds, respectively. The sulfonamide receptors are able to form face-to-face dimers because the bend of the sulfonyl bridge places the terminal arene out of the way with

a 230° bend through the N–S bond. Conversely, bis(amide) **2** is planar through the C(=O)–N bond and risks a steric clash if it adopts the '**U**' confirmation. For **H2⁺•Cl⁻**, the weak Cl⁻ bridging contacts discourage the formation of strong dimers in solution and likely contribute to the decreased fluorescence selectivity.

¹H and DOSY NMR studies

The existence and strength of a **H2⁺•Cl⁻** dimer in solution was probed using ¹H NMR dilution experiments and titration of a competing guest, tetrabutylammonium chloride (TBACl). Figure 5 shows the stacked ¹H NMR spectra of **2** and **H2⁺•Cl⁻** (prepared by bubbling gaseous HCl through a stock solution of **2**) in CDCl₃ at 1.0 mM. The amide NH appears at 8.92 ppm as a broad singlet and shifts to 10.04 ppm upon forming the chloride complex. Based on our prior experience with the water-bound dimers of **1** in solution,[18,24] we expected to observe some broadening and shifting of the water peak from its typical value of 1.55 ppm to ca. 3-4 ppm; however, the shift of the resonance remained unchanged.
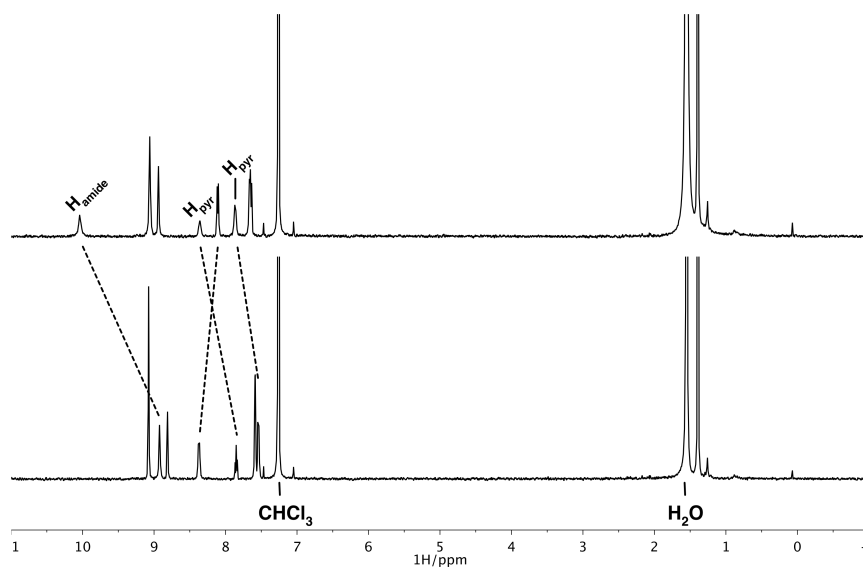
Figure 5. ¹H NMR spectra of **2** (1.0 mM, bottom) and **H2⁺•Cl⁻** (1.0 mM, top) in CDCl₃. Water peak broadening is due to excess HCl.

We next eliminated the formation of a halide-water bridged dimer by observing the shift of the amide and arene protons while adding TBACl. The titration of free base **2** with TBACl from 0 to 18 equivalents is shown in Figure 6. The aromatic peaks remain static and the amide peak shifts downfield with a large excess of Cl⁻. The change in the amide proton ($\Delta\delta$ = 0.22 ppm) is unusual for such an electron-poor amide and coincides with a weak hydrogen bond. The binding isotherm for the titration with Cl⁻ was perfectly linear (Figure 1 in Appendix D) over the range we observed. Based on the concentration of **2,** a linear isotherm and the limits of solubility, the association constant for Cl⁻ is too low for accurate determination by ¹H NMR. The weak association to Cl⁻ further supports our hypothesis that water is not an appropriate bridge for dimerization of **2**.
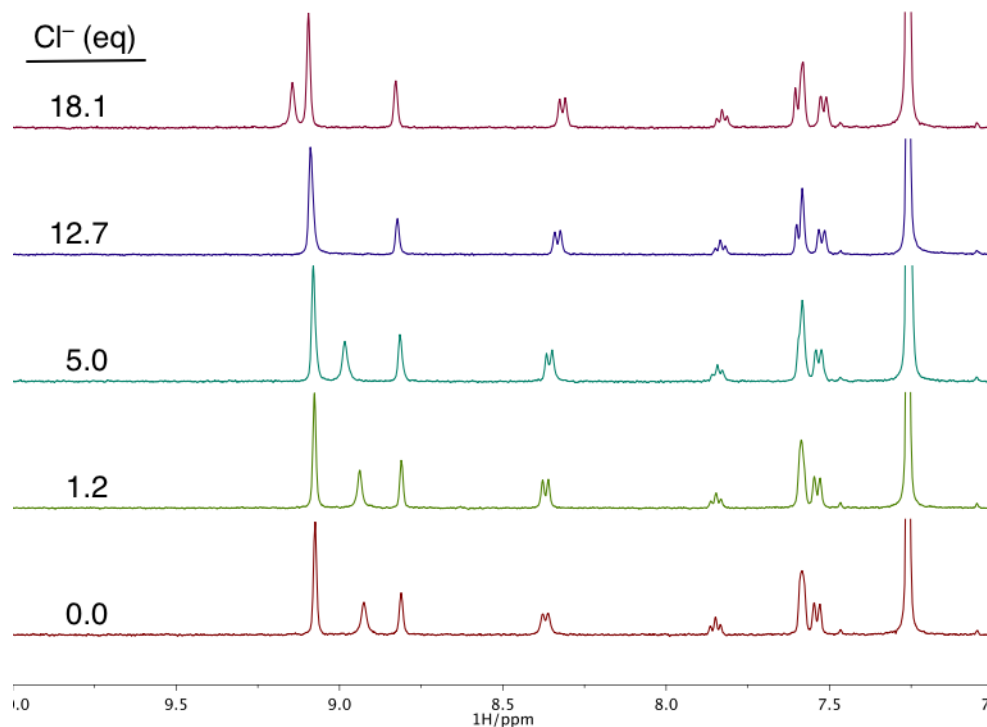
Figure 6. Stacked plot showing **2** titrated with Cl⁻ in water saturated CDCl₃ ([**2**] = 1.0 mM). The amide peak shifts downfield slightly, while other protons remain unchanged.

104

X-ray crystallography pointed towards $\mathbf{H2^+ \cdot Cl^-}$ as a much more likely candidate for dimerization in solution. The ^{1}H NMR spectrum of $\mathbf{H2^+ \cdot Cl^-}$ in Figure 5 was remarkably similar to the spectrum of **2** at equimolar concentration. The water peak remains in place at 1.55 ppm with slight broadening due to the change in ionic strength. The pyridine protons and the amide proton have the largest shifts from **2** to $\mathbf{H2^+ \cdot Cl^-}$. Surprisingly, we do not observe a large shift for the 3,5-dinitroarene peaks as could be expected from anion-π interactions. The 3,5-substitution pattern is optimized for forming anion-π interactions over the alternative C–H hydrogen bond, but neither appears to be significant here. A last test for the presence of an anion-π interaction was to subject **2** to the larger Br^- and I^- ions as their TBA salts. Iodide is noteworthy for forming colored charge-transfer complexes in the presence of electron-poor arenes; however, we did not observe this characteristic color change and thus eliminated anion-π or weak-σ interactions as major contributors.

In a dilution experiment with $\mathbf{H2^+ \cdot Cl^-}$, the addition of $CDCl_3$ down to [**2**] = 0.2 mM resulted in an upfield shift of the amide proton. The small shift (0.15 ppm) was completely mitigated by bubbling additional gaseous HCl into the sample. A second dilution with the addition of HCl saturated $CDCl_3$ resulted in no change of the peaks down to [**2**] = 0.03 mM. The possibility remains for a dimer to be present throughout the dilution and it is simply too strong to break, but more likely the monomer persists over this concentration range (otherwise $K_{dim} > 10^5$ M^{-1}, which is unreasonably high for a dimer held together by only two weak hydrogen bonds).

Diffusion Ordered SpectroscopY (DOSY) is a NMR technique to measure the diffusion constant of each NMR active species via a gradient pulse sequence.[37] The diffusion constant scales with molecule size by eq. **1**:

$$D = k_b T / 6\pi\eta R \tag{1}$$

and correlates with molecular weight.[38] D is the diffusion constant, η is the viscosity, and R

is the radius of a spherical particle. Samples for DOSY were prepared in water-saturated

$CDCl_3$ using the HCl salt $\textbf{H2}^+\bullet\textbf{Cl}^-$ (0.93 mM) and $\textbf{2}$ (1.11 mM). The diffusion constant for

$\textbf{H2}^+\bullet\textbf{Cl}^- = 4.13 \pm 0.34 \times 10^{-10}$ D and $\textbf{2} = 4.55 \pm 0.47 \times 10^{-10}$ D at 298 K. The difference is

statistically insignificant at the 95% confidence interval. Diffusion of residual solvent

$(CHCl_3)$ was the same in both samples, excluding a significant change in solvent viscosity.

These results again indicate that $\textbf{2}$ and $\textbf{H2}^+\bullet\textbf{Cl}^-$ are monomeric in solution.

Conclusion

Substitution of 3,5-dinitrophenyl amides on the 2,6-bis(2-anilinoethynyl)pyridine

scaffold affords a receptor that retains the strong 'OFF-ON' fluorescence response of the

sulfonamide and urea receptors, while also improving upon background fluorescence. The

propensity (or not) to form dimers with HCl highlights the difference in conformation of the

amide from its sulfonamide cousin. In addition, solution studies elucidated a greater

preference for monomers with the amide arms. The low affinity for Cl^- and increased

response to TFA indicate this may be a good strategy for increasing oxoanion selectivity.

Experimental

General Procedures

2,6-Bis(2-ethynylaniline)pyridine $\textbf{3}$ was synthesized using previously reported

procedures (19, 23). ^{1}H and ^{13}C NMR spectra were obtained on an Inova 500 MHz (^{1}H

500.10 MHz, ^{13}C 125.75 MHz) or Bruker Avance-III-HD 600 MHz (^{1}H 599.98 MHz, ^{13}C

150.87 MHz) spectrometer with a Prodigy multinuclear broadband BBO CryoProbe.

Chemical shifts (δ) are expressed in ppm relative to tetramethylsilane (TMS) using residual

non-deuterated solvent (CDCl$_3$: ^{1}H 7.26 ppm, ^{13}C 77.0 ppm). UV-Vis spectra were recorded

on a Hewlett-Packard 8453 UV-Vis spectrophotometer using a 265 nm high-pass filter.

Fluorescence spectra were recorded on a Horiba Jobin-Yvon FluoroMax-4 fluorescence

spectrophotometer equipped with an integrating sphere in O$_2$-containing solvents. Unless

otherwise specified, all reagents were purchased and used as received. Dry solvents were

obtained from distillation using published literature procedures directly before use.

Synthesis of 2

To a vigorously stirred, biphasic mixture of dianiline **3** (100 mg, 0.24 mmol), EtOAc

(10 mL), H$_2$O (10 mL) and K$_2$CO$_3$ (70.8 mg, 0.51 mmol) was added 3,5-dinitrobenzoyl

chloride (111 mg, 0.48 mmol) in EtOAc (2 mL) dropwise via syringe over 2 min. A

precipitate formed after 10 min. After stirring vigorously for 16 h, the precipitate was

isolated and recrystallized from hot EtOAc to yield **2** (62 mg, 45%) as a pale yellow powder.

MP >210 °C (dec) ^{1}H NMR (600 MHz, CDCl$_3$): δ 9.07 (s, 4H), 8.91 (s, 2H), 8.80 (s, 2H),

8.36 (d, J = 8.7 Hz, 2H), 7.84 (t, J = 7.7 Hz, 1H), 7.57–7.60 (m, 4H), 7.53 (d, J = 8.7 Hz,

2H), 1.39 (s, 18H); ^{13}C NMR (151 MHz, CDCl$_3$): δ 176.28, 159.95, 148.65, 148.47, 143.15,

137.67, 137.60, 136.31, 128.73, 128.49, 127.50, 126.23, 121.31, 119.57, 111.08, 96.22, 85.16,

34.79, 31.31; IR (KBr) ν 3389 (NH), 2207 (C≡C), 1655 (C=O); HRMS (ESI) for

C$_{43}$H$_{35}$N$_7$O$_{10}$ [M+H]$^+$: calcd 810.2524, found 810.2555.

Crystal data for 2

Diffraction intensities were collected at 173(2) K on a Bruker Apex2 CCD

diffractometer using MoKα radiation. The space group was determined based on intensity

statistics. Absorption correction was applied by SADABS.[39] The structure was solved by

direct methods and Fourier techniques and refined on F^2 using full matrix least-squares

procedures. All non-H atoms were refined with anisotropic thermal parameters. H atoms

were refined in calculated positions in a rigid group model except those at the N atoms involved in H-bonds. Positions of these H atoms were found on the residual density map and they were refined with isotropic thermal parameters. In the crystal structure there are two solvent CH_2Cl_2 molecules. All calculations were performed by the Bruker SHELXTL (v. 6.10) package.[40]

Crystal data: $C_{45}H_{40}Cl_5N_7O_{10}$, M = 1016.09, 0.20 x 0.10 x 0.02 mm, T = 173(2) K, Triclinic, space group P-1, a = 11.032(2) Å, b = 13.691(2) Å, c = 15.767(3) Å, α = 98.225(4)°, β = 91.235(3)°, γ = 95.894(3)°, V = 2342.9(7) Å^3, Z = 2, D_c = 1.440 Mg/m^3, μ = 0.375 mm^{-1}, F(000) = 1048, $2\theta_{max}$ = 50.0°, 16887 reflections, 8166 independent reflections [R_{int} = 0.0689], R_1 = 0.0727, wR_2 = 0.1380 and GOF = 1.050 for 8166 reflections (616 parameters) with I>2σ(I), R_1 = 0.1622, wR_2 = 0.1730 and GOF = 1.050 for all reflections, max/min residual electron density +0.587/–0.412 eÅ^3. CCDC 1406414.

Bridge to Chapter VI

The results presented in Chapter V describe the use of amide hydrogen bond donors to control the self-assembly of an arylethynyl receptor. The flat geometry and smaller binding pocket in this amide receptor produces a distinct anion binding pocket from that observed in the previously described sulphonamide and urea receptors. Importantly, we have also demonstrated that the 'OFF-ON' fluorescent response is retained in the receptor with electron withdrawing NO_2 groups. In Chapter VI, the fluorescent properties of the phenyl core receptors presented in Chapters II-IV will be further explored. A strategy of variable substitution at two positions, the core and the pendant phenyls, will be used to create a library of fluorescent anion receptors. The optoelectronic properties will be presented and a strategy for developing differential anion sensor arrays will be demonstrated.

CHAPTER VI

OPTOELECTRONIC PROPERTIES AND ANION RESPONSE OF A

1,3-BIS(ARYLETHYNYL)BENZENE RECEPTOR ARRAY

Chapter VI is derived from unpublished, co-authored work performed by undergraduates Leif Winstead and Anne-Lise Emig, and myself. Working under my supervision, Leif and Anne-Lisa synthesized the novel bisurea receptor molecules and performed anion response screens. I performed the synthesis of the penultimate dianilines and the OMe substituted bisureas, along with analysis of the results and writing of this chapter. My advisors, Profs. Darren Johnson and Michael Haley, assisted as editors for this chapter.

Introduction

The development of sensors based on single molecules or discrete molecular assemblies has been a long standing ambition for supramolecular chemistry. A variety of strategies for sensing have been proposed using colorimetric,[1] fluorescence, [2,3] or other techniques[4,5] for signal output. Some signaling examples include dye-displacement assays,[1] aggregation induced emission,[6] and supramolecular gelation.[7] While there continues to be a significant push for supramolecular sensor development, the advancement of technologies from flask to benchtop or field has remained slow.[8] A notable exception is the development of electrochemical sensors for pH and ions based on ISFET technologies.[9] The problem generally centers around the need to develop within a single molecular system the three key factors for efficient sensing: affinity, selectivity, and signal. An example figure of merit for each of these would be limit of detection, competitive interference, and fluorescence

intensity, respectively. The fact that all of these are highly interdependent makes sensor design in a single molecule extremely difficult. One solution to this problem is the introduction of sensing arrays and the use of principle component analysis or similar methods of deconvolution to process complex signals into an analytical sensor output.[10-12]

The first step towards the development of a useful sensor array is the synthesis and characterization of analyte response for a library of receptor molecules. The preparation of such a library is facilitated by identifying a scaffold that provides large sctructural diversity and yet remains easily accessible.[12] Fortunately, previous work in our lab identified such a library can be synthesized from the already reported 2,6-bis(anilinoethynyl)pyridine scaffold **1** in Figure 1.[13] Substitution with electron withdrawing (EWG) and donating (EDG) groups at two positions was demonstrated as an effective means to tune both the emission wavelength (λ_{em}) and the photoluminescent quantum yield (PLQY) of the scaffold. Specifically, variation of the core substituent R was most effective at controlling the emission λ in both penultimate dianilines and the bisureas **1**. In addition, the pendant phenyl substituent R' was effective at altering the PLQY of the receptors, with a limited effect on the λ_{em}.

1
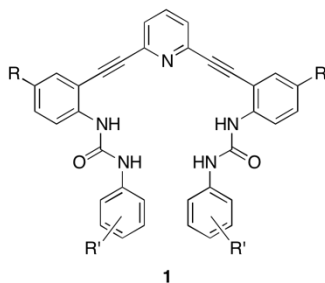
Figure 1. 3,5-bis(arylethynyl)pyridine receptor scaffold with R = *t*-Bu, CO_2Et, CF_3, OMe and R' = 4-OMe, 4-NO_2, 4-H, 2,3,4,5,6-pentafluoro.

While the optoelectronic properties of **1** were studied extensively, the anion response has only been touched upon briefly. A BF_4^- salt of **1•H⁺** (R = CO_2Et, R' = 2,3,4,5,6-pentafluoro) was found to exhibit a large emission increase upon anion exchange with 1 equiv. TBACl in MeCN.[13] The only other example of fluorescence anion response in this scaffold (R = *t*-Bu) was also found to produce an 'OFF-ON' response for Cl⁻, this time with an alternate EWG (R' = NO_2), while the opposite 'ON-OFF' response was observed for an EDG (R' = OMe).[14] From these combined results, a hypothesis has been developed that the presence of an EWG as R' on the pendant phenyl will likely result in a 'turn-ON' response, while the opposite case with an EDG produces a 'turn-OFF' response. In order to test this design principle, we prepared a series of phenyl derived receptors (**2a–d** and **3a–d**) with similar EWG and EDG at R' (see Scheme 1). The optoelectronic properties resulting from R', as well as changes at the core arene (R = *t*-Bu and CF_3), are reported. The new library of compounds has the added benefit of testing the generality of our previously proposed design principles for the pyridine receptors. In addition, screens with multiple anions were performed using a subset of the receptors to probe the change in fluorescence upon anion binding. We have identified the pendant phenyl R' as the key factor in the fluorescence response to anion binding for this scaffold.

Results and Discussion

The synthesis of OMe-urea **2a** (R = *t*-Bu) was previously reported as part of a study into substituent control upon CH hydrogen bond strength and selectivity.[15] The general scheme for the synthesis of arylethynyl bisureas **1** and **2a** is highly amenable to divergent synthesis. Reactions of the penultimate dianiline **5** with commercially available *para*-R'-phenylisocyantes provide a series of electron poor and electron rich ureas, **2b-d**, for

111

comparison to **1** and **2a**. In addition, we sought to test whether the fluorescence emission of this phenyl scaffold could be improved by an EWG on the core (R = CF_3). The dianiline **6** is prepared by Sonogashira cross-coupling of aniline **4** to 1,3-diiodo-5-(trifluoromethyl)benzene. The urea receptors **3a-d** are accessible by similar procedures as for **2a-d**.
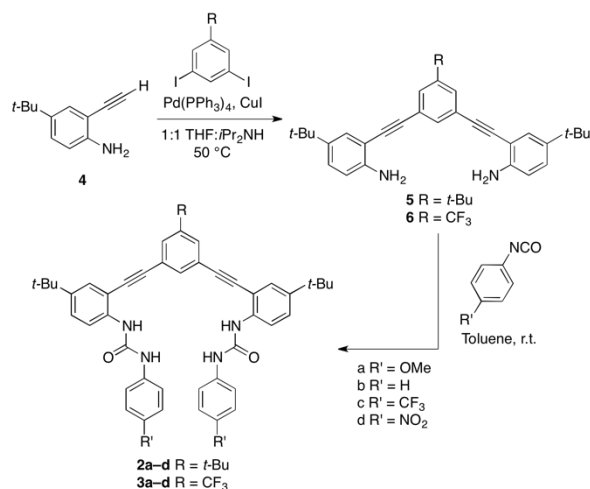
Scheme 1. Divergent synthesis of a fluorescent anion receptor library, **2a-d** and **3a-d**.

With this library of compounds, the absorbance and fluorescence emission properties of the urea receptors were measured in water saturated, basic $CHCl_3$. The UV-vis absorbance spectra shown in Figure 2 have been normalized to molar absorptivity, ε. The pendant phenyl R' group has a strong effect on the absorbance above 310 nm and relatively small changes in absorbance with the core R group appear below 310 nm. For instance, the NO_2 substituted receptors **2d** and **3d** have small variances in intensity but have similar absorbance peaks and overlapping ε for the peak around 365 nm, which is distinct in its intensity from all of the other compounds. This points to the urea acting as the primary

absorber in the 300-365 nm region and correlates well with the absorbance changes for **1**, where the peak at 350 nm shifted ± 15 nm from changes to R' and R near the ureas.[13]
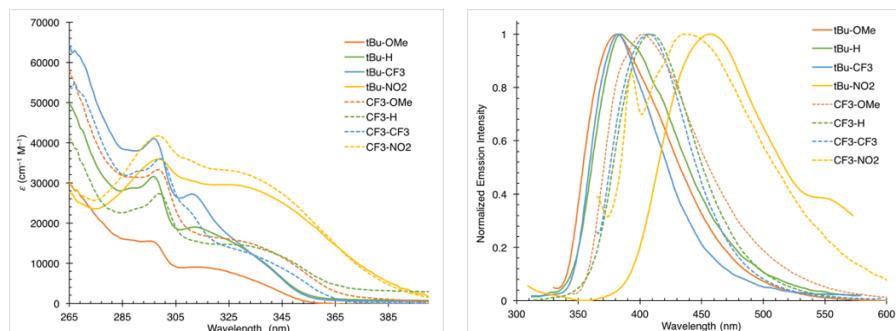
Figure 2. Absorbance (left) and emission (right) spectra of ureas **2a-d** and **3a-d** in H_2O sat. $CHCl_3$.

The emission spectra for **2a-d** and **3a-d** were also measured using the same solvent system. Samples were diluted to an approximate absorbance of 0.1-0.2 (~1-20 μM) for peaks in the 300-350 nm region and emission spectra are normalized to 1 (Figure 2, right). Contrary to trends in the absorbance spectra, emission peaks cluster according to the core substituent (R, *t*-Bu λ_{em} = 382 ± 2 nm and CF_3 λ_{em} = 406 ± 3 nm). Just as for absorbance, the outlier for emission λ is the pendant R' = NO_2 on **2d** and **3d** with λ_{em} = 457 and 437 nm, respectively. The NO_2 substituents acts as a strong fluorescence quencher; **2-3d** have the least intense emission which leads to a prominent H_2O Raman peak at 297 nm (λ_{exc} = 350 nm) in the spectra of **3d**. The emission properties of **2a-d** and **3a-d** are tabulated in Table 1, including Stokes shifts ranging from 66 nm to 163 nm. This receptor library covers a respectable range of λ_{em} and fluorescence intensity with simple substitutions; however, it is difficult to correlate emission intensity of the free receptor with its ability to act as a sensor. Therefore, we must also consider the fluorescence response to anion binding as well.

Table 1. Emission properties of receptors **2a-d** and **3a-d**, and intensity ratio response to anions.

Host	λ_{exc} (nm)	λ_{em} (nm)	Stokes shift (nm)	Cl^{-a}	Br^{-a}	I^{-a}	NO_3^{-a}
2a	315	381	66	—	—	—	—
2b	299	384	85	2.45	1.26	-0.98	2.09
2c	297	382	85	10.72	-0.39	0.46	25.21
2d	294	457	163	58.13	1.39	-0.62	49.91
3a	330	402	72	—	—	—	—
3b	336	409	73	2.04	0.58	-0.96	1.45
3c	350	407	57	1.78	0.48	—	1.38
3d	350	437	87	0.32	-0.70	-0.82	0.05

[a]Intensity ratio, change in emission intensity with 100 equiv. TBA salt calculated by ($IR = I - I_o / I_o$). Values represent a single experiment; therefore, no error is reported.

In order to quickly screen the library of receptors for anion response, a simple methodology for testing the maximum fluorescence intensity change with TBA salt addition was developed. A stock solution of receptor ([H] = 2 μM) was prepared in water saturated, basified CHCl$_3$ and divided into five vials, of which four contained dried salts that were premeasured to provide [X⁻] = 2 mM in 2 mL total volume. The fifth vial was used as a control to measure baseline fluorescence of the receptor. The anions tested (Cl⁻, Br⁻, I⁻, and NO$_3$⁻) were chosen as a representative series of the halides and a non-spherical oxoanion. Fluorescence emission was measured by excitation at the optimal λ_{exc} for the free receptor and anion response is reported as the intensity ratio ($IR = I - I_o / I_o$) in Table 1.

In order to more easily visualize trends, the fluorescence intensity ratios have been converted to a heat map in Figure 3 (left). The dark blue and light blue boxes indicate quenching or weak 'turn-ON' upon anion binding, while orange to yellow are examples of strong 'turn-ON' response. A cut-off of $IR = 2.5$ has been applied to highlight the small

changes in the majority of cases. The first trend that emerges is the general ability of I⁻ to act as a quencher, which is typical for heavy atom quenching. Bromide also produces weak fluorescence changes but most often generates a 'turn-ON' response. The largest 'turn-ON' responses for this array result from addition of Cl⁻ or NO_3^-.
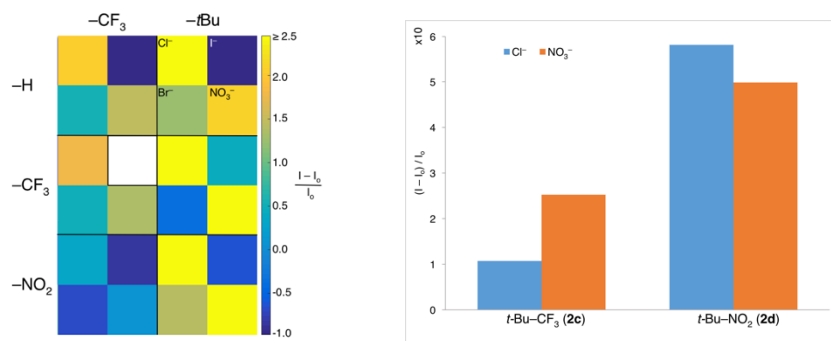
Figure 3. (left) Heat map of anion response for receptors **2a-d** and **3a-d** with 100 equiv. Cl⁻, Br⁻, I⁻, and NO_3^-. Color correspond to intensity ratio (Table 1) with a maximum cut-off at 2.5 to highlight small changes. (right) Anion response to Cl⁻ and NO_3^- for the two most intense receptors, **2c** and **2d**.

The two most effective molecules for fluorescent 'turn-ON' response in this array are **2c** and **2d** (R = t-Bu, R' = CF_3 and NO_2). A graph of the IR for these receptors with Cl⁻ and NO_3^- is shown in Figure 3 which highlights the extreme response observed for **2d** especially (IR = (Cl⁻) 58.13 and (NO_3^-) 49.91). Interestingly, the selectivity for Cl⁻ over NO_3^- appears to switch between **2d** and **2c**. The difference is quite large is these initial studies; however, additional experimental repetitions are required to determine the significance of this result. Insight into the mechanism for this large 'turn-ON' response is obtained by comparing the frontier molecular orbital (MO) maps for **2c** and **2d**.

The structures of free receptors **2c-d** were optimized in the gas phase using Gaussian 09 and molecular orbitals were calculated using B3LYP/6-31G*//B3LYP-D3/6-311G**.[16-18] The HOMO and LUMO orbitals for **2c-d** are shown in Figure 4 to demonstrate

115

the effect of R' upon the frontier MOs. The NO_2 substituted **2d** presents nearly complete

orbital separation between the HOMO and LUMO, with the HOMO residing on the

electron rich core. The MO separation leads to significant charge transfer upon excitation

and likely results in the quenched fluorescence of free **2d**.
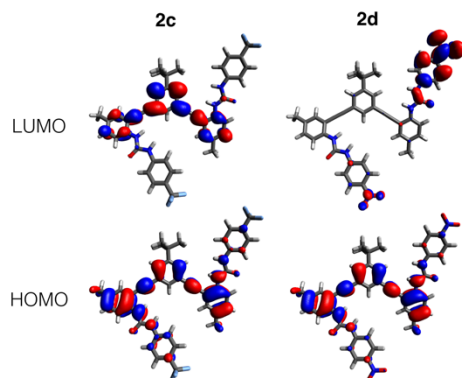
Figure 4. Frontier MO calculated for optimized structure of **2c** and **2d** using Gaussian 09 with B3LYP/6-31G*//B3LYP-D3/6-311G**.

The CF_3 receptor **2c**, however, has predominantly overlapping HOMO and LUMO

with limited ability to undergo charge transfer. **2c** also exhibits a large background

fluorescence for the free receptor. Based upon this comparison, the difference in *IR* for **2c**

and **2d** can be attributed predominantly to a difference in the signal gain for each receptor,

i.e. quenching of **2d** enhances the possible anion response signal range. The open

conformation shown in Figure 4 represents only one asymmetric conformation for these

receptors; it is likely that exploring the other two symmetric conformations along with anion

binding will further elucidate the mechanism for anion response observed in this library.

Conclusion

The study of anion response for an array of fluorescent arylethynyl receptors has helped to better our understanding of design and fluorescent mechanisms for the arylethynyl receptor scaffold. Importantly, we have demonstrated that the aryl CH receptors **2** and **3** not only function similarly to the pyridine **1**, but exhibit exceptional 'turn-ON' response in certain cases. Additionally, we are now able to sense biologically relevant anions without the need to vicariously sense protons simultaneously.[19] The large 'turn-ON' response for **2c** is an exciting prospect as it will be beneficial for developing a Cl⁻ sensing method with very low limit of detection. While computations of the frontier MOs have provided some insight into the mechanism of fluorescence, it would be beneficial to examine alternative conformations and the role of anion binding by this method. The synthetic methods describe here offer an efficient path to divergent synthesis of ever larger receptor arrays. In combination with a greater understanding of molecular sensor design and high-throughput anion screening, this library will hopefully lead to the rapid development of new sensor platforms.

Experimental

General Procedures

^{1}H and ^{13}C NMR spectra were obtained on a Bruker Avance-III-HD 600 MHz (^{1}H 599.98 MHz, ^{13}C 150.87 MHz) spectrometer with a Prodigy multinuclear broadband BBO CryoProbe or an Inova 500 MHz (^{1}H 500.10 MHz, ^{13}C 125.75 MHz). Chemical shifts (δ) are expressed in ppm relative to tetramethylsilane (TMS) using residual non-deuterated solvent (CDCl$_3$: ^{1}H 7.26 ppm, ^{13}C 77.0 ppm; DMSO-d_6: ^{1}H 2.50 ppm, ^{13}C 39.51 ppm). UV-Vis spectra were recorded on a Hewlett-Packard 8453 UV-Vis spectrophotometer using a 265 nm high-pass filter. Fluorescence spectra were recorded on a Horiba Jobin-Yvon

FluoroMax-4 fluorescence spectrophotometer in O_2-containing solvents. Unless otherwise specified, all reagents were purchased and used as received. Dry solvents were obtained from distillation using published literature procedures directly before use. Procedures for the synthesis of 2,6-bis(2-ethynylaniline)pyridine **4**[14] and 1,3-diiodo-5-(trifluoromethyl)benzene[20] have been previously reported.

Synthesis

Aniline 6. 1,3-diiodo-5-(trifluoromethyl)benzene (0.658 g, 1.66 mol) was taken up in dry, N_2-purged THF (20 mL) and i-Pr$_2$NH (20 mL). Pd(PPh$_3$)$_4$ (0.096 g, 0.083 mmol) and CuI (0.063 g, 0.332 mmol) were added, followed by addition of 2-ethynyl-4-t-butylaniline (0.861 g, 4.97 mmol) in THF (7 mL). The reaction was stirred for 16 h at 50 °C then filtered over silica and washed with DCM (100 mL). The crude product was purified by flash silica column chromatography (25% EtOAc in hexanes) to provide **6** (0.456 g, 55%) as a white powder. ^{1}H NMR (600 MHz, DMSO-d_6) δ 8.17 (s, 1H), 8.00 (s, 2H), 7.25 (d, J = 2.4 Hz, 2H), 7.18 (dd, J = 8.6, 2.5 Hz, 2H), 6.69 (d, J = 8.6 Hz, 2H), 5.54 (s, 4H), 1.23 (s, 18H); ^{19}F NMR (565 MHz, DMSO-d_6) δ -61.43; ^{13}C NMR (151 MHz, DMSO-d_6) δ147.99, 137.88, 136.79, 128.20, 127.88, 126.60, 124.84, 114.03, 103.81, 91.29, 90.19, 33.47, 31.24, 31.19. HRMS (ESI) for C$_{31}$H$_{32}$N$_2$F$_3$ [M+H]$^+$: calcd 489.2518, found 489.2501.

General Urea Synthesis. In an oven dried flask, dianiline **5** or **6** (0.1 g) was taken up in dry toluene (40 mL) under dry N_2 and R'-phenylisocyanate (2.3 equiv.) was added. The reaction was allowed to stir at r.t.-60 °C until the dianiline had been consumed as monitored by ^{1}H NMR, typically 24-48 h. The precipitated product was recovered by vacuum filtration and triturated with 95% EtOH until analytically pure.

Urea 2b. Dianiline **5** (0.100 g, 0.22 mmol) was reacted with phenylisocyanate (0.086 g, 0.72 mmol) at 60 ºC according to the general procedure and urea **2b** (0.101 g, 65%) was

isolated as a white powder. ^{1}H NMR (600 MHz, DMSO-d_6) δ 9.45 (s, 2H), 8.22 (s, 2H), 7.99 (d, J = 8.8 Hz, 2H), 7.83 (s, 1H), 7.73 (s, 2H), 7.53 (s, 2H), 7.47 (d, J = 8.0 Hz, 4H), 7.43 (d, J = 9.1 Hz, 2H), 7.27 (t, J = 7.8 Hz, 4H), 6.97 (t, J = 7.5 Hz, 2H), 1.34 (s, 9H), 1.30 (s, 18H); ^{13}C NMR (151 MHz, DMSO-d_6) δ 152.28, 151.79, 144.69, 139.52, 137.79, 131.71, 128.93, 128.85, 128.76, 126.87, 122.68, 122.02, 120.01, 118.26, 111.32, 94.16, 86.27, 34.64, 33.99, 31.03, 30.81.

Urea 2c. Dianiline **5** (0.103 g, 0.22 mmol) was reacted with 4-trifluoromethyl-phenylisocyanate (0.100 g, 0.54 mmol) at r.t. according to the general procedure and urea **2c** (0.063 g, 34%) was isolated as a taupe powder. ^{1}H NMR (600 MHz, DMSO-d_6) δ 9.84 (s, 2H), 8.34 (s, 2H), 7.97 (d, J = 8.7 Hz, 2H), 7.83 (s, 1H), 7.71 (d, J = 1.4 Hz, 2H), 7.67 (d, J = 8.5 Hz, 4H), 7.61 (d, J = 8.6 Hz, 4H), 7.54 (d, J = 2.4 Hz, 2H), 7.45 (dd, J = 8.8, 2.4 Hz, 2H), 1.31 (s, 9H), 1.30 (s, 18H); ^{19}F NMR (282 MHz, DMSO-d_6) δ -60.11; ^{13}C NMR (151 MHz, DMSO-d_6) δ 152.10, 151.80, 145.20, 143.31, 137.38, 131.75, 128.95, 128.82, 126.92, 126.13 (d, J = 3.8 Hz), 124.50 (d, J = 271.1 Hz), 122.65, 121.91 (d, J = 31.6 Hz), 120.30, 117.87, 111.86, 94.21, 86.22, 34.60, 34.03, 31.01, 30.77.

Urea 2d. Dianiline **5** (0.104 g, 0.22 mmol) was reacted with 4-nitrophenylisocyanate (0.084 g, 0.50 mmol) at r.t. according to the general procedure and urea **2d** (0.112 g, 80%) was isolated as a pale yellow powder. ^{1}H NMR (600 MHz, DMSO-d_6) δ 10.14 (s, 2H), 8.45 (s, 2H), 8.16 (d, J = 9.1 Hz, 4H), 7.97 (d, J = 8.7 Hz, 2H), 7.83 (s, 1H), 7.73 – 7.64 (m, 6H), 7.55 (d, J = 2.4 Hz, 2H), 7.47 (dd, J = 8.8, 2.4 Hz, 2H), 1.31 (s, 9H), 1.30 (s, 18H); ^{13}C NMR (151 MHz, DMSO-d_6) δ 151.83, 146.17, 145.52, 141.09, 137.08, 131.81, 128.97, 128.87, 126.95, 125.16, 122.61, 120.42, 117.49, 112.10, 94.28, 86.15, 34.61, 34.06, 31.00, 30.77.

Urea 3a. Dianiline **6** (0.125 g, 0.26 mmol) was reacted with 4-methoxy-phenylisocyanate (0.088 g, 0.59 mmol) at 50 ºC according to the general procedure and urea

3a (0.122 g, 60%) was isolated as a white powder. ^{1}H NMR (600 MHz, DMSO-d_6) δ 9.24 (s, 2H), 8.28 (s, 1H), 8.16 (s, 2H), 8.10 (s, 2H), 8.04 (d, J = 8.8 Hz, 2H), 7.56 (d, J = 2.4 Hz, 2H), 7.46 (dd, J = 9.3, 2.5 Hz, 2H), 7.38 (d, J = 9.0 Hz, 4H), 6.86 (d, J = 9.0 Hz, 4H), 3.70 (s, 6H), 1.30 (s, 18H); ^{19}F NMR (565 MHz, DMSO-d_6) δ -61.49; ^{13}C NMR (151 MHz, DMSO-d_6) δ 154.63, 152.36, 144.44, 138.31, 137.72, 132.37, 130.25 (q, J = 32.6 Hz), 127.81 (d, J = 3.0 Hz), 128.19 (d, J = 223.2 Hz), 124.28, 120.22, 119.69, 114.05, 110.22, 92.24, 88.56, 55.14, 33.98, 31.01, 30.96.

Urea 3b. Dianiline **6** (0.130 g, 0.27 mmol) was reacted with phenylisocyanate (0.110 g, 0.93 mmol) at 60 ºC according to the general procedure and urea **3b** (0.067 g, 35%) was isolated as a white powder. ^{1}H NMR (600 MHz, DMSO-d_6) δ 9.42 (s, 2H), 8.28 (s, 1H), 8.26 (s, 2H), 8.11 (s, 2H), 8.03 (d, J = 8.8 Hz, 2H), 7.50 – 7.42 (m, 6H), 7.28 (t, J = 7.8 Hz, 4H), 6.98 (t, J = 7.3 Hz, 2H); ^{19}F NMR (565 MHz, DMSO-d_6) δ -61.50; ^{13}C NMR (126 MHz, DMSO-d_6) δ 152.22, 144.71, 139.43, 138.10, 128.90 (d, J = 15.7 Hz), 128.84, 127.45, 123.18 (d, J = 273.7 Hz), 119.96, 118.35, 110.54, 92.23, 88.55, 33.99, 30.99.

Urea 3c. Dianiline **6** (0.100 g, 0.22 mmol) was reacted with 4-trifluoromethyl-phenylisocyanate (0.086 g, 0.46 mmol) at r.t. according to the general procedure and urea **3c** (0.047 g, 27%) was isolated as a white powder. ^{1}H NMR (600 MHz, DMSO-d_6) δ 9.82 (s, 2H), 8.38 (s, 2H), 8.29 (s, 1H), 8.09 (s, 2H), 8.02 (d, J = 8.8 Hz, 2H), 7.68 (d, J = 8.5 Hz, 4H), 7.64 – 7.56 (m, 6H), 7.49 (dd, J = 8.8, 2.4 Hz, 2H), 1.30 (s, 18H); ^{19}F NMR (565 MHz, DMSO-d_6) δ -60.15, -61.54; ^{13}C NMR (151 MHz, DMSO-d_6) δ 152.05, 145.17, 143.22, 137.81, 137.68, 129.04, 127.87 (d, J = 5.5 Hz), 127.50 (d, J = 54.3 Hz), 126.12 (d, J = 3.5 Hz), 124.50 (d, J = 270.8 Hz), 124.22, 120.19, 117.94, 111.01, 92.31, 88.47, 34.04, 30.98.

Urea 3d. Dianiline **6** (0.103 g, 0.22 mmol) was reacted with 4-nitro-phenylisocyanate (0.086 g, 0.53 mmol) at r.t. according to the general procedure and urea **3d** (0.063 g, 36%)

was isolated as a yellow powder. ^{1}H NMR (600 MHz, DMSO-d_6) δ 10.10 (s, 2H), 8.48 (s, 2H), 8.28 (s, 1H), 8.16 (d, J = 8.7 Hz, 4H), 8.09 (s, 2H), 8.01 (d, J = 8.8 Hz, 2H), 7.60 (d, J = 9.2 Hz, 4H), 7.60 (d, J = 2.4 Hz, 2H), 7.50 (dd, J = 8.6, 2.5 Hz, 2H), 1.31 (s, 18H); ^{19}F NMR (565 MHz, DMSO-d_6) δ -61.53; ^{13}C NMR (151 MHz, DMSO-d_6) δ 151.79, 146.09, 145.51, 141.15, 137.83, 137.39, 129.09, 127.91 (d, J = 7.0 Hz), 127.55, 125.16, 124.19, 123.32 (d, J = 273.1 Hz), 120.33, 117.56, 111.27, 92.37, 88.40, 34.08, 30.98.

Bridge to Chapter VII

The results presented in Chapter VI describe the application of the CH arylethynyl scaffold to fluorescent anion sensing. The optoelectronic properties of the phenyl receptors follow the same trends as the pyridine receptors studied previously. Significantly, two receptors have been identified as exceptional 'turn-ON' fluorescent receptors for Cl$^-$ and NO$_3^-$. The calculated frontier MOs provide a possible explanation for the fluorescence intensities and further work with this library will provide a greater understanding of the anion sensing mechanism. The final Chapter VII will offer possible future directions for the aryl CH hydrogen bonding receptors we have described throughout this dissertation.

CHAPTER VII

CONCLUDING REMARKS AND FUTURE DIRECTIONS

<u>Concluding Remarks</u>

The goal of this dissertation has been to explore the role of aryl CH hydrogen bonds in anion binding. In the course of this work, we have increased our fundamental understanding of this non-traditional interaction and the breadth of possibility it holds for designing supramolecular systems. We first demonstrated the ability of this hydrogen bond donor to replace a traditional strong donor, specifically an N^+–H donor, in an anion receptor with no loss of function. The comparison of these two hydrogen bond donors with different polarizations provides an important estimate of the binding energy for C–$H\cdots Cl^-$ hydrogen bonds. Notably, the strength of this interaction is comparable to weak, traditional O–H and N–H hydrogen bonds.

Furthermore, we explored the possibility to control the strength and selectivity of this interaction through inclusion of electron withdrawing and donating groups. The hydrogen bond strength can be predicted across a series of similar receptors using empirical σ parameters and by computed electrostatic potentials. The substituent effects on the aryl CH hydrogen bond provide a wide energy range for tuning binding strength without the fear of compromising the useful pK_a regime through ionization, due to benzene's high pK_a. In addition, we discovered the importance of considering both the resonance and inductive contribution of substituents on the formation of an aryl CH hydrogen bond. The partial covalent bond character in this interaction leads to selectivity based on both host substitution and anionic guest polarizability and basicity. These characteristics of anions are

generalized by hard-soft acid-base theory and future studies may be able to place the CH hydrogen bond into this series.

Deuterium labeling studies corroborated the importance of this interaction through the measurement of equilibrium isotope effects. The zero-point energy change upon heavy atom labeling results from a narrower potential energy surface. The incorporation of a deuterium into the CH hydrogen bond results in the weakening of the C–H···Cl$^-$ interaction. This change arises as the deuterium stretches between the C and Cl$^-$ in hydrogen bond formation and is direct evidence for the partial covalency in this interaction. The observed EIE for anion binding to Cl$^-$ corroborates results from computation and substituent studies that point to lp: $\longrightarrow \sigma^*$ donation taking place upon CH hydrogen bond formation.

Considering the entire receptor anion binding pocket, we have prepared a truncated bisamide receptor and studied its self-assembly in solution and the solid state. The lack of anion binding in solution underscores the influence of the urea as a directing group for this receptor scaffold. In addition, the retention of fluorescence sensing with the bis(amide)arylethynyl scaffold solidifies the importance of the arylethynyl backbone for sensing. The weak anion binding and strong fluorescence response points to protonation as the main sensing mechanism. However, this hypothesis bears further study specifically in light of the fluorescence response of the aryl CH receptors.

Finally, the aryl CH receptor scaffold has been shown to act as a fluorescent anion receptor with equal potency to the pyridine class of receptors. The results of anion screening for a small sensor array have identified promising receptors for further development of selective sensors and possibly a differential anion sensing scheme. The presence of an EWG on the pendant phenyl leads to a 'turn-ON' response, which is desirable for low background

123

signal in sensing. In addition, the 'turn-ON' fluorescence response without a pH sensitive pyridine is a promising development for future molecular chloride probes that function in cells at physiological pH.

Future Directions

The research presented herein has demonstrated the impact aryl CH hydrogen bonds can have upon supramolecular structure and selective guest binding. Future work in this area will continue to explore the design of CH arylethynyl anion receptors for fluorescent anion sensing applications. The preliminary work in Chapter 6 on the assembly of a fluorescent array can be expanded to include additional structures from this dissertation. As well, completing the fluorescence screen against the electron donating pendant phenyls and relevant anions will allow a complete structure-activity relationship to be developed for anion sensing. With the plethora of data obtained in these studies, it would be beneficial to apply machine learning methods, such as principle component analysis and neural networks, to the identification of key sensor design factors and possible combinations of receptors for analyte discrimination. This strategy may be applied to other structures, for example receptors **1-3** in Scheme 1.
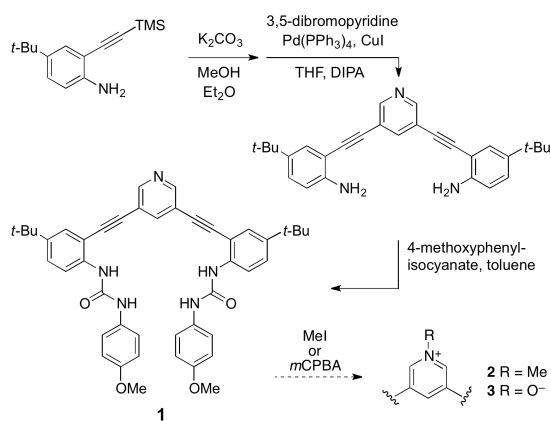
Scheme 1. Preliminary synthesis of a 3,5-pyridine CH receptor and proposed modifications.

The synthesis of 3,5-bis(arylethynyl)-pyridine receptor **1** is already underway. The flipped pyridine receptor will provide a binding pocket with five persistent hydrogen bond donors and an exterior nitrogen which will polarize the CH donor. A synthetic route to receptor **1** is shown in Scheme 1. In addition, the pyridine nitrogen can be further functionalized by protonation, methylation (**2**), or conversion to the N-oxide (**3**) to increase CH polarization. These modifications will allow for separation of pyridine-pyridinium ionization from alkyne rotation in the binding event, and provide a way to study how each contributes to the fluorescence response.

SUPPLEMENTARY INFORMATION FOR CHAPTER II

Titrations

NMR Titrations

Tetrabutylammonium chloride with 5. A stock solution of **5** (1.48 mg, [R]=0.69 mM) in CDCl$_3$ (3 mL) was prepared and used in the dilution of TBACl guest solution (5.05 mg, [G]=7.57 mM). The remaining stock solution (0.6 mL) was used as the starting volume in an NMR tube. The calculated association constants for Cl$^-$ with **5** had large error and were not consistent across titrations; therefore, reported association constants were determined using UV-Vis titrations. The procedure for this titration is provided for comparison of structural characteristics apparent in the NMR (downfield shifts of urea and aryl protons) to crystallographic data.
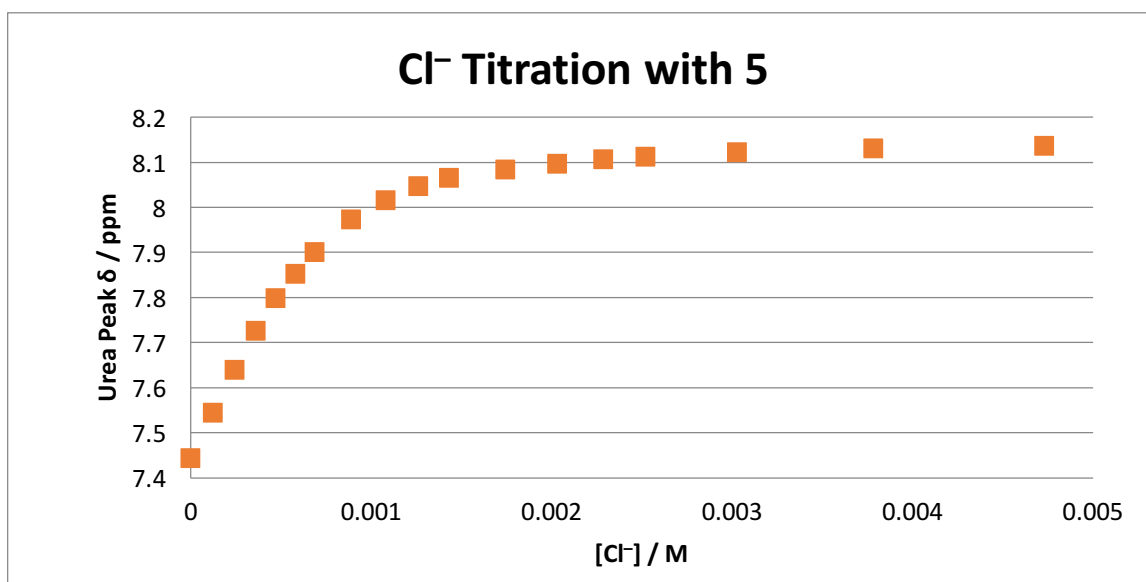
Figure 1. Binding isotherm for Cl$^-$ titration of **5** in CDCl$_3$ by ^{1}H NMR.

Table 1. Representative titration data for Cl⁻ with **5**.

	Guest (μL)	[**5**] (M)	[Cl⁻] (M)	Equiv.	δ (ppm)
0	0	6.86E-04	0.00E+00	0.00	7.443
1	10	6.86E-04	1.24E-04	0.18	7.545
2	20	6.86E-04	2.44E-04	0.36	7.640
3	30	6.86E-04	3.61E-04	0.53	7.726
4	40	6.86E-04	4.73E-04	0.69	7.798
5	50	6.86E-04	5.82E-04	0.85	7.852
6	60	6.86E-04	6.88E-04	1.00	7.900
7	80	6.86E-04	8.91E-04	1.30	7.973
8	100	6.86E-04	1.08E-03	1.58	8.016
9	120	6.86E-04	1.26E-03	1.84	8.047
10	140	6.86E-04	1.43E-03	2.09	8.065
11	180	6.86E-04	1.75E-03	2.55	8.084
12	220	6.86E-04	2.03E-03	2.96	8.097
13	260	6.86E-04	2.29E-03	3.34	8.106
14	300	6.86E-04	2.52E-03	3.68	8.112
15	400	6.86E-04	3.03E-03	4.41	8.122
16	600	6.86E-04	3.79E-03	5.52	8.130
17	1000	6.86E-04	4.73E-03	6.90	8.137

Tetrabutylammonium bromide with 5. A stock solution of **5** (1.98 mg, [R]=0.92 mM) in CDCl₃ (3 mL) was prepared and used in the dilution of TBABr guest solution (19.58 mg, [G]=26.41 mM). The remaining stock solution (0.6 mL) was used as the starting volume in an NMR tube.
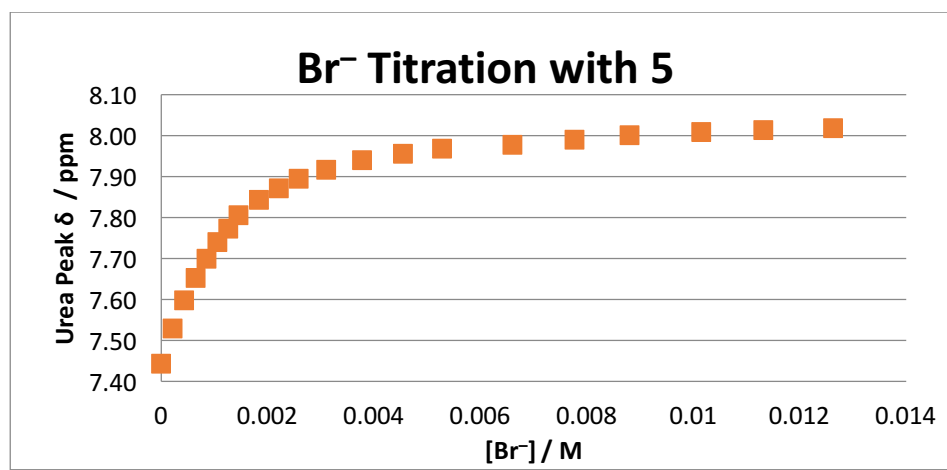
Figure 2. Binding isotherm for Br⁻ titration of **5** in CDCl₃ by ¹H NMR.

Table 2. Representative titration data for Br⁻ with **5**.

	Guest (μL)	[5] (M)	[Br⁻] (M)	Equiv.	δ (ppm)
0	0	9.18E-04	0.00E+00	0.00	7.443
1	5	9.18E-04	2.18E-04	0.24	7.528
2	10	9.18E-04	4.33E-04	0.47	7.597
3	15	9.18E-04	6.44E-04	0.70	7.652
4	20	9.18E-04	8.52E-04	0.93	7.699
5	25	9.18E-04	1.06E-03	1.15	7.739
6	30	9.18E-04	1.26E-03	1.37	7.773
7	35	9.18E-04	1.46E-03	1.59	7.805
8	45	9.18E-04	1.84E-03	2.01	7.842
9	55	9.18E-04	2.22E-03	2.42	7.871
10	65	9.18E-04	2.58E-03	2.81	7.894
11	80	9.18E-04	3.11E-03	3.38	7.916
12	100	9.18E-04	3.77E-03	4.11	7.939
13	125	9.18E-04	4.55E-03	4.96	7.955
14	150	9.18E-04	5.28E-03	5.75	7.968
15	200	9.18E-04	6.60E-03	7.19	7.977
16	250	9.18E-04	7.77E-03	8.46	7.990
17	300	9.18E-04	8.80E-03	9.59	8.000
18	375	9.18E-04	1.02E-02	11.06	8.008
19	450	9.18E-04	1.13E-02	12.33	8.013
20	550	9.18E-04	1.26E-02	13.76	8.017
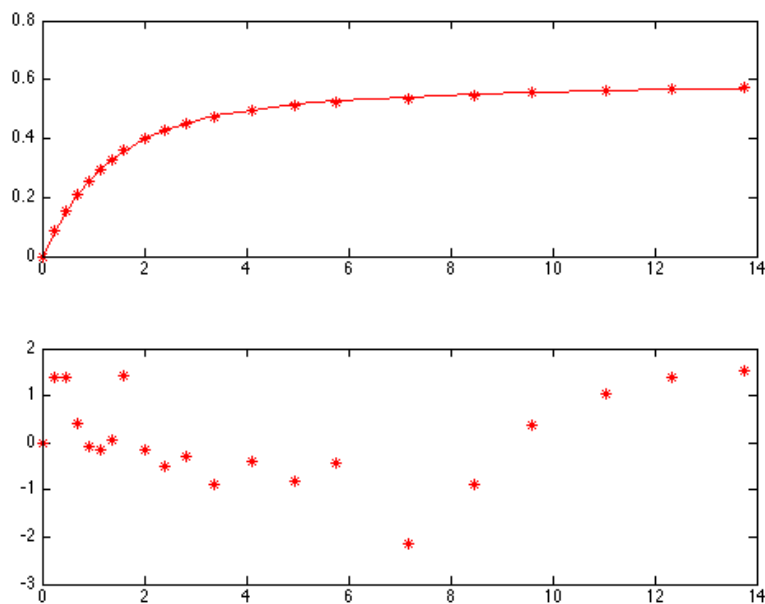
Figure 3. Matlab fit for the binding isotherm of Br⁻ titration with **5**.
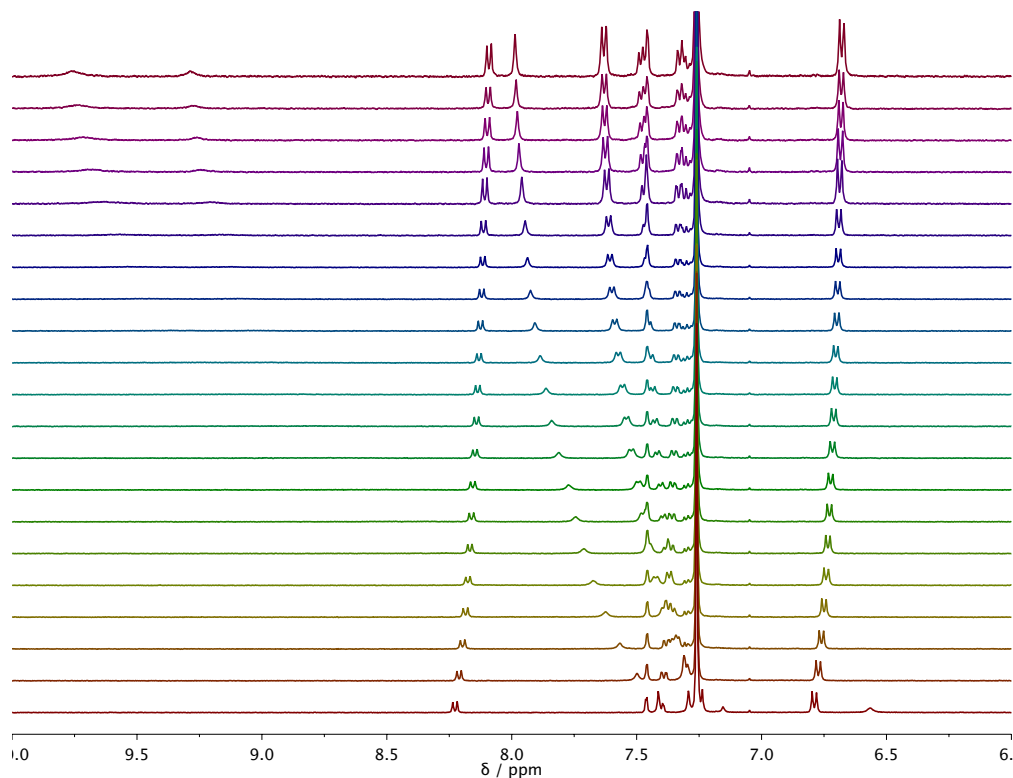
Figure 4. ^{1}H NMR spectra of Br$^-$ titration with **5**.

Tetrabutylammonium iodide with 5. A stock solution of **5** (4.05 mg, [R]=1.88 mM) in CDCl$_3$ (3 mL) was prepared and used in the dilution of TBAI guest solution (50.21 mg, [G]=58.47 mM). The remaining stock solution (0.6 mL) was used as the starting volume in an NMR tube.

Table 3. Representative titration data for I$^-$ with **5**.

	Guest (µL)	[5] (M)	[I$^-$] (M)	Equiv.	δ (ppm)
0	0	1.88E-03	0.00E+00	0.00	7.418
1	5	1.88E-03	4.83E-04	0.26	7.442
2	10	1.88E-03	9.58E-04	0.51	7.460
3	15	1.88E-03	1.43E-03	0.76	7.486
4	20	1.88E-03	1.89E-03	1.00	7.505
5	25	1.88E-03	2.34E-03	1.25	7.524
6	30	1.88E-03	2.78E-03	1.48	7.540
7	35	1.88E-03	3.22E-03	1.72	7.555

8	40	1.88E-03	3.65E-03	1.95	7.570
9	50	1.88E-03	4.50E-03	2.39	7.594
10	60	1.88E-03	5.32E-03	2.83	7.616
11	70	1.88E-03	6.11E-03	3.25	7.635
12	80	1.88E-03	6.88E-03	3.66	7.650
13	90	1.88E-03	7.63E-03	4.06	7.666
14	115	1.88E-03	9.40E-03	5.01	7.693
15	140	1.88E-03	1.11E-02	5.89	7.715
16	190	1.88E-03	1.41E-02	7.49	7.744
17	240	1.88E-03	1.67E-02	8.90	7.765
18	290	1.88E-03	1.91E-02	10.14	7.776
19	390	1.88E-03	2.30E-02	12.26	7.794
20	590	1.88E-03	2.90E-02	15.44	7.812
21	1090	1.88E-03	3.77E-02	20.08	7.824
22	1590	1.88E-03	4.24E-02	22.60	7.828
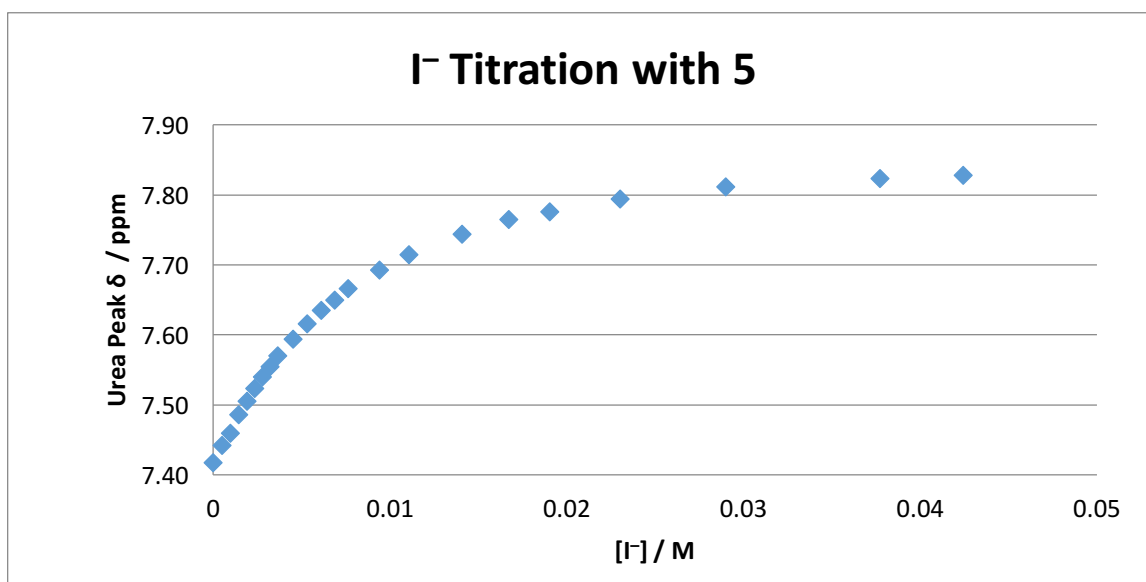
Figure 5. Binding isotherm for I⁻ titration of **5** in CDCl$_3$ by ^{1}H NMR.
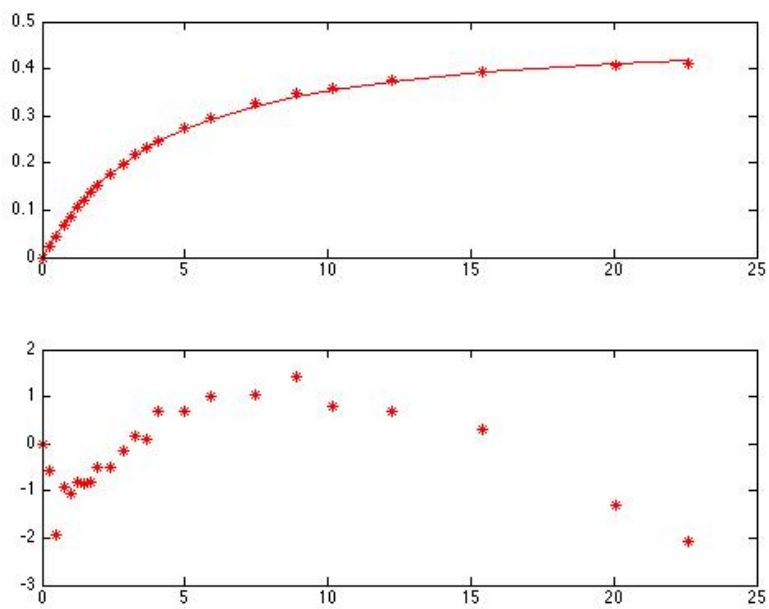
Figure 6. Matlab fit for the binding isotherm of I⁻ titration with **5**.
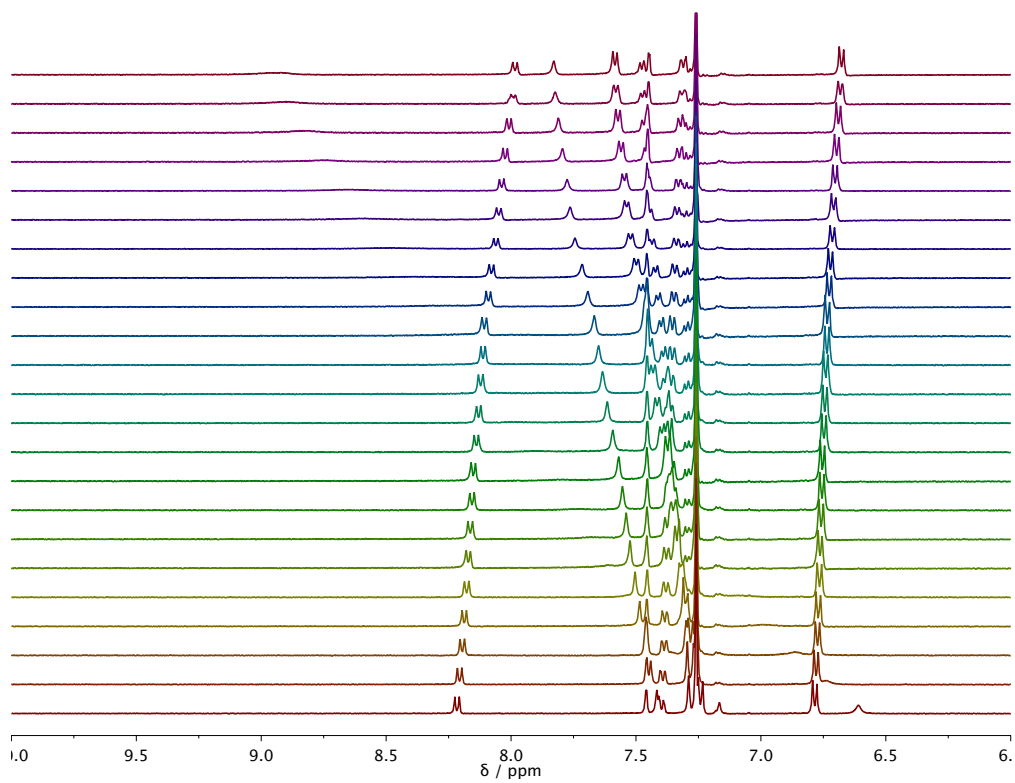
Figure 7. ¹H NMR spectra of I⁻ titration with **5**.

Tetrabutylammonium chloride with 2. A stock solution of **2** (2.87 mg, [**2**]=1.33 mM) in CDCl$_3$ (3 mL) was prepared and used in the dilution of TBACl guest solution (21.34 mg, [G]=33.38 mM). The remaining stock solution (0.6 mL) was used as the starting volume in an NMR tube.

Table 4. Representative titration data for Cl$^-$ with **5**.

	Guest (μL)	[**2**] (M)	[Cl$^-$] (M)	δ H1 (ppm)	δ H2 (ppm)
0	0	1.33E-03	0.00E+00	7.716	7.716
1	5	1.33E-03	2.76E-04	8.017	7.827
2	10	1.33E-03	5.47E-04	8.226	7.920
3	15	1.33E-03	8.14E-04	8.422	7.995
4	20	1.33E-03	1.08E-03	8.574	8.060
5	25	1.33E-03	1.34E-03	8.692	8.111
6	30	1.33E-03	1.59E-03	8.816	8.158
7	40	1.33E-03	2.09E-03	8.990	8.231
8	50	1.33E-03	2.57E-03	9.112	8.286
9	60	1.33E-03	3.03E-03	9.230	8.331
10	70	1.33E-03	3.49E-03	9.301	8.368
11	100	1.33E-03	4.77E-03	9.484	8.449
12	125	1.33E-03	5.76E-03	9.593	8.494
13	150	1.33E-03	6.68E-03	9.655	8.529
14	200	1.33E-03	8.35E-03	9.766	8.581
15	250	1.33E-03	9.82E-03	9.837	8.615
16	350	1.33E-03	1.23E-02	9.936	8.664
17	450	1.33E-03	1.43E-02	9.995	8.695
18	650	1.33E-03	1.74E-02	10.073	8.733
19	850	1.33E-03	1.96E-02	10.107	8.758
20	1050	1.33E-03	2.12E-02	10.140	8.773
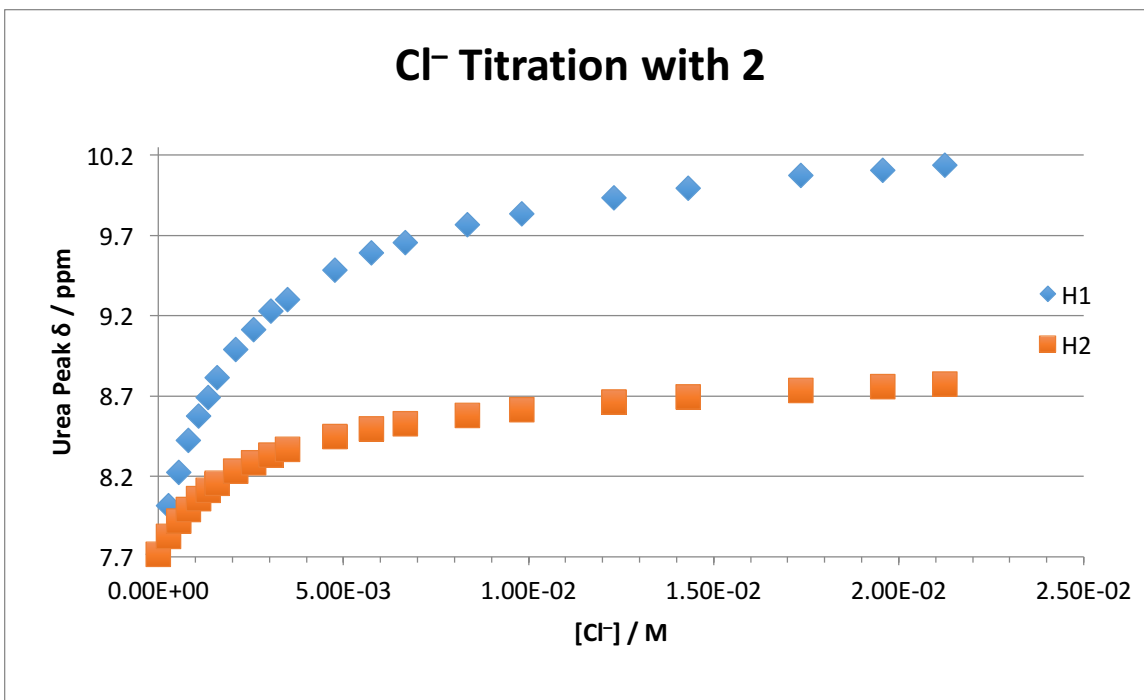
Figure 8. Binding isotherm for Cl⁻ titration of **2** in CDCl$_3$ by ^{1}H NMR.
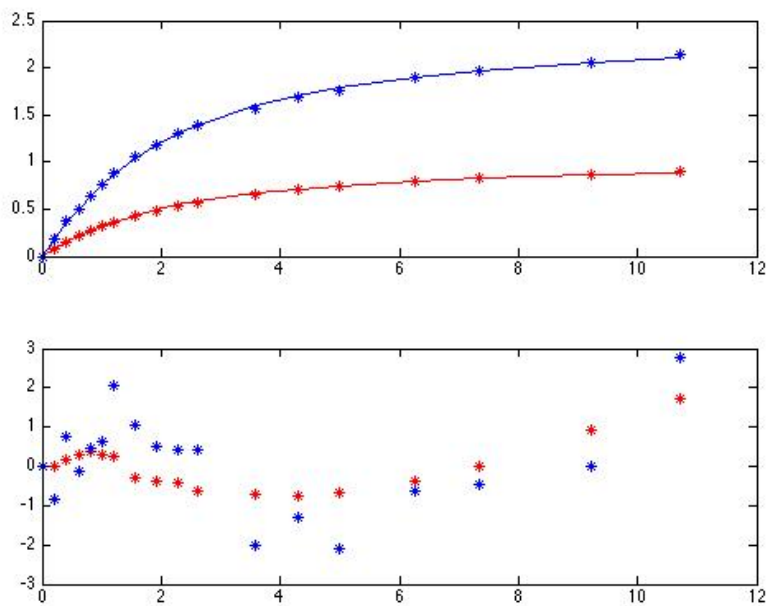
Figure 9. Matlab fit for the binding isotherm of Cl⁻ titration with **2**.
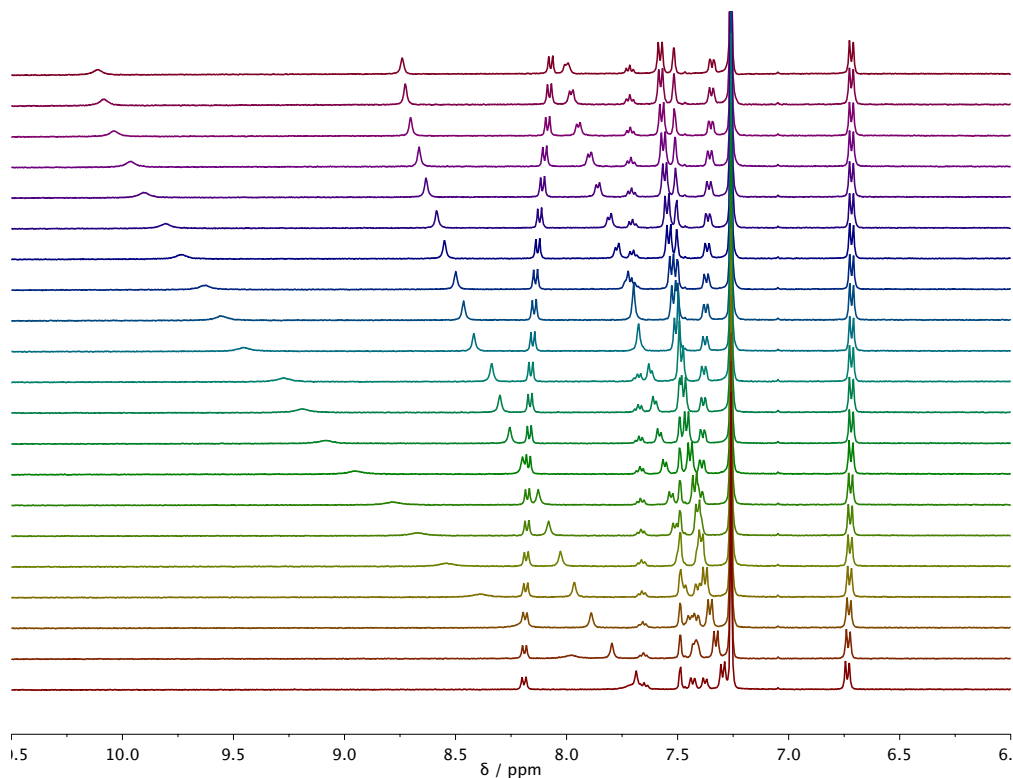
Figure 10. ^{1}H NMR spectra of Cl$^-$ titration with **2**.

UV–Vis Titrations

       Tetrabutylammonium chloride with 5. A stock solution of **5** was prepared using serial dilution to a final volume of 5 mL (1.28 mg, [**5**] = 10.68 μM). A 2 mL solution of TBACl (2.96 mg, 2.13 mM) was prepared by serial dilution with the stock solution of **5**. The starting volume in the cuvette was 2.0 mL.

Table 5. Representative titration data for Cl$^-$ with **5**.

	Guest (μL)	[5] (M)	[Cl$^-$] (M)	Equiv.
00	0	1.07E-05	0.00E+00	0.00
01	5	1.07E-05	5.31E-06	0.50
02	10	1.07E-05	1.06E-05	0.99
03	15	1.07E-05	1.59E-05	1.48
04	20	1.07E-05	2.11E-05	1.97
05	25	1.07E-05	2.63E-05	2.46

134

06	30	1.07E-05	3.15E-05	2.95
07	40	1.07E-05	4.18E-05	3.91
08	50	1.07E-05	5.20E-05	4.86
09	60	1.07E-05	6.20E-05	5.81
10	70	1.07E-05	7.20E-05	6.74
11	80	1.07E-05	8.19E-05	7.67
12	100	1.07E-05	1.01E-04	9.49
13	120	1.07E-05	1.21E-04	11.29
14	140	1.07E-05	1.39E-04	13.04
15	180	1.07E-05	1.76E-04	16.46
16	220	1.07E-05	2.11E-04	19.76
17	300	1.07E-05	2.78E-04	26.01
18	400	1.07E-05	3.55E-04	33.23
19	600	1.07E-05	4.92E-04	46.01
20	800	1.07E-05	6.09E-04	56.97
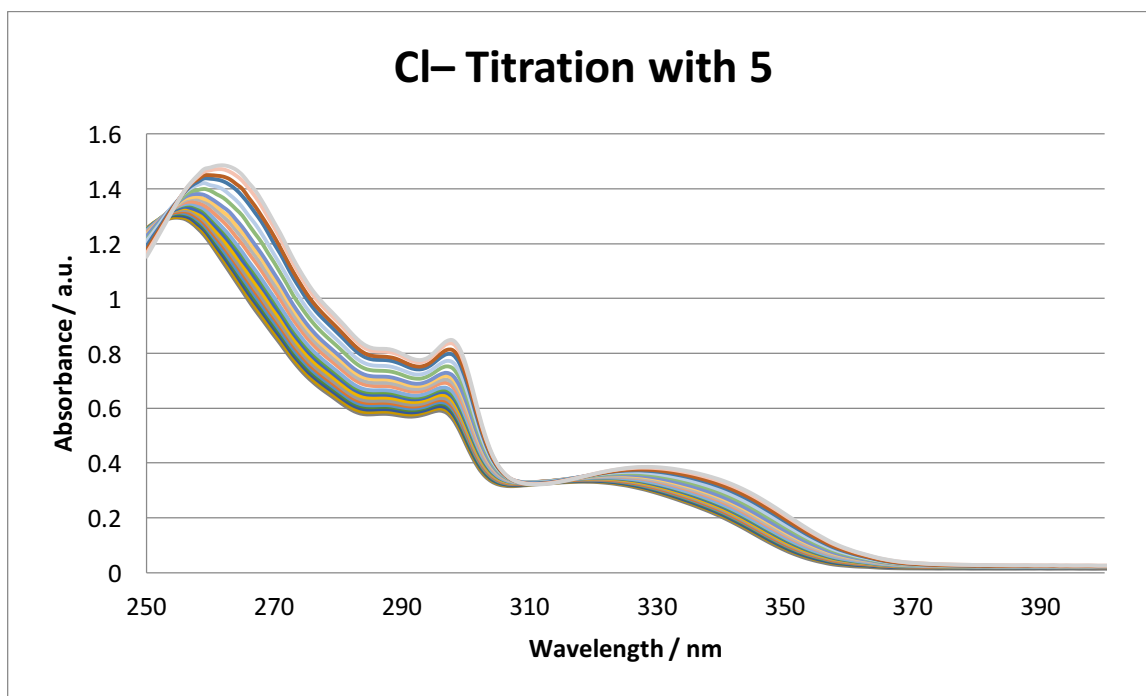
Figure 11. UV-Vis spectra of **5** titrated with Cl⁻ in water saturated CHCl$_3$.
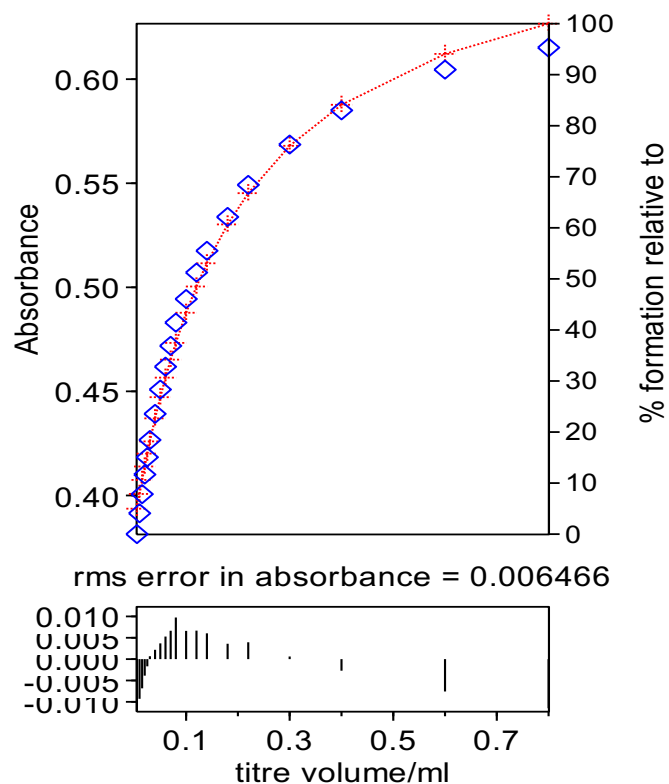
Figure 12. HyperQuad fit for the binding isotherm of Cl⁻ titration with **5**.

Tetrabutylammonium chloride with 3. A stock solution of **3** was prepared using serial dilution to a final volume of 5 mL (1.50 mg, [**3**] = 14.99 µM). A 2 mL solution of TBACl (7.20 mg, 2.07 mM) was prepared by serial dilution with the stock solution of **3**. The starting volume in the cuvette was 2.0 mL.

Table 6. Representative titration data for Cl⁻ with **3**.

	Guest (µL)	[3] (M)	[Cl⁻] (M)	Equiv.
00	0	1.50E-05	0.00E+00	0.00
01	5	1.50E-05	5.17E-06	0.34
02	10	1.50E-05	1.03E-05	0.69
03	15	1.50E-05	1.54E-05	1.03
04	20	1.50E-05	2.05E-05	1.37
05	25	1.50E-05	2.56E-05	1.71
06	30	1.50E-05	3.06E-05	2.04

07	40	1.50E-05	4.06E-05	2.71
08	50	1.50E-05	5.05E-05	3.37
09	60	1.50E-05	6.04E-05	4.03
10	70	1.50E-05	7.01E-05	4.68
11	80	1.50E-05	7.97E-05	5.32
12	90	1.50E-05	8.92E-05	5.95
13	100	1.50E-05	9.87E-05	6.58
14	120	1.50E-05	1.17E-04	7.83
15	140	1.50E-05	1.36E-04	9.05
16	160	1.50E-05	1.54E-04	10.24
17	200	1.50E-05	1.88E-04	12.57
18	250	1.50E-05	2.30E-04	15.36
19	300	1.50E-05	2.70E-04	18.03
20	350	1.50E-05	3.09E-04	20.59
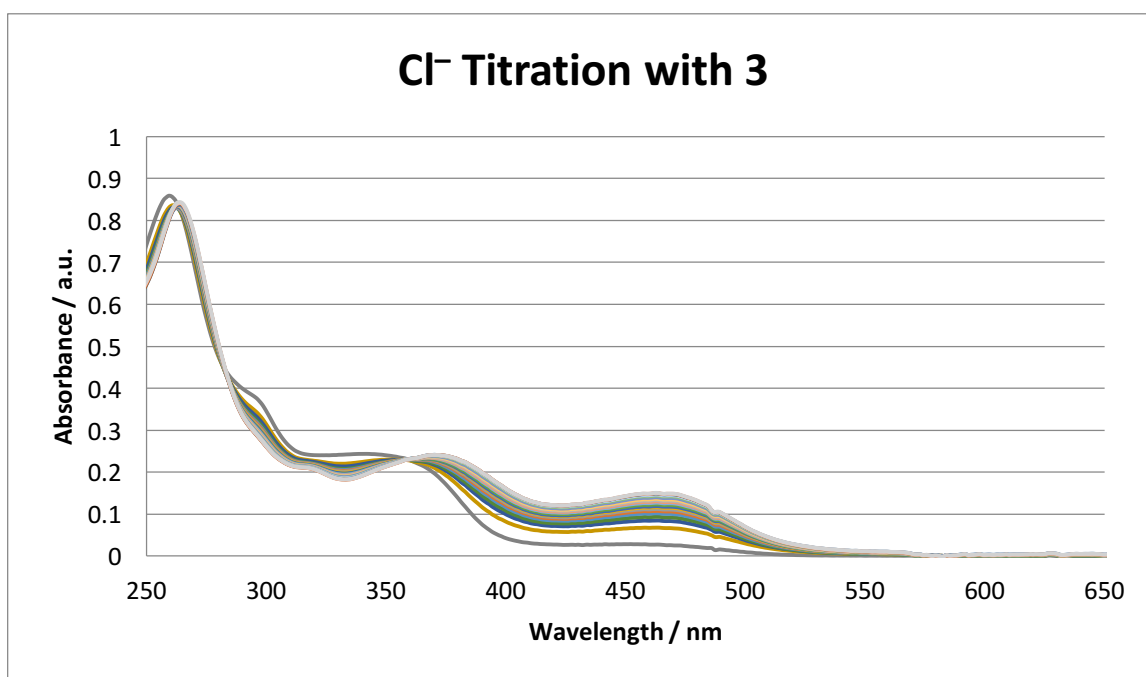
Figure 13. UV-Vis spectra of **3** titrated with Cl⁻ in water saturated CHCl₃.
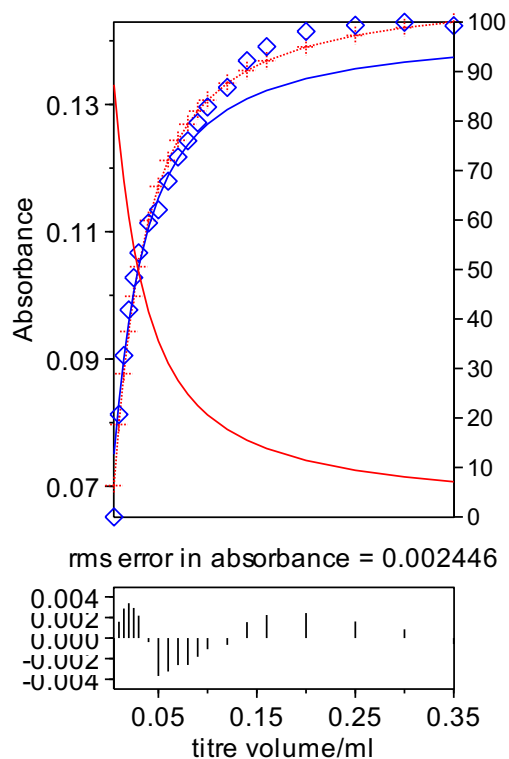
Figure 14. HyperQuad fit for the binding isotherm of Cl⁻ titration with **3**.

<u>Fluorescence Spectra</u>
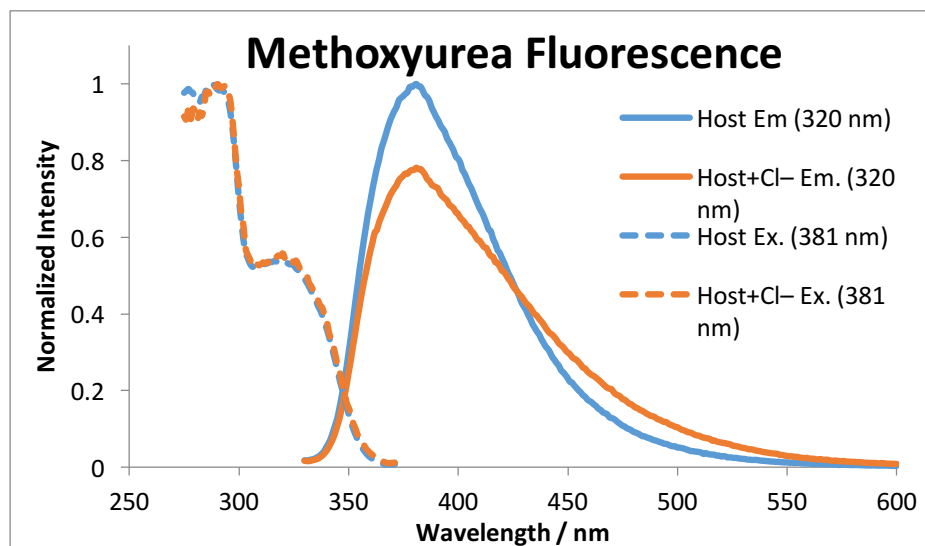
Figure 15. Fluorescence emission and excitation spectra of **5** and **5** with one equivalent of TBACl in CHCl₃.

NMR Spectra
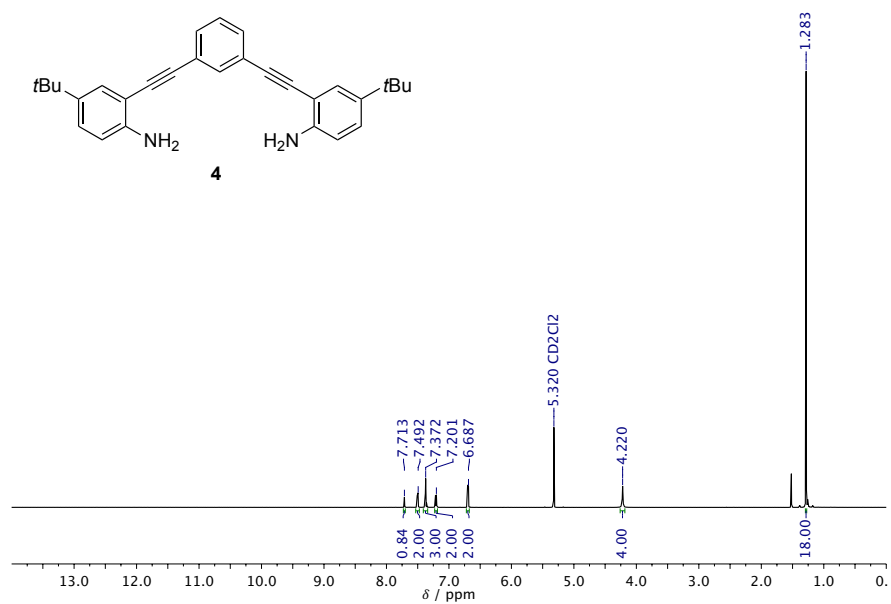
Figure 16. ^{1}H NMR spectra of **4** in CD$_2$Cl$_2$.
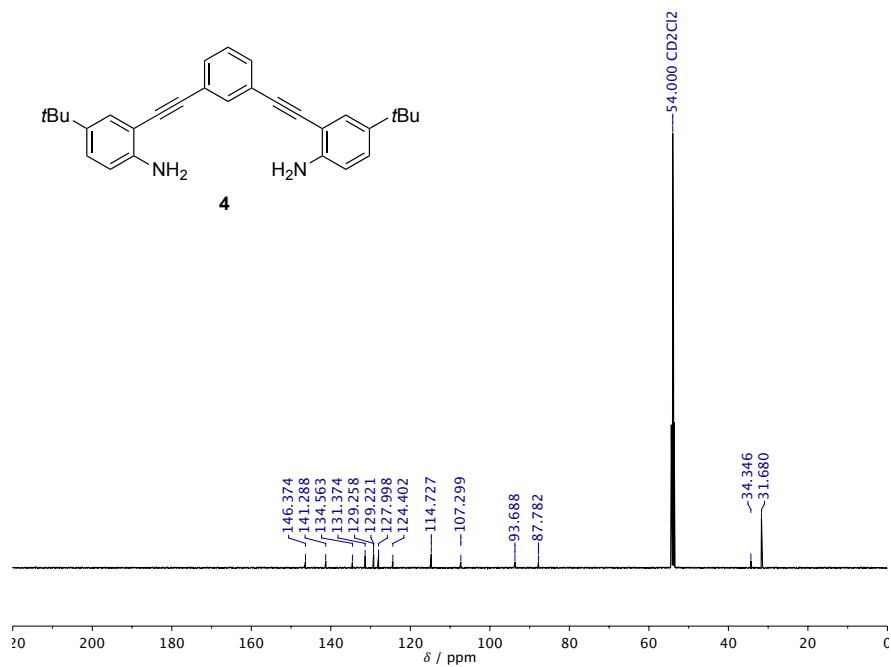
Figure 17. ^{13}C NMR spectra of **4** in CD$_2$Cl$_2$.
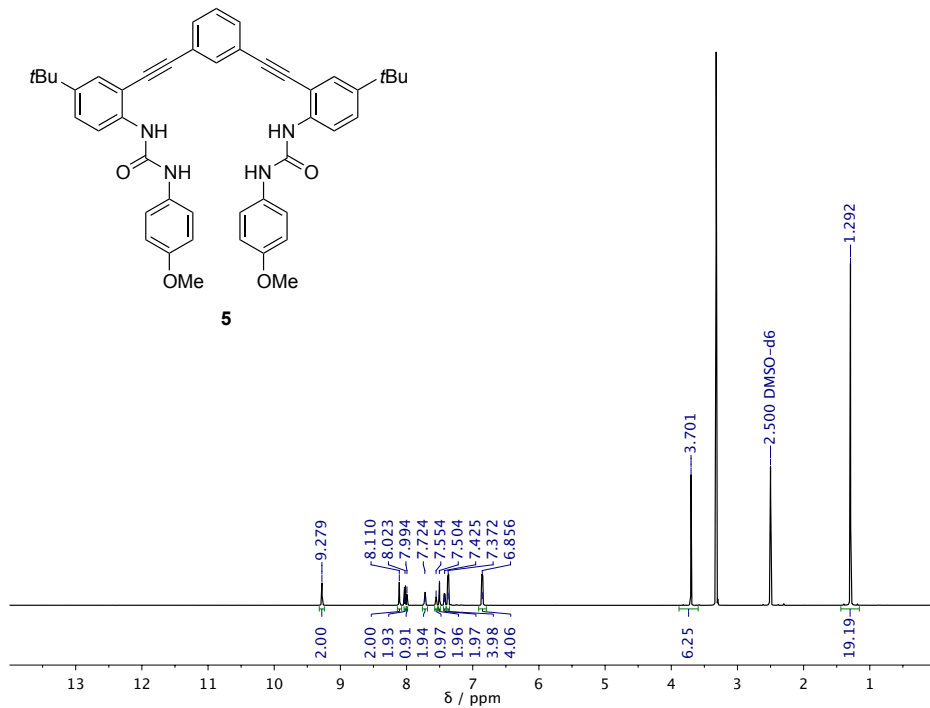
Figure 18. ¹H NMR spectra of **5** in DMSO–d_6.
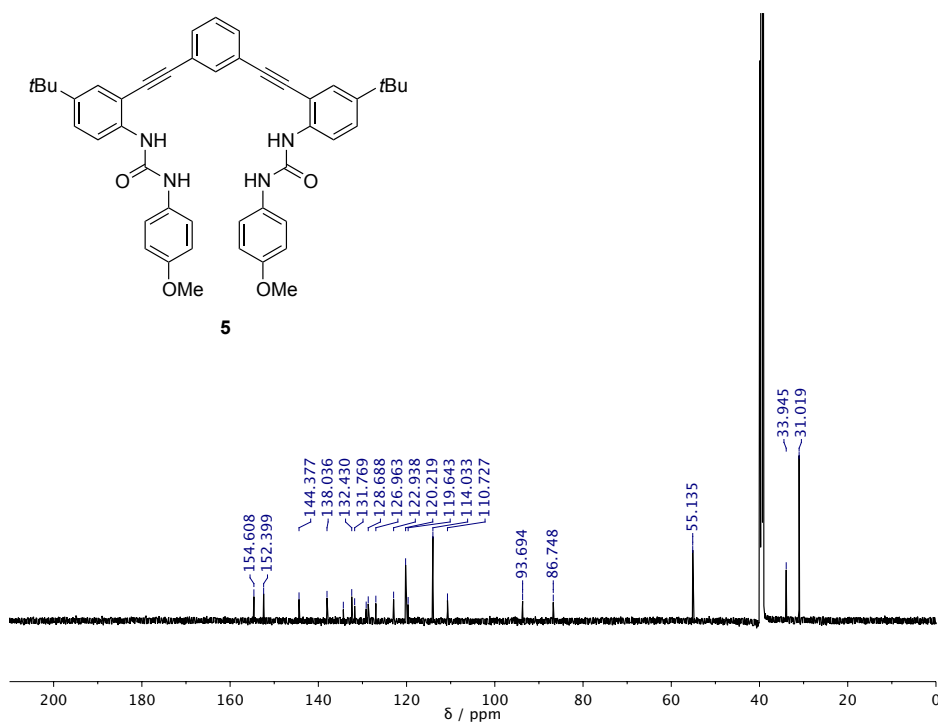
Figure 19. ¹³C NMR spectra of **5** in DMSO–d_6.
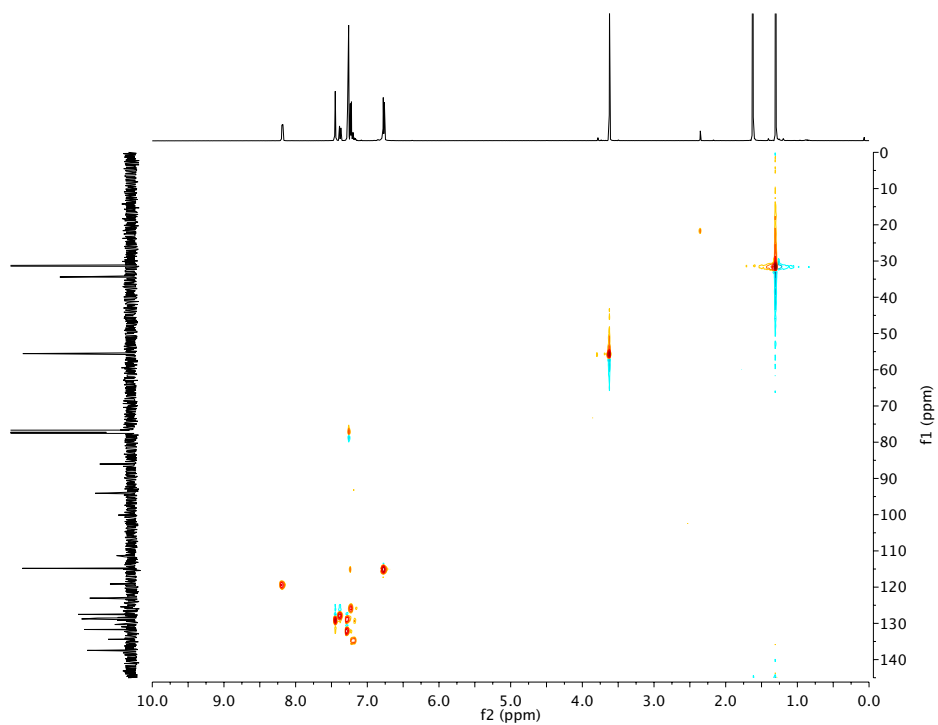
Figure 20. 2D ^{1}H–^{13}C HSQC NMR spectra of **5** in CDCl$_3$.
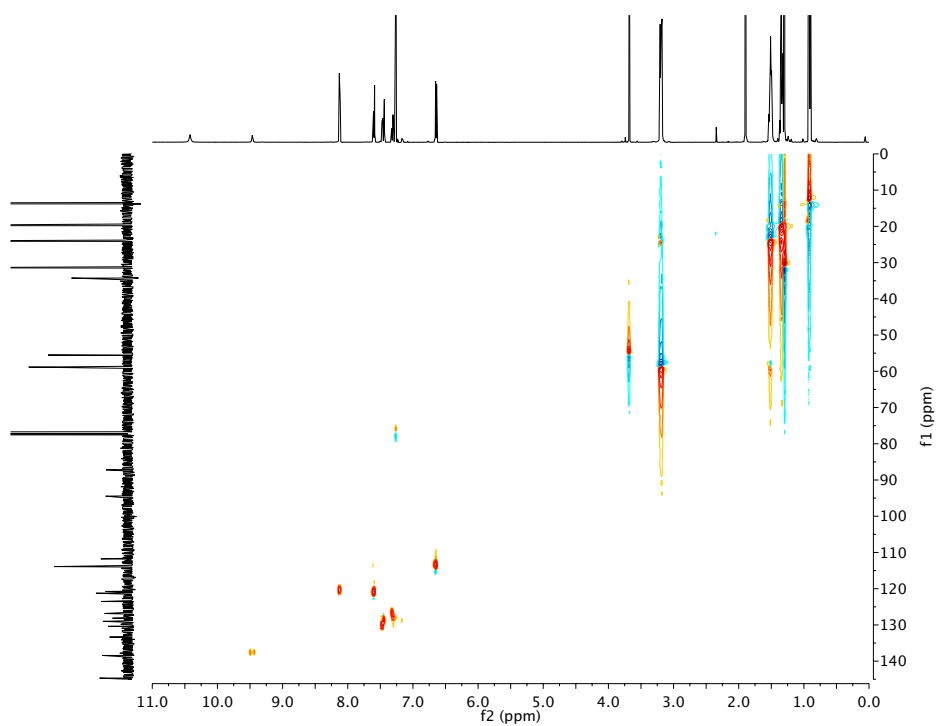
Figure 21. 2D ^{1}H–^{13}C HSQC NMR spectra of **5•Cl$^-$** in CDCl$_3$.
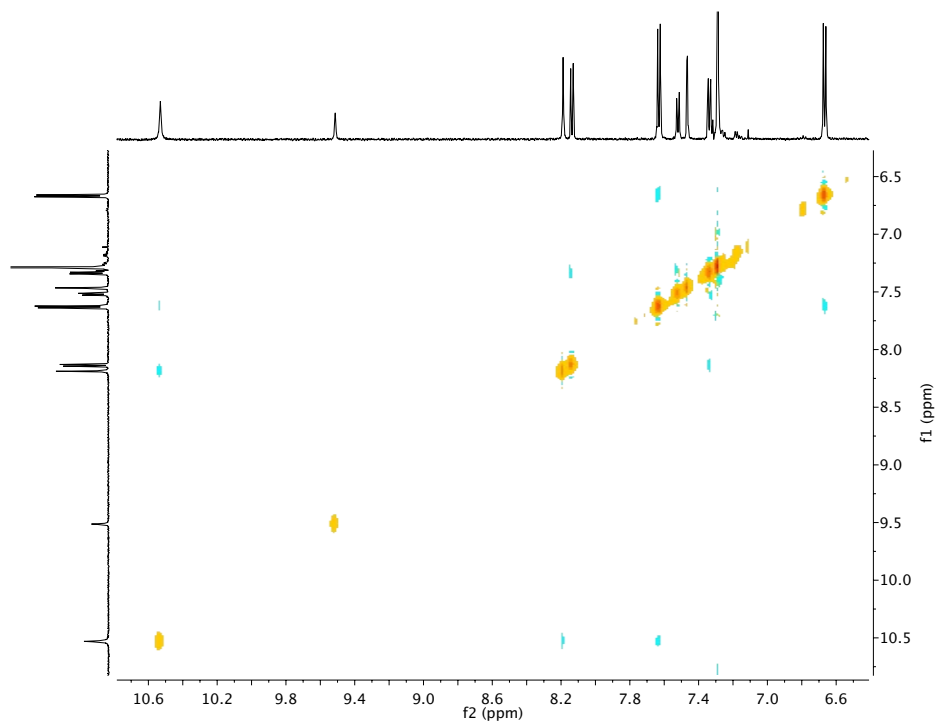
Figure 22. 2D ^1H–^1H ROESY NMR spectra of **5•Cl⁻** in CDCl$_3$.

High Resolution MS of 4 and 5
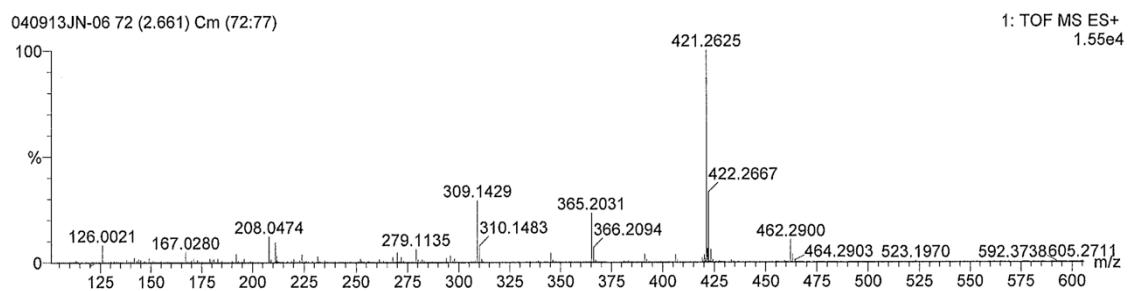
Figure 23. High resolution MS of **4**.
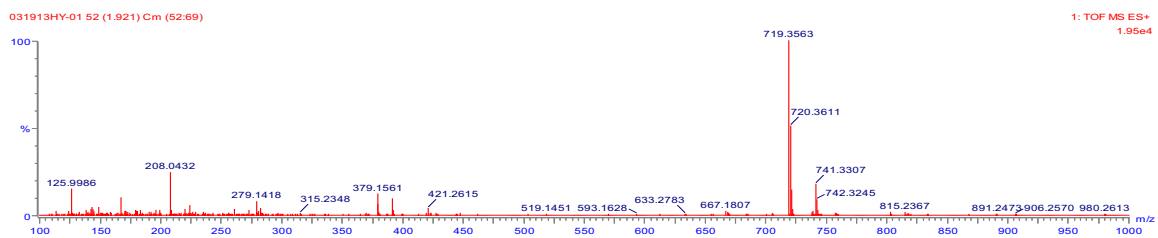
Figure 24. High resolution MS of **5**.

SUPPLEMENTARY INFORMATION FOR CHAPTER III

<u>Titrations</u>

^{1}H NMR Titrations

Table 1. Titration of **1a** with NO_3^-. (Stock $[NO_3^-]$ = 20.1 mM)

	Guest (µL)	[**1a**] (M)	$[NO_3^-]$ (M)	Equiv.	δ (ppm)
0	0	7.42E-04	0.00E+00	0.00	7.443
1	5	7.42E-04	1.01E-07	0.22	7.570
2	10	7.42E-04	2.01E-07	0.44	7.688
3	15	7.42E-04	3.02E-07	0.66	7.770
4	20	7.42E-04	4.02E-07	0.87	7.853
5	25	7.42E-04	5.03E-07	1.08	7.919
6	35	7.42E-04	7.04E-07	1.49	8.005
7	45	7.42E-04	9.05E-07	1.89	8.068
8	55	7.42E-04	1.11E-06	2.28	8.109
9	65	7.42E-04	1.31E-06	2.65	8.137
10	75	7.42E-04	1.51E-06	3.01	8.158
11	85	7.42E-04	1.71E-06	3.36	8.172
12	100	7.42E-04	2.01E-06	3.87	8.190
13	125	7.42E-04	2.51E-06	4.67	8.208
14	150	7.42E-04	3.02E-06	5.42	8.221
15	200	7.42E-04	4.02E-06	6.78	8.235
16	250	7.42E-04	5.03E-06	7.97	8.244
17	350	7.42E-04	7.04E-06	9.98	8.257
18	450	7.42E-04	9.05E-06	11.61	8.265
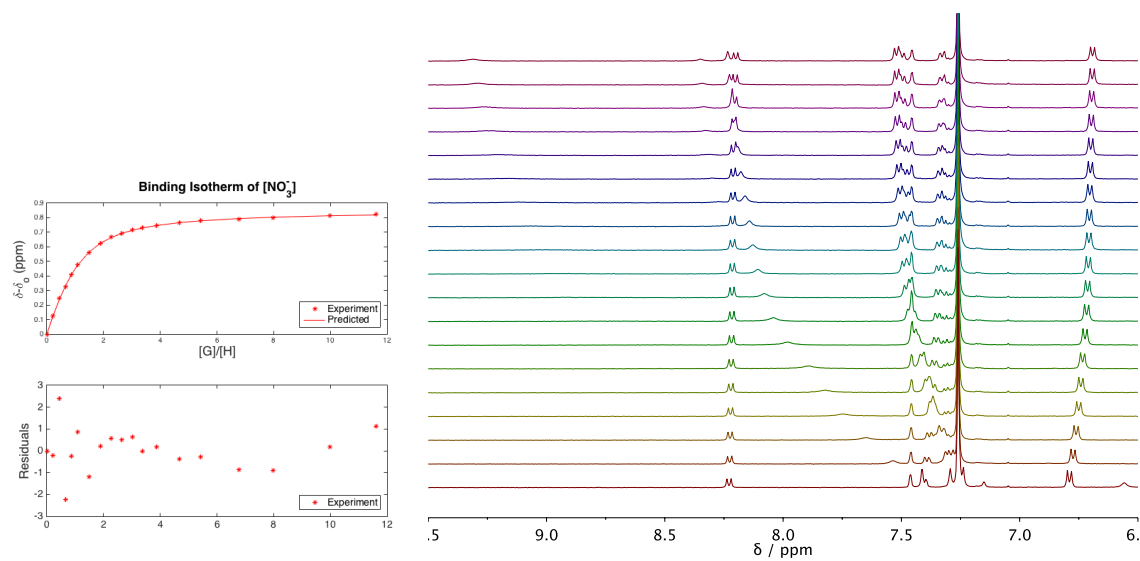
Figure 1. Binding isotherm for NO_3^- titration of **1a** in $CDCl_3$ by ^1H NMR. ^1H NMR stacked plot of **1a** (0.742 mM) titrated with TBA NO_3^- (0-11.6 equiv., bottom to top) in $CDCl_3$.

Table 2. Titration of **1b** with Cl^-. (Stock $[Cl^-]$ = 12.1 mM)

	Guest (µL)	**[1b]** (M)	$[Cl^-]$ (M)	Equiv.	δ (ppm)
0	0	3.77E-04	0.00E+00	0.00	7.467
1	4	3.77E-04	7.99E-05	0.21	7.550
2	8	3.77E-04	1.59E-04	0.42	7.655
3	12	3.77E-04	2.37E-04	0.63	7.832
4	16	3.77E-04	3.13E-04	0.83	7.940
5	20	3.77E-04	3.89E-04	1.03	8.000
6	24	3.77E-04	4.64E-04	1.23	8.033
7	28	3.77E-04	5.38E-04	1.43	8.053
8	32	3.77E-04	6.11E-04	1.62	8.066
9	37	3.77E-04	7.01E-04	1.86	8.076
10	45	3.77E-04	8.42E-04	2.23	8.086
11	55	3.77E-04	1.01E-03	2.69	8.093
12	65	3.77E-04	1.18E-03	3.13	8.098
13	80	3.77E-04	1.42E-03	3.76	8.102
14	100	3.77E-04	1.72E-03	4.57	8.106
15	125	3.77E-04	2.08E-03	5.52	8.108
16	150	3.77E-04	2.41E-03	6.40	8.110
17	200	3.77E-04	3.02E-03	8.00	8.112
18	250	3.77E-04	3.55E-03	9.41	8.113
19	350	3.77E-04	4.44E-03	11.79	8.115
20	450	3.77E-04	5.17E-03	13.71	8.116
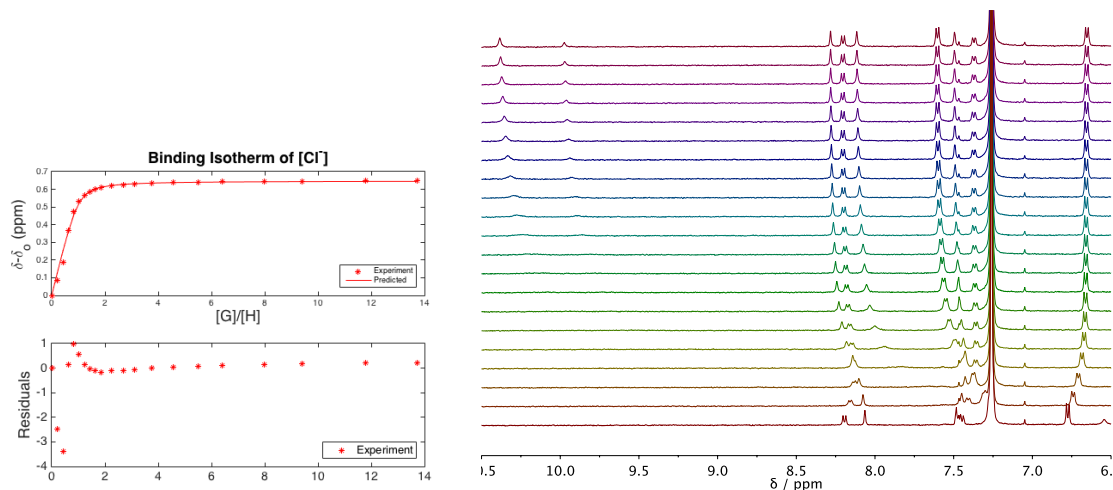
Figure 2. Binding isotherm for Cl⁻ titration of **1b** in CDCl$_3$ by ¹H NMR. ¹H NMR stacked plot of **1b** (0.377 mM) titrated with TBA Cl⁻ (0-13.7 equiv., bottom to top) in CDCl$_3$.

Table 3. Titration of **1b** with Br⁻. (Stock [Br⁻] = 18.8 mM)

	Guest (µL)	[**1b**] (M)	[Cl⁻] (M)	Equiv.	δ (ppm)
0	0	4.76E-04	0.00E+00	0.00	7.486
1	5	4.76E-04	9.39E-08	0.33	7.524
2	10	4.76E-04	1.88E-07	0.65	7.683
3	15	4.76E-04	2.82E-07	0.96	7.769
4	20	4.76E-04	3.76E-07	1.27	7.820
5	30	4.76E-04	5.64E-07	1.88	7.877
6	40	4.76E-04	7.51E-07	2.47	7.906
7	50	4.76E-04	9.39E-07	3.04	7.924
8	60	4.76E-04	1.13E-06	3.59	7.935
9	80	4.76E-04	1.50E-06	4.65	7.949
10	100	4.76E-04	1.88E-06	5.64	7.958
11	125	4.76E-04	2.35E-06	6.81	7.965
12	150	4.76E-04	2.82E-06	7.90	7.969
13	200	4.76E-04	3.76E-06	9.87	7.975
14	300	4.76E-04	5.64E-06	13.17	7.981
15	400	4.76E-04	7.51E-06	15.80	7.984
16	600	4.76E-04	1.13E-05	19.75	7.988
17	800	4.76E-04	1.50E-05	22.57	7.989
18	1000	4.76E-04	1.88E-05	24.69	7.990
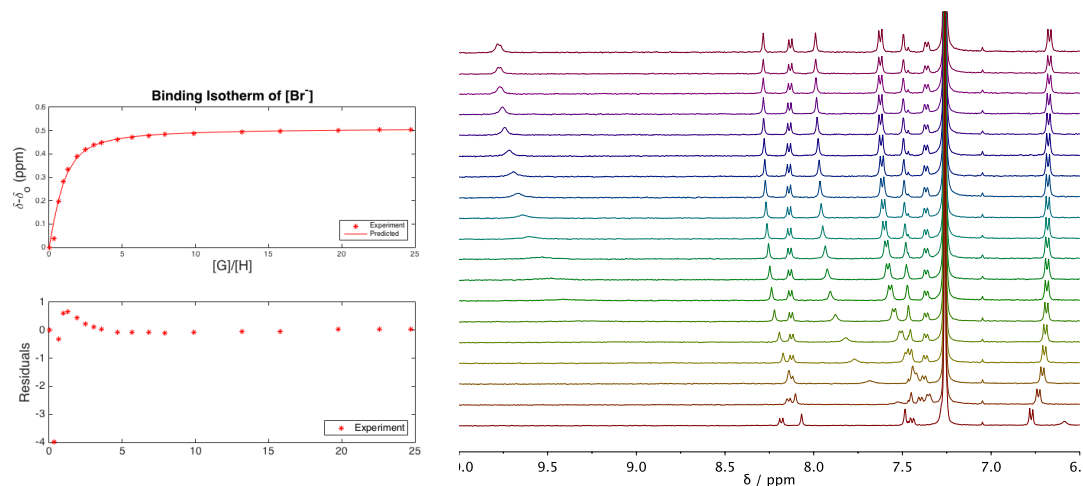
Figure 3. Binding isotherm for Br⁻ titration of **1b** in CDCl₃ by ¹H NMR. ¹H NMR stacked plot of **1b** (0.476 mM) titrated with TBA Br⁻ (0-24.7 equiv., bottom to top) in CDCl₃.

Table 4. Titration of **1b** with I⁻. (Stock [I⁻] = 62.5 mM)

	Guest (μL)	[**1b**] (M)	[I⁻] (M)	Equiv.	δ (ppm)
0	0	1.27E-03	0.00E+00	0.00	8.062
1	5	1.27E-03	3.13E-07	0.41	8.094
2	10	1.27E-03	6.25E-07	0.81	8.115
3	15	1.27E-03	9.38E-07	1.20	8.133
4	20	1.27E-03	1.25E-06	1.59	8.147
5	30	1.27E-03	1.88E-06	2.35	8.169
6	40	1.27E-03	2.50E-06	3.09	8.184
7	50	1.27E-03	3.13E-06	3.80	8.196
8	65	1.27E-03	4.06E-06	4.83	8.209
9	80	1.27E-03	5.00E-06	5.81	8.218
10	100	1.27E-03	6.25E-06	7.06	8.227
11	120	1.27E-03	7.50E-06	8.23	8.234
12	160	1.27E-03	1.00E-05	10.40	8.243
13	200	1.27E-03	1.25E-05	12.35	8.248
14	250	1.27E-03	1.56E-05	14.53	8.252
15	300	1.27E-03	1.88E-05	16.47	8.255
16	400	1.27E-03	2.50E-05	19.76	8.259
17	600	1.27E-03	3.75E-05	24.70	8.262
18	800	1.27E-03	5.00E-05	28.23	8.263
19	1200	1.27E-03	7.50E-05	32.93	8.264

Figure 4. Binding isotherm for I^- titration of **1b** in $CDCl_3$ by ^1H NMR. ^1H NMR stacked plot of **1b** (1.27 mM) titrated with TBA I^- (0-32.9 equiv., bottom to top) in $CDCl_3$.

Table 5. Titration of **1b** with NO_3^-. (Stock $[NO_3^-]$ = 27.1 mM)

	Guest (μL)	[**1b**] (M)	$[NO_3^-]$ (M)	Equiv.	δ (ppm)
0	0	4.45E-04	0.00E+00	0.00	7.284
1	5	4.45E-04	1.35E-07	0.50	7.719
2	10	4.45E-04	2.71E-07	1.00	7.997
3	15	4.45E-04	4.06E-07	1.48	8.105
4	20	4.45E-04	5.42E-07	1.96	8.15
5	25	4.45E-04	6.77E-07	2.43	8.174
6	30	4.45E-04	8.13E-07	2.90	8.188
7	35	4.45E-04	9.48E-07	3.35	8.197
8	40	4.45E-04	1.08E-06	3.80	8.204
9	50	4.45E-04	1.35E-06	4.68	8.213
10	60	4.45E-04	1.63E-06	5.53	8.219
11	80	4.45E-04	2.17E-06	7.16	8.228
12	100	4.45E-04	2.71E-06	8.69	8.231
13	150	4.45E-04	4.06E-06	12.17	8.238
14	200	4.45E-04	5.42E-06	15.22	8.244
15	300	4.45E-04	8.13E-06	20.29	8.248
16	400	4.45E-04	1.08E-05	24.34	8.251
17	600	4.45E-04	1.63E-05	30.43	8.254

147

Figure 5. Binding isotherm for NO_3^- titration of **1b** in $CDCl_3$ by ^1H NMR. ^1H NMR stacked plot of **1b** (0.445 mM) titrated with TBA NO_3^- (0-30.4 equiv., bottom to top) in $CDCl_3$.

Table 6. Titration of **1c** with Cl^-. (Stock $[Cl^-]$ = 27.4 mM)

	Guest (µL)	[**1c**] (M)	[Cl] (M)	Equiv.	δ (ppm)
0	0	7.43E-04	0.00E+00	0.00	7.027
1	5	7.43E-04	2.26E-04	0.30	7.573
2	10	7.43E-04	4.49E-04	0.60	7.791
3	15	7.43E-04	6.68E-04	0.90	7.92
4	20	7.43E-04	8.83E-04	1.19	7.989
5	25	7.43E-04	1.10E-03	1.47	8.02
6	30	7.43E-04	1.30E-03	1.75	8.037
7	40	7.43E-04	1.71E-03	2.30	8.053
8	50	7.43E-04	2.11E-03	2.83	8.062
9	60	7.43E-04	2.49E-03	3.35	8.067
10	80	7.43E-04	3.22E-03	4.33	8.073
11	100	7.43E-04	3.91E-03	5.26	8.077
12	150	7.43E-04	5.48E-03	7.37	8.084
13	200	7.43E-04	6.84E-03	9.21	8.087
14	300	7.43E-04	9.13E-03	12.28	8.093
15	400	7.43E-04	1.10E-02	14.73	8.097
16	600	7.43E-04	1.37E-02	18.41	8.102
17	1100	7.43E-04	1.77E-02	23.83	8.106
18	1600	7.43E-04	1.99E-02	26.78	8.106
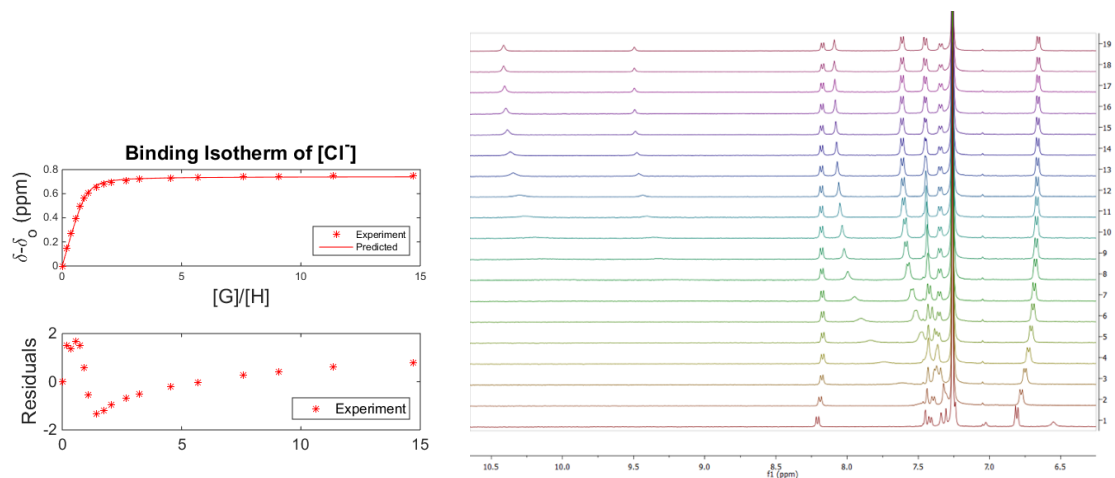
Figure 6. Binding isotherm for Cl⁻ titration of **1c** in CDCl₃ by ¹H NMR. ¹H NMR stacked plot of **1c** (0.743 mM) titrated with TBA Cl⁻ (0-26.78 equiv., bottom to top) in CDCl₃.

Table 7. Titration of **1c** with Br⁻. (Stock [Br⁻] = 24.5 mM)

|	Guest (µL)	[**1c**] (M)	[Br⁻] (M)	Equiv.	δ (ppm)
0	0	5.18E-04	0.00E+00	0.00	7.042
1	5	5.18E-04	2.03E-04	0.39	7.479
2	10	5.18E-04	4.02E-04	0.78	7.592
3	15	5.18E-04	5.98E-04	1.16	7.672
4	20	5.18E-04	7.91E-04	1.53	7.722
5	25	5.18E-04	9.81E-04	1.89	7.761
6	30	5.18E-04	1.17E-03	2.26	7.79
7	40	5.18E-04	1.53E-03	2.96	7.828
8	50	5.18E-04	1.89E-03	3.64	7.852
9	60	5.18E-04	2.23E-03	4.31	7.87
10	80	5.18E-04	2.88E-03	5.57	7.891
11	150	5.18E-04	4.90E-03	9.47	7.905
12	200	5.18E-04	6.13E-03	11.84	7.924
13	300	5.18E-04	8.17E-03	15.79	7.935
14	400	5.18E-04	9.81E-03	18.95	7.946
15	600	5.18E-04	1.23E-02	23.68	7.952
16	1000	5.18E-04	1.53E-02	29.60	7.958
17	1500	5.18E-04	1.75E-02	33.83	7.962
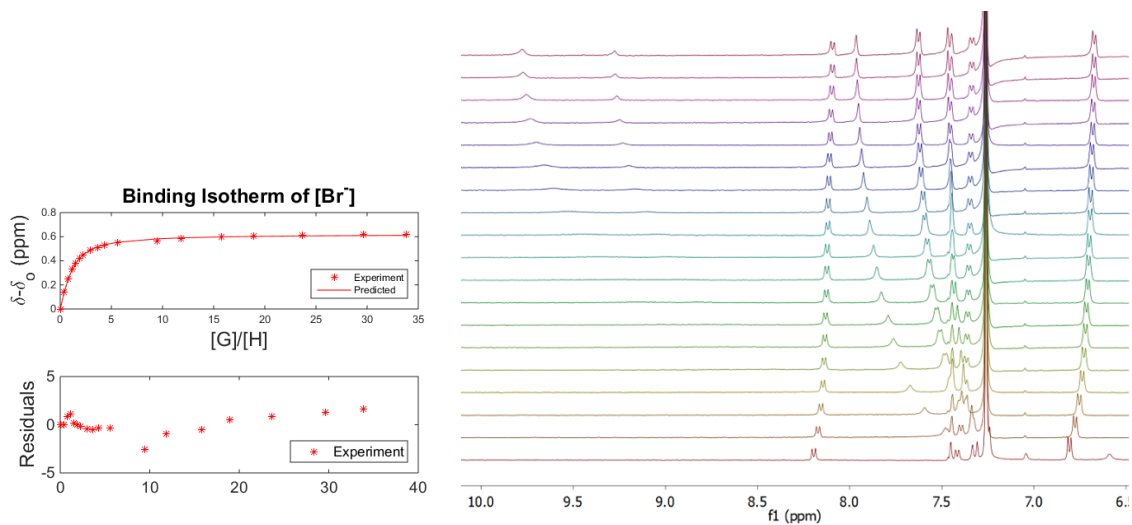
Figure 7. Binding isotherm for Br⁻ titration of **1c** in CDCl$_3$ by ^{1}H NMR. ^{1}H NMR stacked plot of **1c** (0.518 mM) titrated with TBA Br⁻ (0-33.83 equiv., bottom to top) in CDCl$_3$.

Table 8. Titration of **1c** with I⁻. (Stock [I⁻] = 70.3 mM)

|	Guest (μL)	[**1c**] (M)	[I⁻] (M)	Equiv.	δ (ppm)
0	0	7.35E-04	0.00E+00	0	7.339
1	5	7.35E-04	5.81E-04	0.79	7.41
2	10	7.35E-04	1.15E-03	1.57	7.463
3	15	7.35E-04	1.72E-03	2.34	7.506
4	20	7.35E-04	2.27E-03	3.09	7.537
5	25	7.35E-04	2.81E-03	3.83	7.567
6	30	7.35E-04	3.35E-03	4.56	7.592
7	40	7.35E-04	4.40E-03	5.98	7.627
8	50	7.35E-04	5.41E-03	7.37	7.654
9	60	7.35E-04	6.39E-03	8.70	7.673
10	80	7.35E-04	8.27E-03	11.26	7.703
11	100	7.35E-04	1.00E-02	13.68	7.723
12	150	7.35E-04	1.41E-02	19.15	7.754
13	200	7.35E-04	1.76E-02	23.94	7.774
14	300	7.35E-04	2.34E-02	31.92	7.789
15	400	7.35E-04	2.81E-02	38.30	7.809
16	600	7.35E-04	3.52E-02	47.88	7.813
17	900	7.35E-04	4.22E-02	57.45	7.817
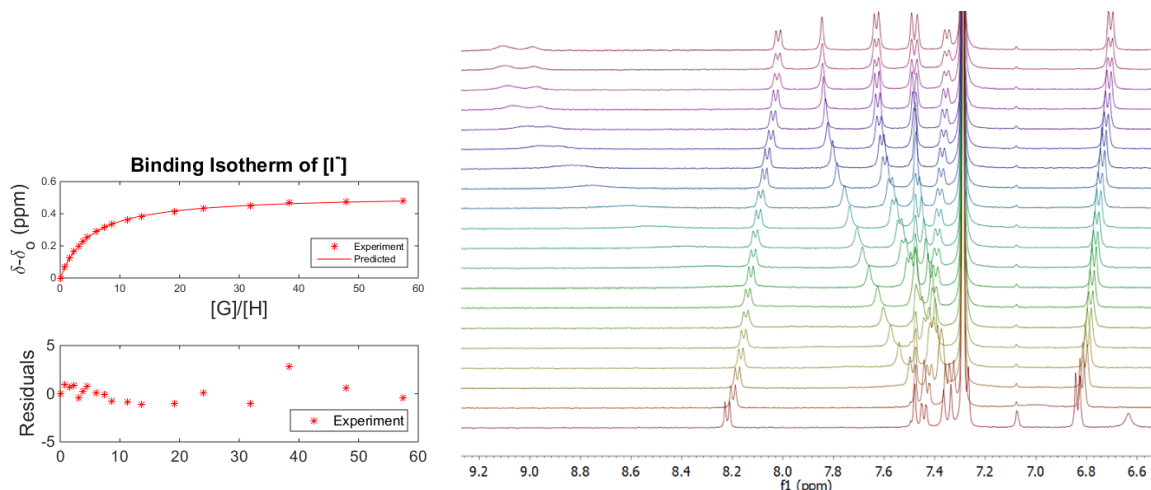
Figure 8. Binding isotherm for I⁻ titration of **1c** in CDCl₃ by ¹H NMR. ¹H NMR stacked plot of **1c** (0.734 mM) titrated with TBA I⁻ (0-57.45 equiv., bottom to top) in CDCl₃.

Table 9. Titration of **1d** with Cl⁻. (Stock [Cl⁻] = 26.4 mM)

|	Guest (µL)	[**1d**] (M)	[Cl⁻] (M)	Equiv.	δ (ppm)
0	0	6.65E-04	0.00E+00	0	7.342
1	5	6.65E-04	2.19E-04	0.33	7.586
2	10	6.65E-04	4.33E-04	0.65	7.78
3	15	6.65E-04	6.45E-04	0.97	7.904
4	20	6.65E-04	8.53E-04	1.28	7.971
5	25	6.65E-04	1.06E-03	1.59	8.013
6	30	6.65E-04	1.26E-03	1.89	8.034
7	40	6.65E-04	1.65E-03	2.48	8.055
8	50	6.65E-04	2.03E-03	3.06	8.071
9	60	6.65E-04	2.40E-03	3.61	8.079
10	80	6.65E-04	3.11E-03	4.68	8.089
11	100	6.65E-04	3.78E-03	5.68	8.095
12	150	6.65E-04	5.29E-03	7.95	8.104
13	200	6.65E-04	6.61E-03	9.94	8.11
14	300	6.65E-04	8.81E-03	13.25	8.117
15	400	6.65E-04	1.06E-02	15.90	8.121
16	600	6.65E-04	1.32E-02	19.88	8.126
17	900	6.65E-04	1.59E-02	23.86	8.127
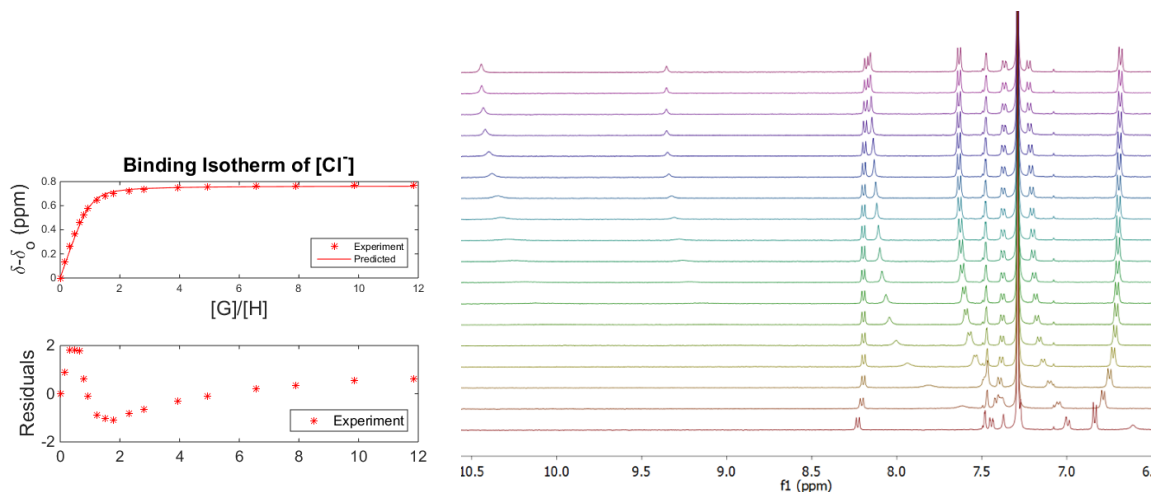
Figure 9. Binding isotherm for Cl⁻ titration of **1d** in CDCl₃ by ¹H NMR. ¹H NMR stacked plot of **1d** (0.665 mM) titrated with TBA Cl⁻ (0-23.86 equiv., bottom to top) in CDCl₃.

Table 10. Titration of **1d** with Br⁻. (Stock [Br⁻] = 31.8 mM)

	Guest (µL)	[1d] (M)	[Br⁻] (M)	Equiv.	δ (ppm)
0	0	9.32E-04	0.00E+00	0	7.338
1	5	9.32E-04	2.63E-04	0.28	7.473
2	10	9.32E-04	5.22E-04	0.56	7.58
3	15	9.32E-04	7.77E-04	0.83	7.669
4	20	9.32E-04	1.03E-03	1.10	7.726
5	25	9.32E-04	1.27E-03	1.37	7.768
6	30	9.32E-04	1.52E-03	1.63	7.806
7	40	9.32E-04	1.99E-03	2.14	7.841
8	50	9.32E-04	2.45E-03	2.63	7.869
9	60	9.32E-04	2.90E-03	3.11	7.886
10	80	9.32E-04	3.75E-03	4.02	7.91
11	100	9.32E-04	4.55E-03	4.89	7.924
12	150	9.32E-04	6.37E-03	6.84	7.944
13	200	9.32E-04	7.97E-03	8.55	7.955
14	300	9.32E-04	1.06E-02	11.40	7.97
15	400	9.32E-04	1.27E-02	13.68	7.975
16	600	9.32E-04	1.59E-02	17.10	7.982
17	900	9.32E-04	1.91E-02	20.52	7.987
18	1300	9.32E-04	2.18E-02	23.40	7.989
19	1800	9.32E-04	2.40E-02	25.65	7.991

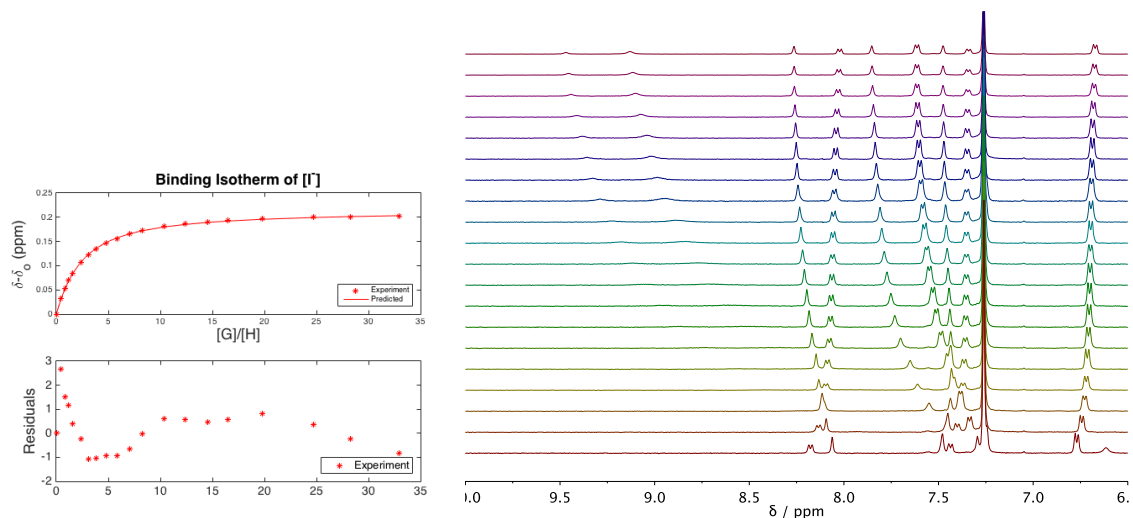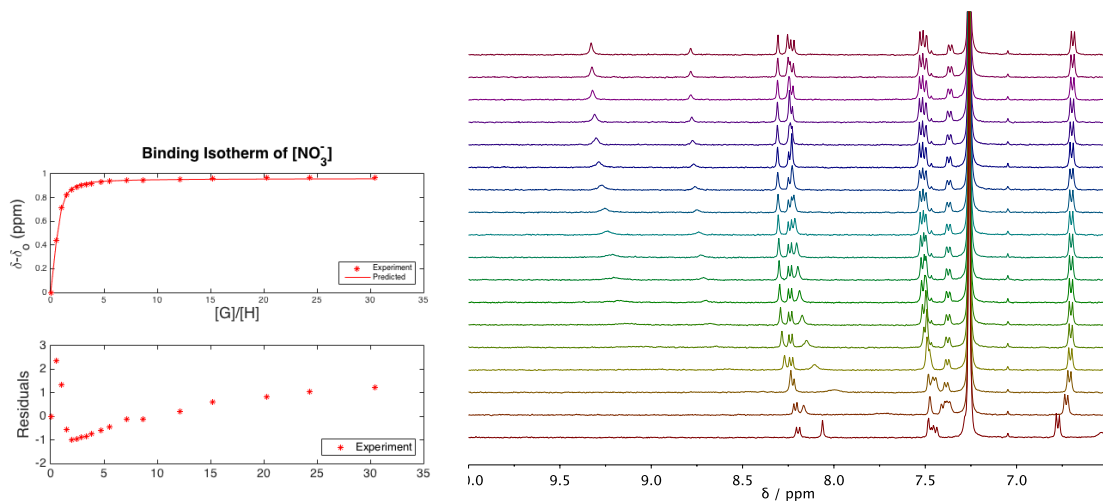**Figure 10.** Binding isotherm for Br⁻ titration of **1d** in CDCl₃ by ¹H NMR. ¹H NMR stacked plot of **1d** (0.932 mM) titrated with TBA Br⁻ (0-25.65 equiv., bottom to top) in CDCl₃.

Table 11. Titration of **1d** with I⁻. (Stock [I⁻] = 90.2 mM)

|	Guest (µL)	[**1d**] (M)	[I⁻] (M)	Equiv.	δ (ppm)
0	0	8.73E-04	0.00E+00	0	7.342
1	5	8.73E-04	7.46E-04	0.85	7.421
2	10	8.73E-04	1.48E-03	1.69	7.477
3	15	8.73E-04	2.20E-03	2.52	7.519
4	20	8.73E-04	2.91E-03	3.33	7.556
5	25	8.73E-04	3.61E-03	4.13	7.583
6	30	8.73E-04	4.30E-03	4.92	7.609
7	40	8.73E-04	5.64E-03	6.46	7.642
8	50	8.73E-04	6.94E-03	7.95	7.669
9	60	8.73E-04	8.20E-03	9.40	7.689
10	80	8.73E-04	1.06E-02	12.16	7.721
11	110	8.73E-04	1.40E-02	16.01	7.742
12	150	8.73E-04	1.80E-02	20.67	7.773
13	200	8.73E-04	2.26E-02	25.84	7.79
14	300	8.73E-04	3.01E-02	34.45	7.808
15	400	8.73E-04	3.61E-02	41.34	7.817
16	600	8.73E-04	4.51E-02	51.68	7.825
17	900	8.73E-04	5.41E-02	62.01	7.83
18	1300	8.73E-04	6.17E-02	70.72	7.832
19	1650	8.73E-04	6.62E-02	75.79	7.832
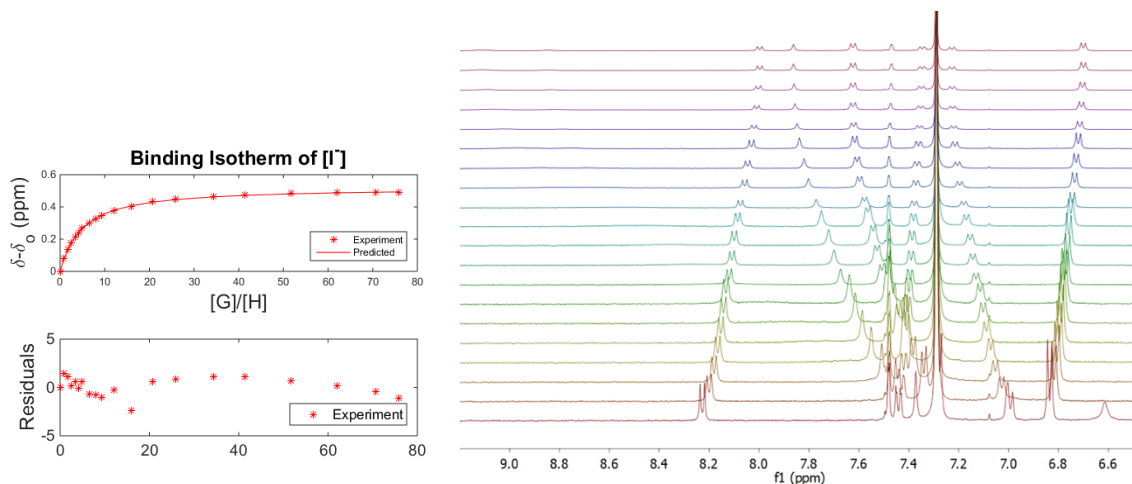
Figure 11. Binding isotherm for I⁻ titration of **1d** in CDCl₃ by ¹H NMR. ¹H NMR stacked plot of **1d** (0.873 mM) titrated with TBA I⁻ (0-75.79 equiv., bottom to top) in CDCl₃.

Table 12. Titration of **1e** with Cl⁻. (Stock [Cl⁻] = 39.1 mM)

|	Guest (μL)	**[1e]** (M)	[Cl⁻] (M)	Equiv.	δ (ppm)
0	0	7.74E-04	7.74E-04	0.00	7.453
1	5	7.74E-04	7.74E-04	0.42	7.743
2	10	7.74E-04	7.74E-04	0.83	7.911
3	15	7.74E-04	7.74E-04	1.23	7.988
4	20	7.74E-04	7.74E-04	1.63	8.021
5	25	7.74E-04	7.74E-04	2.02	8.039
6	30	7.74E-04	7.74E-04	2.40	8.050
7	40	7.74E-04	7.74E-04	3.16	8.064
8	50	7.74E-04	7.74E-04	3.88	8.072
9	60	7.74E-04	7.74E-04	4.59	8.077
10	80	7.74E-04	7.74E-04	5.94	8.083
11	100	7.74E-04	7.74E-04	7.21	8.087
12	150	7.74E-04	7.74E-04	10.10	8.092
13	200	7.74E-04	7.74E-04	12.62	8.095
14	300	7.74E-04	7.74E-04	16.83	8.098
15	400	7.74E-04	7.74E-04	20.20	8.100
16	600	7.74E-04	7.74E-04	25.25	8.103
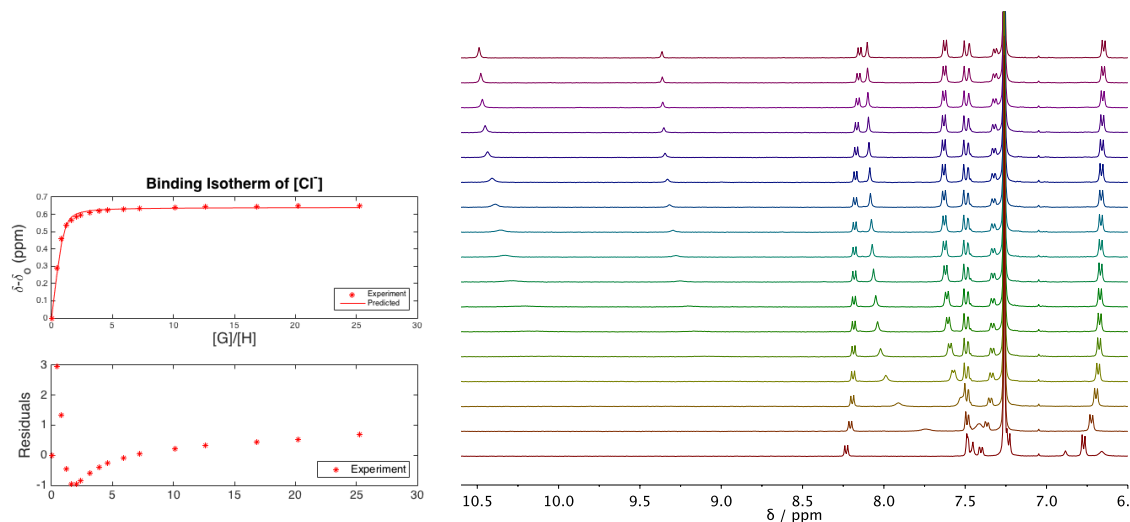
Figure 12. Binding isotherm for Cl⁻ titration of **1e** in CDCl$_3$ by ¹H NMR. ¹H NMR stacked plot of **1e** (0.774 mM) titrated with TBA Cl⁻ (0-25 equiv., bottom to top) in CDCl$_3$.

Table 13. Titration of **1e** with Br⁻ (Stock [Br⁻] = 44.4 mM).

|	Guest (µL)	[**1e**] (M)	[Br⁻] (M)	Equiv.	δ (ppm)
0	0	1.08E-03	0.00E+00	0.00	7.473
1	5	1.08E-03	3.67E-04	0.34	7.588
2	10	1.08E-03	7.28E-04	0.67	7.676
3	15	1.08E-03	1.08E-03	1.00	7.739
4	20	1.08E-03	1.43E-03	1.32	7.785
5	25	1.08E-03	1.78E-03	1.64	7.821
6	30	1.08E-03	2.11E-03	1.95	7.847
7	40	1.08E-03	2.77E-03	2.56	7.884
8	50	1.08E-03	3.42E-03	3.15	7.907
9	60	1.08E-03	4.04E-03	3.72	7.925
10	80	1.08E-03	5.22E-03	4.82	7.946
11	100	1.08E-03	6.34E-03	5.85	7.961
12	150	1.08E-03	8.88E-03	8.19	7.978
13	200	1.08E-03	1.11E-02	10.24	7.994
14	300	1.08E-03	1.48E-02	13.65	8.001
15	400	1.08E-03	1.78E-02	16.39	8.005
16	600	1.08E-03	2.22E-02	20.48	8.008
17	800	1.08E-03	2.54E-02	23.41	8.009
18	1000	1.08E-03	2.77E-02	25.60	8.01
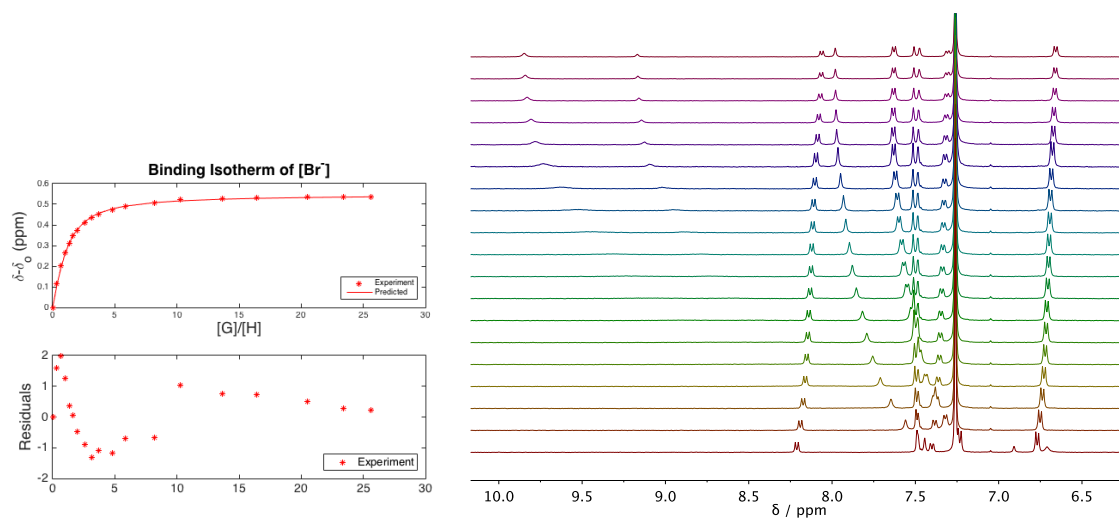
Figure 13. Binding isotherm for Br⁻ titration of **1e** in CDCl₃ by ¹H NMR. ¹H NMR stacked plot of **1e** (1.08 mM) titrated with TBA Br⁻ (0-26 equiv., bottom to top) in CDCl₃.

Table 14. Titration of **1e** with I⁻. (Stock [I⁻] = 99.1 mM)

	Guest (µL)	[**1e**] (M)	[I⁻] (M)	Equiv.	δ (ppm)
0	0	1.15E-03	0.00E+00	0.00	7.445
1	5	1.15E-03	8.19E-04	0.71	7.493
2	10	1.15E-03	1.62E-03	1.41	7.523
3	20	1.15E-03	3.20E-03	2.78	7.573
4	30	1.15E-03	4.72E-03	4.11	7.612
5	40	1.15E-03	6.19E-03	5.39	7.641
6	50	1.15E-03	7.62E-03	6.64	7.665
7	60	1.15E-03	9.01E-03	7.85	7.684
8	80	1.15E-03	1.17E-02	10.15	7.713
9	100	1.15E-03	1.42E-02	12.33	7.733
10	150	1.15E-03	1.98E-02	17.26	7.764
11	200	1.15E-03	2.48E-02	21.58	7.782
12	300	1.15E-03	3.30E-02	28.77	7.799
13	400	1.15E-03	3.96E-02	34.52	7.808
14	500	1.15E-03	4.51E-02	39.23	7.813
15	600	1.15E-03	4.96E-02	43.15	7.816
16	800	1.15E-03	5.66E-02	49.32	7.819
17	1000	1.15E-03	6.19E-02	53.94	7.820
18	1500	1.15E-03	7.08E-02	61.65	7.821
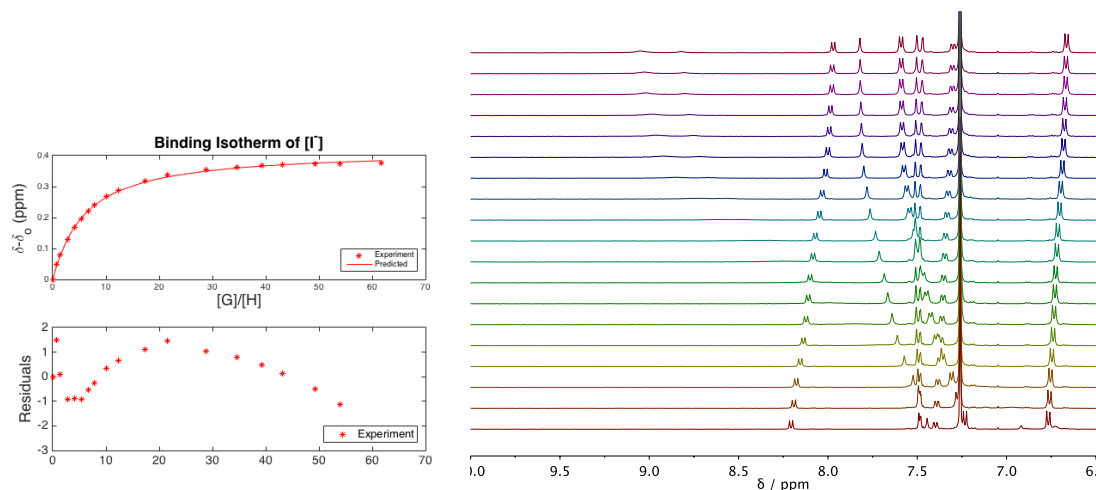
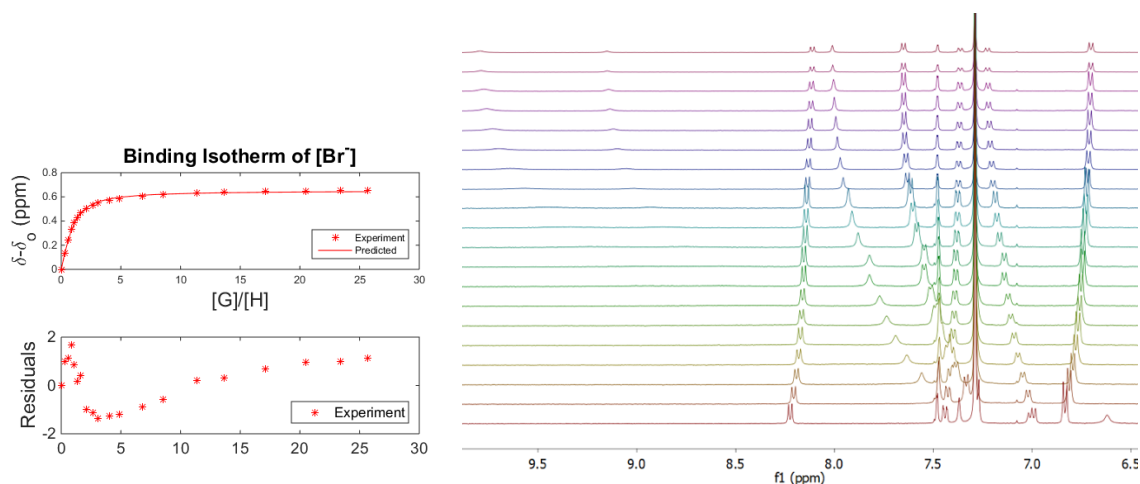**Figure 4.** Binding isotherm for I⁻ titration of **1e** in CDCl₃ by ¹H NMR. ¹H NMR stacked plot of **1b** (1.15 mM) titrated with TBA I⁻ (0-62 equiv., bottom to top) in CDCl₃.

Table 15. Titration of **1e** with NO_3^-. (Stock $[NO_3^-]$ = 40.6 mM)

|	Guest (μL)	[1e] (M)	$[NO_3^-]$ (M)	Equiv.	δ (ppm)
0	0	9.46E-04	0.00E+00	0.00	7.495
1	5	9.46E-04	3.36E-04	0.35	7.692
2	10	9.46E-04	6.66E-04	0.70	7.864
3	15	9.46E-04	9.91E-04	1.05	7.977
4	20	9.46E-04	1.31E-03	1.38	8.05
5	25	9.46E-04	1.63E-03	1.72	8.099
6	30	9.46E-04	1.93E-03	2.04	8.131
7	40	9.46E-04	2.54E-03	2.68	8.172
8	50	9.46E-04	3.13E-03	3.30	8.194
9	60	9.46E-04	3.69E-03	3.90	8.211
10	80	9.46E-04	4.78E-03	5.05	8.229
11	100	9.46E-04	5.80E-03	6.13	8.243
12	150	9.46E-04	8.13E-03	8.59	8.256
13	200	9.46E-04	1.02E-02	10.73	8.264
14	300	9.46E-04	1.35E-02	14.31	8.272
15	400	9.46E-04	1.63E-02	17.17	8.275
16	600	9.46E-04	2.03E-02	21.47	8.28
17	800	9.46E-04	2.32E-02	24.53	8.282
18	1000	9.46E-04	2.54E-02	26.83	8.283
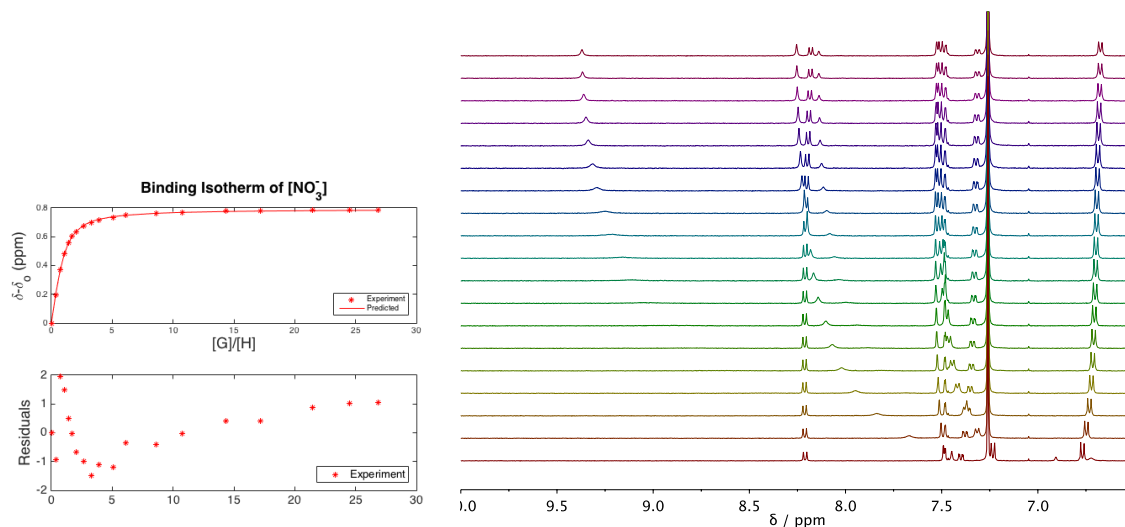
Figure 15. Binding isotherm for NO_3^- titration of **1e** in $CDCl_3$ by ^1H NMR. ^1H NMR stacked plot of **1e** (0.946 mM) titrated with TBA NO_3^- (0-27 equiv., bottom to top) in $CDCl_3$.

Table 16. Titration of **1f** with Cl^-. (Stock [Cl^-] = 41.2 mM)

|	Guest (µL)	[**1f**] (M)	[Cl^-] (M)	Equiv.	δ (ppm)
0	0	7.12E-04	0.00E+00	0	7.399
1	5	7.12E-04	3.41E-04	0.48	7.676
2	10	7.12E-04	6.76E-04	0.95	7.859
3	15	7.12E-04	1.01E-03	1.41	7.955
4	20	7.12E-04	1.33E-03	1.87	8.004
5	25	7.12E-04	1.65E-03	2.32	8.032
6	30	7.12E-04	1.96E-03	2.76	8.048
7	40	7.12E-04	2.58E-03	3.62	8.068
8	50	7.12E-04	3.17E-03	4.45	8.078
9	60	7.12E-04	3.75E-03	5.26	8.086
10	80	7.12E-04	4.85E-03	6.81	8.095
11	100	7.12E-04	5.89E-03	8.27	8.103
12	150	7.12E-04	8.24E-03	11.58	8.114
13	200	7.12E-04	1.03E-02	14.47	8.123
14	300	7.12E-04	1.37E-02	19.29	8.134
15	400	7.12E-04	1.65E-02	23.15	8.14
16	600	7.12E-04	2.06E-02	28.94	8.148
17	800	7.12E-04	2.36E-02	33.08	8.15
18	1100	7.12E-04	2.67E-02	37.45	8.151
19	1500	7.12E-04	2.94E-02	41.34	8.151
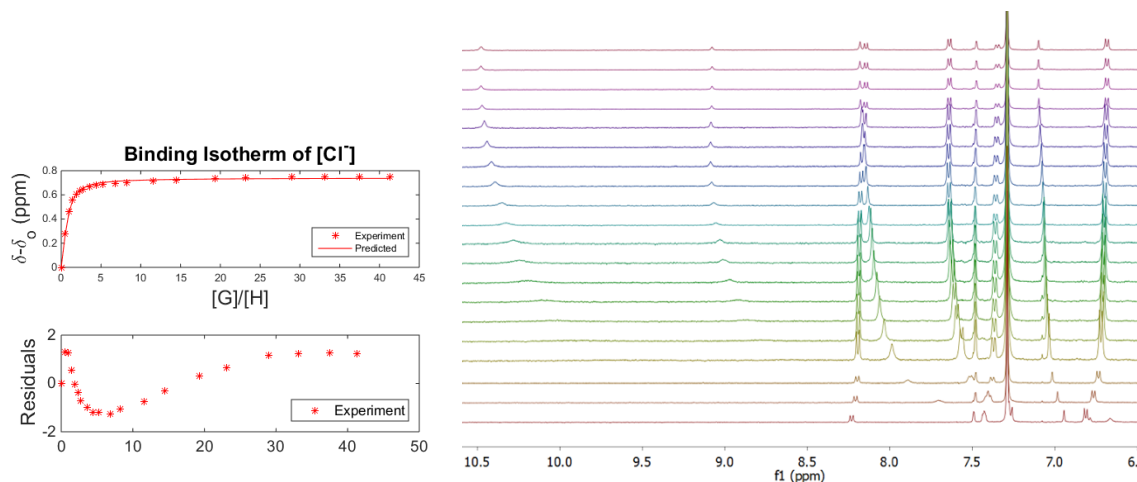
Figure 16. Binding isotherm for Cl⁻ titration of **1f** in CDCl₃ by ¹H NMR. ¹H NMR stacked plot of **1f** (0.712 mM) titrated with TBA Cl⁻ (0-41.34 equiv., bottom to top) in CDCl₃.

Table 17. Titration of **1f** with Br⁻. (Stock [Br⁻] = 35.2 mM)

|	Guest (μL)	[**1f**] (M)	[Br⁻] (M)	Equiv.	δ (ppm)
0	0	7.34E-04	0.00E+00	0	7.399
1	5	7.34E-04	2.91E-04	0.40	7.514
2	10	7.34E-04	5.78E-04	0.79	7.599
3	15	7.34E-04	8.60E-04	1.17	7.663
4	20	7.34E-04	1.14E-03	1.55	7.711
5	25	7.34E-04	1.41E-03	1.92	7.75
6	30	7.34E-04	1.68E-03	2.29	7.779
7	40	7.34E-04	2.20E-03	3.00	7.819
8	50	7.34E-04	2.71E-03	3.69	7.846
9	60	7.34E-04	3.20E-03	4.36	7.871
10	80	7.34E-04	4.15E-03	5.65	7.897
11	100	7.34E-04	5.03E-03	6.86	7.912
12	150	7.34E-04	7.05E-03	9.60	7.94
13	200	7.34E-04	8.81E-03	12.00	7.955
14	300	7.34E-04	1.17E-02	16.00	7.972
15	400	7.34E-04	1.41E-02	19.19	7.981
16	600	7.34E-04	1.76E-02	23.99	7.99
17	800	7.34E-04	2.01E-02	27.42	7.994
18	1100	7.34E-04	2.28E-02	31.05	7.994
19	1500	7.34E-04	0.025173	34.27	7.994
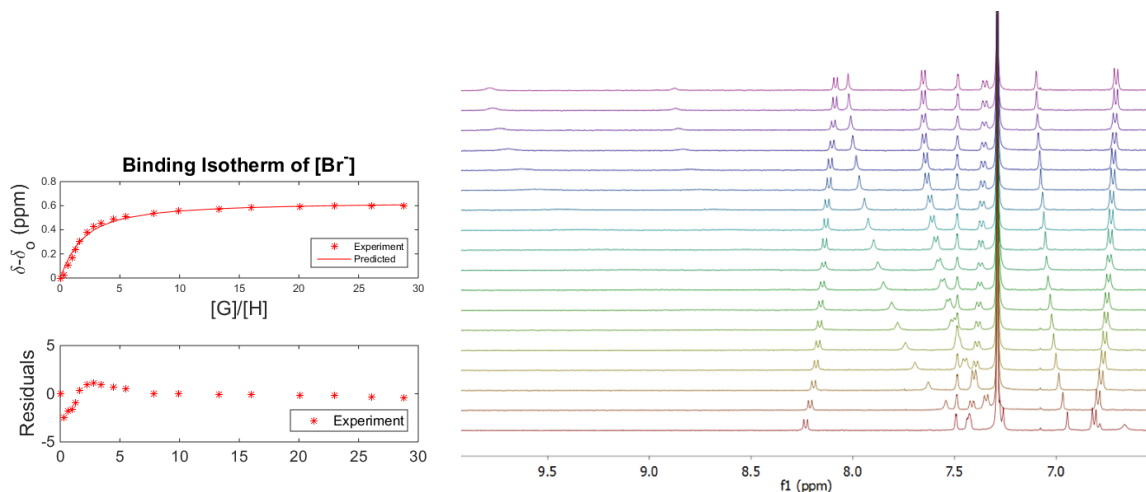
Figure 17. Binding isotherm for Br⁻ titration of **1f** in CDCl₃ by ¹H NMR. ¹H NMR stacked plot of **1f** (0.734 mM) titrated with TBA Br⁻ (0-34.27 equiv., bottom to top) in CDCl₃.

Table 18. Titration of **1f** with I⁻. (Stock [I⁻] = 81.2 mM)

|	Guest (µL)	[**1f**] (M)	[I⁻] (M)	Equiv.	δ (ppm)
0	0	6.54E-04	0.00E+00	0	7.394
1	5	6.54E-04	6.71E-04	1.03	7.44
2	10	6.54E-04	1.33E-03	2.03	7.478
3	15	6.54E-04	1.98E-03	3.03	7.508
4	20	6.54E-04	2.62E-03	4.00	7.535
5	25	6.54E-04	3.25E-03	4.96	7.556
6	30	6.54E-04	3.86E-03	5.91	7.575
7	40	6.54E-04	5.07E-03	7.75	7.608
8	50	6.54E-04	6.24E-03	9.54	7.635
9	60	6.54E-04	7.38E-03	11.28	7.658
10	80	6.54E-04	9.55E-03	14.59	7.689
11	100	6.54E-04	1.16E-02	17.72	7.711
12	150	6.54E-04	1.62E-02	24.81	7.748
13	200	6.54E-04	2.03E-02	31.01	7.771
14	300	6.54E-04	2.71E-02	41.35	7.797
15	400	6.54E-04	3.25E-02	49.62	7.811
16	600	6.54E-04	4.06E-02	62.02	7.821
17	800	6.54E-04	4.64E-02	70.88	7.826
18	1100	6.54E-04	5.25E-02	80.26	7.827
19	1500	6.54E-04	5.80E-02	88.6	7.825
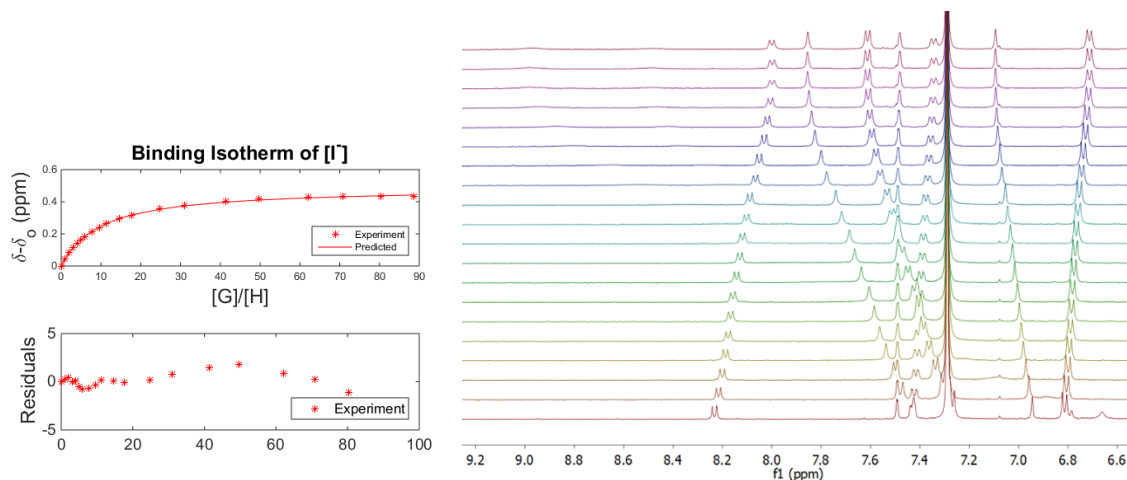
Figure 18. Binding isotherm for I^- titration of **1f** in $CDCl_3$ by ^1H NMR. ^1H NMR stacked plot of **1f** (0.654 mM) titrated with TBA I^- (0-88.60 equiv., bottom to top) in $CDCl_3$.

Table 19. Titration of **1g** with Cl^-. (Stock $[Cl^-]$ = 48.3 mM).

|	Guest (μL)	**[1g]** (M)	$[Cl^-]$ (M)	Equiv.	δ (ppm)
0	0	8.27E-04	0.00E+00	0.00	7.468
1	5	8.27E-04	4.00E-04	0.48	7.720
2	10	8.27E-04	7.92E-04	0.96	7.870
3	20	8.27E-04	1.56E-03	1.89	7.946
4	30	8.27E-04	2.30E-03	2.78	7.988
5	50	8.27E-04	3.72E-03	4.50	8.014
6	70	8.27E-04	5.05E-03	6.11	8.032
7	90	8.27E-04	6.31E-03	7.63	8.054
8	110	8.27E-04	7.49E-03	9.06	8.068
9	130	8.27E-04	8.61E-03	10.41	8.078
10	150	8.27E-04	9.67E-03	11.69	8.091
11	190	8.27E-04	1.16E-02	14.06	8.100
12	240	8.27E-04	1.38E-02	16.70	8.114
13	300	8.27E-04	1.61E-02	19.49	8.123
14	400	8.27E-04	1.93E-02	23.39	8.135
15	500	8.27E-04	2.20E-02	26.58	8.143
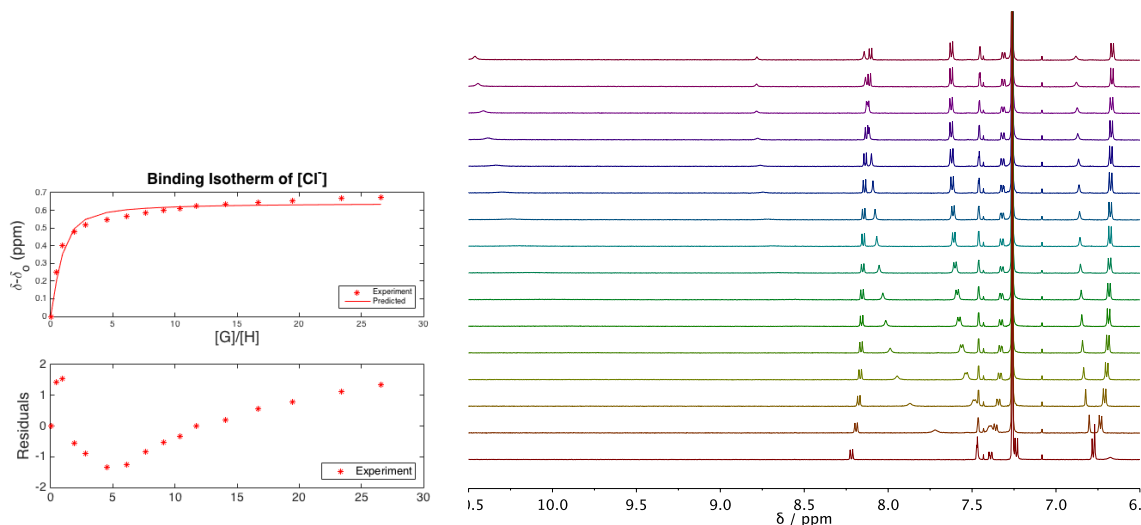
Figure 19. Binding isotherm for Cl⁻ titration of **1g** in CDCl$_3$ by ¹H NMR. ¹H NMR stacked plot of **1g** (0.827 mM) titrated with TBA Cl⁻ (0-27 equiv., bottom to top) in CDCl$_3$.

Table 20. Titration of **1g** with Br⁻. (Stock [Br⁻] = 46.9 mM)

|	Guest (µL)	**[1g]** (M)	[Br⁻] (M)	Equiv.	δ (ppm)
0	0	1.17E-03	0.00E+00	0.00	7.466
1	5	1.17E-03	3.87E-04	0.33	7.557
2	10	1.17E-03	7.68E-04	0.66	7.629
3	15	1.17E-03	1.14E-03	0.97	7.685
4	20	1.17E-03	1.51E-03	1.29	7.730
5	30	1.17E-03	2.23E-03	1.90	7.792
6	40	1.17E-03	2.93E-03	2.50	7.832
7	50	1.17E-03	3.61E-03	3.07	7.861
8	60	1.17E-03	4.26E-03	3.63	7.882
9	80	1.17E-03	5.51E-03	4.70	7.910
10	100	1.17E-03	6.70E-03	5.71	7.930
11	125	1.17E-03	8.08E-03	6.89	7.947
12	150	1.17E-03	9.37E-03	7.99	7.959
13	200	1.17E-03	1.17E-02	9.99	7.975
14	300	1.17E-03	1.56E-02	13.32	7.994
15	400	1.17E-03	1.87E-02	15.99	8.005
16	600	1.17E-03	2.34E-02	19.99	8.013
17	800	1.17E-03	2.68E-02	22.84	8.022
18	1000	1.17E-03	2.93E-02	24.98	8.036
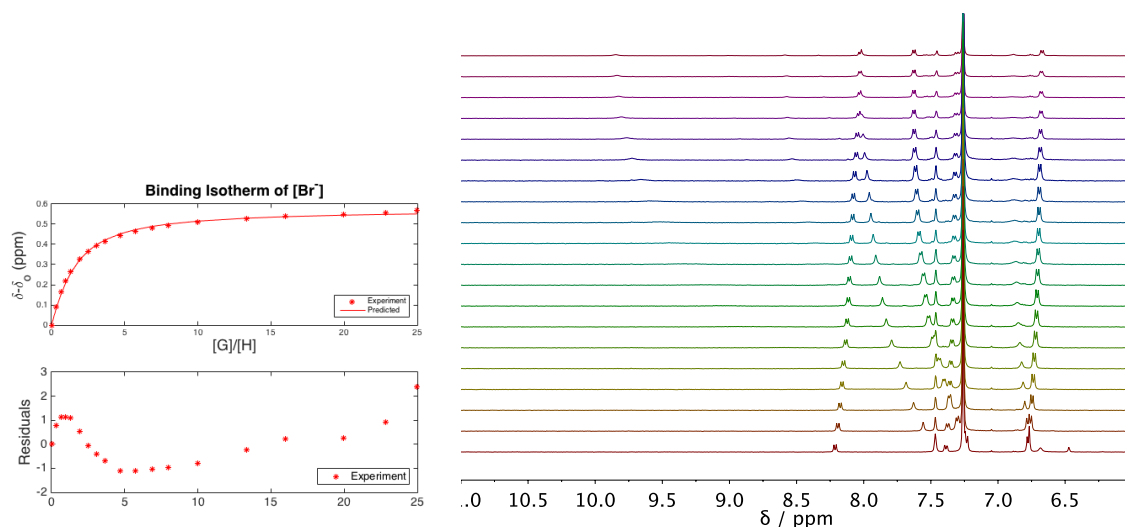
Figure 20. Binding isotherm for Br⁻ titration of **1g** in CDCl₃ by ¹H NMR. ¹H NMR stacked plot of **1g** (1.17 mM) titrated with TBA Br⁻ (0-25 equiv., bottom to top) in CDCl₃.

Table 21. Titration of **1g** with I⁻. (Stock [I⁻] = 113 mM)

|	Guest (µL)	[**1g**] (M)	[I⁻] (M)	Equiv.	δ (ppm)
0	0	1.21E-03	0.00E+00	0.00	7.466
1	5	1.21E-03	9.38E-04	0.78	7.498
2	10	1.21E-03	1.86E-03	1.54	7.524
3	20	1.21E-03	3.66E-03	3.03	7.565
4	30	1.21E-03	5.40E-03	4.48	7.6
5	40	1.21E-03	7.09E-03	5.87	7.628
6	50	1.21E-03	8.73E-03	7.23	7.651
7	60	1.21E-03	1.03E-02	8.54	7.671
8	80	1.21E-03	1.33E-02	11.06	7.701
9	100	1.21E-03	1.62E-02	13.43	7.724
10	150	1.21E-03	2.27E-02	18.80	7.761
11	200	1.21E-03	2.84E-02	23.49	7.782
12	300	1.21E-03	3.78E-02	31.33	7.804
13	400	1.21E-03	4.54E-02	37.59	7.815
14	500	1.21E-03	5.16E-02	42.72	7.822
15	600	1.21E-03	5.67E-02	46.99	7.826
16	800	1.21E-03	6.48E-02	53.70	7.83
17	1000	1.21E-03	7.09E-02	58.74	7.831
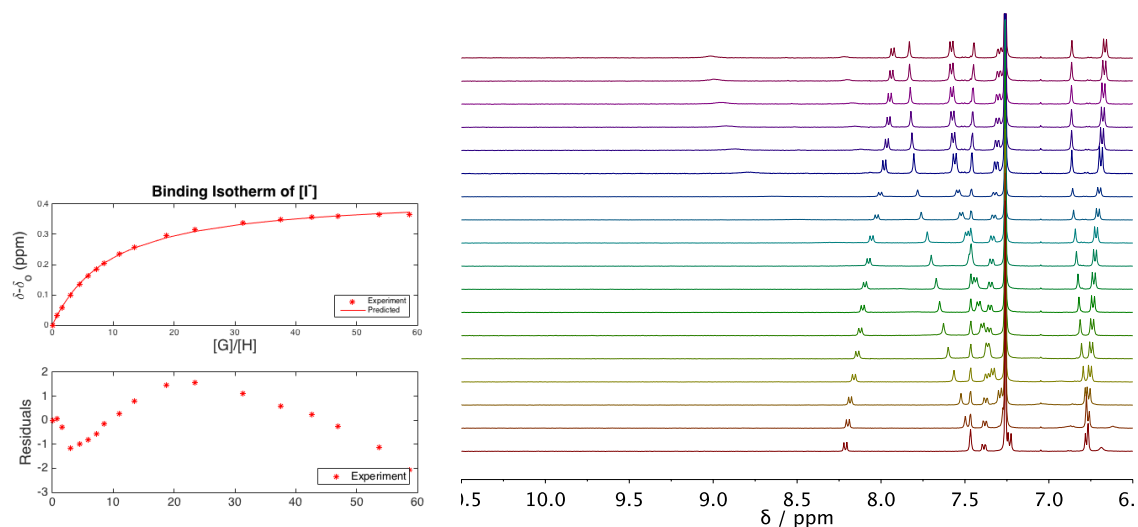
Figure 21. Binding isotherm for I⁻ titration of **1g** in CDCl₃ by ¹H NMR. ¹H NMR stacked plot of **1g** (1.21 mM) titrated with TBA I⁻ (0-59 equiv., bottom to top) in CDCl₃.

Table 22. Titration of **1g** with NO_3^-. (Stock $[NO_3^-]$ = 37.3 mM)

|	Guest (µL)	**[1g]** (M)	$[NO_3^-]$ (M)	Equiv.	δ (ppm)
0	0	9.19E-04	0.00E+00	0.00	7.467
1	5	9.19E-04	3.09E-04	0.34	7.638
2	10	9.19E-04	6.12E-04	0.67	7.772
3	15	9.19E-04	9.11E-04	0.99	7.877
4	20	9.19E-04	1.21E-03	1.31	7.946
5	30	9.19E-04	1.78E-03	1.94	8.034
6	40	9.19E-04	2.33E-03	2.54	8.084
7	50	9.19E-04	2.87E-03	3.13	8.117
8	60	9.19E-04	3.40E-03	3.70	8.139
9	80	9.19E-04	4.39E-03	4.78	8.167
10	100	9.19E-04	5.34E-03	5.81	8.185
11	125	9.19E-04	6.44E-03	7.01	8.2
12	150	9.19E-04	7.47E-03	8.13	8.209
13	200	9.19E-04	9.34E-03	10.17	8.221
14	300	9.19E-04	1.25E-02	13.55	8.234
15	400	9.19E-04	1.49E-02	16.26	8.241
16	600	9.19E-04	1.87E-02	20.33	8.248
17	800	9.19E-04	2.13E-02	23.24	8.251
18	1000	9.19E-04	2.33E-02	25.41	8.253
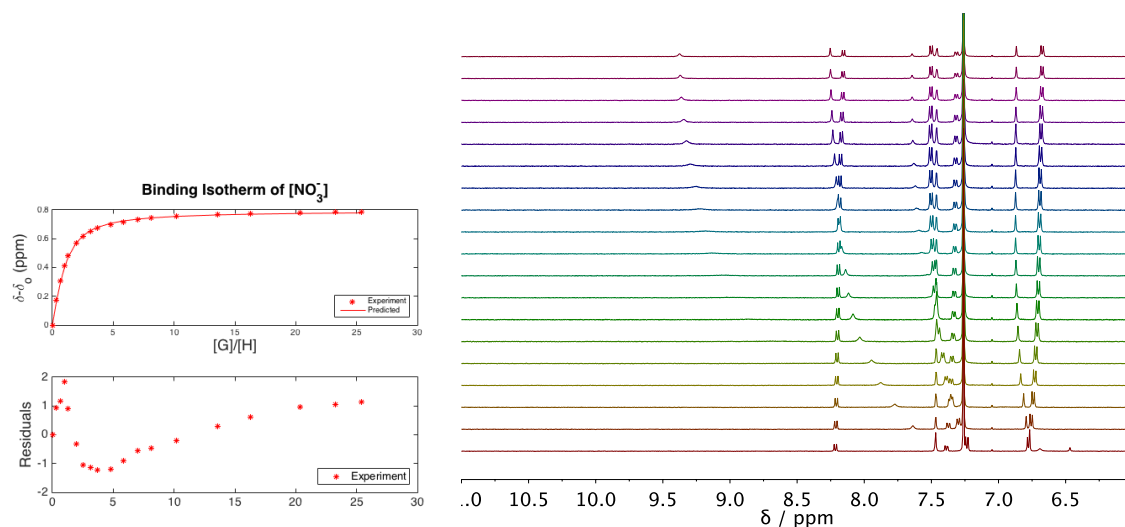
Figure 22. Binding isotherm for NO_3^- titration of **1g** in $CDCl_3$ by ^1H NMR. ^1H NMR stacked plot of **1g** (0.919 mM) titrated with TBA NO_3^- (0-25 equiv., bottom to top) in $CDCl_3$.

UV-vis Titrations

Table 23. Titration of **1a** with NO_3^-. (Stock $[NO_3^-]$ = 2.97 mM).

|	Guest (µL)	[**1a**] (M)	$[NO_3^-]$ (M)	Equiv.
0	0	1.14E-05	0.00E+00	0.00
1	5	1.14E-05	7.41E-06	0.65
2	20	1.14E-05	2.94E-05	2.59
3	30	1.14E-05	4.39E-05	3.87
4	50	1.14E-05	7.25E-05	6.39
5	70	1.14E-05	1.01E-04	8.86
6	90	1.14E-05	1.28E-04	11.28
7	110	1.14E-05	1.55E-04	13.65
8	130	1.14E-05	1.81E-04	15.98
9	150	1.14E-05	2.07E-04	18.27
10	190	1.14E-05	2.58E-04	22.72
11	230	1.14E-05	3.07E-04	27.01
12	270	1.14E-05	3.54E-04	31.15
13	310	1.14E-05	3.99E-04	35.14
14	360	1.14E-05	4.53E-04	39.94
15	410	1.14E-05	5.06E-04	44.55
16	510	1.14E-05	6.04E-04	53.21
17	710	1.14E-05	7.79E-04	68.61
18	910	1.14E-05	9.30E-04	81.89
19	1110	1.14E-05	1.06E-03	93.46
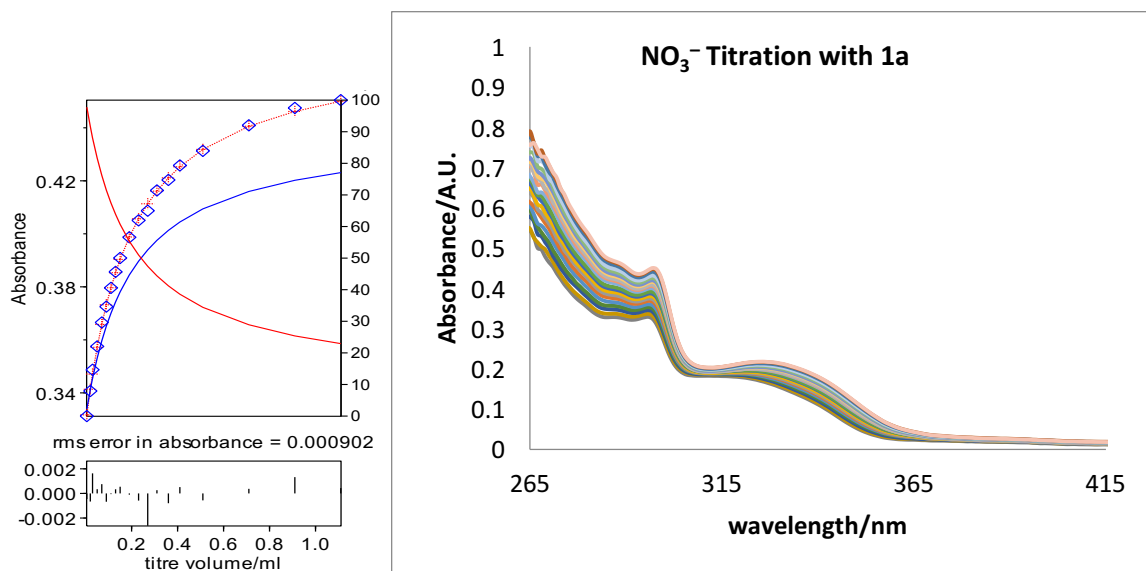
Figure 23. Binding isotherm for NO_3^- titration of **1a** in $CHCl_3$ by UV-vis. Stacked spectra of **1a** (11.4 μM) titrated with TBA NO_3^- (0-93 equiv., increasing abs.) in $CDCl_3$.

Table 24. Titration of **1b** with Cl^-. (Stock $[Cl^-]$ = 2.42 mM)

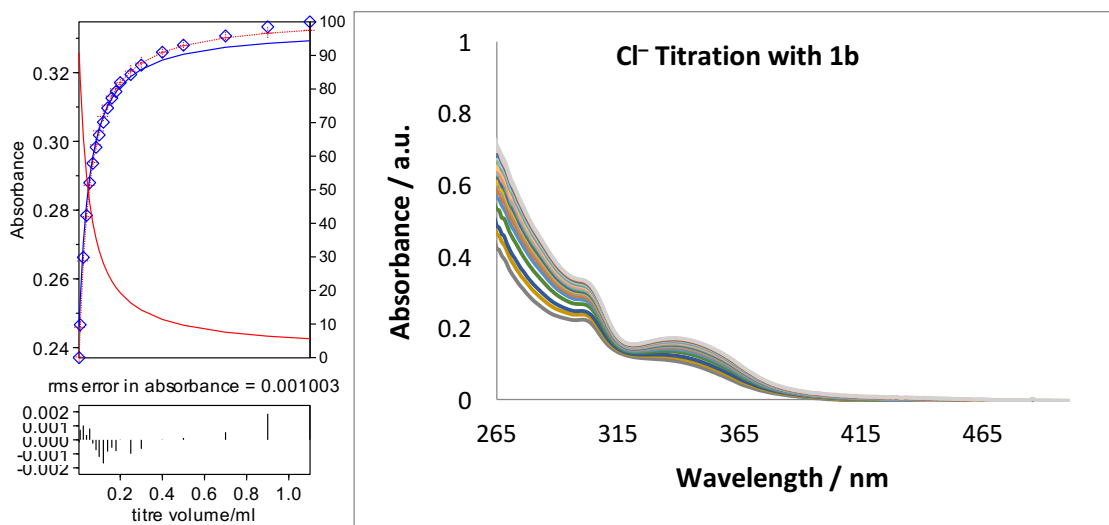|	Guest (μL)	[1b] (M)	$[Cl^-]$ (M)	Equiv.
0	0	1.04E-05	0.00E+00	0.00
1	5	1.04E-05	6.03E-06	0.58
2	10	1.04E-05	1.20E-05	1.16
3	25	1.04E-05	2.99E-05	2.88
4	40	1.04E-05	4.74E-05	4.57
5	55	1.04E-05	6.47E-05	6.24
6	70	1.04E-05	8.18E-05	7.89
7	85	1.04E-05	9.86E-05	9.51
8	100	1.04E-05	1.15E-04	11.11
9	120	1.04E-05	1.37E-04	13.20
10	140	1.04E-05	1.58E-04	15.26
11	160	1.04E-05	1.79E-04	17.27
12	180	1.04E-05	2.00E-04	19.26
13	200	1.04E-05	2.20E-04	21.20
14	250	1.04E-05	2.69E-04	25.91
15	300	1.04E-05	3.15E-04	30.42
16	400	1.04E-05	4.03E-04	38.87
17	500	1.04E-05	4.84E-04	46.64
18	700	1.04E-05	6.27E-04	60.46
19	900	1.04E-05	7.50E-04	72.38
20	1100	1.04E-05	8.58E-04	82.75

Figure 24. Binding isotherm for Cl⁻ titration of **1b** in CHCl₃ by UV-vis. Stacked spectra of **1b** (10.4 μM) titrated with TBA Cl⁻ (0-83 equiv., increasing abs.) in CDCl₃.

Table 25. Titration of **1b** with Br⁻. (Stock [Br⁻] = 2.61 mM)

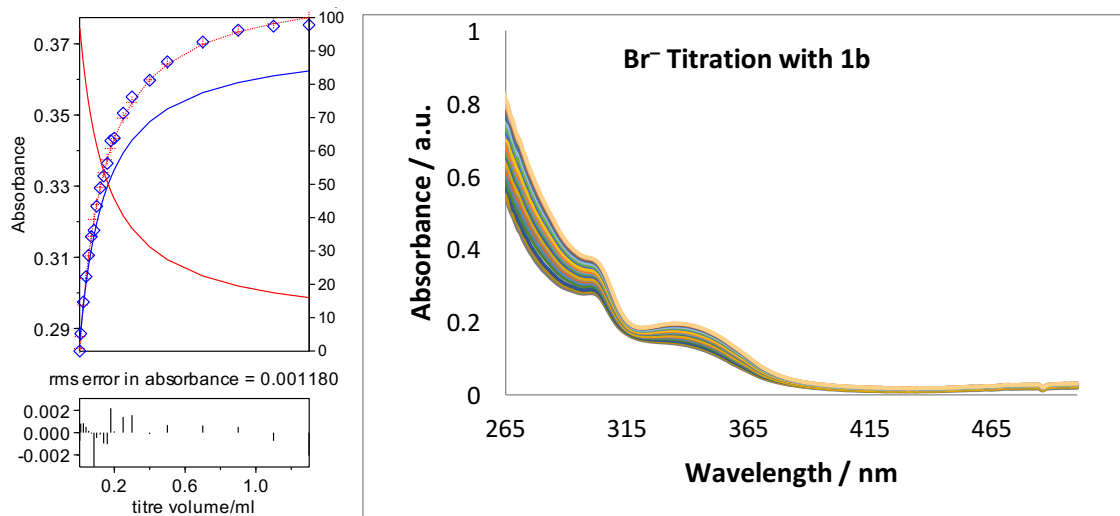|	Guest (μL)	[**1b**] (M)	[Br⁻] (M)	Equiv.
0	0	9.72E-06	0.00E+00	0.00
1	5	9.72E-06	6.52E-06	0.67
2	10	9.72E-06	1.30E-05	1.34
3	25	9.72E-06	3.23E-05	3.32
4	40	9.72E-06	5.12E-05	5.27
5	55	9.72E-06	6.99E-05	7.20
6	70	9.72E-06	8.84E-05	9.09
7	85	9.72E-06	1.07E-04	10.96
8	100	9.72E-06	1.24E-04	12.81
9	120	9.72E-06	1.48E-04	15.22
10	140	9.72E-06	1.71E-04	17.59
11	160	9.72E-06	1.94E-04	19.92
12	180	9.72E-06	2.16E-04	22.21
13	200	9.72E-06	2.38E-04	24.45
14	250	9.72E-06	2.90E-04	29.88
15	300	9.72E-06	3.41E-04	35.08
16	400	9.72E-06	4.36E-04	44.82
17	500	9.72E-06	5.23E-04	53.79
18	700	9.72E-06	6.78E-04	69.72
19	900	9.72E-06	8.11E-04	83.46
20	1100	9.72E-06	9.27E-04	95.43
21	1300	9.72E-06	1.03E-03	105.94

Figure 25. Binding isotherm for Br⁻ titration of **1b** in CHCl₃ by UV-vis. Stacked spectra of **1b** (9.72 µM) titrated with TBA Br⁻ (0-105 equiv., increasing abs.) in CDCl₃.

Table 26. Titration of **1b** with NO_3^-. (Stock $[NO_3^-]$ = 2.35 mM).

	Guest (µL)	[**1b**] (M)	$[NO_3^-]$ (M)	Equiv.
00	0	1.02E-05	0.00E+00	0.00
01	5	1.02E-05	5.87E-06	0.58
02	10	1.02E-05	1.17E-05	1.15
03	25	1.02E-05	2.91E-05	2.85
04	40	1.02E-05	4.62E-05	4.52
05	55	1.02E-05	6.30E-05	6.17
06	70	1.02E-05	7.96E-05	7.80
07	85	1.02E-05	9.60E-05	9.40
08	100	1.02E-05	1.12E-04	10.98
09	130	1.02E-05	1.44E-04	14.08
10	160	1.02E-05	1.74E-04	17.08
11	190	1.02E-05	2.04E-04	20.01
12	220	1.02E-05	2.33E-04	22.86
13	250	1.02E-05	2.62E-04	25.63
14	300	1.02E-05	3.07E-04	30.08
15	400	1.02E-05	3.92E-04	38.44
16	500	1.02E-05	4.71E-04	46.13
17	700	1.02E-05	6.11E-04	59.79
18	900	1.02E-05	7.31E-04	71.58
19	1100	1.02E-05	8.36E-04	81.84

Figure 26. Binding isotherm for NO_3^- titration of **1b** in $CHCl_3$ by UV-vis. Stacked spectra of **1b** (10.2 μM) titrated with TBA NO_3^- (0-82 equiv., increasing abs.) in $CDCl_3$.

Table 27. Titration of **1c** with Cl^-. (Stock $[Cl^-]$ = 2.39 mM).

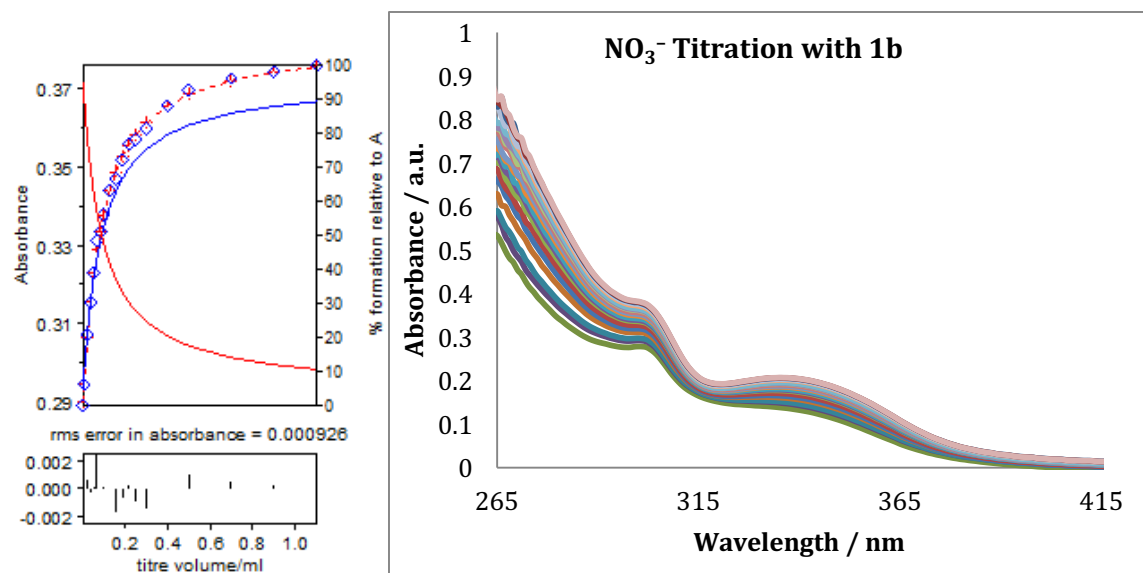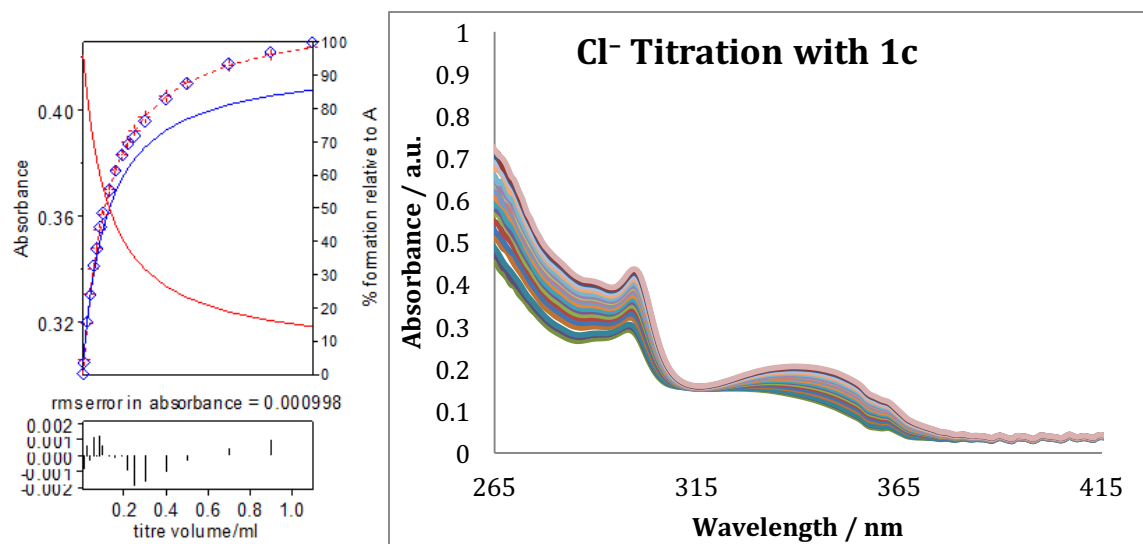|	Guest (μL)	**[1c]** (M)	$[Cl^-]$ (M)	Equiv.
00	0	1.02E-05	0.00E+00	0.00
01	5	1.02E-05	5.97E-06	0.59
02	10	1.02E-05	1.19E-05	1.17
03	25	1.02E-05	2.95E-05	2.90
04	40	1.02E-05	4.69E-05	4.61
05	55	1.02E-05	6.40E-05	6.29
06	70	1.02E-05	8.09E-05	7.95
07	85	1.02E-05	9.75E-05	9.58
08	100	1.02E-05	1.14E-04	11.19
09	130	1.02E-05	1.46E-04	14.34
10	160	1.02E-05	1.77E-04	17.41
11	190	1.02E-05	2.08E-04	20.39
12	220	1.02E-05	2.37E-04	23.29
13	250	1.02E-05	2.66E-04	26.11
14	300	1.02E-05	3.12E-04	30.65
15	400	1.02E-05	3.99E-04	39.17
16	500	1.02E-05	4.79E-04	47.00
17	700	1.02E-05	6.20E-04	60.93
18	900	1.02E-05	7.43E-04	72.94
19	1100	1.02E-05	8.49E-04	83.39

Figure 27. Binding isotherm for Cl⁻ titration of **1c** in CHCl₃ by UV-vis. Stacked spectra of **1c** (10.2 μM) titrated with TBA Cl⁻ (0-83 equiv., increasing abs.) in CDCl₃.

Table 28. Titration of **1c** with Br⁻. (Stock [Br⁻] = 2.36 mM).

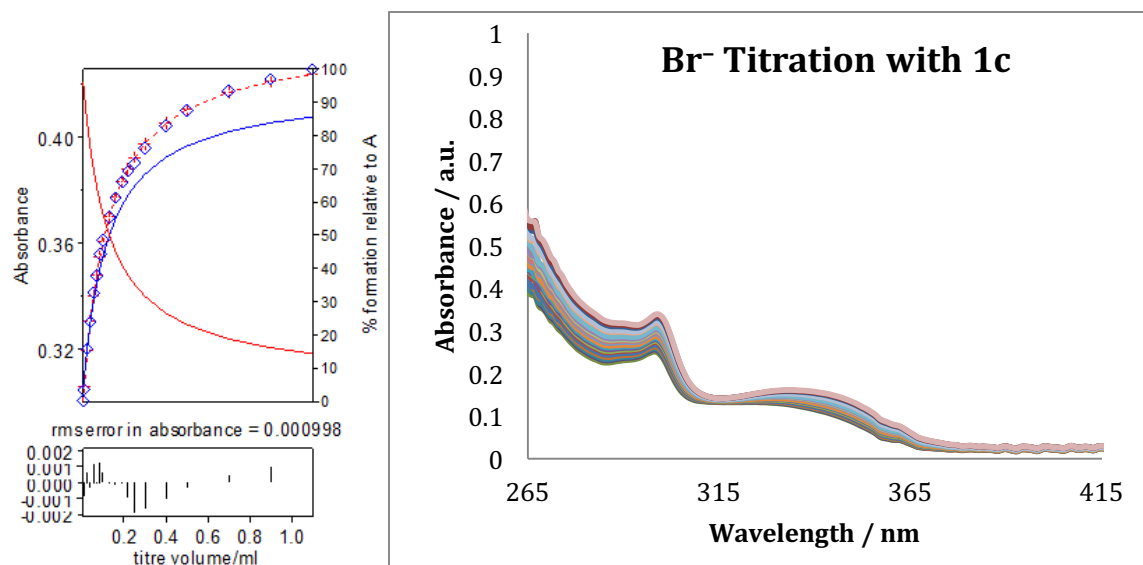|	Guest (μL)	[1c] (M)	[Br–] (M)	Equiv.
00	0	1.02E-05	0.00E+00	0.00
01	5	1.02E-05	5.88E-06	0.58
02	10	1.02E-05	1.17E-05	1.15
03	25	1.02E-05	2.91E-05	2.87
04	40	1.02E-05	4.62E-05	4.55
05	55	1.02E-05	6.31E-05	6.21
06	70	1.02E-05	7.97E-05	7.85
07	85	1.02E-05	9.61E-05	9.46
08	100	1.02E-05	1.12E-04	11.05
09	130	1.02E-05	1.44E-04	14.16
10	160	1.02E-05	1.75E-04	17.19
11	190	1.02E-05	2.04E-04	20.13
12	220	1.02E-05	2.34E-04	23.00
13	250	1.02E-05	2.62E-04	25.79
14	300	1.02E-05	3.07E-04	30.27
15	400	1.02E-05	3.93E-04	38.68
16	500	1.02E-05	4.71E-04	46.41
17	700	1.02E-05	6.11E-04	60.17
18	900	1.02E-05	7.31E-04	72.02
19	1100	1.02E-05	8.36E-04	82.35

Figure 28. Binding isotherm for Br⁻ titration of **1c** in CHCl₃ by UV-vis. Stacked spectra of **1c** (10.2 μM) titrated with TBA Br⁻ (0-82 equiv., increasing abs.) in CDCl₃.

Table 29. Titration of **1c** with NO_3^-. (Stock $[NO_3^-]$ = 2.35 mM).

	Guest (μL)	[**1c**] (M)	$[NO_3^-]$ (M)	Equiv.
00	0	1.02E-05	0.00E+00	0.00
01	5	1.02E-05	5.85E-06	0.57
02	10	1.02E-05	1.17E-05	1.14
03	25	1.02E-05	2.90E-05	2.83
04	40	1.02E-05	4.60E-05	4.49
05	55	1.02E-05	6.28E-05	6.13
06	70	1.02E-05	7.94E-05	7.75
07	85	1.02E-05	9.57E-05	9.34
08	100	1.02E-05	1.12E-04	10.91
09	130	1.02E-05	1.43E-04	13.98
10	160	1.02E-05	1.74E-04	16.97
11	190	1.02E-05	2.04E-04	19.87
12	220	1.02E-05	2.33E-04	22.70
13	250	1.02E-05	2.61E-04	25.45
14	300	1.02E-05	3.06E-04	29.88
15	400	1.02E-05	3.91E-04	38.18
16	500	1.02E-05	4.69E-04	45.81
17	700	1.02E-05	6.09E-04	59.39
18	900	1.02E-05	7.28E-04	71.09
19	1100	1.02E-05	8.33E-04	81.28
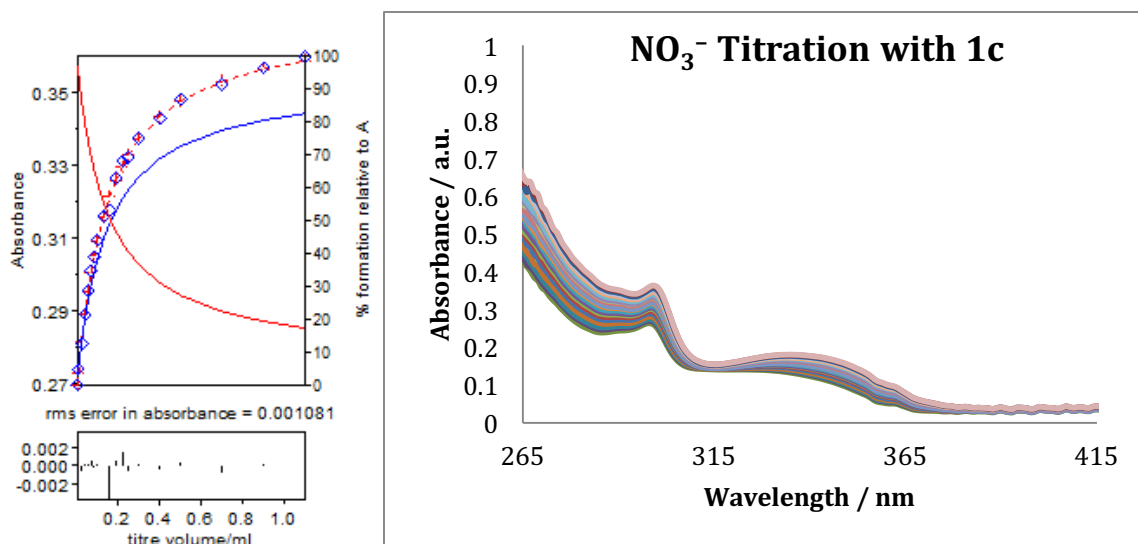
Figure 29. Binding isotherm for NO_3^- titration of **1c** in $CHCl_3$ by UV-vis. Stacked spectra of **1c** (10.2 μM) titrated with TBA NO_3^- (0-81 equiv., increasing abs.) in $CDCl_3$.

Table 30. Titration of **1d** with Cl^-. (Stock $[Cl^-]$ = 2.46 mM).

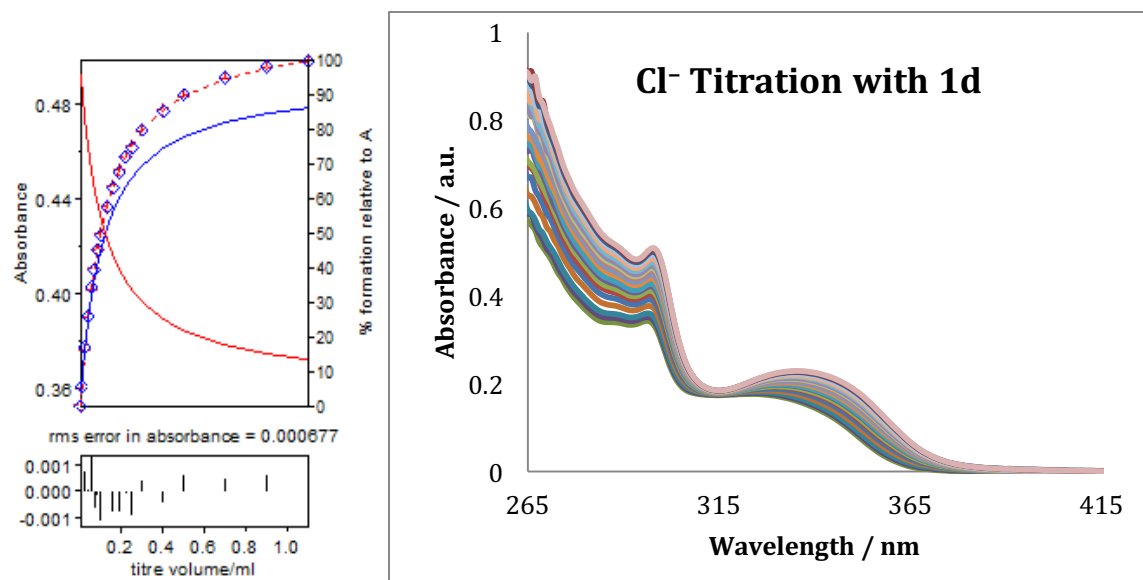|	Guest (μL)	[1d] (M)	[Cl⁻] (M)	Equiv.
00	0	1.08E-05	0.00E+00	0.00
01	5	1.08E-05	6.13E-06	0.57
02	10	1.08E-05	1.22E-05	1.13
03	25	1.08E-05	3.03E-05	2.81
04	40	1.08E-05	4.82E-05	4.46
05	55	1.08E-05	6.58E-05	6.09
06	70	1.08E-05	8.31E-05	7.69
07	85	1.08E-05	1.00E-04	9.28
08	100	1.08E-05	1.17E-04	10.83
09	130	1.08E-05	1.50E-04	13.89
10	160	1.08E-05	1.82E-04	16.85
11	190	1.08E-05	2.13E-04	19.74
12	220	1.08E-05	2.44E-04	22.55
13	250	1.08E-05	2.73E-04	25.28
14	300	1.08E-05	3.21E-04	29.68
15	400	1.08E-05	4.10E-04	37.92
16	500	1.08E-05	4.92E-04	45.50
17	700	1.08E-05	6.37E-04	58.99
18	900	1.08E-05	7.63E-04	70.61
19	1100	1.08E-05	8.72E-04	80.73

Figure 30. Binding isotherm for Cl⁻ titration of **1d** in CHCl₃ by UV-vis. Stacked spectra of **1d** (10.8 μM) titrated with TBA Cl⁻ (0-81 equiv., increasing abs.) in CDCl₃.

Table 31. Titration of **1d** with Br⁻. (Stock [Br⁻] = 2.39 mM).

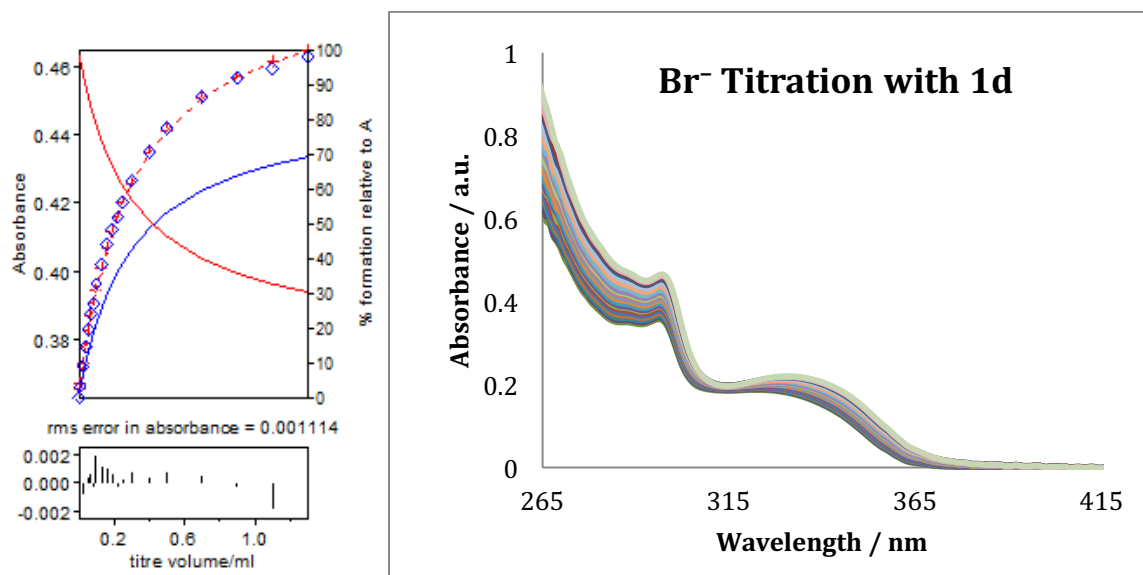|	Guest (μL)	[**1d**] (M)	[Br⁻] (M)	Equiv.
00	0	1.26E-05	0.00E+00	0.00
01	5	1.26E-05	5.96E-06	0.47
02	10	1.26E-05	1.19E-05	0.94
03	25	1.26E-05	2.95E-05	2.34
04	40	1.26E-05	4.68E-05	3.71
05	55	1.26E-05	6.39E-05	5.07
06	70	1.26E-05	8.08E-05	6.40
07	85	1.26E-05	9.74E-05	7.72
08	100	1.26E-05	1.14E-04	9.01
09	130	1.26E-05	1.46E-04	11.55
10	160	1.26E-05	1.77E-04	14.02
11	190	1.26E-05	2.07E-04	16.42
12	220	1.26E-05	2.37E-04	18.76
13	250	1.26E-05	2.65E-04	21.03
14	300	1.26E-05	3.12E-04	24.69
15	400	1.26E-05	3.98E-04	31.55
16	500	1.26E-05	4.78E-04	37.86
17	700	1.26E-05	6.19E-04	49.08
18	900	1.26E-05	7.42E-04	58.75
19	1100	1.26E-05	8.48E-04	67.18
20	1300	1.26E-05	9.41E-04	74.58

Figure 31. Binding isotherm for Br⁻ titration of **1d** in CHCl₃ by UV-vis. Stacked spectra of **1d** (12.6 µM) titrated with TBA Br⁻ (0-75 equiv., increasing abs.) in CDCl₃.

Table 32. Titration of **1d** with NO_3^-. (Stock $[NO_3^-]$ = 2.35 mM).

	Guest (µL)	[**1d**] (M)	$[NO_3^-]$ (M)	Equiv.
00	0	1.03E-05	0.00E+00	0.00
01	5	1.03E-05	5.86E-06	0.57
02	10	1.03E-05	1.17E-05	1.14
03	25	1.03E-05	2.90E-05	2.83
04	40	1.03E-05	4.60E-05	4.49
05	55	1.03E-05	6.29E-05	6.13
06	70	1.03E-05	7.94E-05	7.74
07	85	1.03E-05	9.57E-05	9.33
08	100	1.03E-05	1.12E-04	10.90
09	130	1.03E-05	1.43E-04	13.97
10	160	1.03E-05	1.74E-04	16.96
11	190	1.03E-05	2.04E-04	19.86
12	220	1.03E-05	2.33E-04	22.68
13	250	1.03E-05	2.61E-04	25.43
14	300	1.03E-05	3.06E-04	29.86
15	400	1.03E-05	3.91E-04	38.15
16	500	1.03E-05	4.70E-04	45.78
17	700	1.03E-05	6.09E-04	59.35
18	900	1.03E-05	7.29E-04	71.04
19	1100	1.03E-05	8.33E-04	81.22
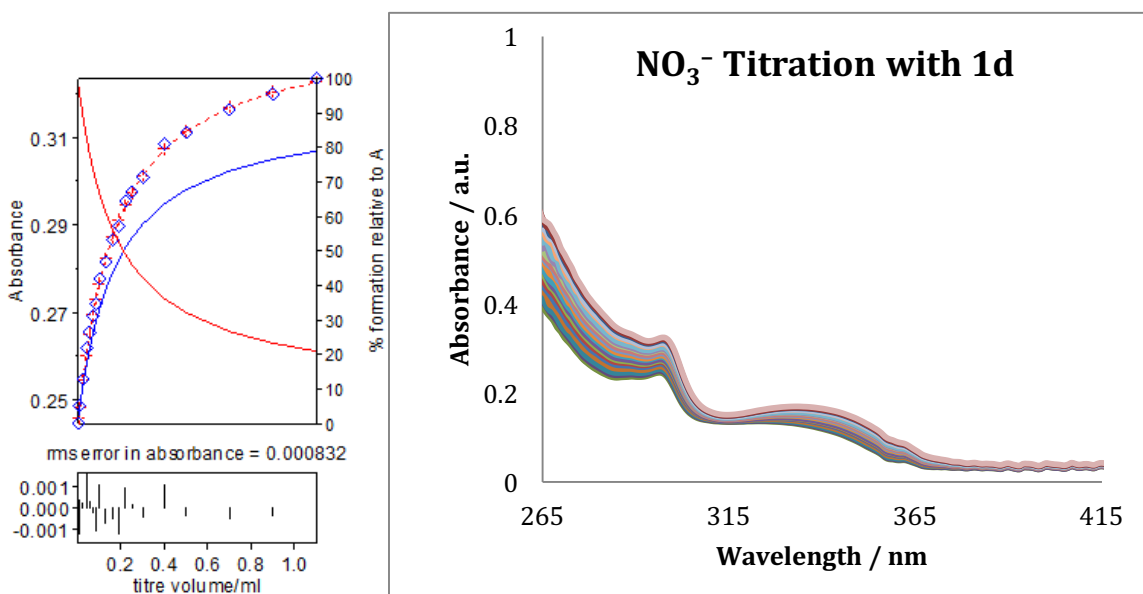
Figure 32. Binding isotherm for NO_3^- titration of **1d** in $CHCl_3$ by UV-vis. Stacked spectra of **1d** (10.3 μM) titrated with TBA NO_3^- (0-81 equiv., increasing abs.) in $CDCl_3$.

Table 33. Titration of **1e** with Cl^-. (Stock $[Cl^-]$ = 5.11 mM)

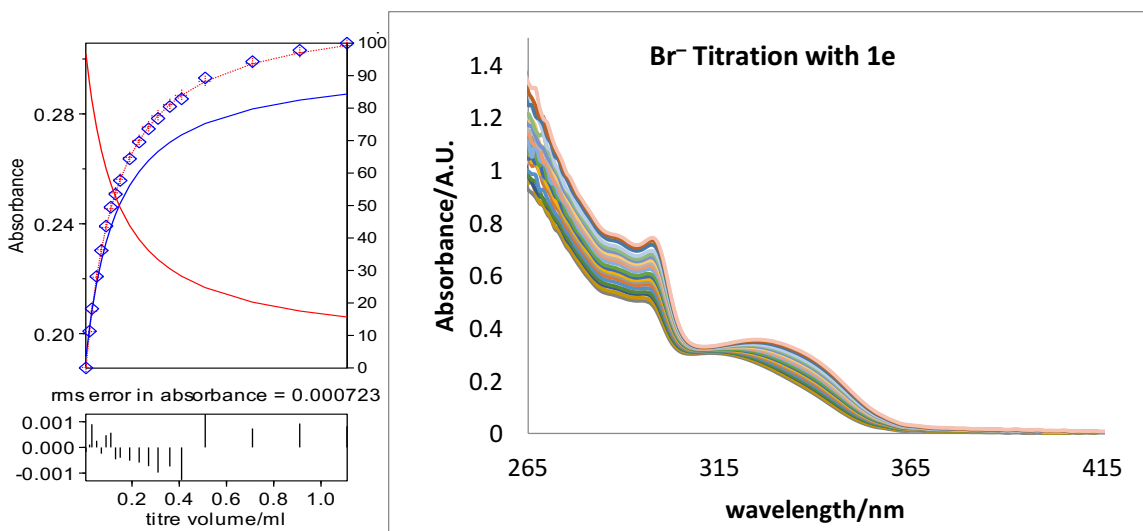|	Guest (μL)	**[1e]** (M)	$[Cl^-]$ (M)	Equiv.
0	0	2.26E-05	0.00E+00	0.00
1	5	2.26E-05	1.27E-05	0.56
2	10	2.26E-05	2.54E-05	1.12
3	15	2.26E-05	3.80E-05	1.68
4	25	2.26E-05	6.31E-05	2.79
5	50	2.26E-05	1.25E-04	5.50
6	80	2.26E-05	1.97E-04	8.68
7	110	2.26E-05	2.66E-04	11.76
8	150	2.26E-05	3.56E-04	15.74
9	200	2.26E-05	4.64E-04	20.51
10	250	2.26E-05	5.68E-04	25.07
11	300	2.26E-05	6.66E-04	29.43
12	400	2.26E-05	8.52E-04	37.60
13	500	2.26E-05	1.02E-03	45.13
14	700	2.26E-05	1.32E-03	58.50
15	900	2.26E-05	1.59E-03	70.02
16	1300	2.26E-05	2.01E-03	88.88
17	1700	2.26E-05	2.35E-03	103.67
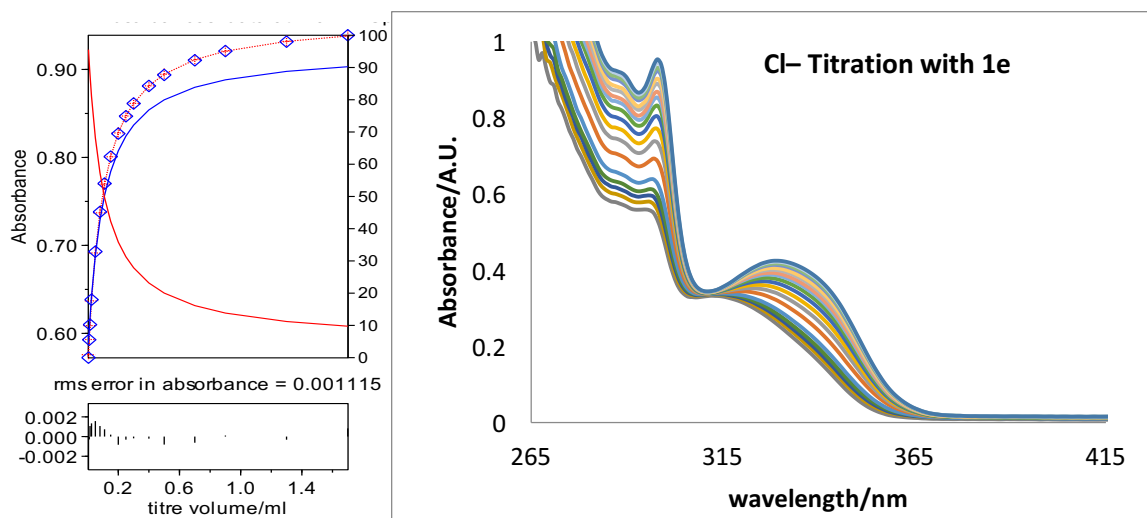
Figure 33. Binding isotherm for Cl⁻ titration of **1e** in CHCl₃ by UV-vis. Stacked spectra of **1e** (22.6 μM) titrated with TBA Cl⁻ (0-104 equiv., increasing abs.) in CDCl₃.

Table 34. Titration of **1e** with Br⁻. (Stock [Br⁻] = 4.65 mM).

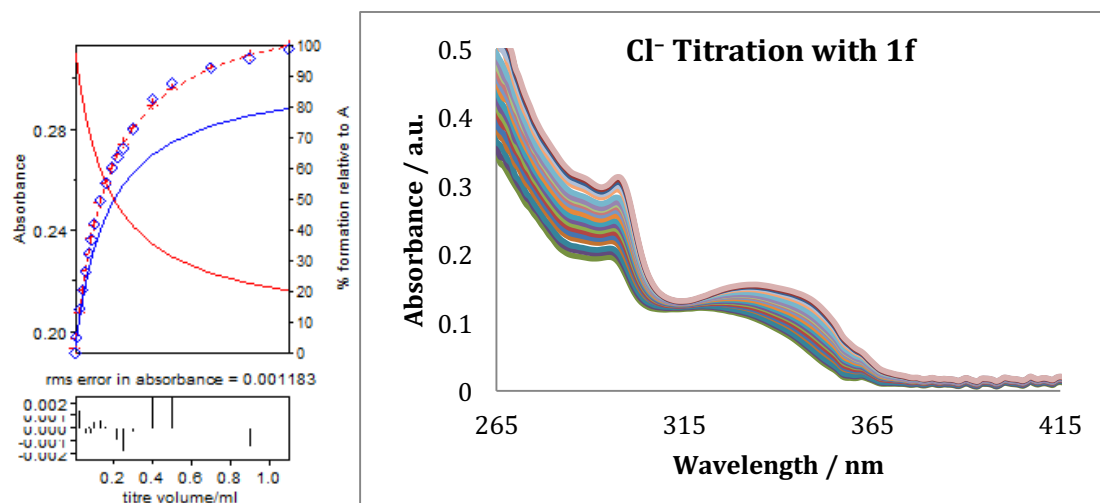|	Guest (μL)	[**1e**] (M)	[Br⁻] (M)	Equiv.
0	0	2.28E-05	0.00E+00	0.00
1	5	2.28E-05	1.16E-05	0.51
2	20	2.28E-05	4.60E-05	2.02
3	30	2.28E-05	6.87E-05	3.01
4	50	2.28E-05	1.13E-04	4.97
5	70	2.28E-05	1.57E-04	6.89
6	90	2.28E-05	2.00E-04	8.77
7	110	2.28E-05	2.42E-04	10.62
8	130	2.28E-05	2.84E-04	12.44
9	150	2.28E-05	3.24E-04	14.22
10	190	2.28E-05	4.03E-04	17.68
11	230	2.28E-05	4.79E-04	21.02
12	270	2.28E-05	5.53E-04	24.24
13	310	2.28E-05	6.24E-04	27.35
14	360	2.28E-05	7.09E-04	31.08
15	410	2.28E-05	7.91E-04	34.67
16	510	2.28E-05	9.45E-04	41.40
17	710	2.28E-05	1.22E-03	53.39
18	910	2.28E-05	1.45E-03	63.72
19	1110	2.28E-05	1.66E-03	72.73

Figure 34. Binding isotherm for Br⁻ titration of **1e** in CHCl₃ by UV-vis. Stacked spectra of **1e** (22.8 μM) titrated with TBA Br⁻ (0-72 equiv., increasing abs.) in CDCl₃.

Table 35. Titration of **1e** with NO_3^-. (Stock $[NO_3^-]$ = 5.05 mM).

|	Guest (μL)	[**1e**] (M)	$[NO_3^-]$ (M)	Equiv.
0	0	2.13E-05	0.00E+00	0.00
1	5	2.13E-05	1.26E-05	0.59
2	20	2.13E-05	5.00E-05	2.35
3	30	2.13E-05	7.47E-05	3.50
4	50	2.13E-05	1.23E-04	5.78
5	70	2.13E-05	1.71E-04	8.01
6	90	2.13E-05	2.18E-04	10.20
7	110	2.13E-05	2.63E-04	12.35
8	130	2.13E-05	3.08E-04	14.46
9	150	2.13E-05	3.52E-04	16.53
10	190	2.13E-05	4.38E-04	20.56
11	230	2.13E-05	5.21E-04	24.44
12	270	2.13E-05	6.01E-04	28.19
13	310	2.13E-05	6.78E-04	31.80
14	360	2.13E-05	7.71E-04	36.15
15	410	2.13E-05	8.59E-04	40.31
16	510	2.13E-05	1.03E-03	48.15
17	710	2.13E-05	1.32E-03	62.08
18	910	2.13E-05	1.58E-03	74.10
19	1110	2.13E-05	1.80E-03	84.58
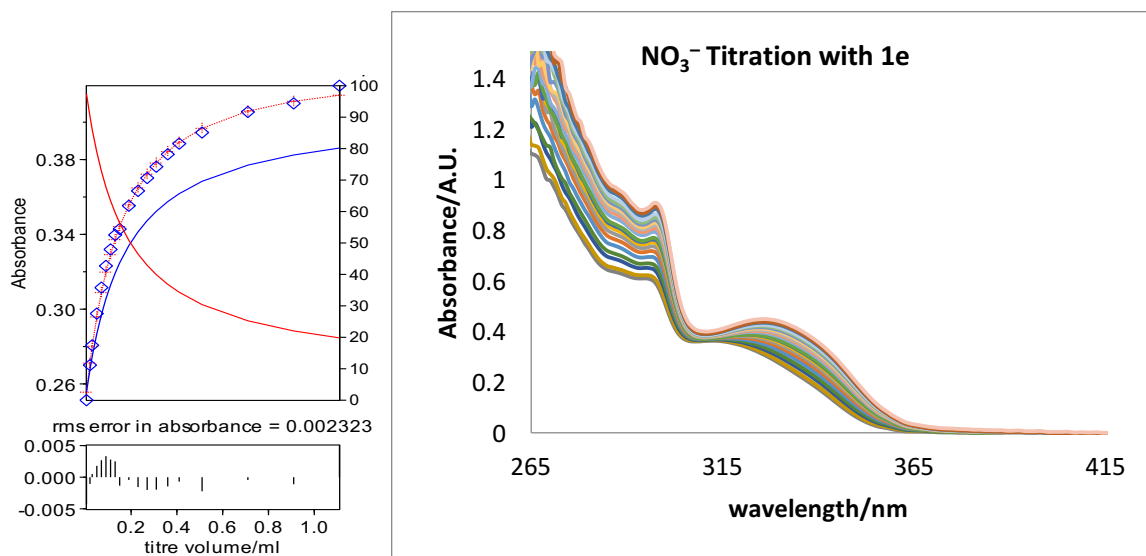
Figure 35. Binding isotherm for NO_3^- titration of **1e** in $CHCl_3$ by UV-vis. Stacked spectra of **1e** (21.3 μM) titrated with TBA NO_3^- (0-85 equiv., increasing abs.) in $CDCl_3$.

Table 36. Titration of **1f** with Cl^-. (Stock $[Cl^-]$ = 2.41 mM)

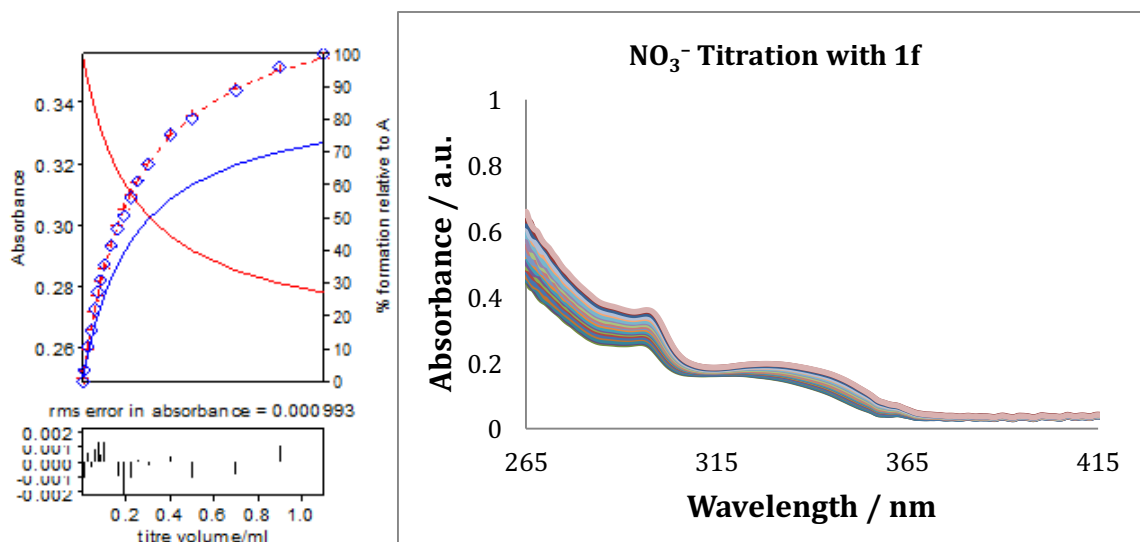|	Guest (μL)	**[1f]** (M)	[Cl–] (M)	Equiv.
00	0	1.03E-05	0.00E+00	0.00
01	5	1.03E-05	6.01E-06	0.58
02	10	1.03E-05	1.20E-05	1.16
03	25	1.03E-05	2.97E-05	2.88
04	40	1.03E-05	4.72E-05	4.57
05	55	1.03E-05	6.45E-05	6.24
06	70	1.03E-05	8.15E-05	7.88
07	85	1.03E-05	9.82E-05	9.50
08	100	1.03E-05	1.15E-04	11.10
09	130	1.03E-05	1.47E-04	14.23
10	160	1.03E-05	1.78E-04	17.27
11	190	1.03E-05	2.09E-04	20.23
12	220	1.03E-05	2.39E-04	23.10
13	250	1.03E-05	2.68E-04	25.90
14	300	1.03E-05	3.14E-04	30.41
15	400	1.03E-05	4.02E-04	38.85
16	500	1.03E-05	4.82E-04	46.62
17	700	1.03E-05	6.25E-04	60.44
18	900	1.03E-05	7.48E-04	72.35
19	1100	1.03E-05	8.55E-04	82.72

Figure 36. Binding isotherm for Cl⁻ titration of **1f** in CHCl₃ by UV-vis. Stacked spectra of **1f** (10.34 μM) titrated with TBA Cl⁻ (0-83 equiv., increasing abs.) in CDCl₃.

Table 37. Titration of **1f** with Br⁻. (Stock [Br⁻] = 11.19 mM).

|	Guest (μL)	[**1f**] (M)	[Br–] (M)	Equiv.
00	0	1.05E-05	0.00E+00	0.00
01	5	1.05E-05	2.79E-05	2.65
02	10	1.05E-05	5.57E-05	5.29
03	25	1.05E-05	1.38E-04	13.12
04	40	1.05E-05	2.19E-04	20.84
05	55	1.05E-05	3.00E-04	28.44
06	70	1.05E-05	3.78E-04	35.94
07	85	1.05E-05	4.56E-04	43.33
08	100	1.05E-05	5.33E-04	50.61
09	130	1.05E-05	6.83E-04	64.87
10	160	1.05E-05	8.29E-04	78.73
11	190	1.05E-05	9.71E-04	92.21
12	220	1.05E-05	1.11E-03	105.32
13	250	1.05E-05	1.24E-03	118.09
14	300	1.05E-05	1.46E-03	138.62
15	350	1.05E-05	1.67E-03	158.29
16	400	1.05E-05	1.87E-03	177.13
17	500	1.05E-05	2.24E-03	212.56
18	600	1.05E-05	2.58E-03	245.26
19	800	1.05E-05	3.20E-03	303.65
20	1000	1.05E-05	3.73E-03	354.26
21	1200	1.05E-05	4.20E-03	398.55
22	1400	1.05E-05	4.61E-03	437.62
23	1600	1.05E-05	4.97E-03	472.35
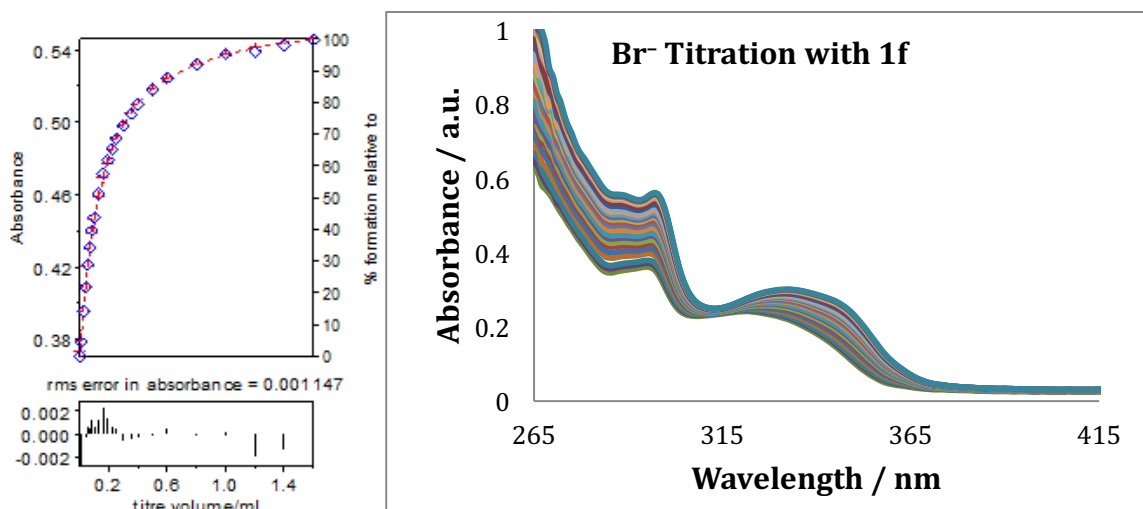
Figure 37. Binding isotherm for Br⁻ titration of **1f** in CHCl₃ by UV-vis. Stacked spectra of **1f** (10.53 μM) titrated with TBA Br⁻ (0-472 equiv., increasing abs.) in CDCl₃.

Table 38. Titration of **1f** with NO_3^-. (Stock [Br⁻] = 2.28 mM).

|	Guest (µL)	[**1f**] (M)	$[NO_3^-]$ (M)	Equiv.
00	0	1.01E-05	0.00E+00	0.00
01	5	1.01E-05	5.69E-06	0.56
02	10	1.01E-05	1.14E-05	1.13
03	25	1.01E-05	2.82E-05	2.79
04	40	1.01E-05	4.48E-05	4.44
05	55	1.01E-05	6.11E-05	6.05
06	70	1.01E-05	7.72E-05	7.65
07	85	1.01E-05	9.31E-05	9.22
08	100	1.01E-05	1.09E-04	10.77
09	130	1.01E-05	1.39E-04	13.81
10	160	1.01E-05	1.69E-04	16.76
11	190	1.01E-05	1.98E-04	19.63
12	220	1.01E-05	2.26E-04	22.42
13	250	1.01E-05	2.54E-04	25.14
14	300	1.01E-05	2.98E-04	29.51
15	400	1.01E-05	3.81E-04	37.70
16	500	1.01E-05	4.57E-04	45.24
17	700	1.01E-05	5.92E-04	58.65
18	900	1.01E-05	7.09E-04	70.21
19	1100	1.01E-05	8.10E-04	80.27

Figure 38. Binding isotherm for NO_3^- titration of **1f** in $CHCl_3$ by UV-vis. Stacked spectra of **1f** (10.1 μM) titrated with TBA NO_3^- (0-80 equiv., increasing abs.) in $CDCl_3$.

Table 39. Titration of **1g** with Cl^-. (Stock $[Cl^-]$ = 9.87 mM).

	Guest (μL)	**[1g]** (M)	$[Cl^-]$ (M)	Equiv.
0	0	3.94E-05	0.00E+00	0.00
1	5	3.94E-05	2.46E-05	0.63
2	10	3.94E-05	4.91E-05	1.25
3	20	3.94E-05	9.77E-05	2.48
4	30	3.94E-05	1.46E-04	3.70
5	50	3.94E-05	2.41E-04	6.11
6	70	3.94E-05	3.34E-04	8.48
7	90	3.94E-05	4.25E-04	10.80
8	110	3.94E-05	5.15E-04	13.07
9	130	3.94E-05	6.02E-04	15.30
10	150	3.94E-05	6.89E-04	17.49
11	190	3.94E-05	8.56E-04	21.75
12	230	3.94E-05	1.02E-03	25.86
13	270	3.94E-05	1.17E-03	29.82
14	310	3.94E-05	1.32E-03	33.64
15	360	3.94E-05	1.51E-03	38.24
16	410	3.94E-05	1.68E-03	42.65
17	510	3.94E-05	2.01E-03	50.94
18	710	3.94E-05	2.59E-03	65.68
19	910	3.94E-05	3.09E-03	78.40
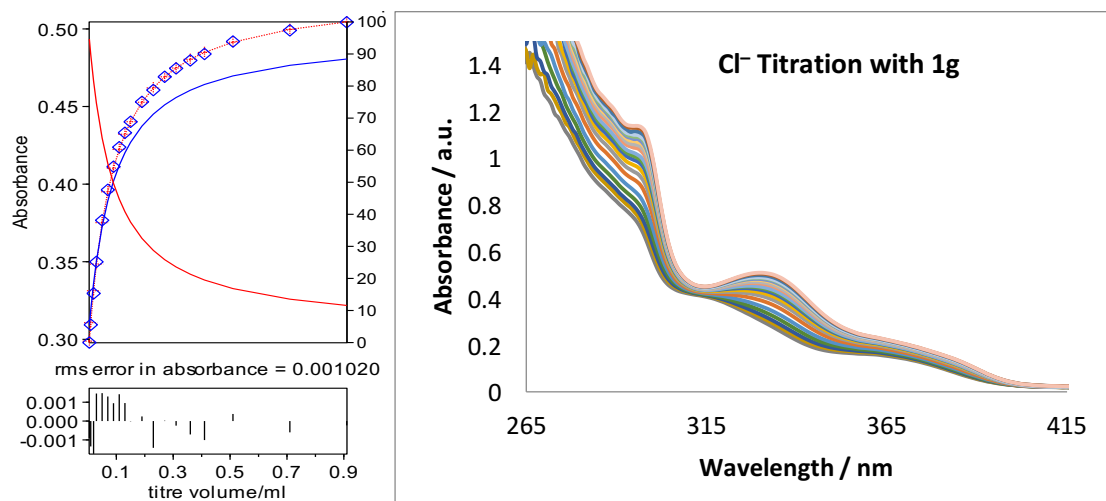
Figure 39. Binding isotherm for Cl⁻ titration of **1g** in CHCl₃ by UV-vis. Stacked spectra of **1g** (39.4 μM) titrated with TBA Cl⁻ (0-78 equiv., increasing abs.) in CDCl₃.

Table 40. Titration of **1g** with Br⁻. (Stock [Br⁻] = 7.39 mM).

	Guest (μL)	[1g] (M)	[Br⁻] (M)	Equiv.
0	0	3.22E-05	0.00E+00	0.00
1	5	3.22E-05	1.84E-05	0.57
2	20	3.22E-05	7.32E-05	2.28
3	30	3.22E-05	1.09E-04	3.40
4	50	3.22E-05	1.80E-04	5.60
5	70	3.22E-05	2.50E-04	7.77
6	90	3.22E-05	3.18E-04	9.90
7	110	3.22E-05	3.85E-04	11.98
8	130	3.22E-05	4.51E-04	14.02
9	150	3.22E-05	5.15E-04	16.03
10	190	3.22E-05	6.41E-04	19.94
11	230	3.22E-05	7.62E-04	23.70
12	270	3.22E-05	8.79E-04	27.33
13	310	3.22E-05	9.92E-04	30.84
14	360	3.22E-05	1.13E-03	35.05
15	410	3.22E-05	1.26E-03	39.09
16	510	3.22E-05	1.50E-03	46.69
17	710	3.22E-05	1.94E-03	60.20
18	910	3.22E-05	2.31E-03	71.86
19	1110	3.22E-05	2.64E-03	82.02
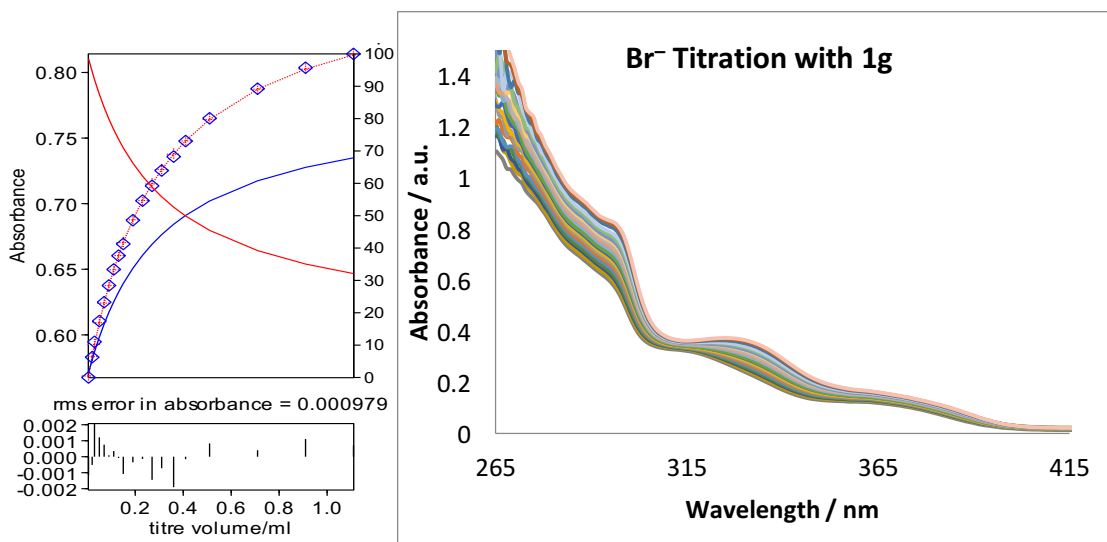
Figure 40. Binding isotherm for Br⁻ titration of **1g** in CHCl₃ by UV-vis. Stacked spectra of **1g** (32.2 μM) titrated with TBA Br⁻ (0-82 equiv., increasing abs.) in CDCl₃.

Table 41. Titration of **1g** with NO_3^-. (Stock $[NO_3^-]$ = 7.91 mM)

	Guest (μL)	**[1g]** (M)	$[NO_3^-]$ (M)	Equiv.
0	0	3.56E-05	0.00E+00	0.00
1	5	3.56E-05	1.97E-05	0.55
2	20	3.56E-05	7.83E-05	2.20
3	30	3.56E-05	1.17E-04	3.28
4	50	3.56E-05	1.93E-04	5.41
5	70	3.56E-05	2.67E-04	7.51
6	90	3.56E-05	3.40E-04	9.56
7	110	3.56E-05	4.12E-04	11.57
8	130	3.56E-05	4.83E-04	13.55
9	150	3.56E-05	5.52E-04	15.49
10	190	3.56E-05	6.86E-04	19.26
11	230	3.56E-05	8.15E-04	22.89
12	270	3.56E-05	9.40E-04	26.40
13	310	3.56E-05	1.06E-03	29.79
14	360	3.56E-05	1.21E-03	33.86
15	410	3.56E-05	1.35E-03	37.76
16	510	3.56E-05	1.61E-03	45.10
17	710	3.56E-05	2.07E-03	58.16
18	910	3.56E-05	2.47E-03	69.42
19	1110	3.56E-05	2.82E-03	79.23
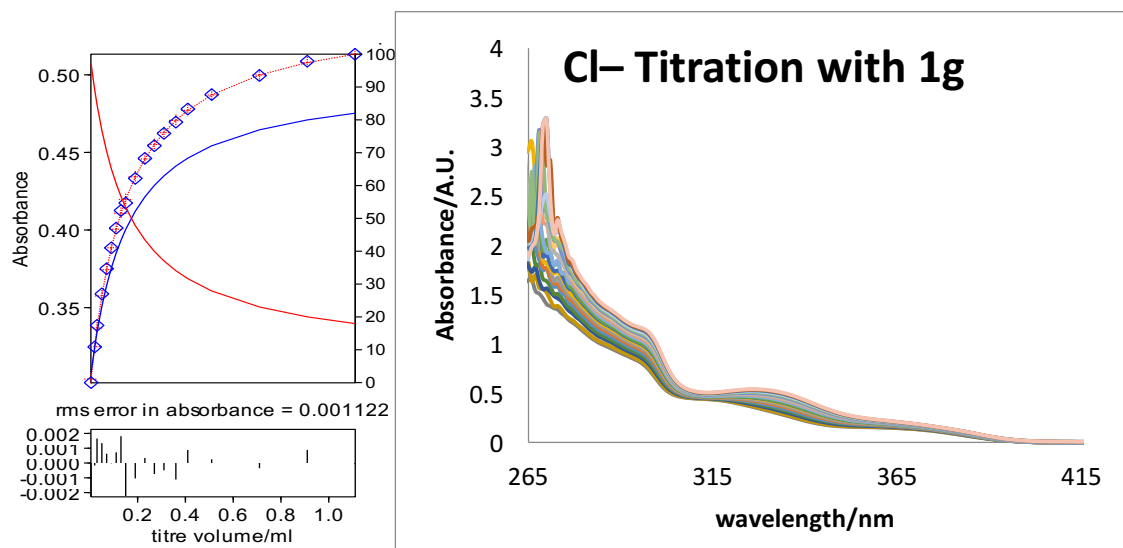
Figure 41. Binding isotherm for NO_3^- titration of **1g** in $CHCl_3$ by UV-vis. Stacked spectra of **1g** (35.6 μM) titrated with TBA NO_3^- (0-79 equiv., increasing abs.) in $CDCl_3$.

Job Plots

      UV-Vis Job Plot Conditions. UV-Vis Job plots were carried out on an HP 8453 UV-Vis spectrometer. Water-saturated $CHCl_3$ was prepared in the ame manner as for ^1H data. Job plots were obtained by $\Delta\lambda_{max}$ of the anion-bound complex highest peak. Hamilton gas-tight syringes were used during serial dilutions and titrations.

      Tetrabutylammonium nitrate with 1b. A stock solution of **1b** was prepared using serial dilution to a final volume of 5 mL (1.32 mg, [**1b**] = 77.76 μM). A 5 mL solution of $TBANO_3$ (6.41 mg, 77.69 μM) was prepared by serial dilution. The volume in the cuvette was 2.0 mL.
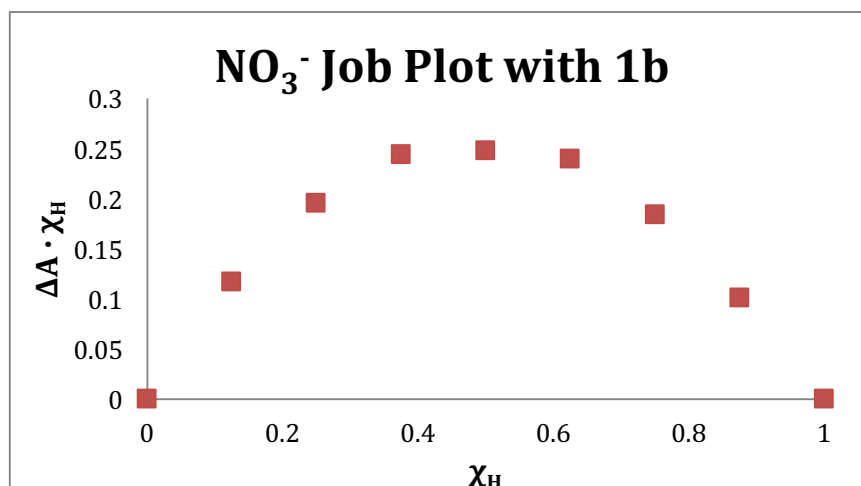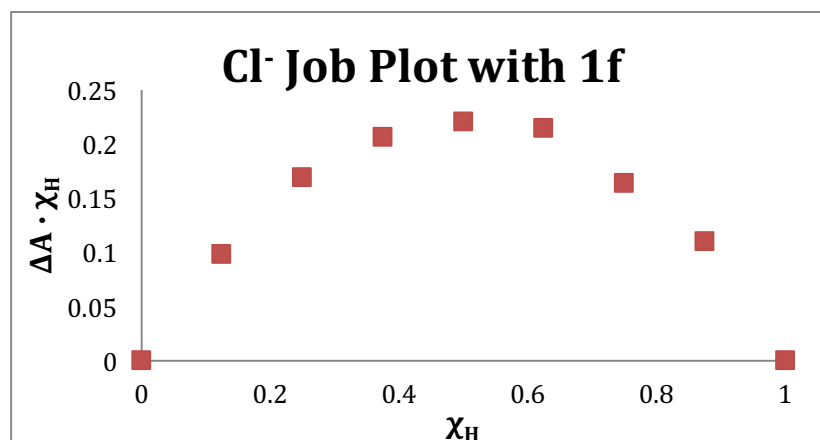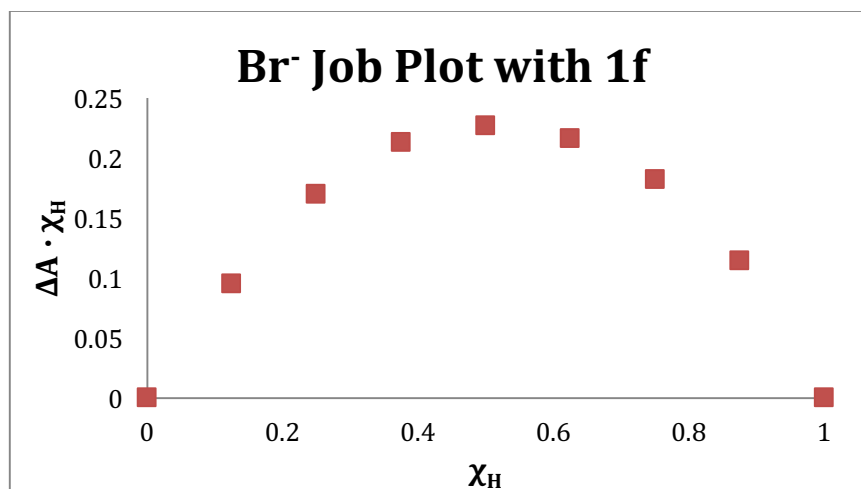
Figure 42. Job plot of **1b** with NO_3^- in water-saturated $CHCl_3$.

Tetrabutylammonium chloride with 1c. A stock solution of **1c** was prepared using serial dilution to a final volume of 5 mL (1.23 mg, [**1c**] = 75.11 μM). A 5 mL solution of TBACl (15.18 mg, 75.10 μM) was prepared by serial dilution. The volume in the cuvette was 2.0 mL.
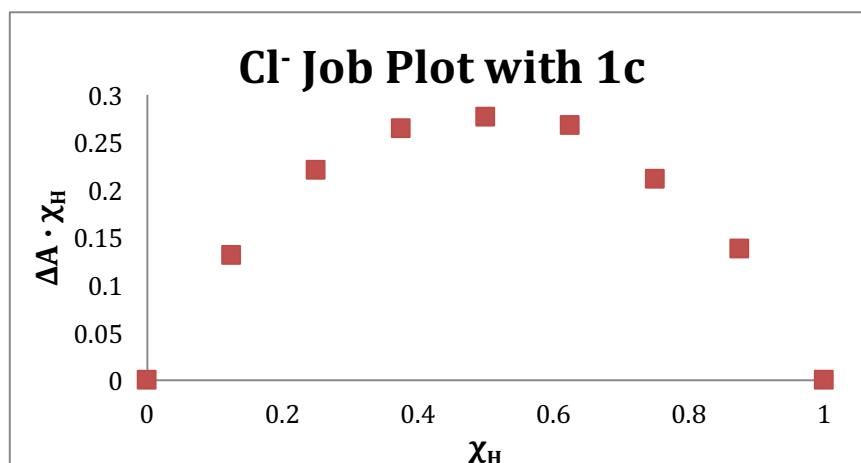
Figure 43. Job plot of **1c** with Cl^- in water-saturated $CHCl_3$.

Tetrabutylammonium bromide with 1c. A stock solution of **1c** was prepared using serial dilution to a final volume of 5 mL (1.25 mg, [**1c**] = 48.95 μM). A 5 mL solution

of TBABr (8.96 mg, 48.85 μM) was prepared by serial dilution. The volume in the cuvette was 2.0 mL.
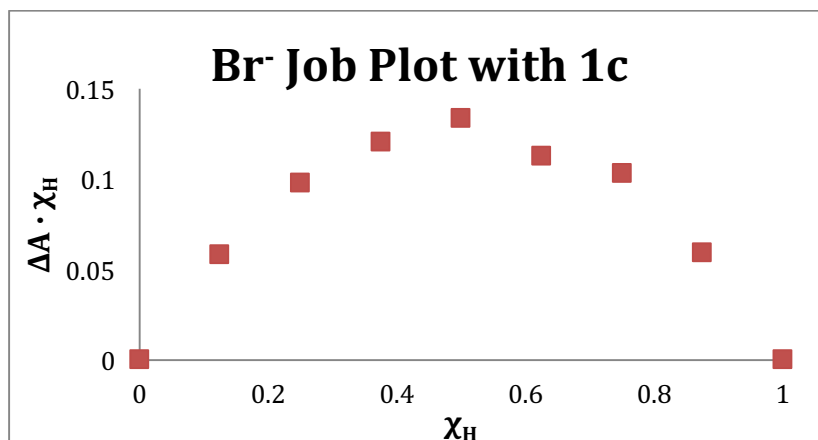
Figure 44. Job plot of **1c** with Br^- in water-saturated $CHCl_3$.

Tetrabutylammonium nitrate with 1c. A stock solution of **1c** was prepared using serial dilution to a final volume of 5 mL (1.36 mg, [**1c**] = 72.21 μM). A 5 mL solution of TBANO$_3$ (7.72 mg, 72.26 μM) was prepared by serial dilution. The volume in the cuvette was 2.0 mL.
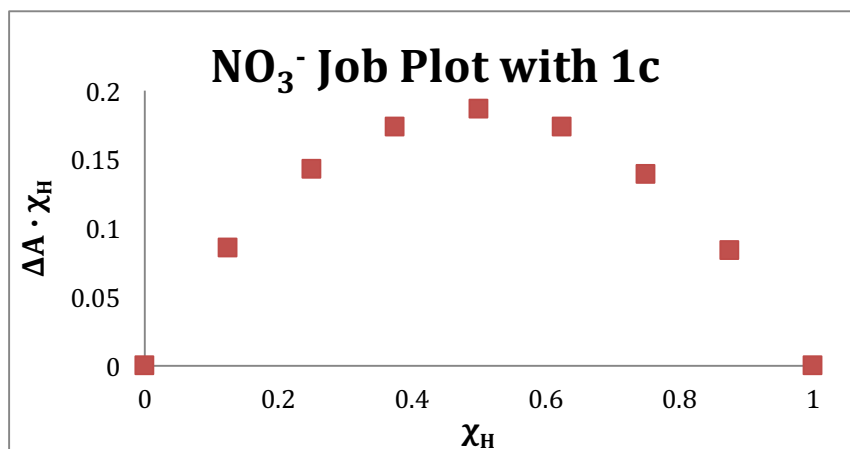
Figure 45. Job plot of **1c** with NO_3^- in water-saturated $CHCl_3$.

Tetrabutylammonium chloride with 1d. A stock solution of **1d** was prepared using serial dilution to a final volume of 5 mL (1.55 mg, [**1d**] = 71.52 µM). A 5 mL solution of TBACl (10.60 mg, 71.51 µM) was prepared by serial dilution. The volume in the cuvette was 2.0 mL.
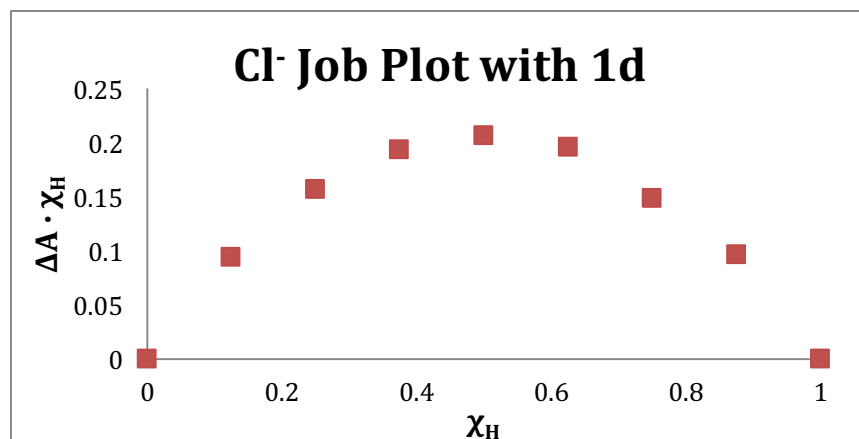
Figure 46. Job plot of **1d** with Cl⁻ in water-saturated CHCl₃.

Tetrabutylammonium bromide with 1d. A stock solution of **1d** was prepared using serial dilution to a final volume of 5 mL (1.18 mg, [**1d**] = 71.26 µM). A 5 mL solution of TBABr (10.07 mg, 71.22 µM) was prepared by serial dilution. The volume in the cuvette was 2.0 mL.
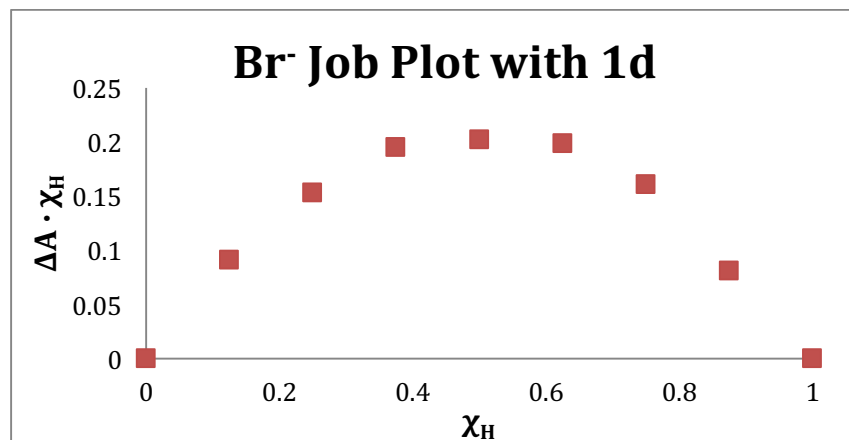
Figure 47. Job plot of **1d** with Br⁻ in water-saturated CHCl₃.

Tetrabutylammonium nitrate with 1d. A stock solution of **1d** was prepared using serial dilution to a final volume of 5 mL (1.65 mg, [**1d**] = 70.53 μM). A 5 mL solution of TBANO$_3$ (5.83 mg, 70.56 μM) was prepared by serial dilution. The volume in the cuvette was 2.0 mL.
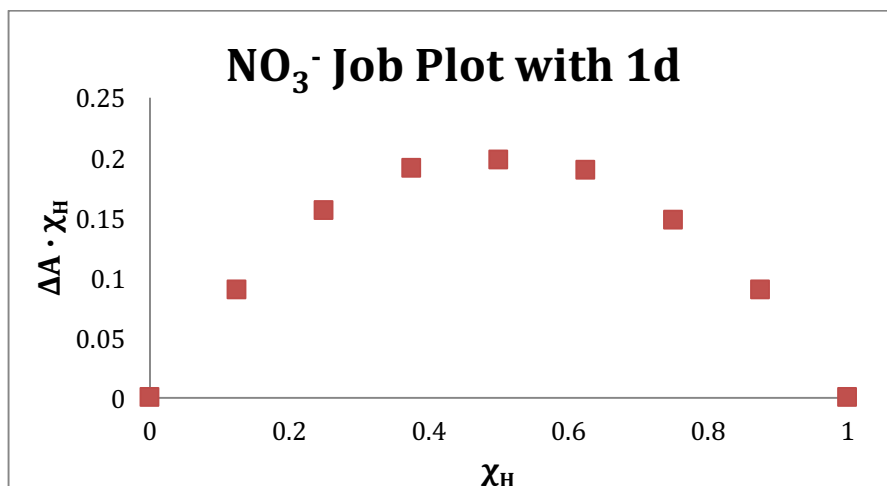
Figure 48. Job plot of **1d** with NO$_3^-$ in water-saturated CHCl$_3$.

Tetrabutylammonium chloride with 1f. A stock solution of **1f** was prepared using serial dilution to a final volume of 5 mL (1.85 mg, [**1f**] = 69.17 μM). A 5 mL solution of TBACl (18.54 mg, 69.16 μM) was prepared by serial dilution. The volume in the cuvette was 2.0 mL.

Figure 49. Job plot of **1f** with Cl⁻ in water-saturated CHCl₃.

Tetrabutylammonium bromide with 1f. A stock solution of **1f** was prepared using serial dilution to a final volume of 5 mL (1,76 mg, [**1f**] = 70.50 µM). A 5 mL solution of TBABr (29.32 mg, 70.49 µM) was prepared by serial dilution. The volume in the cuvette was 2.0 mL.

Figure 50. Job plot of **1f** with Br⁻ in water-saturated CHCl₃.

Tetrabutylammonium nitrate with 1f. A stock solution of **1f** was prepared using serial dilution to a final volume of 5 mL (2.12 mg, [**1f**] = 70.77 µM). A 5 mL solution of

TBANO$_3$ (6.47 mg, 70.75 µM) was prepared by serial dilution. The volume in the cuvette was 2.0 mL.
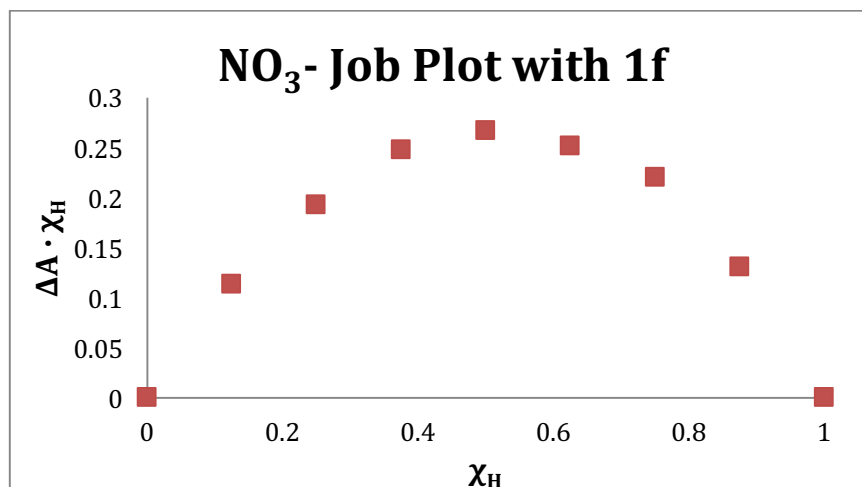
Figure 51. Job plot of **1f** with NO$_3^-$ in water-saturated CHCl$_3$.

Fitting Data and Results
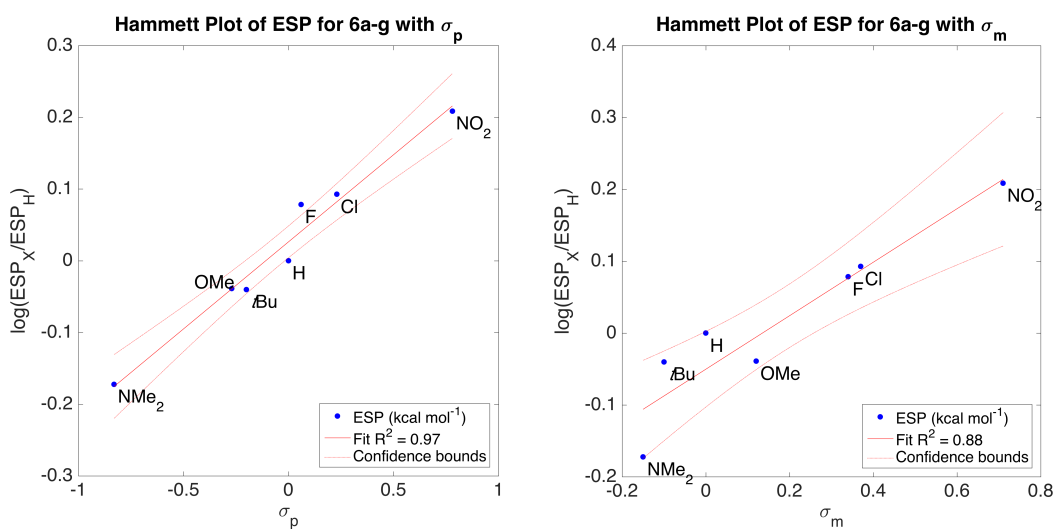
Figure 52. Hammett plots of the ESP for the C-H hydrogen bond donor in **6a-g**. ESP fit with σ$_p$ ($\boldsymbol{\rho}$ = 0.243, i = 0.026) is superior to σ$_m$ ($\boldsymbol{\rho}$ = 0.372, i = -0.050).

Table 42. Mulliken atomic charge and ESP values for 5a-g.

X	Mulliken atomic charges							ESP values		
	H (CH)	C (CH)	H_1	$N_1{}^a$	H_2	H_3	$N_2{}^b$	C– H	N– $H_2{}^c$	N– $H_3{}^c$
$N(Me)_2$	0.168	-0.362	0.388	-0.596	0.382	0.418	-0.789	36.3	55.9	47.5
t-Bu	0.174	-0.321	0.386	-0.605	0.381	0.416	-0.779	39.2	57.0	48.6
H	0.175	-0.273	0.387	-0.613	0.381	0.417	-0.775	39.2	57.8	50.1
F	0.177	-0.279	0.387	-0.613	0.381	0.418	-0.774	43.1	59.5	51.6
NO3	0.186	-0.250	0.385	-0.608	0.381	0.417	-0.775	48.6	62.6	53.6

*Mulliken charges are given as a fraction of one electronic charge. ESP values are reported here in kcal/mol. [a]Areneethynyl attached nitrogen. [b]Terminal nitrogen. [c]Hydrogens on terminal nitrogen.

Table 43. Coefficients and Fitting Statistics for Mulliken charges and ESP of 5a-g with σ_p.

		ρ	i	N	R^2	F
Charge	**C (CH)**	-0.104(±0.021)	0.029(±0.011)	5	0.90	25.7
	N1	-0.008(±0.005)	-0.607(±0.003)	5	0.43	2.3
	N2	0.005(±0.002)	0.002(±0.001)	5	0.68	6.3
ESP	**C–H**	0.080(±0.015)	0.023(±0.008)	5	0.90	28
	N–H2	0.032(±0.006)	0.007(±0.003)	5	0.91	29
	N–H3	0.034(±0.006)	0.002(±0.003)	7	0.91	29

Table 44. Coefficients and Fitting Statistics for Hammett Plots of σ_+ and σ_-.

K_a (X$^-$)	ρ	i	N	R^2	F
Cl$^-$ (σ_+)	0.35(±0.07)	0.08(±0.06)	7	0.83	24
Br$^-$ (σ_+)	0.34(±0.07)	0.14(±0.05)	7	0.84	26
I$^-$ (σ_+)	0.27(±0.07)	0.21(±0.06)	7	0.73	14
NO$_3{}^-$ (σ_+)	0.30(±0.06)	0.15(±0.05)	7	0.81	21
Cl$^-$ (σ_-)	0.52(±0.11)	–0.08(±0.05)	7	0.83	24
Br$^-$ (σ_-)	0.49(±0.12)	–0.02(±0.06)	7	0.77	17
I$^-$ (σ_-)	0.41(±0.10)	–0.08(±0.05)	7	0.77	16
NO$_3{}^-$ (σ_-)	0.41(±0.12)	–0.02(±0.06)	7	0.71	13

NMR Spectra
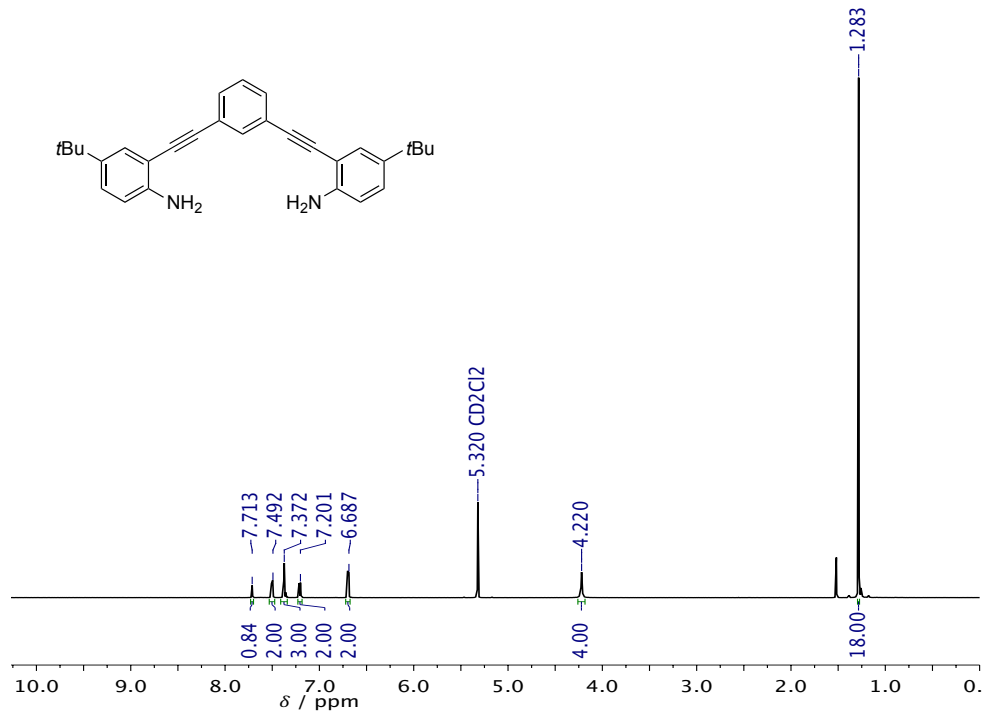
Figure 53. ^{1}H NMR spectrum of **2a** in CD$_2$Cl$_2$.
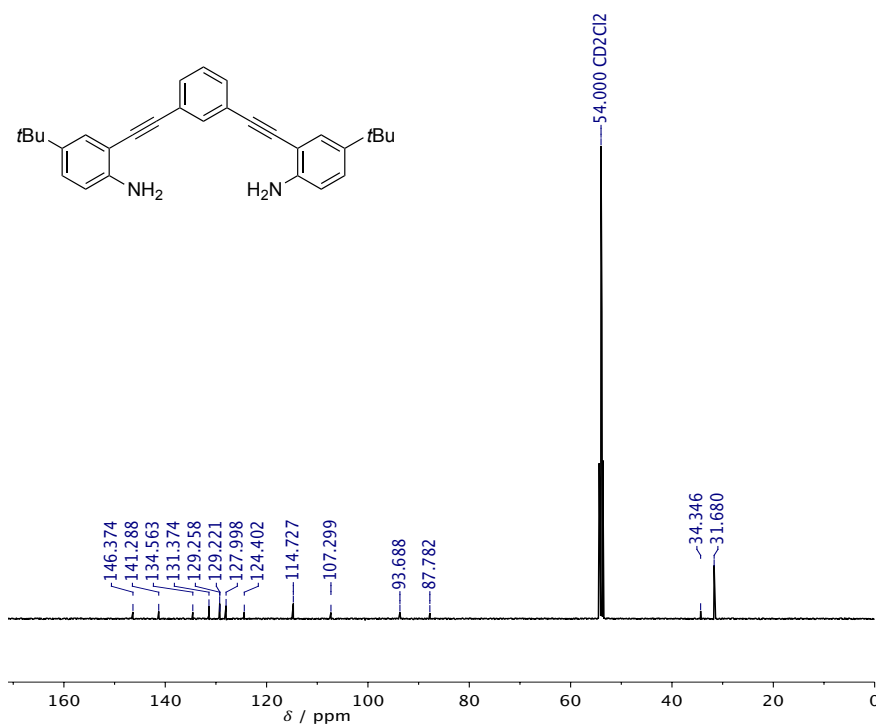
Figure 54. ^{13}C NMR spectrum of **2a** in CD$_2$Cl$_2$.
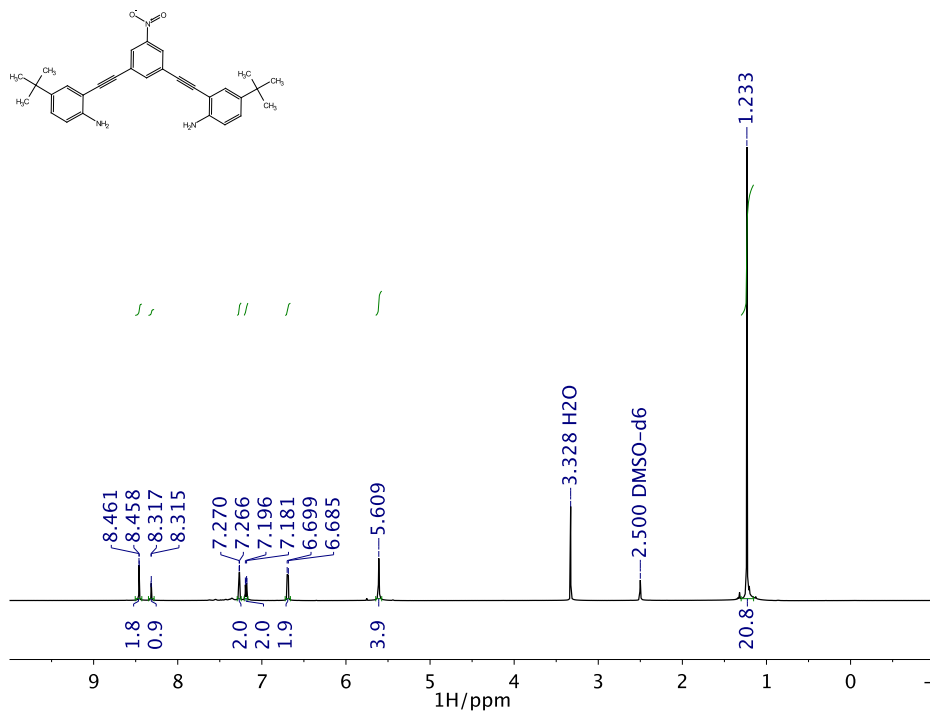
Figure 55. ^{1}H NMR spectrum of **2b** in DMSO-d_6.
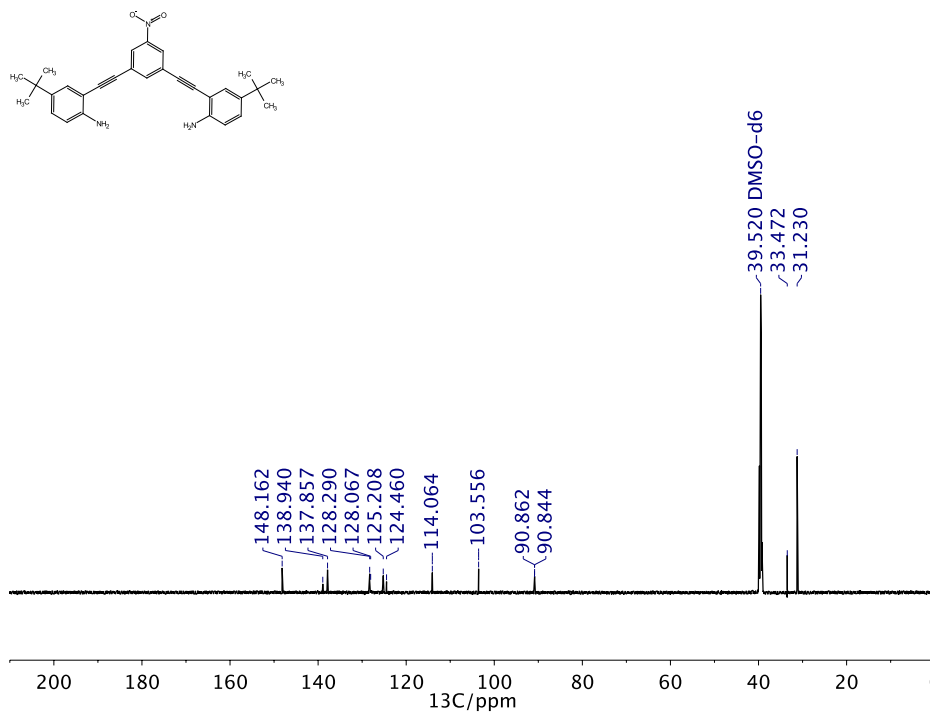
Figure 56. ^{13}C NMR spectrum of **2b** in DMSO-d_6.
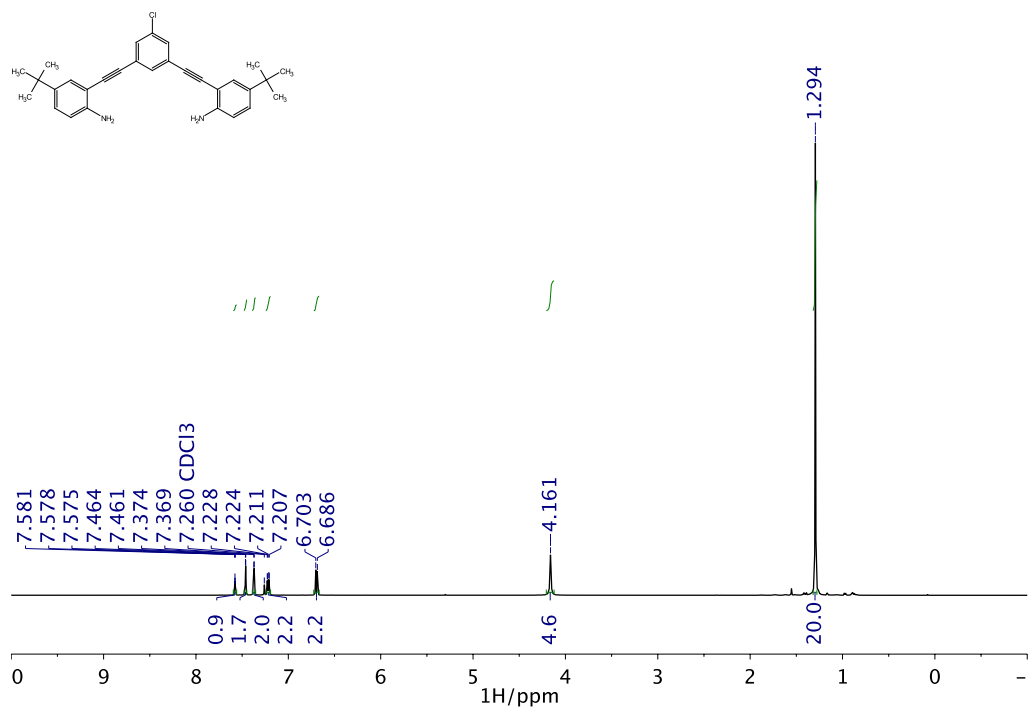
Figure 57. ^{1}H NMR spectrum of **2c** in CDCl$_3$.
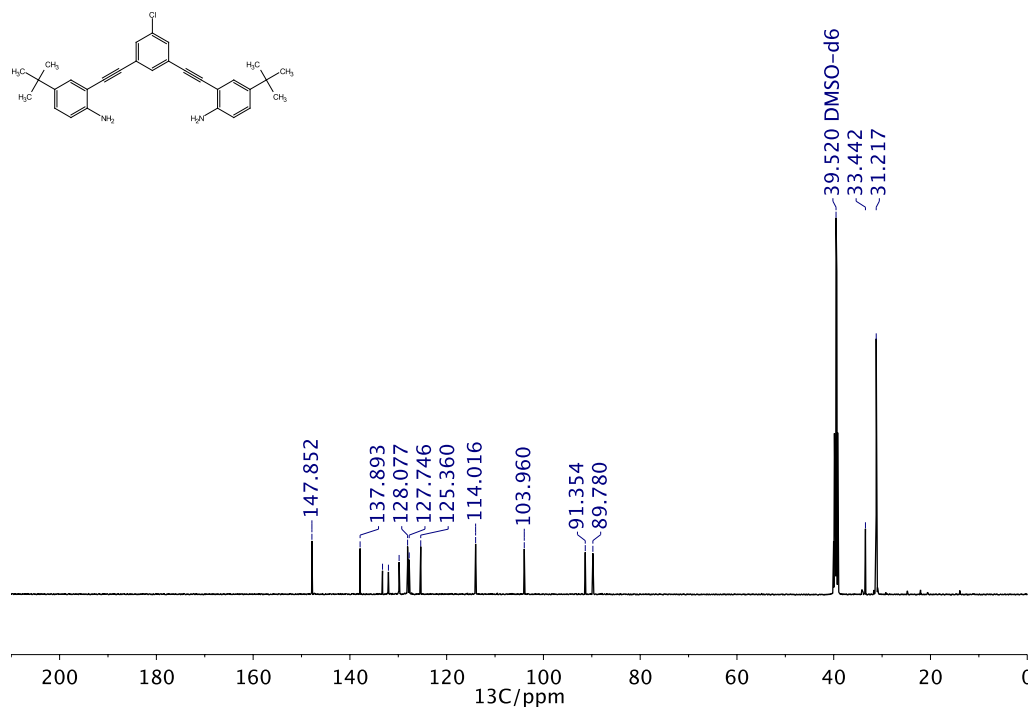
Figure 58. ^{13}C NMR spectrum of **2c** in DMSO-d_6.
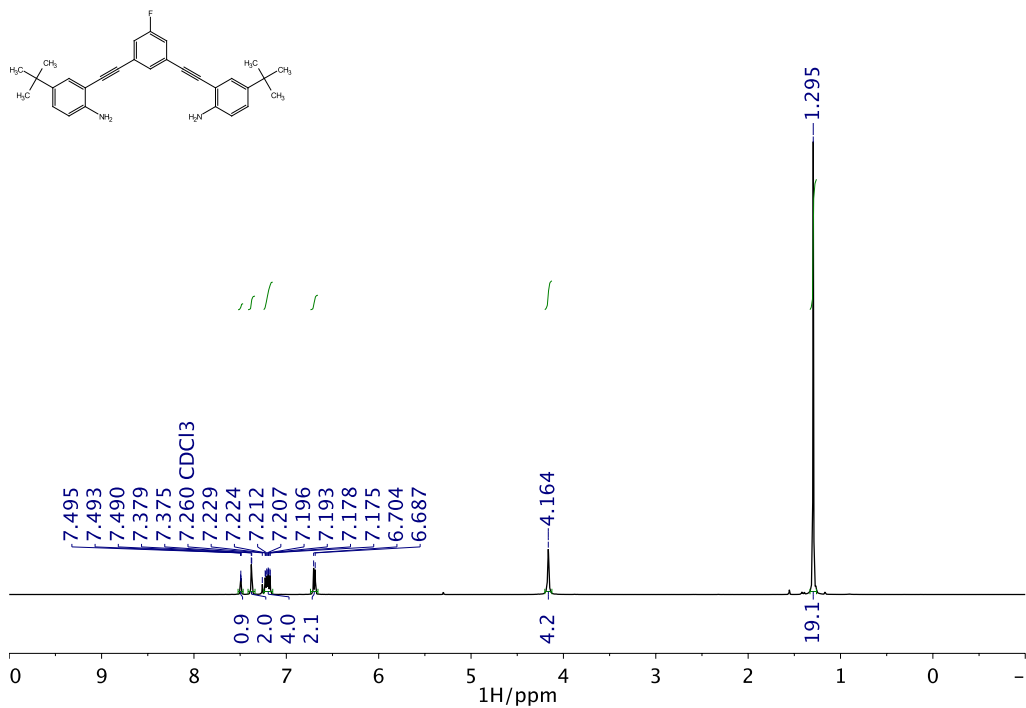
Figure 59. ^{1}H NMR spectrum of **2d** in CDCl$_3$.
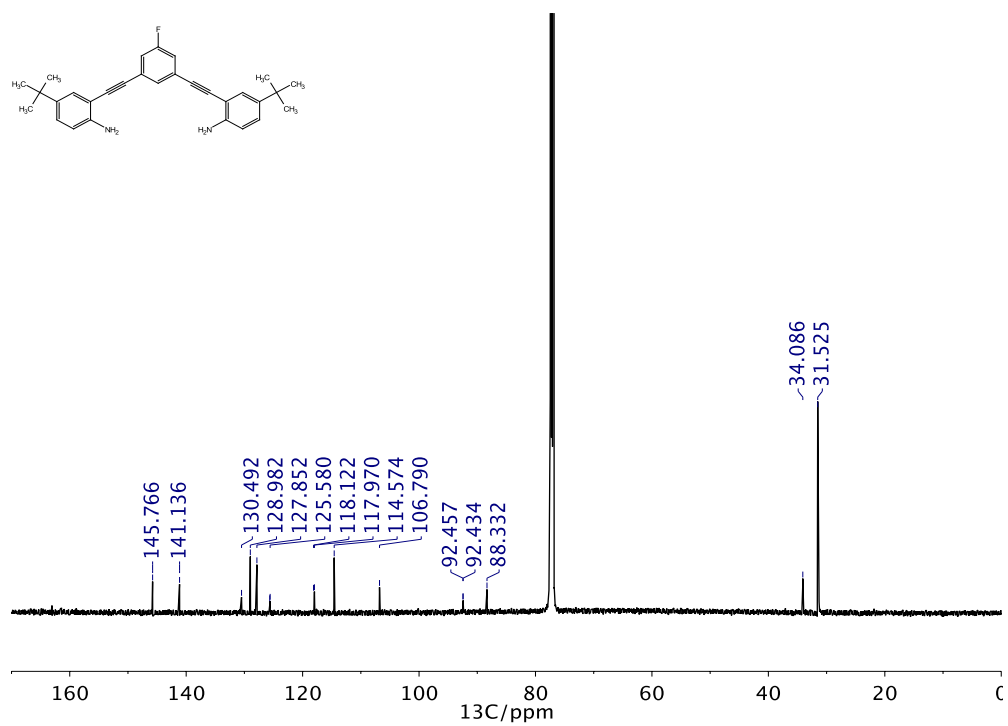
Figure 60. ^{13}C NMR spectrum of **2d** in CDCl$_3$.
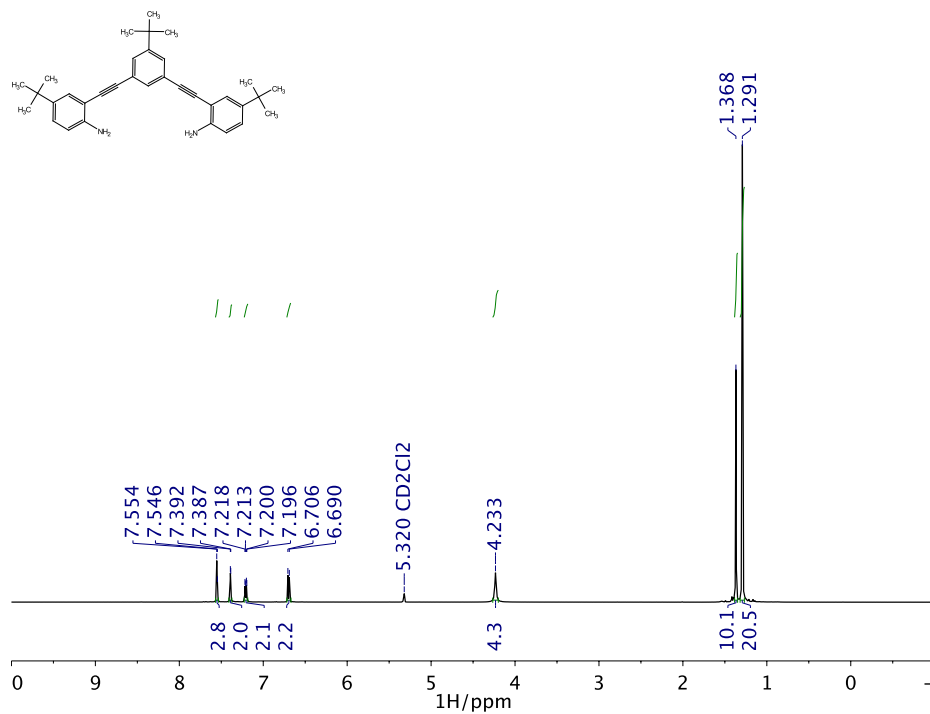
Figure 61. ^{1}H NMR spectrum of **2e** in CD$_2$Cl$_2$.
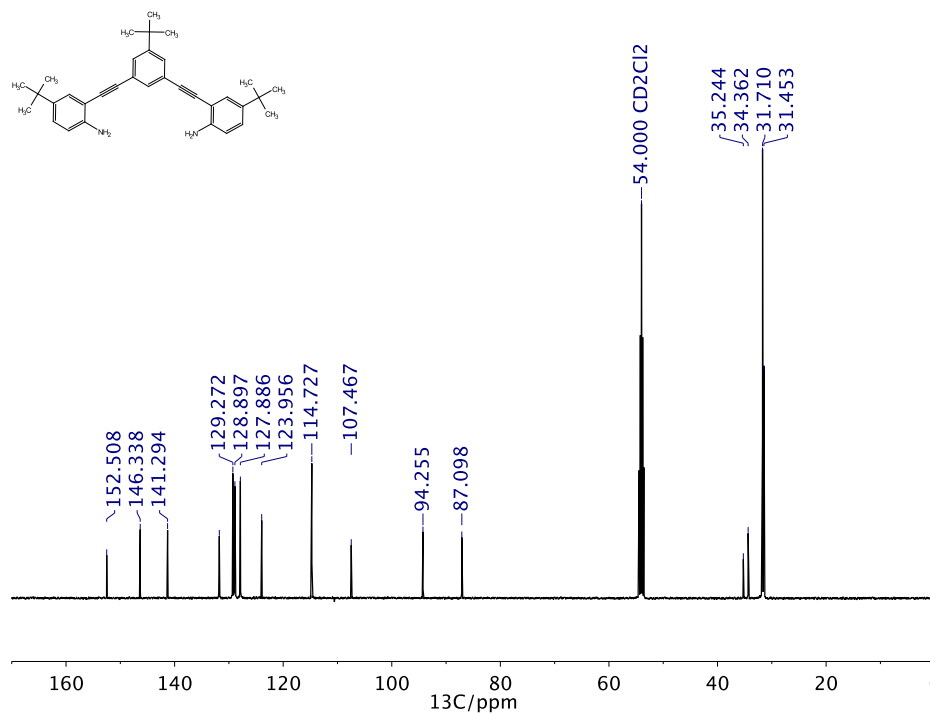
Figure 62. ^{13}C NMR spectrum of **2e** in CD$_2$Cl$_2$.

196
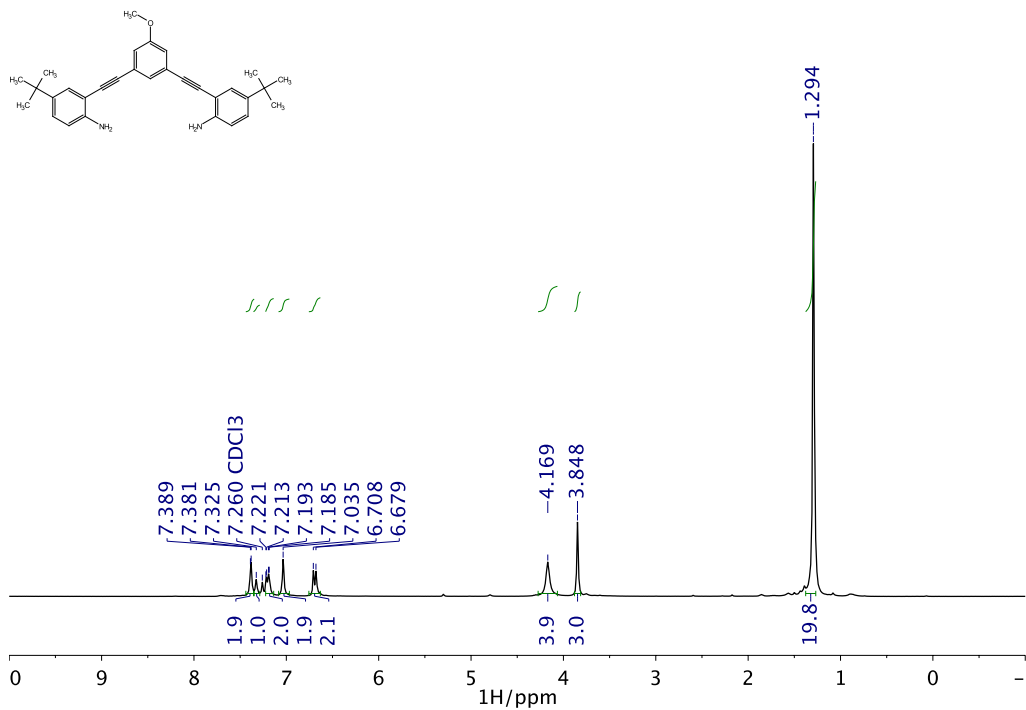
Figure 63. ^{1}H NMR spectrum of **2f** in CDCl$_3$.
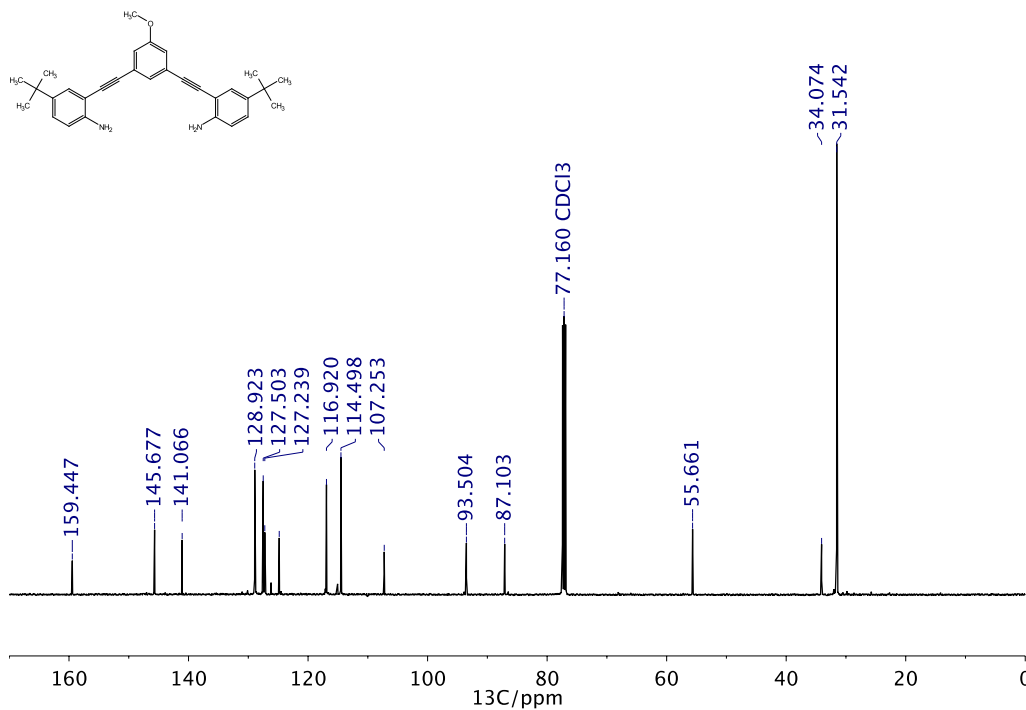
Figure 64. ^{13}C NMR spectrum of **2f** in CDCl$_3$.
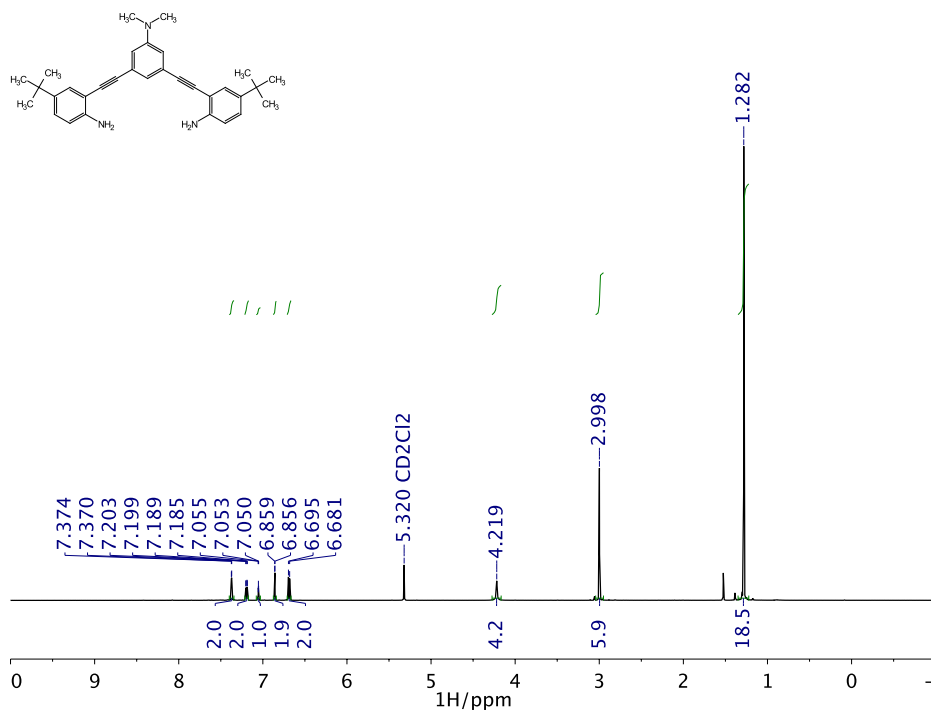
Figure 65. ^{1}H NMR spectrum of **2g** in CD$_2$Cl$_2$.
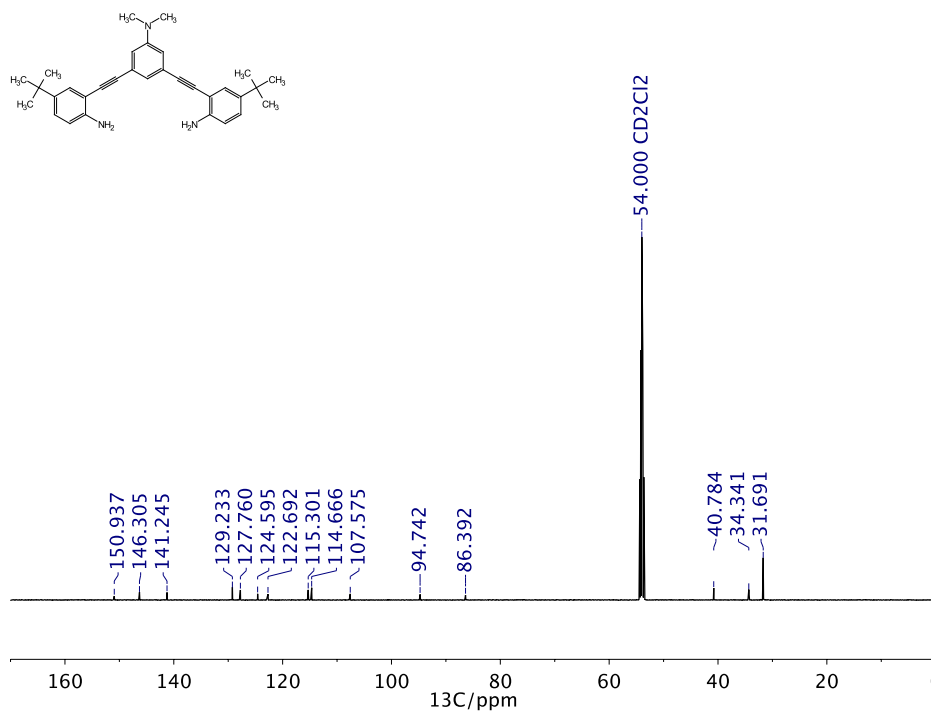
Figure 66. ^{13}C NMR spectrum of **2g** in CD$_2$Cl$_2$.
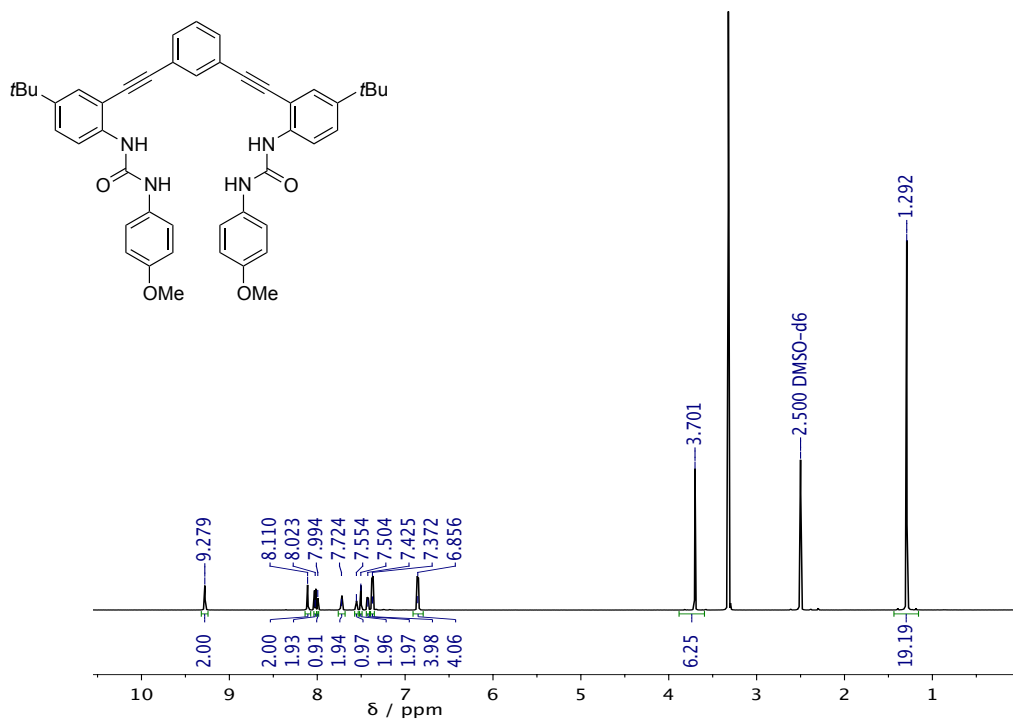
Figure 67. ^{1}H NMR spectrum of **1a** in DMSO–d_6.
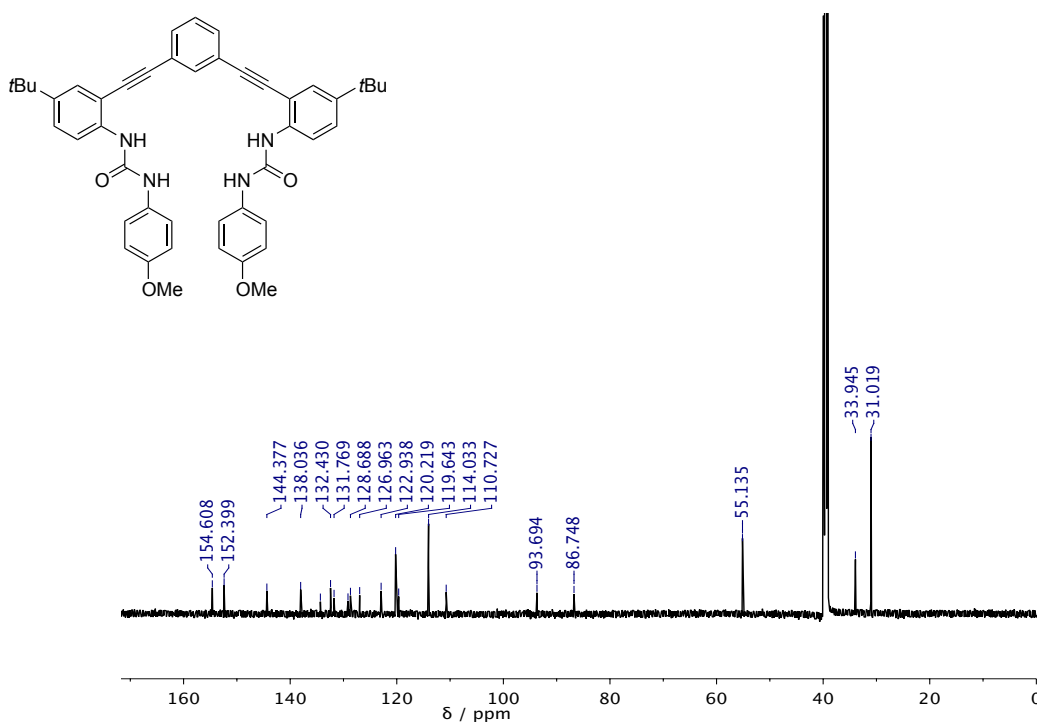
Figure 68. ^{13}C NMR spectrum of **1a** in DMSO–d_6.
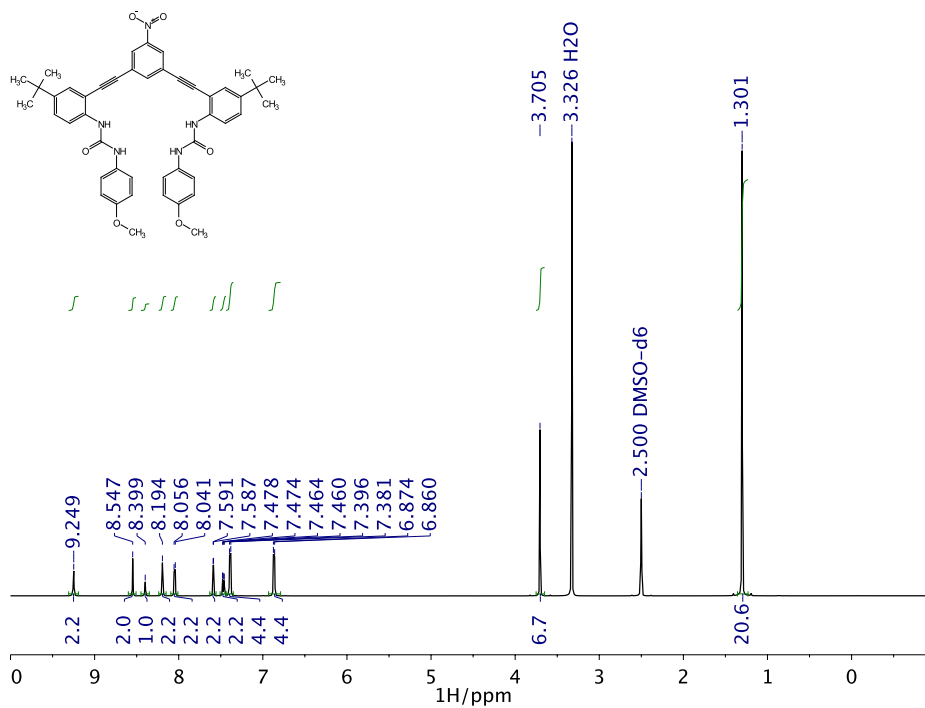
Figure 69. ^{1}H NMR spectrum of **1b** in DMSO–d_6.
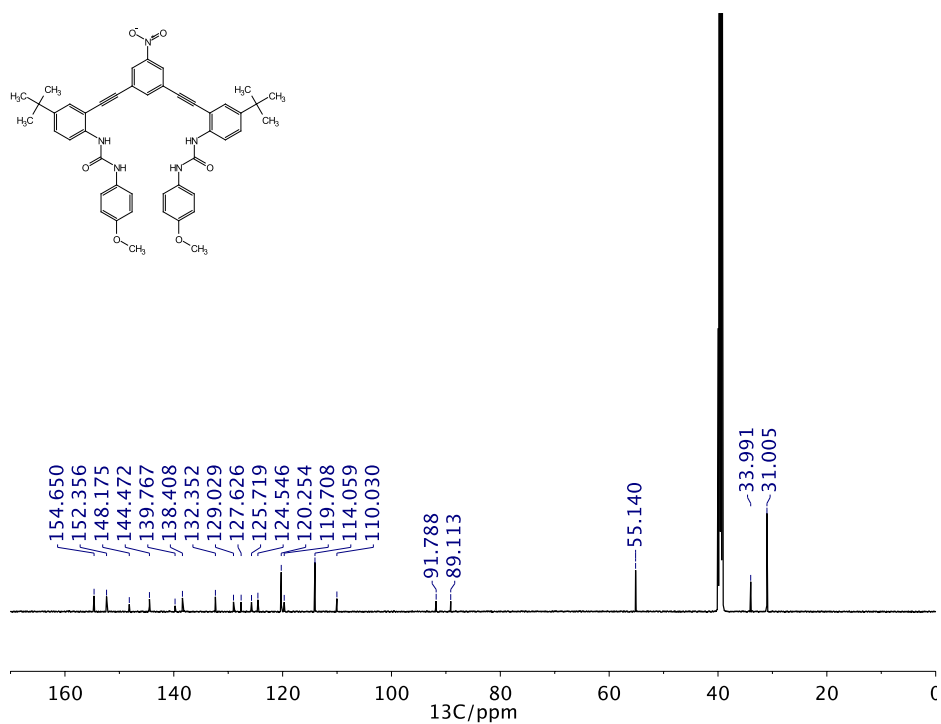
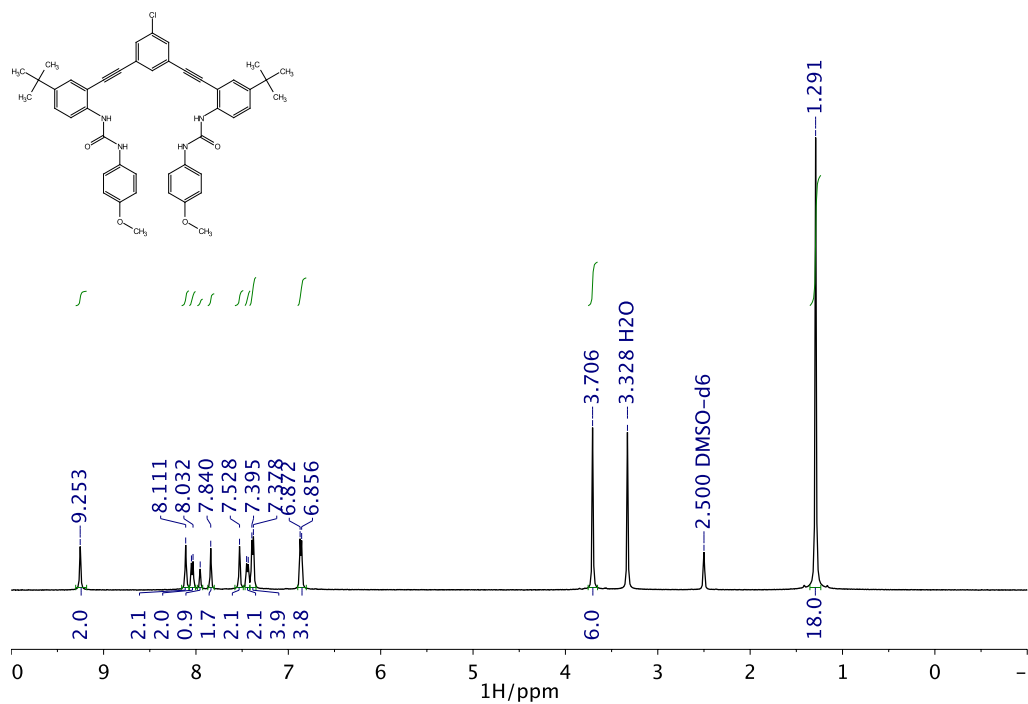**Figure 70.** ^{13}C NMR spectrum of **1b** in DMSO–d_6.

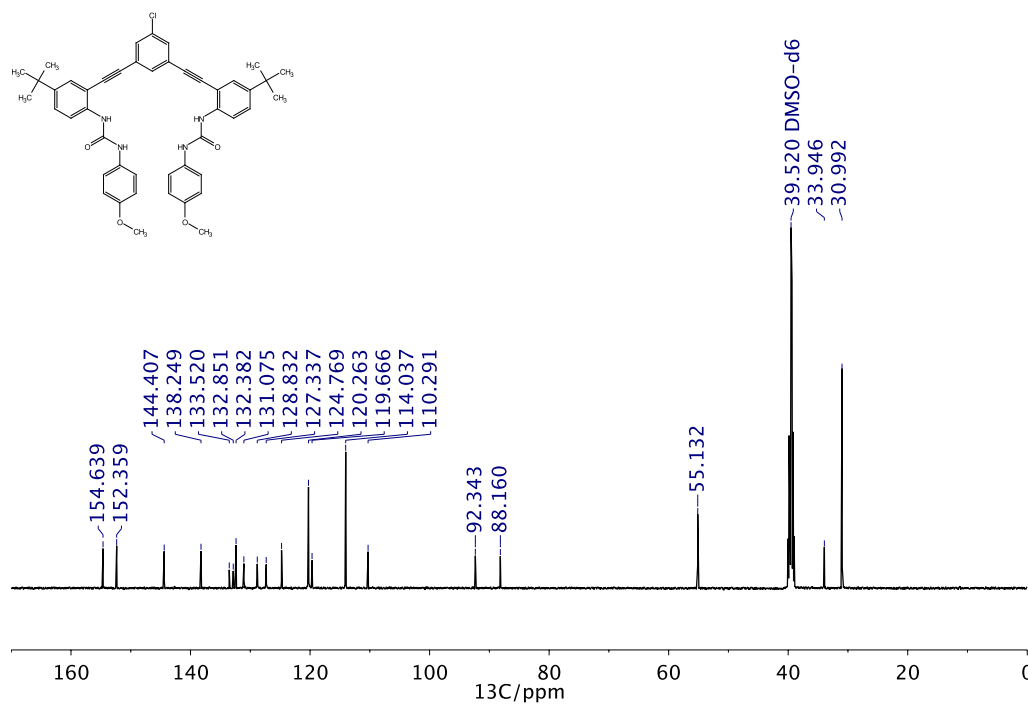**Figure 71.** ^{1}H NMR spectrum of **1c** in DMSO–d_6.

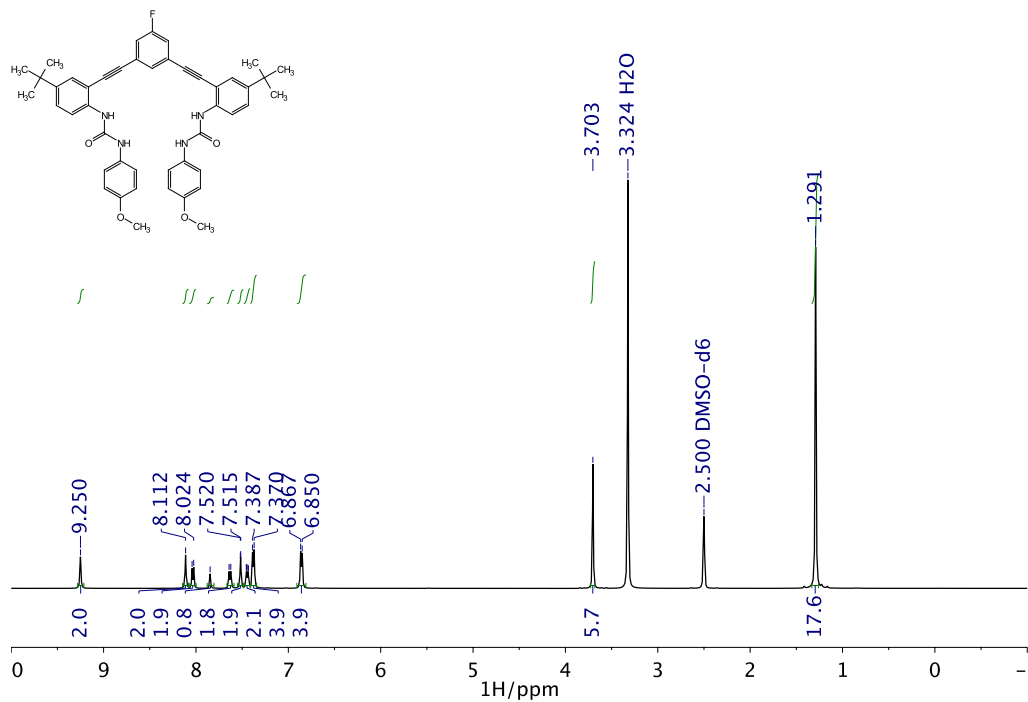**Figure 72.** ^{13}C NMR spectrum of **1c** in DMSO–d_6.

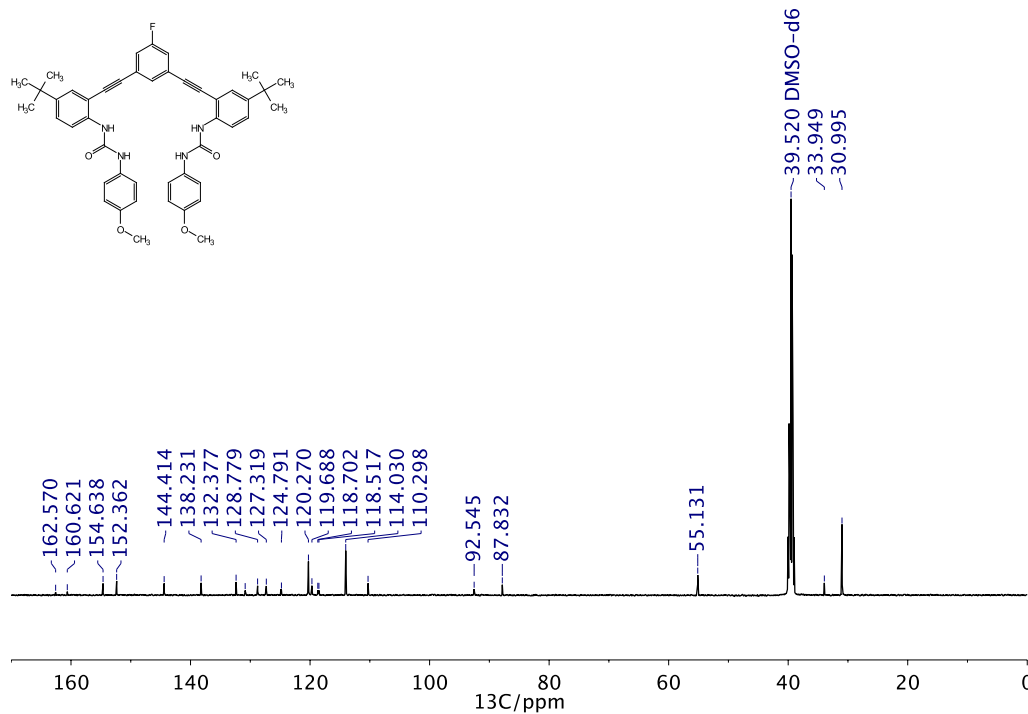**Figure 73.** ^{1}H NMR spectrum of **1d** in DMSO–d_6.

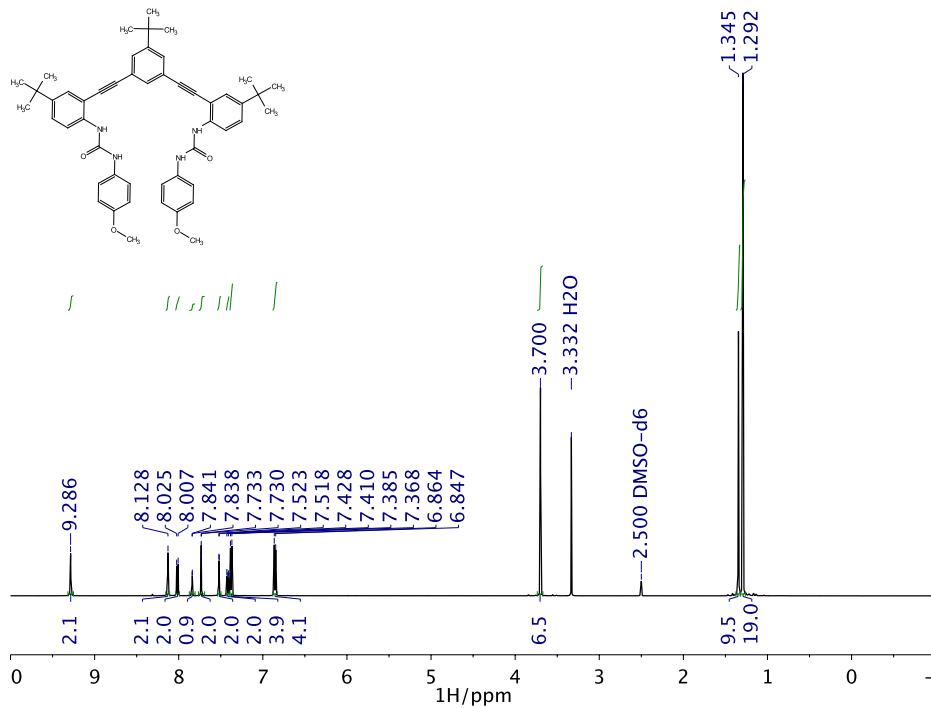**Figure 74.** ^{13}C NMR spectrum of **1d** in DMSO–d_6.

Figure 75. ^{1}H NMR spectrum of **1e** in DMSO–d_6.
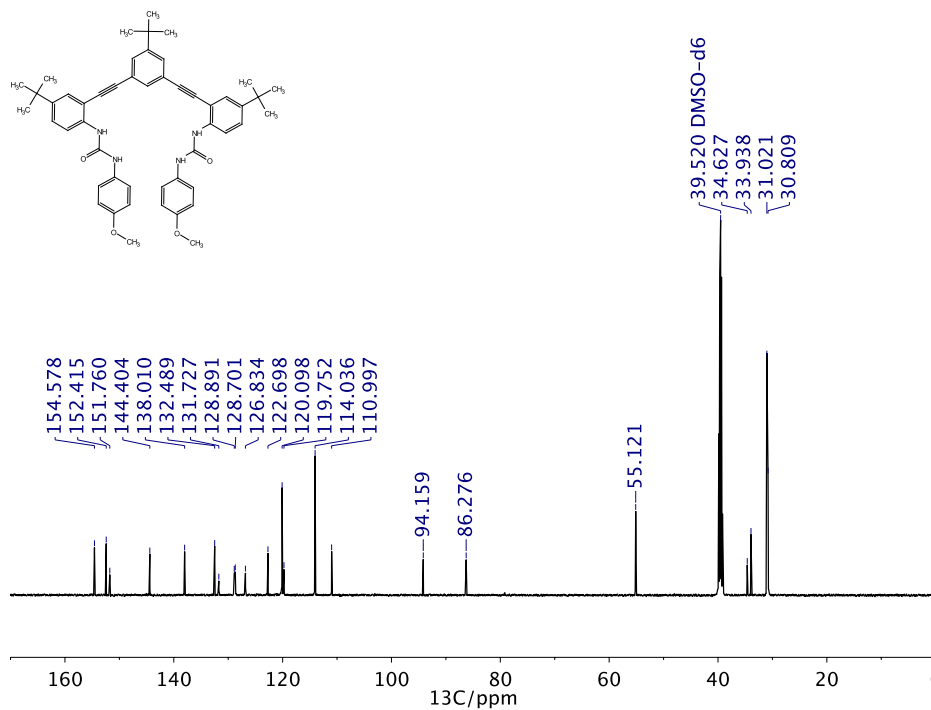

Figure 76. ^{13}C NMR spectrum of **1e** in DMSO–d_6.
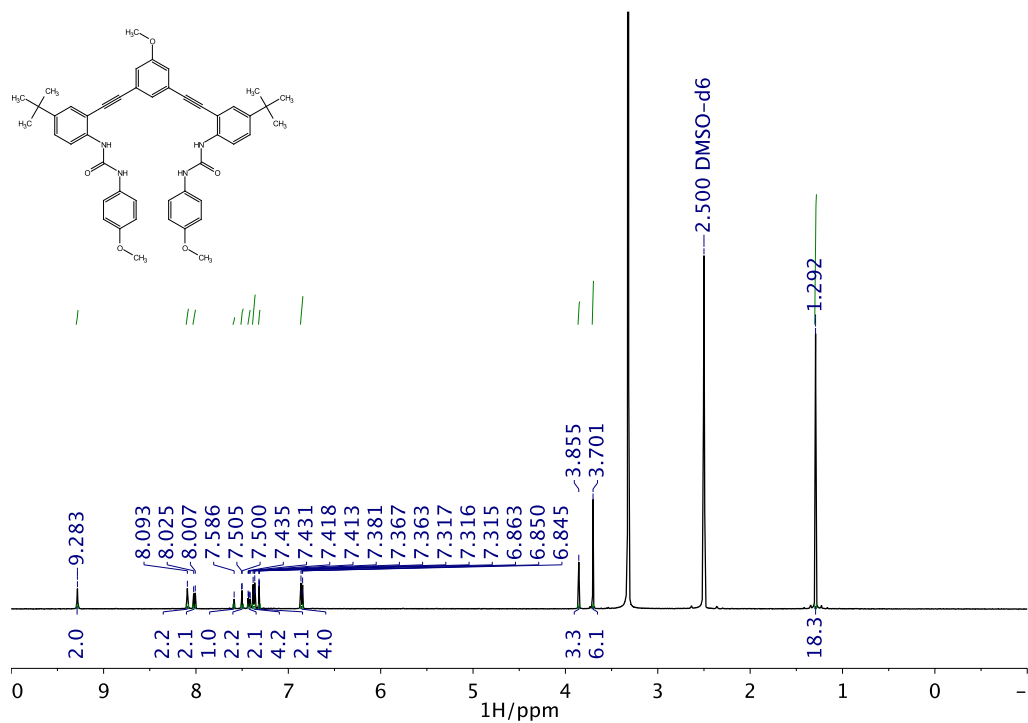
Figure 77. ^{1}H NMR spectrum of **1f** in DMSO–d_6.
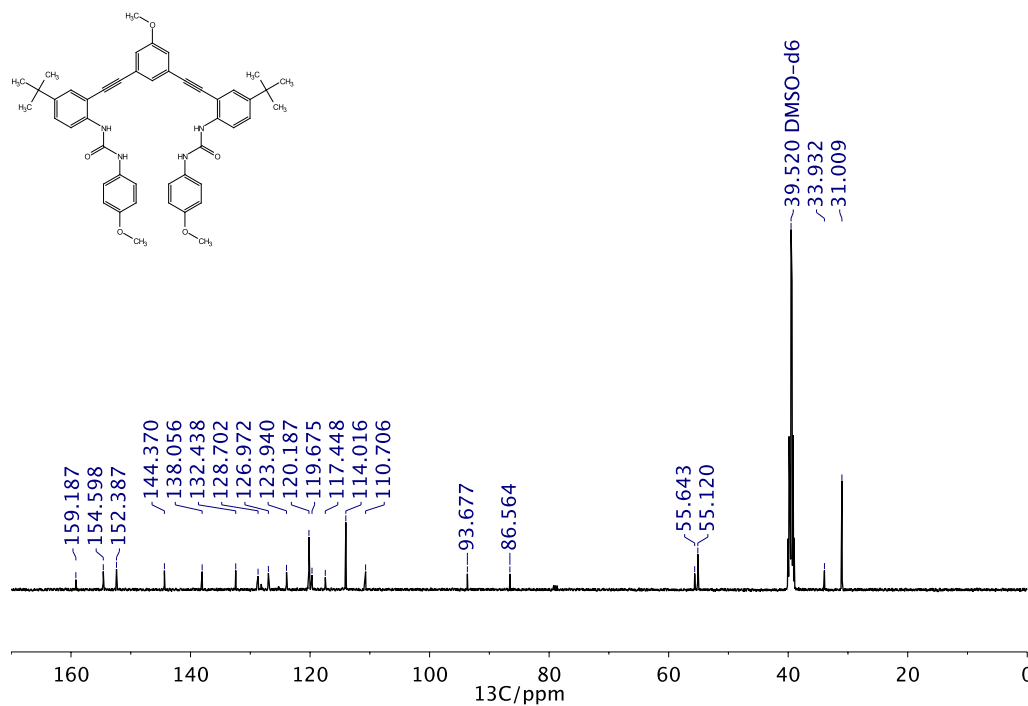
Figure 78. ^{13}C NMR spectrum of **1f** in DMSO–d_6.
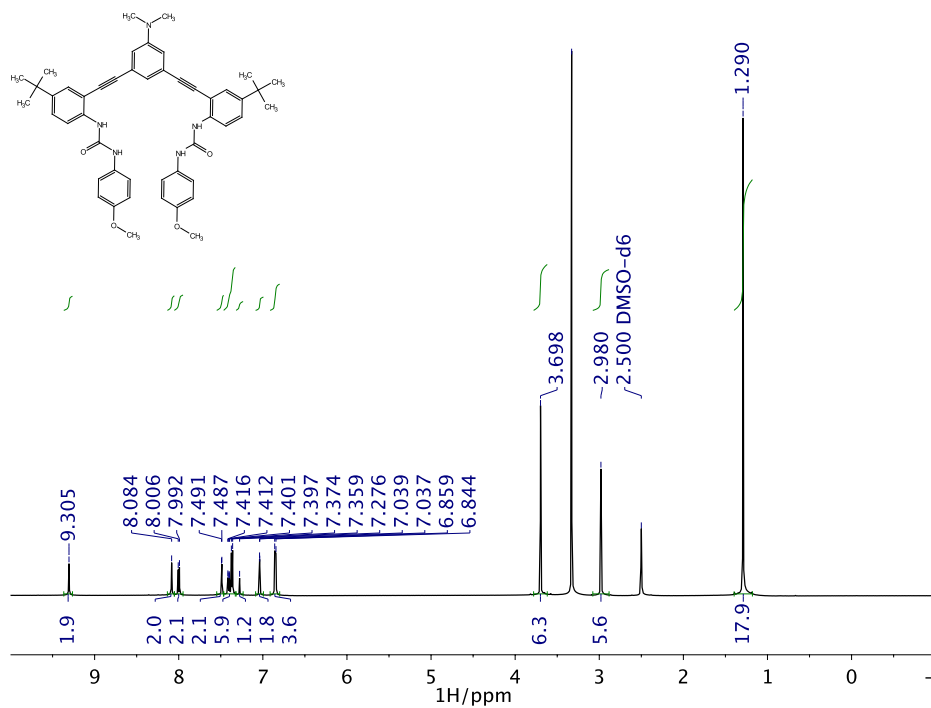
Figure 79. ^{1}H NMR spectrum of **1g** in DMSO–d_6.
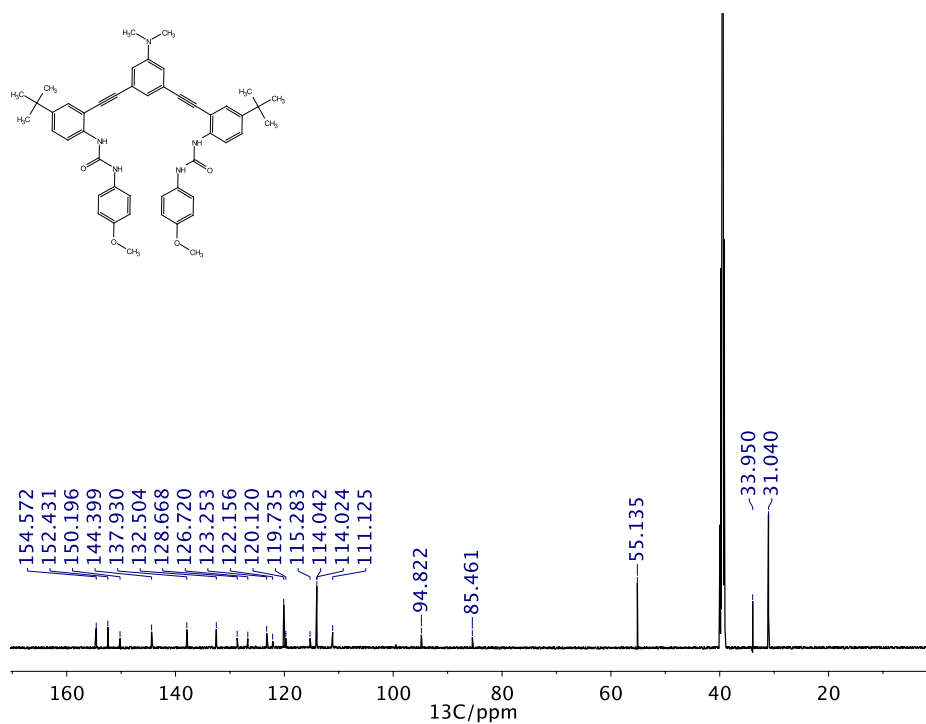
Figure 80. ^{13}C NMR spectrum of **1g** in DMSO–d_6.

SUPPLEMENTARY INFORMATION FOR CHAPTER IV

<u>NMR Spectra</u>
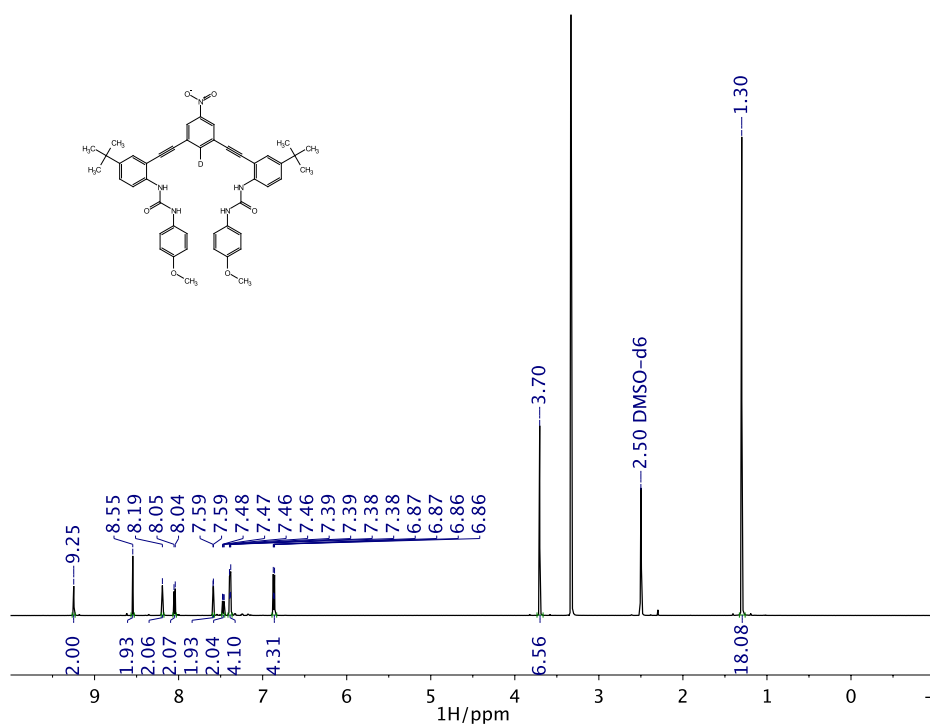
Figure 1. ^{1}H NMR of **2D** in DMSO-d_6.

Figure 2. ^{2}H NMR of **2D** in acetone-d_6.

Figure 3. ^{13}C NMR of **2D** in DMSO-d_6.

207
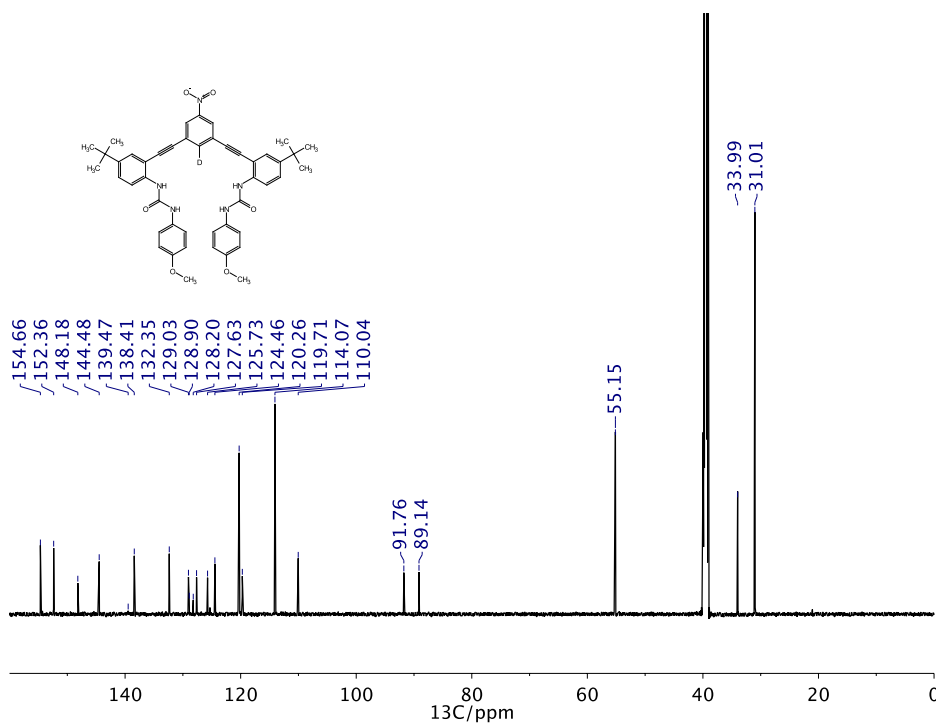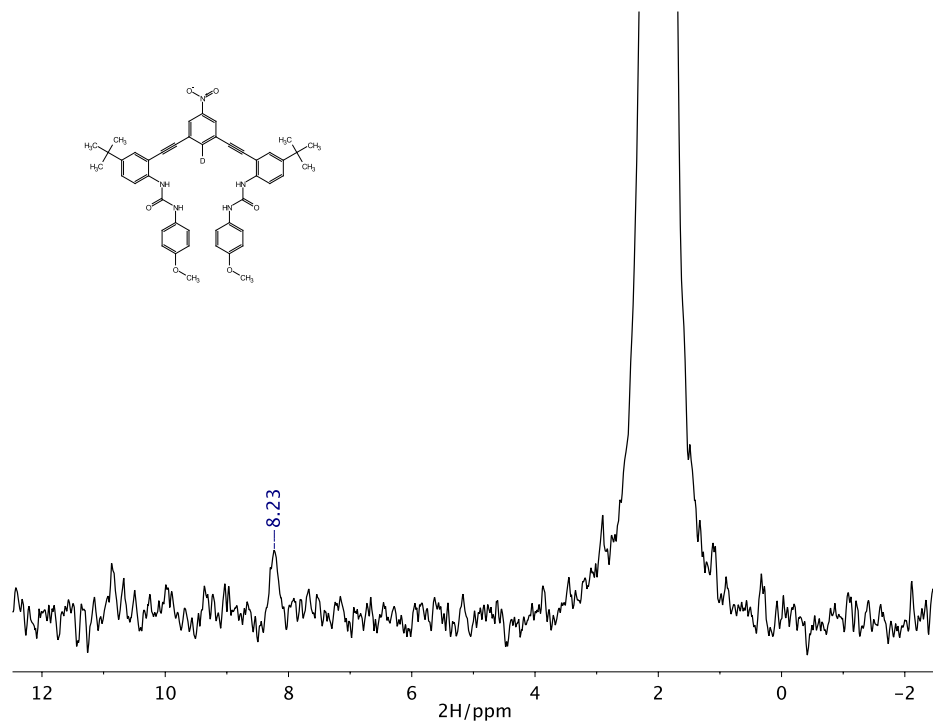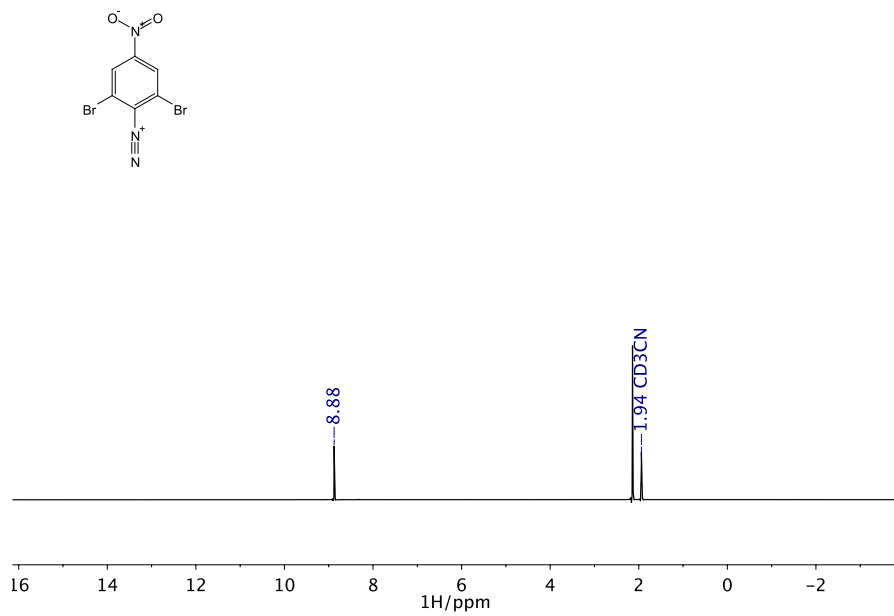
Figure 4. ^{1}H NMR of **3** in CD$_3$CN.
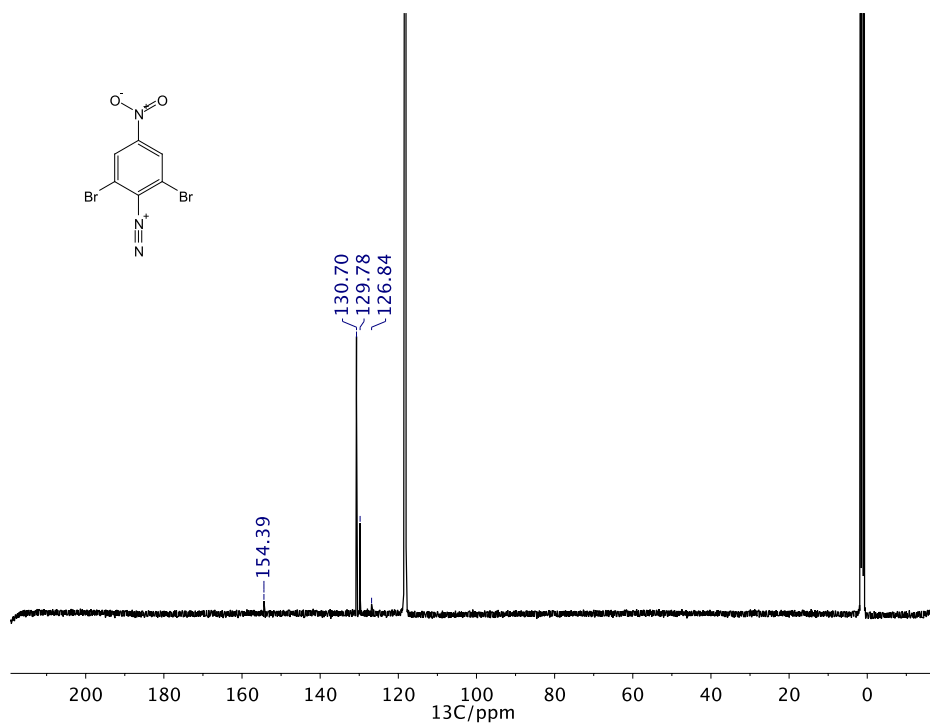
Figure 5. ^{13}C NMR of **3** in CD$_3$CN.
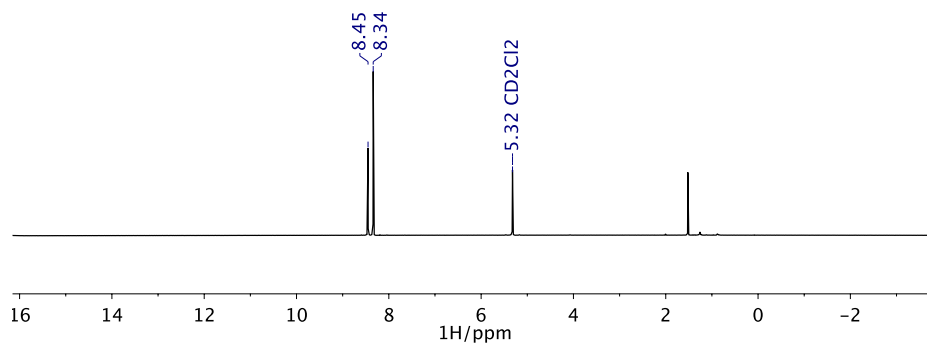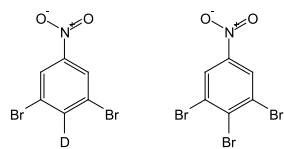
Figure 6. ^{1}H NMR of **4** in CD$_2$Cl$_2$.
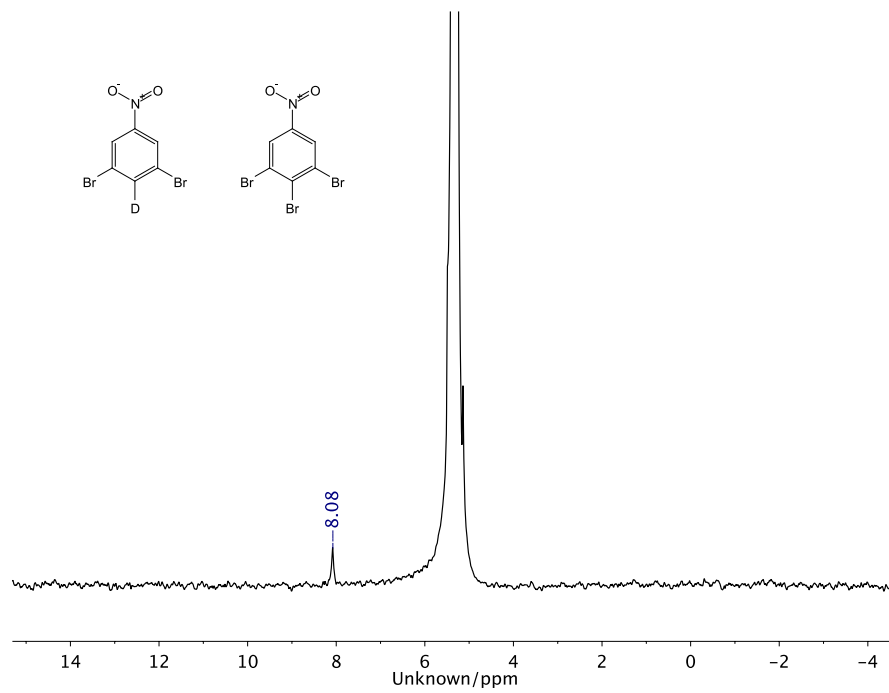
Figure 7. ^{2}H NMR of **4** in CH$_2$Cl$_2$.

209
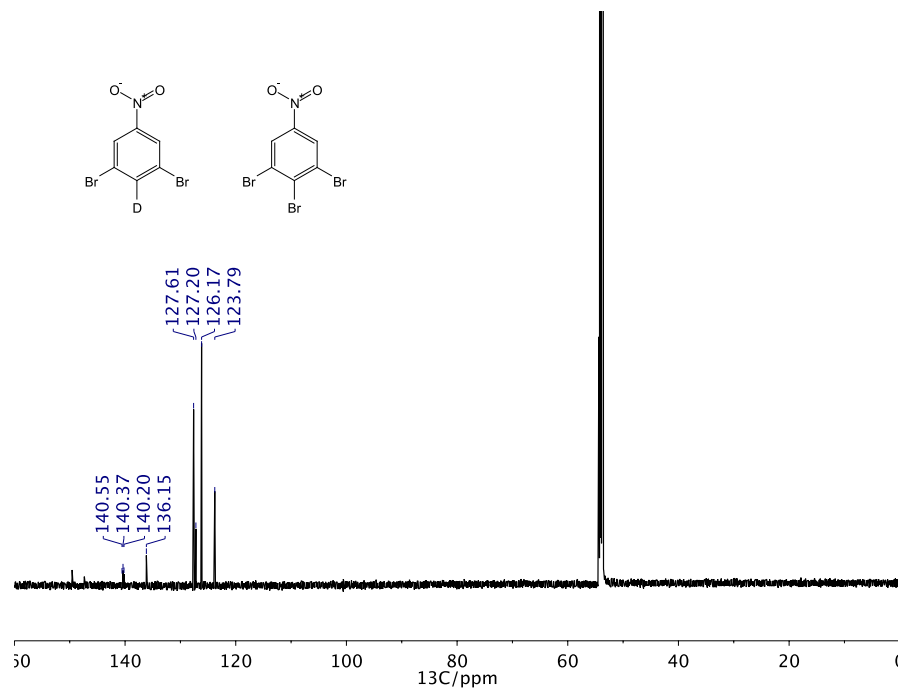
Figure 8. ^{13}C NMR of **4** in CD$_2$Cl$_2$.
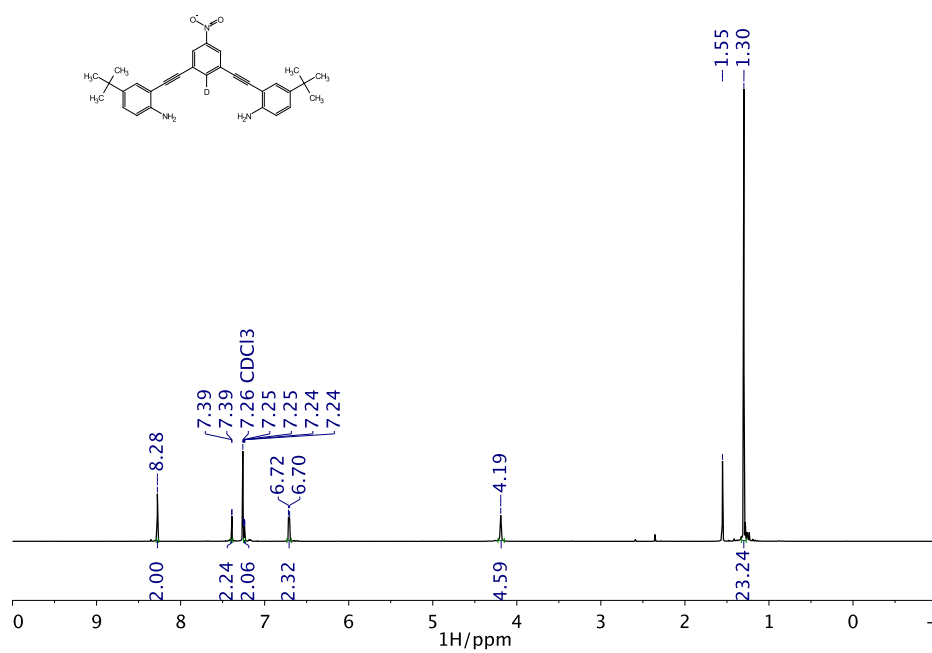
Figure 9. ^{1}H NMR of **5** in CD$_2$Cl$_2$.
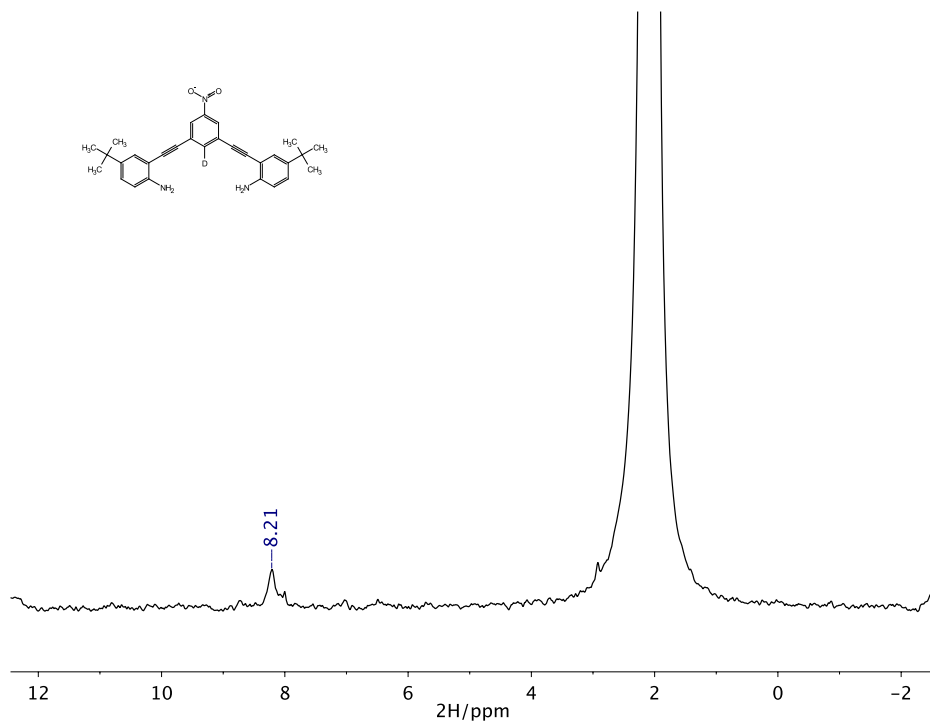
Figure 10. ^{2}H NMR of **5** in acetone-d_6.
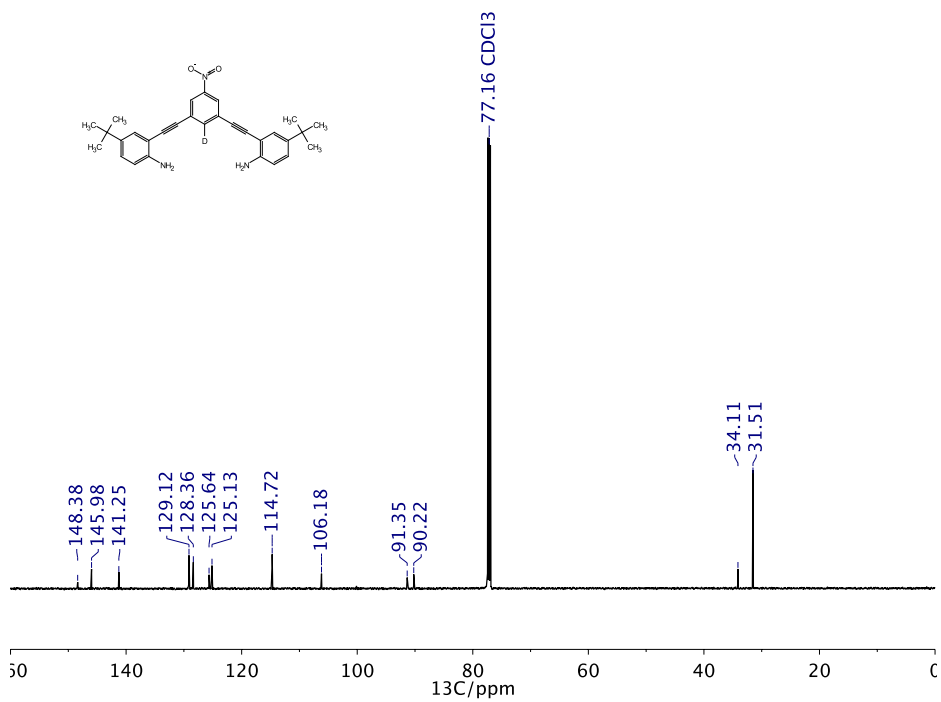
Figure 11. ^{13}C NMR of **5** in CD$_2$Cl$_2$.

211

Atomic Coordinates

[2•Cl⁻][TBA⁺]

E = -2091557.8003629

Cl	0.36501	0.54073	1.00701
O	0.12579	5.35520	-1.25345
O	-5.63368	2.78360	-2.87605
O	-1.94906	-3.45117	3.43886
O	-4.02107	1.81659	6.85528
N	1.52348	4.07458	0.09901
H	1.69473	3.12087	0.43683
N	-0.53999	3.24632	-0.55251
H	-0.32151	2.46010	0.08618
N	-0.22221	-3.01323	1.93559
H	0.50733	-2.33125	1.70037
N	-1.05629	-1.31089	3.26058
H	-0.48032	-0.70712	2.64532
N	-1.48883	-1.49469	-2.62248
C	3.81063	-0.40505	0.57642
H	2.76576	-0.10023	0.71183
C	4.82161	0.58265	0.51916
C	6.17108	0.18478	0.35900
H	6.97917	0.91697	0.31171
C	6.46007	-1.17718	0.25039
C	5.47907	-2.17033	0.29556
H	5.76352	-3.22038	0.20894
C	4.13015	-1.77751	0.46538
C	4.47228	1.95791	0.59770
C	4.15993	3.14786	0.63203
C	3.85639	4.53354	0.63681
C	2.54358	5.00889	0.31835
C	2.32004	6.40128	0.26572
H	1.32686	6.76309	0.00066
C	3.35981	7.29582	0.53292
H	3.15589	8.37096	0.48826
C	4.64582	6.83847	0.86662
C	4.88605	5.46692	0.91623
H	5.87917	5.07952	1.16299
C	0.34416	4.31480	-0.62404
C	-1.80435	3.20635	-1.17095
C	-2.10119	3.88299	-2.37201
H	-1.34257	4.52329	-2.82398
C	-3.36829	3.76843	-2.96495
H	-3.56263	4.31501	-3.89156
C	-4.36389	2.97146	-2.37275

C	-4.07663	2.30242	-1.16652
H	-4.86940	1.71843	-0.68762
C	-2.81783	2.42136	-0.57307
H	-2.60987	1.91304	0.37496
C	-5.99364	3.55784	-4.01667
H	-7.04825	3.32073	-4.22100
H	-5.38390	3.29398	-4.90351
H	-5.89165	4.64230	-3.82044
C	3.09421	-2.75149	0.53212
C	2.20327	-3.59789	0.61041
C	1.18311	-4.57959	0.71832
C	-0.04301	-4.29320	1.40841
C	-1.02113	-5.31164	1.49550
H	-1.93723	-5.10533	2.04813
C	-0.79254	-6.56672	0.92398
H	-1.56731	-7.33564	1.01546
C	0.40537	-6.85489	0.24823
C	1.38184	-5.86348	0.15246
H	2.33125	-6.05947	-0.35563
C	-1.15094	-2.64615	2.93769
C	-1.85187	-0.60652	4.19418
C	-2.73268	-1.21762	5.10636
H	-2.83896	-2.30246	5.10395
C	-3.47211	-0.43604	6.00805
H	-4.14596	-0.94187	6.70449
C	-3.34379	0.96328	6.01497
C	-2.46117	1.57508	5.10291
H	-2.36364	2.66479	5.11447
C	-1.72636	0.80290	4.20674
H	-1.04022	1.28621	3.50185
C	-4.89752	1.22399	7.80611
H	-5.32614	2.05827	8.38141
H	-4.35740	0.54459	8.49435
H	-5.71607	0.66035	7.31634
C	-0.70985	-0.33226	-3.26466
H	-1.37250	0.54402	-3.18275
H	-0.61951	-0.58726	-4.33439
C	0.66233	0.00189	-2.68000
H	0.59836	0.21355	-1.59624
H	1.36306	-0.84386	-2.80916
C	1.23661	1.23369	-3.41082
H	1.25603	1.04125	-4.50237
H	0.56026	2.09634	-3.25693
C	2.64676	1.59268	-2.92721
H	3.03960	2.46431	-3.47687
H	3.35019	0.75432	-3.07671
H	2.65042	1.84669	-1.85411
C	-2.03408	-1.02519	-1.26090

H	-2.55146	-0.07517	-1.46354
H	-1.15429	-0.77766	-0.63998
C	-2.96399	-1.99459	-0.52256
H	-2.39893	-2.84796	-0.10636
H	-3.73924	-2.41147	-1.19305
C	-3.68133	-1.25326	0.62705
H	-2.93144	-0.77532	1.28236
H	-4.28780	-0.43460	0.19452
C	-4.57798	-2.17858	1.45923
H	-5.11542	-1.60206	2.23055
H	-3.98269	-2.94496	1.98327
H	-5.33113	-2.68486	0.82783
C	-0.58490	-2.70757	-2.39081
H	-1.21332	-3.46134	-1.89047
H	0.17173	-2.37729	-1.66159
C	0.07984	-3.30506	-3.63490
H	0.58644	-2.52020	-4.22656
H	-0.67336	-3.77127	-4.29644
C	1.11739	-4.37264	-3.23501
H	1.88401	-3.90854	-2.58601
H	0.62939	-5.15063	-2.61848
C	1.78731	-5.01747	-4.45464
H	2.52987	-5.77057	-4.14262
H	2.31289	-4.26605	-5.07023
H	1.04820	-5.52439	-5.10031
C	-2.62777	-1.88380	-3.56582
H	-2.14901	-2.18705	-4.51041
H	-3.09433	-2.78141	-3.12970
C	-3.67546	-0.80143	-3.83599
H	-3.21431	0.06628	-4.34123
H	-4.11055	-0.42176	-2.89517
C	-4.81442	-1.34769	-4.71887
H	-4.39397	-1.80885	-5.63372
H	-5.33928	-2.15754	-4.17659
C	-5.81383	-0.24947	-5.10652
H	-6.67259	-0.66993	-5.65585
H	-5.33732	0.50667	-5.75570
H	-6.19730	0.27598	-4.21434
H	5.45222	7.54634	1.08109
H	0.57902	-7.84372	-0.18718
N	7.87361	-1.58948	0.07133
O	8.10634	-2.80302	-0.04614
O	8.73381	-0.69587	0.04760

2

E = -1372925.0404770

O	-1.10047	1.91685	0.00037
O	1.10000	1.91694	-0.00013
O	7.72311	-0.56646	-0.00095
O	7.25106	6.06855	0.00006
O	-7.72303	-0.56620	-0.00018
O	-7.25069	6.06871	-0.00091
N	-0.00020	1.34295	-0.00006
N	5.65142	-1.63453	-0.00040
N	5.75253	0.66702	0.00165
N	-5.65142	-1.63445	0.00160
N	-5.75237	0.66711	0.00142
C	-0.00004	-2.92203	-0.00097
H	0.00005	-4.01500	-0.00112
C	1.23269	-2.22581	-0.00092
C	1.22208	-0.80876	-0.00067
H	2.14794	-0.23170	-0.00062
C	-0.00015	-0.13959	-0.00048
C	-1.22229	-0.80887	-0.00057
H	-2.14820	-0.23189	-0.00048
C	-1.23281	-2.22595	-0.00079
C	2.47994	-2.90470	-0.00098
C	3.58513	-3.45144	-0.00090
C	4.91865	-3.93235	-0.00066
C	6.00010	-2.98357	-0.00042
C	7.32747	-3.45722	-0.00021
H	8.14076	-2.73109	-0.00012
C	7.57460	-4.83347	-0.00018
H	8.61334	-5.18038	-0.00001
C	6.52580	-5.76989	-0.00040
C	5.20723	-5.31754	-0.00066
H	4.37116	-6.02332	-0.00085
C	6.49099	-0.50876	-0.00002
C	6.22207	2.00101	0.00115
C	5.24827	3.02486	0.00103
H	4.18091	2.76709	0.00117
C	5.62334	4.36560	0.00071
H	4.87014	5.15862	0.00062
C	6.98695	4.72099	0.00041
C	7.95897	3.70521	0.00049
H	9.02459	3.94788	0.00027
C	7.58320	2.35352	0.00090
H	8.33920	1.56802	0.00099
C	8.62052	6.45910	-0.00021
H	8.61851	7.55912	-0.00042

H	9.15006	6.09402	-0.90167
H	9.15031	6.09437	0.90125
C	-2.48006	-2.90483	-0.00070
C	-3.58527	-3.45155	-0.00042
C	-4.91883	-3.93234	0.00008
C	-6.00021	-2.98347	0.00102
C	-7.32761	-3.45702	0.00156
H	-8.14085	-2.73083	0.00212
C	-7.57486	-4.83325	0.00117
H	-8.61363	-5.18008	0.00157
C	-6.52614	-5.76974	0.00027
C	-5.20753	-5.31750	-0.00027
H	-4.37153	-6.02336	-0.00099
C	-6.49090	-0.50862	0.00087
C	-6.22187	2.00113	0.00076
C	-7.58298	2.35369	-0.00081
H	-8.33902	1.56822	-0.00147
C	-7.95870	3.70539	-0.00141
H	-9.02431	3.94810	-0.00262
C	-6.98664	4.72113	-0.00044
C	-5.62305	4.36570	0.00110
H	-4.86982	5.15869	0.00178
C	-5.24803	3.02494	0.00167
H	-4.18067	2.76713	0.00271
C	-8.62013	6.45932	-0.00255
H	-8.61808	7.55934	-0.00267
H	-9.15088	6.09454	0.89832
H	-9.14875	6.09434	-0.90459
H	4.63967	-1.48484	-0.00104
H	4.73604	0.58991	0.00316
H	-4.63966	-1.48485	0.00039
H	-4.73588	0.58996	0.00395
H	-6.73889	-6.84276	0.00001
H	6.73848	-6.84291	-0.00040

Titrations, Dilutions, and DOSY

Titrations and Dilutions

General Procedures. Receptor concentration was kept constant by preparing a stock solution of receptor and diluting a guest with the stock receptor solution. Tetrabutylammonium salts were purchased from TCI America or Fluka and dried by heating to 70 °C *in vacuo* before use. Hamilton gas-tight syringes were used for all titrations and additions were made through septa when available. ^{1}H NMR titrations were carried out on an Inova 500 MHz spectrometer ([1]H 500.10 MHz). Chemical shifts (δ) are expressed in ppm relative to tetramethylsilane (TMS) using residual non-deuterated solvent ($CDCl_3$: [1]H 7.26 ppm, [13]C 77.0 ppm). $CDCl_3$ was prepared by passing over activated alumina; 1:1 v/v $CDCl_3$ and deionized water was mixed in a separatory funnel and the organic layer was collected. When noted, HCl saturated solutions were prepared by bubbling HCl gas ten times with a glass pipette and used immediately. DOSY were processed using the Varian VnmrJ 3.2 RevisionJ software package.

^{1}H NMR Titration of 2 with Tetrabutylammonium Chloride. A stock solution of **2** (2.50 mg, [**2**] = 1.03 mM) in $CDCl_3$ (3 mL) was prepared and used in the dilution of TBACl guest solution (16.71 mg, [G] = 26.14 mM). The remaining stock solution (0.6 mL) was used as the starting volume in an NMR tube. The binding isotherm was linear through 18 equiv. of Cl^{−}, which indicates $K_a \ll 80$ M[−1] at this receptor concentration; therefore, an association constant determined by ^{1}H NMR would be unreliable. The titration is provided

for comparison of structural characteristics apparent in the NMR to crystallographic data and assists in proton signal assignment.

Table 1. Titration data for Cl⁻ with **2**.

|	Guest (µL)	[**5**] (M)	[Cl⁻] (M)	Equiv.	δ (ppm)
0	0	1.03E-03	0.00E+00	0.00	8.925
1	5	1.03E-03	2.16E-04	0.21	8.925
2	10	1.03E-03	4.29E-04	0.42	8.928
3	20	1.03E-03	8.43E-04	0.82	8.933
4	30	1.03E-03	1.24E-03	1.21	8.938
5	50	1.03E-03	2.01E-03	1.95	8.946
6	70	1.03E-03	2.73E-03	2.65	8.954
7	100	1.03E-03	3.73E-03	3.63	8.967
8	150	1.03E-03	5.23E-03	5.08	8.984
9	200	1.03E-03	6.54E-03	6.35	9.002
10	300	1.03E-03	8.71E-03	8.47	9.028
11	400	1.03E-03	1.05E-02	10.16	9.049
12	600	1.03E-03	1.31E-02	12.70	9.088
13	800	1.03E-03	1.49E-02	14.52	9.106
14	1000	1.03E-03	1.63E-02	15.88	9.120
15	1250	1.03E-03	1.77E-02	17.16	9.135
16	1500	1.03E-03	1.87E-02	18.14	9.144
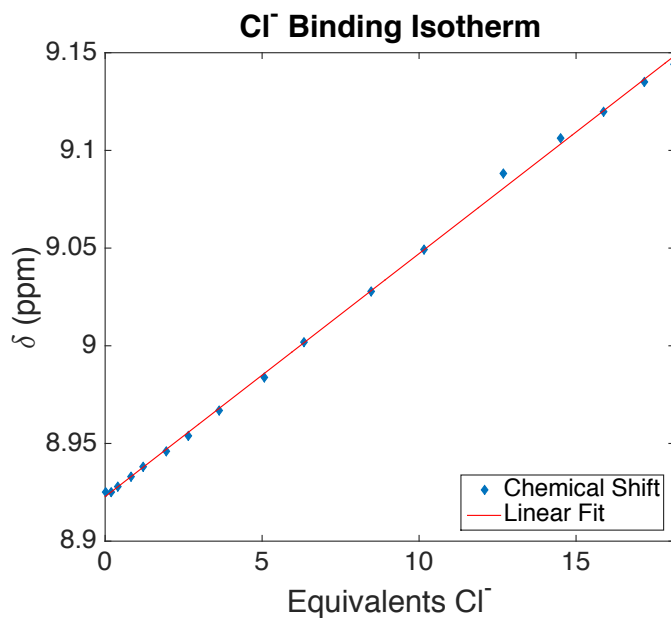
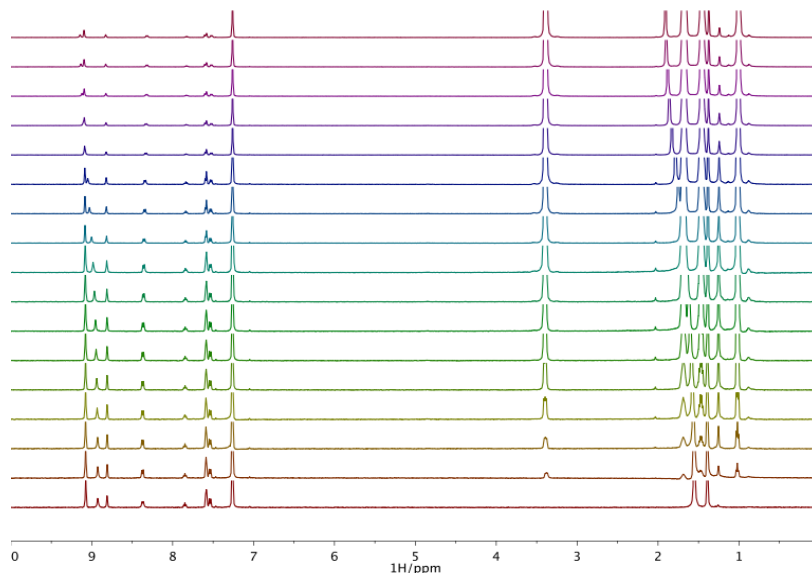**Figure 1.** Binding isotherm for Cl⁻ titration with **2**.

Figure 2. ^{1}H NMR spectra of Cl$^-$ titration with **2**.

^{1}H NMR Dilution of (H2$^+$•Cl$^-$) with CDCl$_3$. A stock solution of **2** (2.44 mg, [**2**] = 1.00 mM) in CDCl$_3$ (3 mL) was prepared. The solution was saturated with HCl and 500μL was transferred to an NMR tube. Aliquots of CDCl$_3$ (without HCl) were added by Hamilton syringe and the ^{1}H NMR spectrum was recorded after each addition. After the final addition, the contents of the NMR tube were transferred to a vial and saturated with HCl. 500 μL of the saturated solution were transferred to a new NMR tube and a final ^{1}H NMR spectrum was recorded.

Table 2. Data from dilution of **2** with CDCl$_3$.

	Added CDCl$_3$ (μL)	[**2**] (M)	Dilution Factor	Additive
0	0	1.00E-03	0	—
1	50	9.13E-04	0.1	—
2	100	8.37E-04	0.2	—
3	150	7.73E-04	0.3	—
4	200	7.17E-04	0.4	—
5	250	6.70E-04	0.5	—
6	300	6.28E-04	0.6	—
7	350	5.91E-04	0.7	—

Table 2. continued

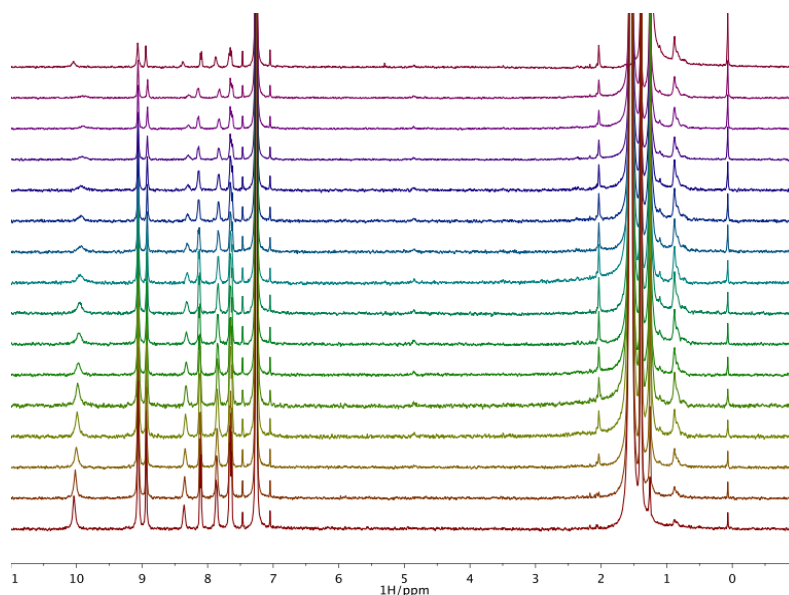|	Added CDCl$_3$ (µL)	[**2**] (M)	Dilution Factor	Additive
8	450	5.29E-04	0.9	—
9	650	4.37E-04	1.3	—
10	850	3.72E-04	1.7	—
11	1050	3.24E-04	2.1	—
12	1250	2.87E-04	2.5	—
13	1450	2.58E-04	2.9	—
14	1650	2.34E-04	3.3	—
15	1650	2.34E-04	3.3	HCl (g)

Figure 3. ^{1}H NMR spectra of **2** diluted with CDCl$_3$. Spectra correspond to Table 2 with point 0 on the bottom and 15 on the top.

^{1}H NMR Dilution of (H2$^+$•Cl$^-$) with CDCl$_3$ (HCl saturated). A stock solution of **2** (1.44 mg, [**2**] = 0.89 mM) in CDCl$_3$ (2 mL) was prepared. The solution was saturated with HCl and 500µL was transferred to an NMR tube. Aliquots of CDCl$_3$ (saturated with HCl) were added by Hamilton syringe and the ^{1}H NMR spectrum was recorded after each addition. After the addition of 1.50 mL, 250 µL of the solution was transferred to a new NMR tube and the dilution was continued.

Table 3. Data from dilution of **2** with CDCl$_3$.

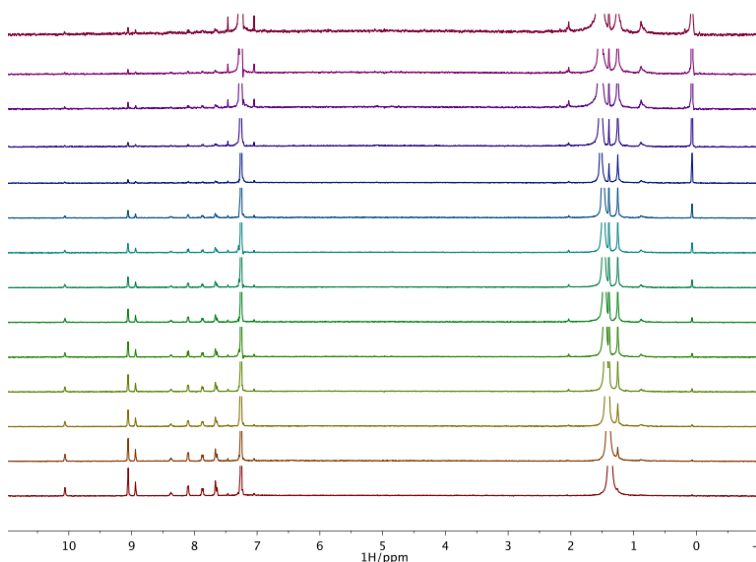|	Added CDCl$_3$ (µL)	[**2**] (M)	Dilution Factor
0	0	8.89E-04	0.0
1	100	7.41E-04	0.2
2	200	6.35E-04	0.4
3	300	5.56E-04	0.6
4	400	4.94E-04	0.8
5	500	4.45E-04	1.0
6	750	3.56E-04	1.5
7	1000	2.96E-04	2.0
8	1500	2.22E-04	3.0
9	250	1.11E-04	7.0
10	500	7.41E-05	11.0
11	750	5.56E-05	15.0
12	1250	3.70E-05	23.0
13	1750	2.78E-05	31.0

Figure 4. ^{1}H NMR spectra of **(H2$^+$•Cl$^-$)** diluted with CDCl$_3$ (HCl saturated). Spectra correspond to Table 3 with point 0 on the bottom.

^{1}H DOSY NMR

General DOSY Procedures. The DOSY experiments were performed using the gradient stimulated echo with spin-lock and convection compensation (DgsteSL_cc) pulse sequences. All Varian software standard default settings were kept for DOSY unless otherwise stated. The diffusion delay was increased to 75 ms, the number of increments was

increased to 20, and the highest gradient value was set to 20,000. The alternate gradient sign

on odd scans and lock gating during gradient portions were also selected. The arrayed

spectra were processed using VnmrJ 3.2 Revision A with standard DOSY parameters and

non-uniform gradient compensation.

DOSY NMR of 2. A stock solution of **2** (0.9 mg, [**2**] = 1.11 mM) in $CDCl_3$ (1 mL)

was prepared and 600 μL was transferred to an NMR tube. DOSY NMR spectra was

collected and processed following the general procedures.

DOSY NMR of HCl Salt (H2$^+$•Cl$^-$). Amide **2** (4.4 mg, 0.005 mmol) was dissolved

in $CHCl_3$ (6 mL) in a vial. HCl was bubbled ten times through the solution with a glass

pipette, which produced a bright yellow solution. The solvent and excess HCl were removed

in vacuo overnight to produce **H2$^+$•Cl$^-$** (5.4 mg) as a yellow powder. **H2$^+$•Cl$^-$** (1.57 mg,

[**H2$^+$•Cl$^-$**] = 1.86 mM) was dissolved in $CDCl_3$ (1 mL) and 400 μL was transferred to an

NMR tube. Solvent (400 μL) was added to dilute to a final concentration of 0.93 mM.

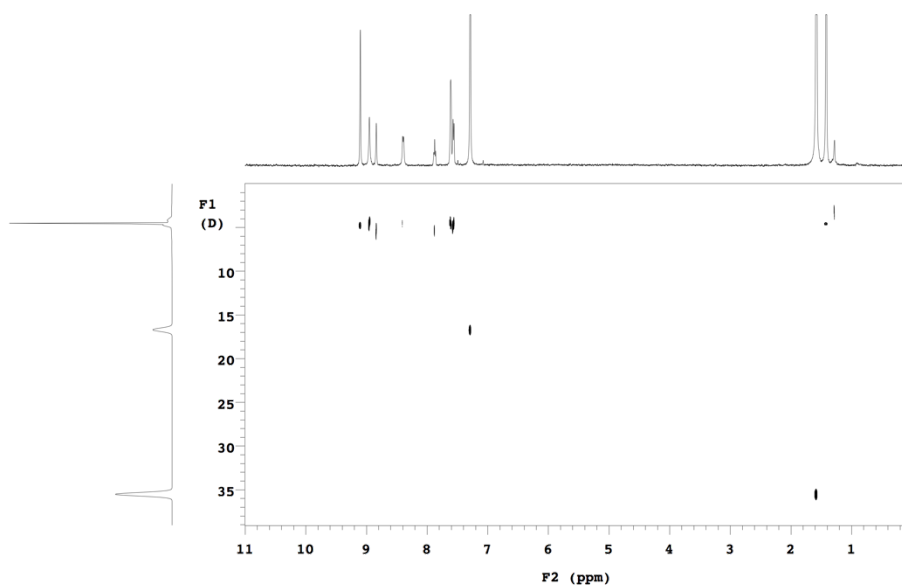DOSY NMR was collected and processed following the general procedures.

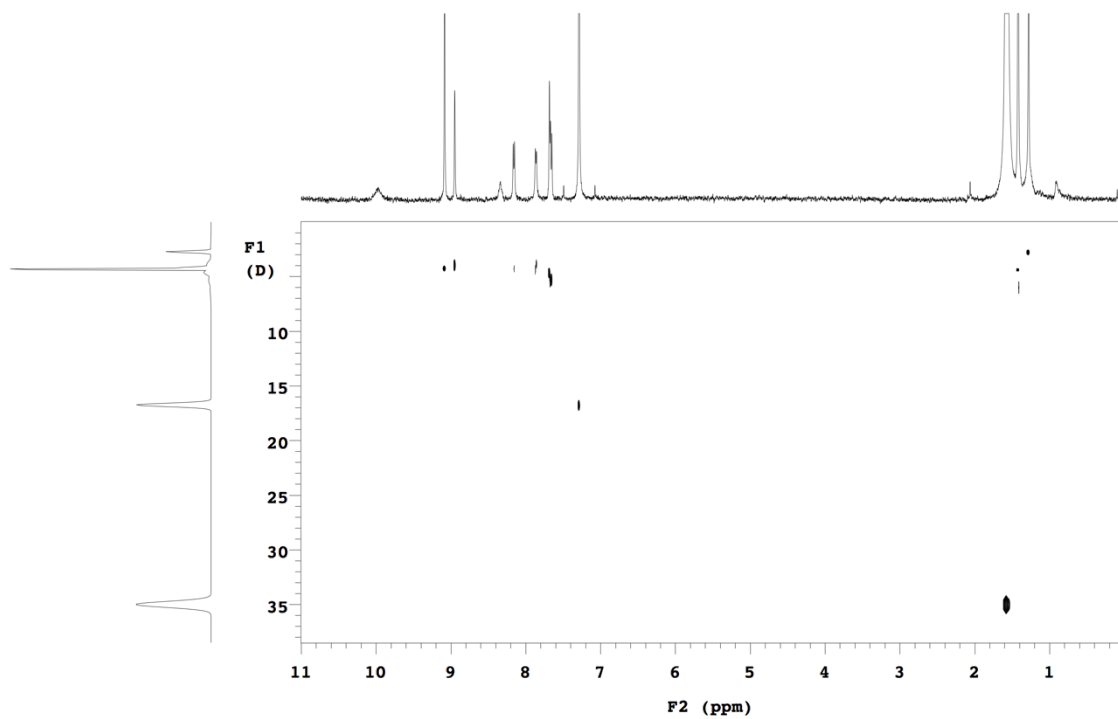**Figure 5.** ^{1}H DOSY NMR spectra of **2**.

Figure 6. ^{1}H DOSY NMR spectra of **(H2$^+$•Cl$^-$)**.
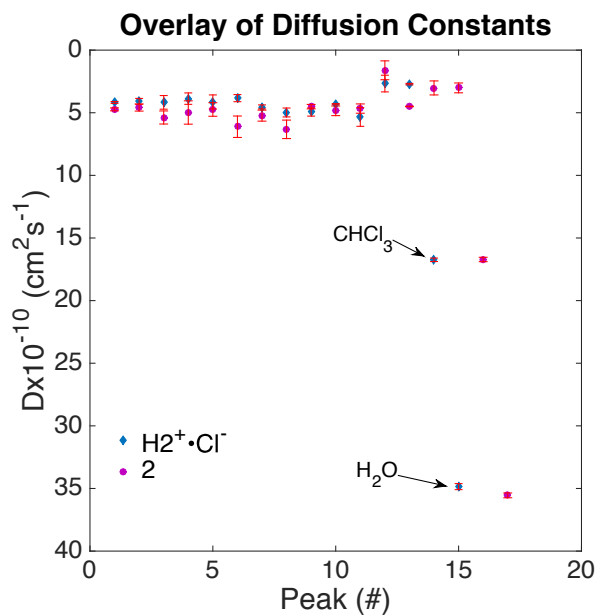

Figure 7. ^{1}H DOSY NMR of **(H2$^+$•Cl$^-$)** and **2**.
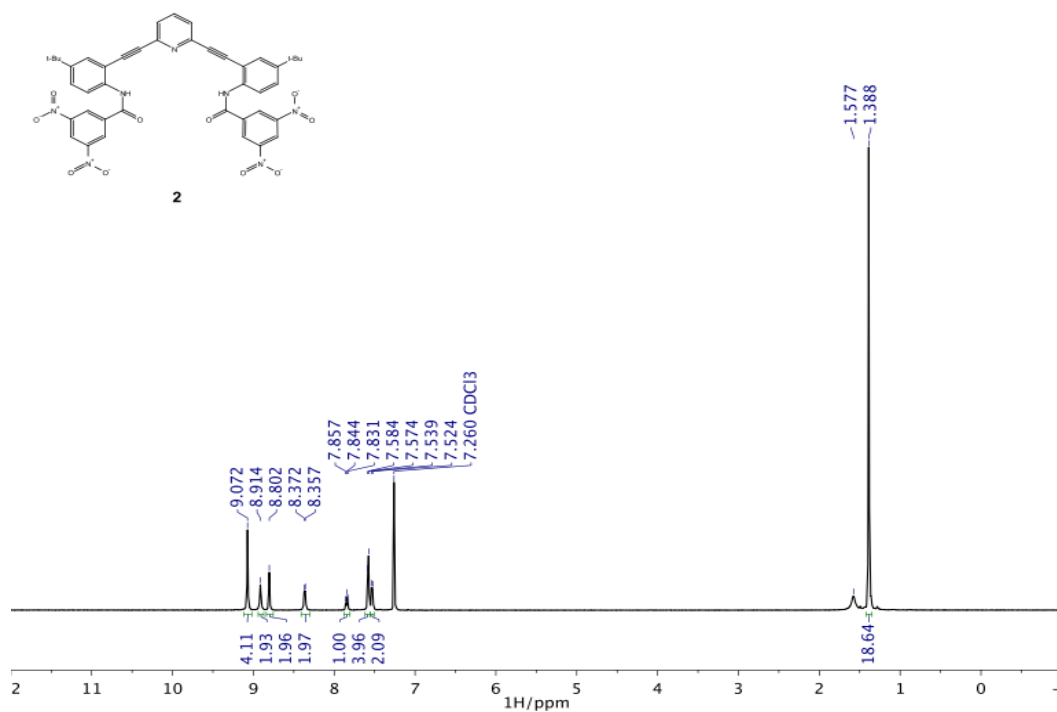
NMR Spectra

Figure 8. ^{1}H NMR spectrum of **2** in CDCl$_3$.
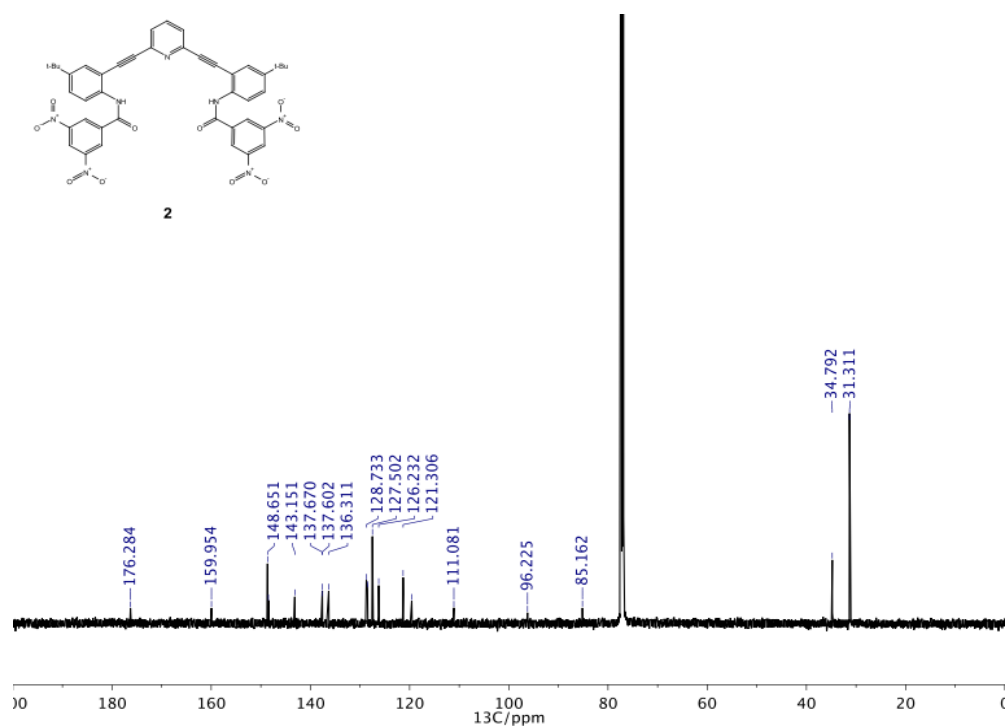
Figure 9. ^{13}C NMR spectrum of **2** in CDCl$_3$.

SUPPLEMENTARY INFORMATION FOR CHAPTER III

NMR Spectra
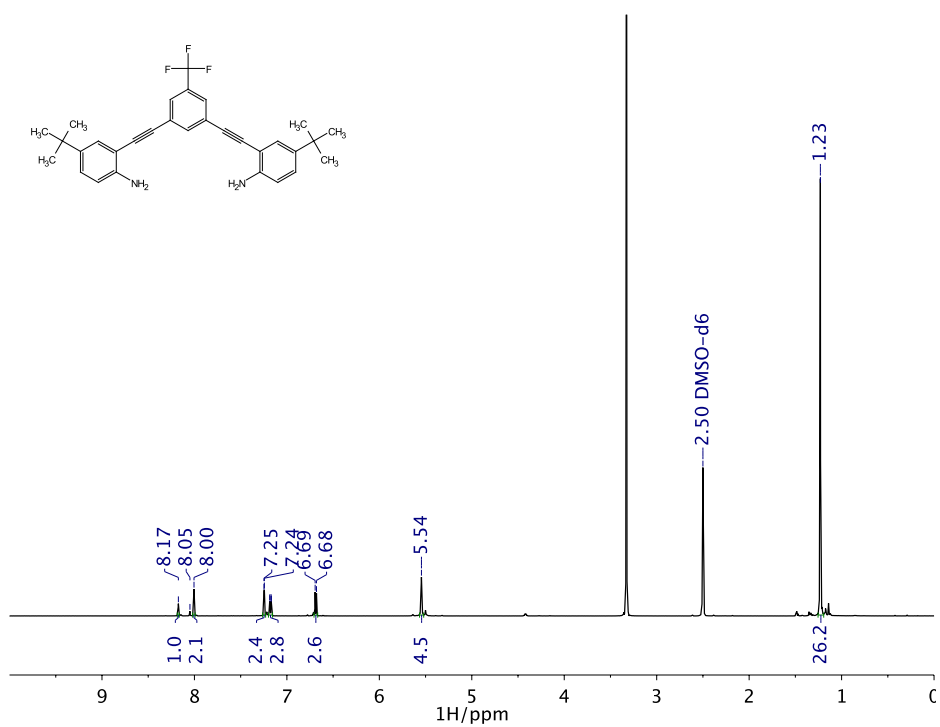
Figure 1. ^{1}H NMR of **6** in DMSO-d_6.
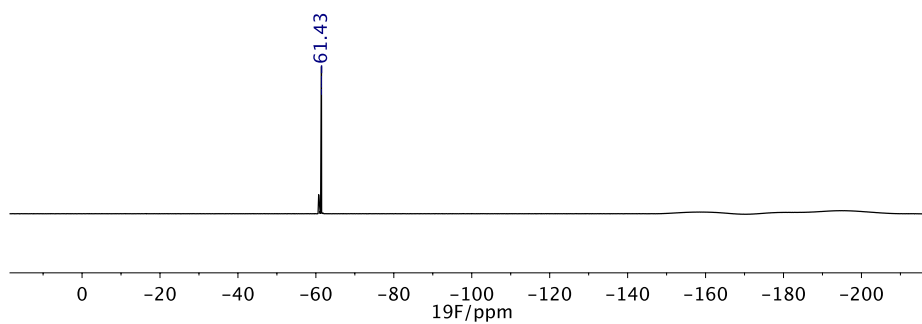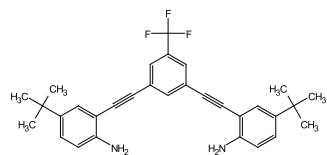
Figure 2. ^{19}F NMR of **6** in DMSO-d_6.
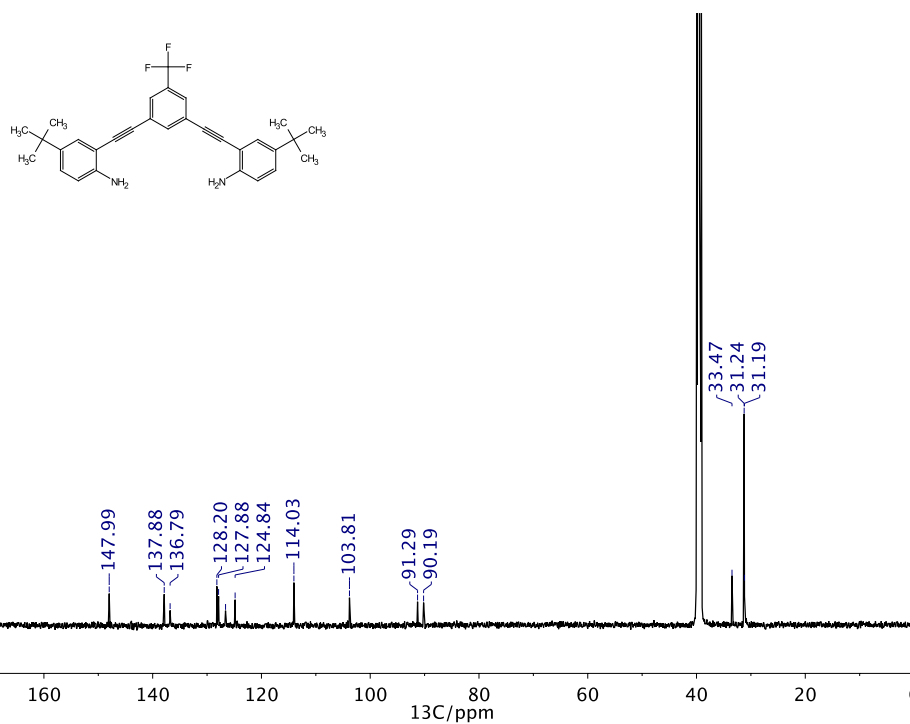
Figure 3. ^{13}C NMR of **6** in DMSO-d_6.
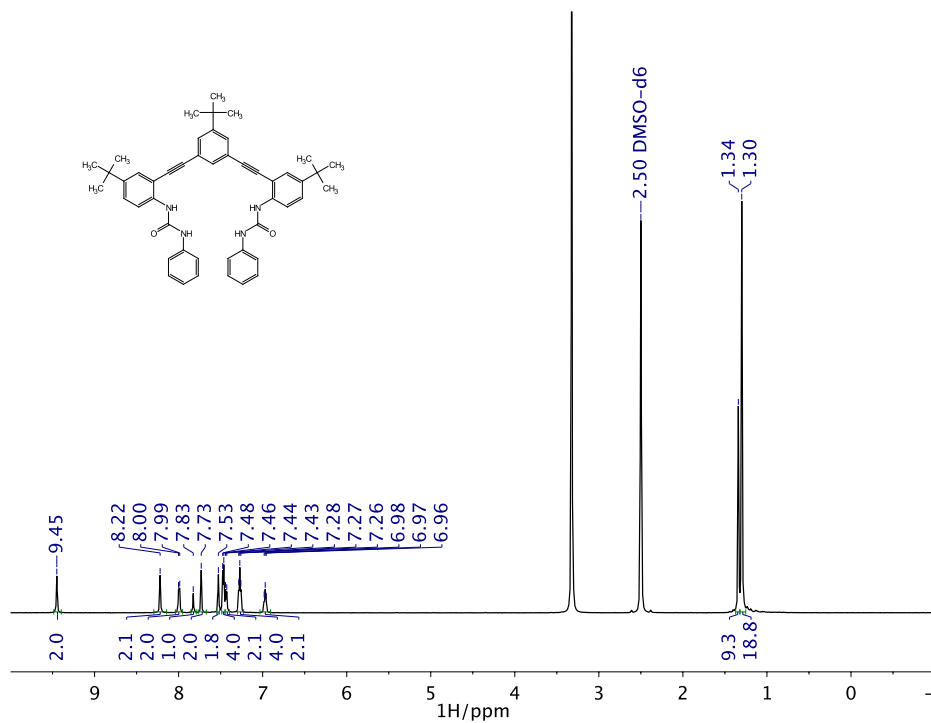
Figure 4. ^{1}H NMR of **2b** in DMSO-d_6.
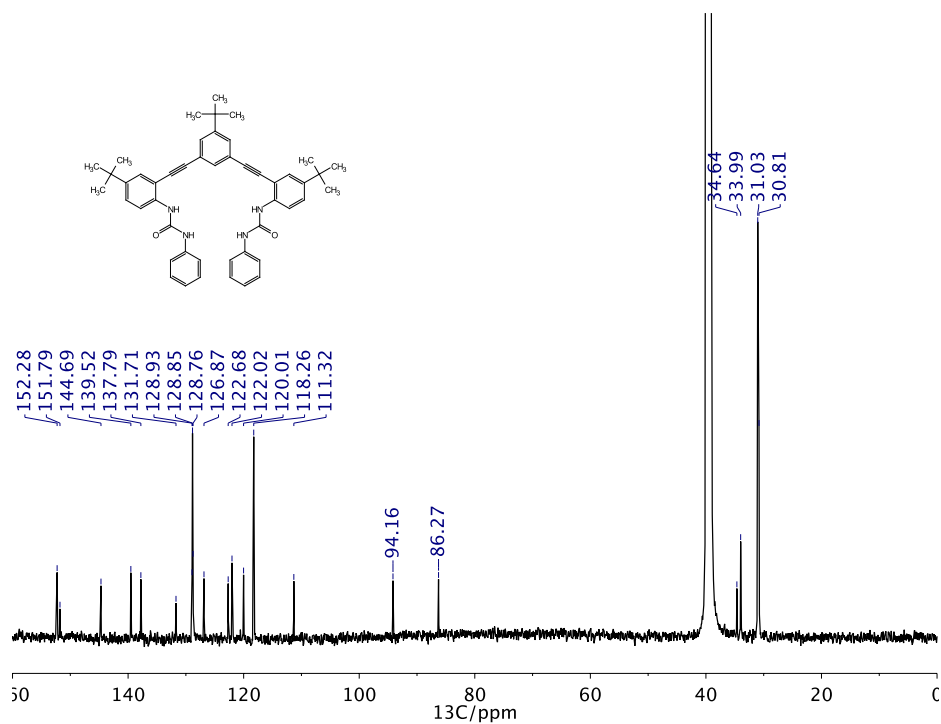
Figure 5. ^{13}C NMR of **2b** in DMSO-d_6.
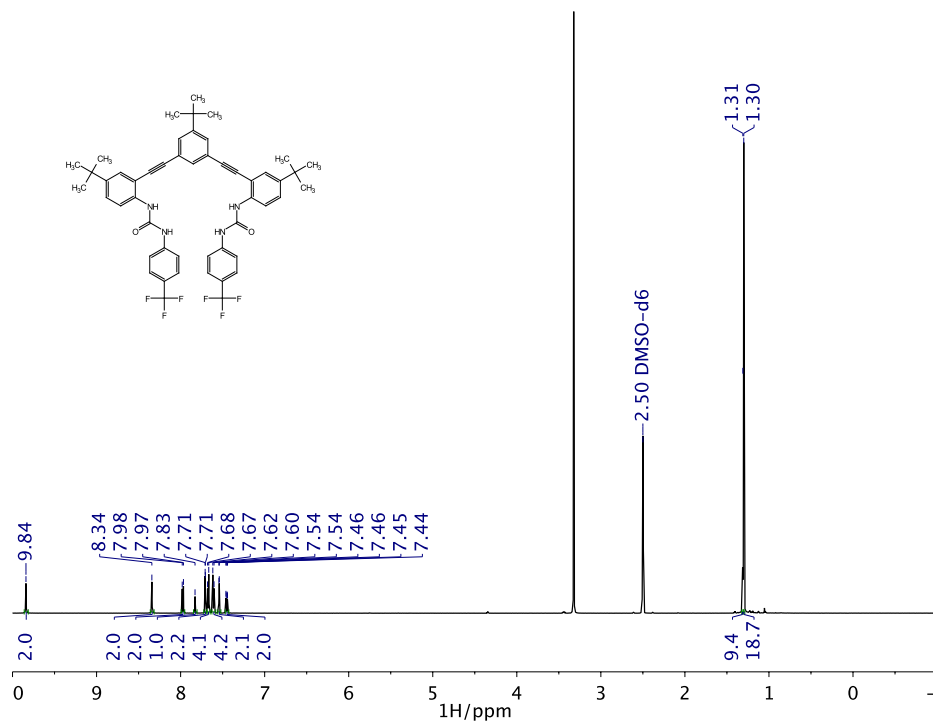
Figure 6. ^{1}H NMR of **2c** in DMSO-d_6.
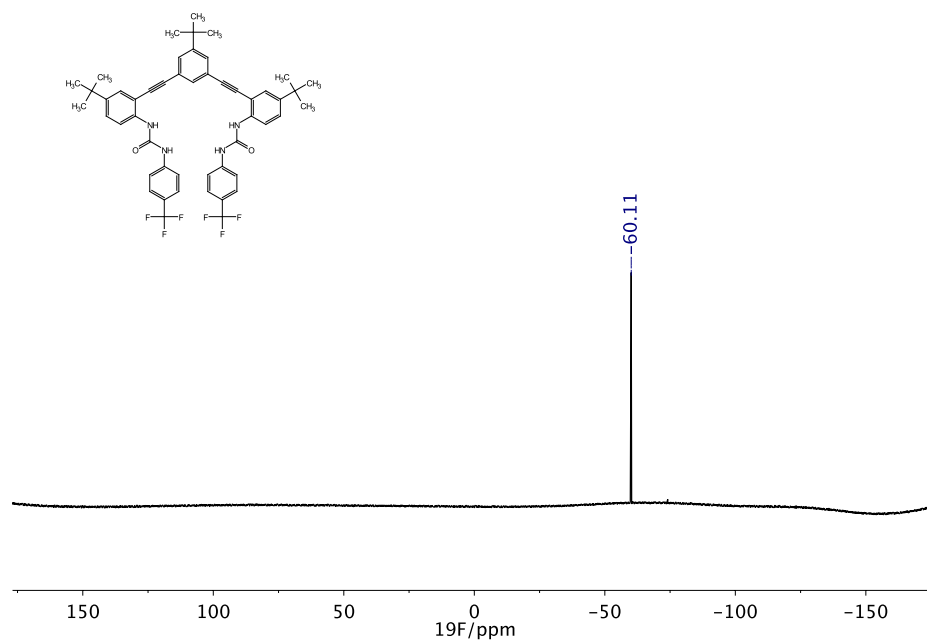
Figure 7. ^{19}F NMR of **2c** in DMSO-d_6.
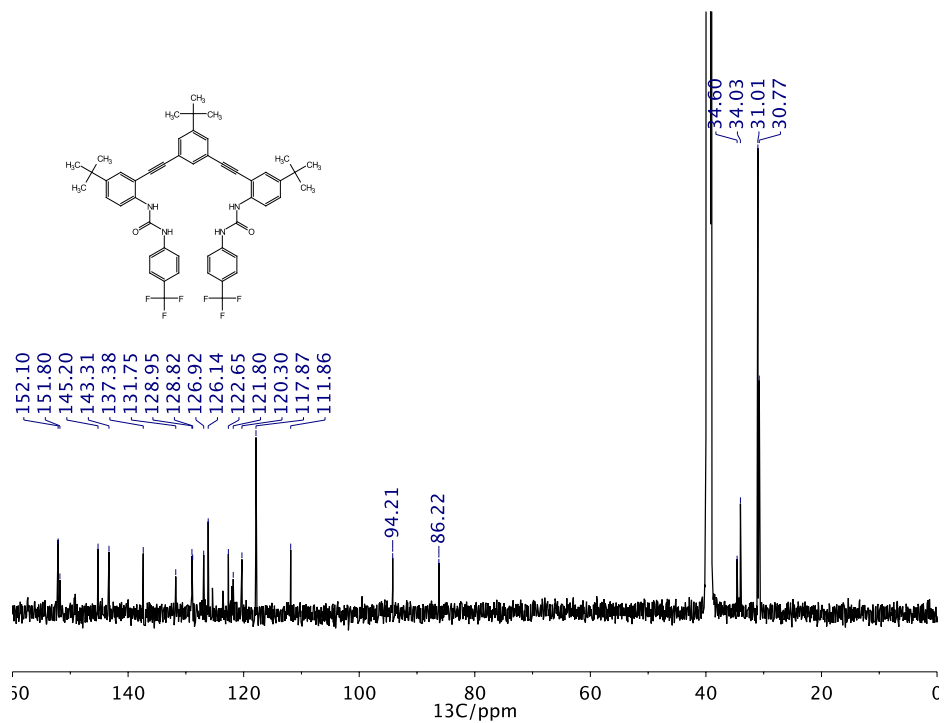
Figure 8. ^{13}C NMR of **2c** in DMSO-d_6.
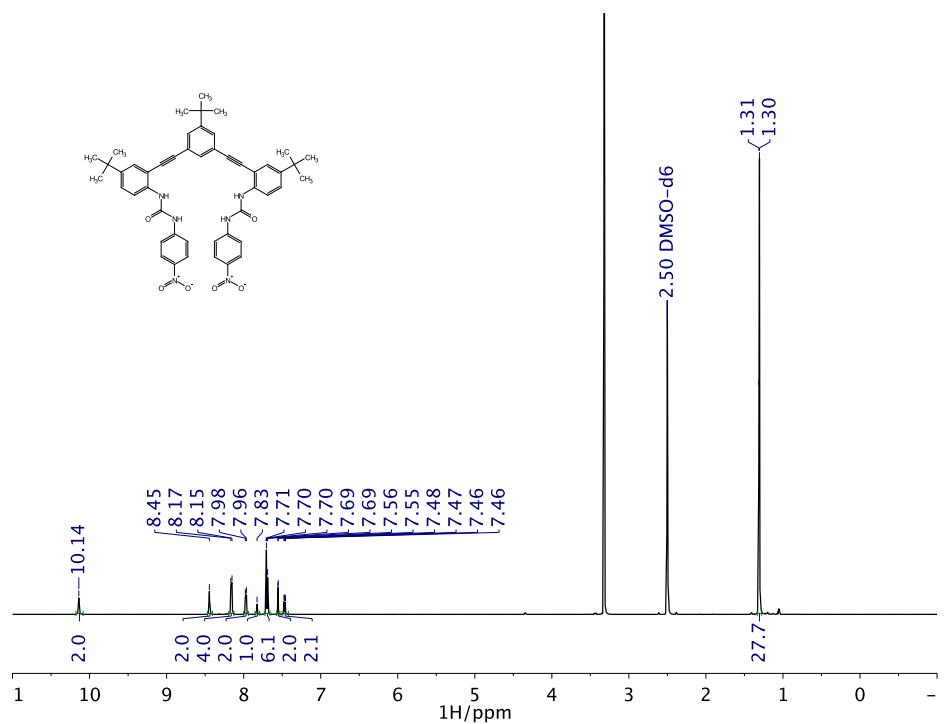
Figure 9. ^{1}H NMR of **2d** in DMSO-d_6.
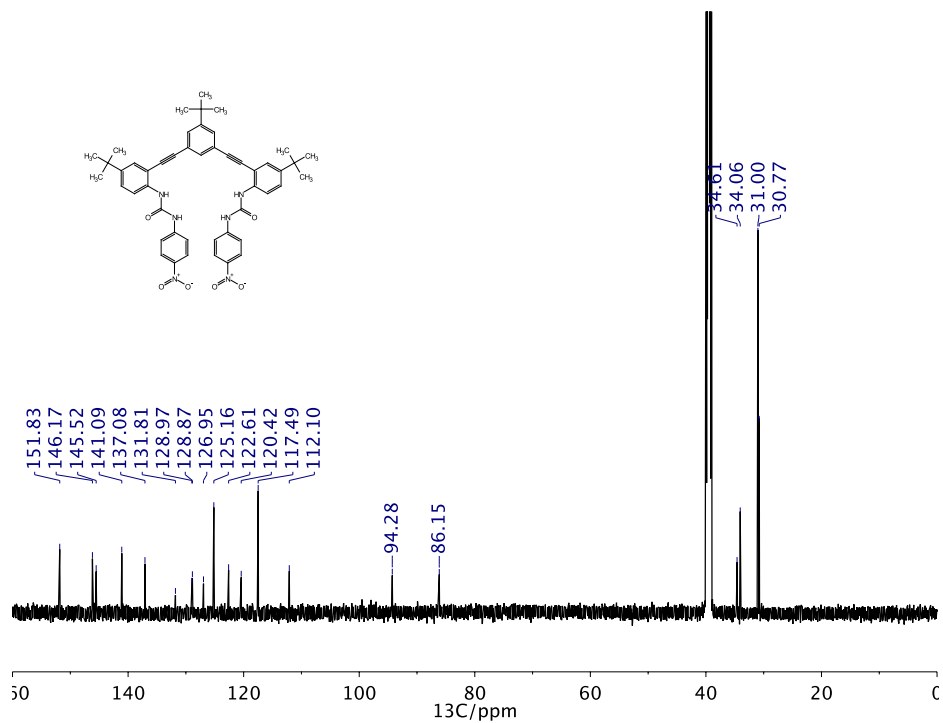
Figure 10. ¹³C NMR of **2d** in DMSO-*d₆*.
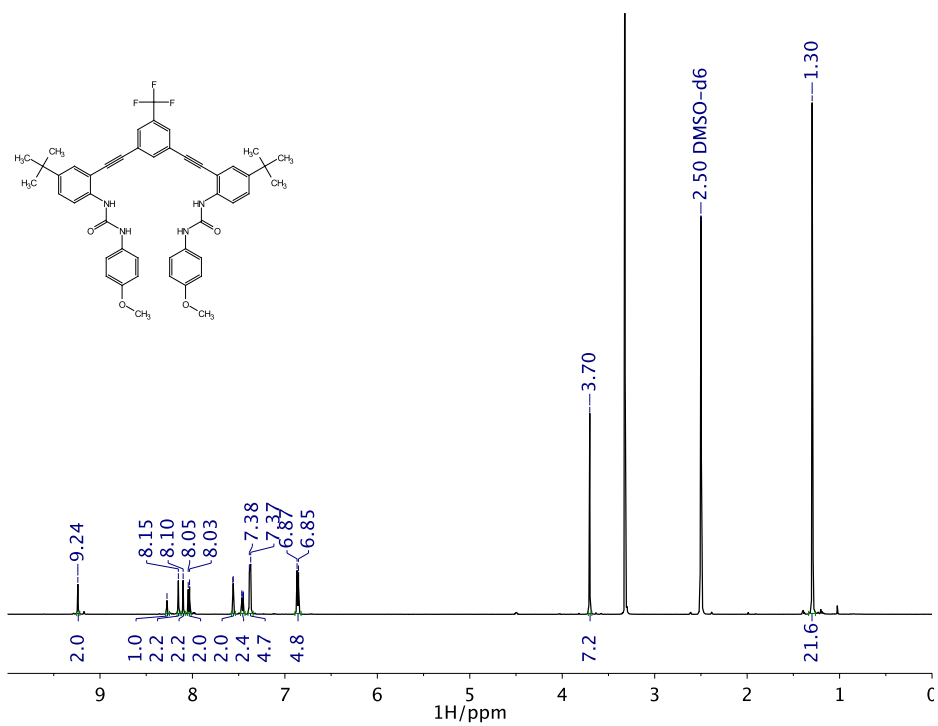
Figure 11. ¹H NMR of **3a** in DMSO-*d₆*.

230
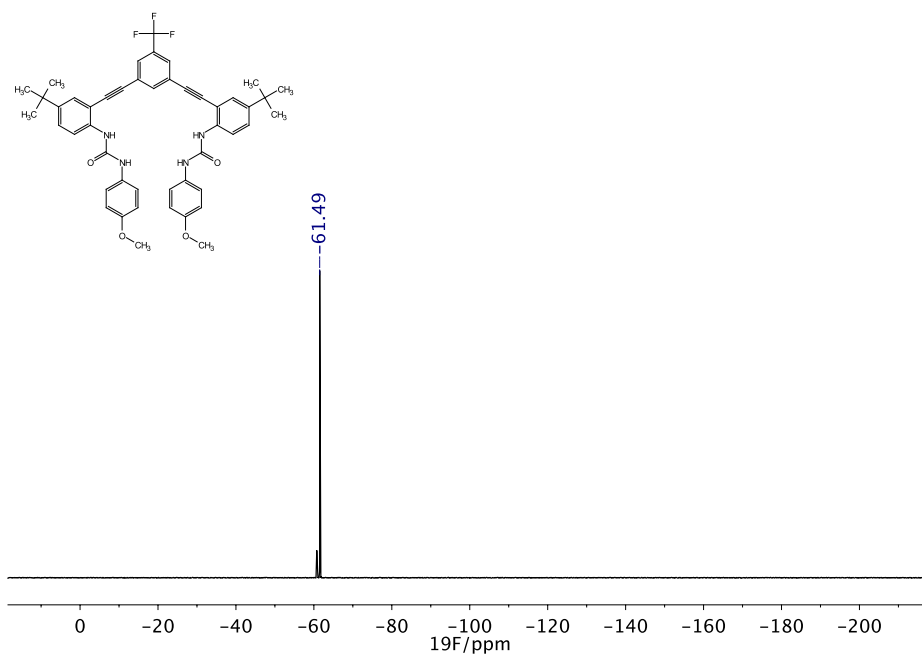
Figure 12. ^{19}F NMR of **3a** in DMSO-d_6.
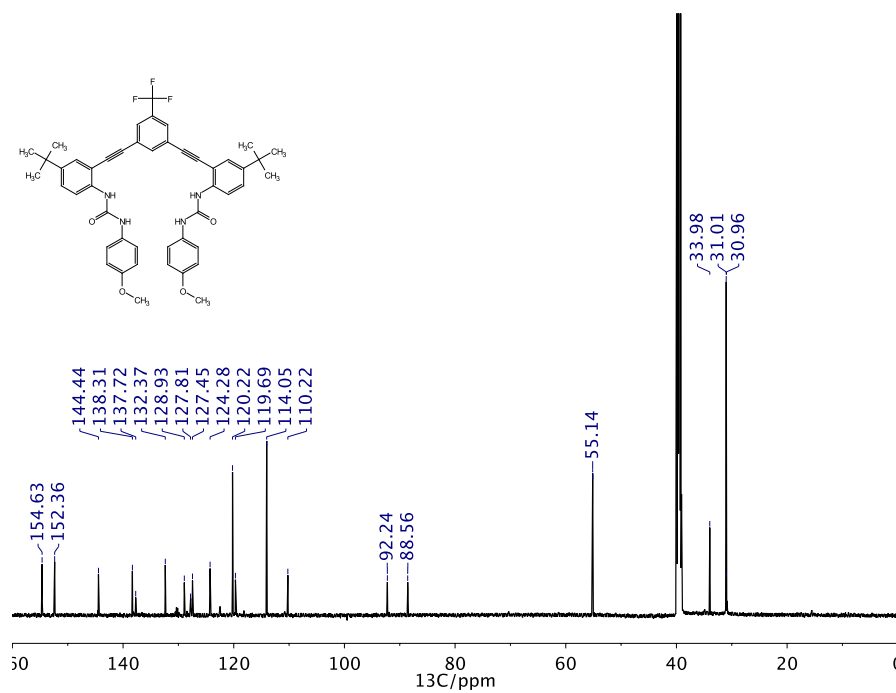
Figure 13. ^{13}C NMR of **3a** in DMSO-d_6.

231
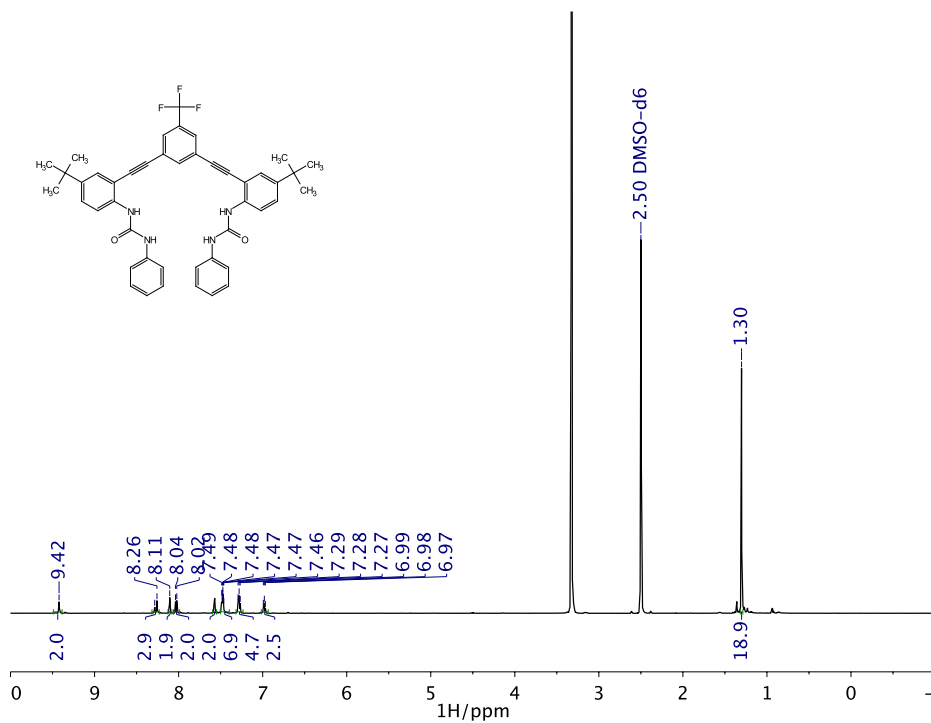
Figure 14. ^{1}H NMR of **3b** in DMSO-d_6.
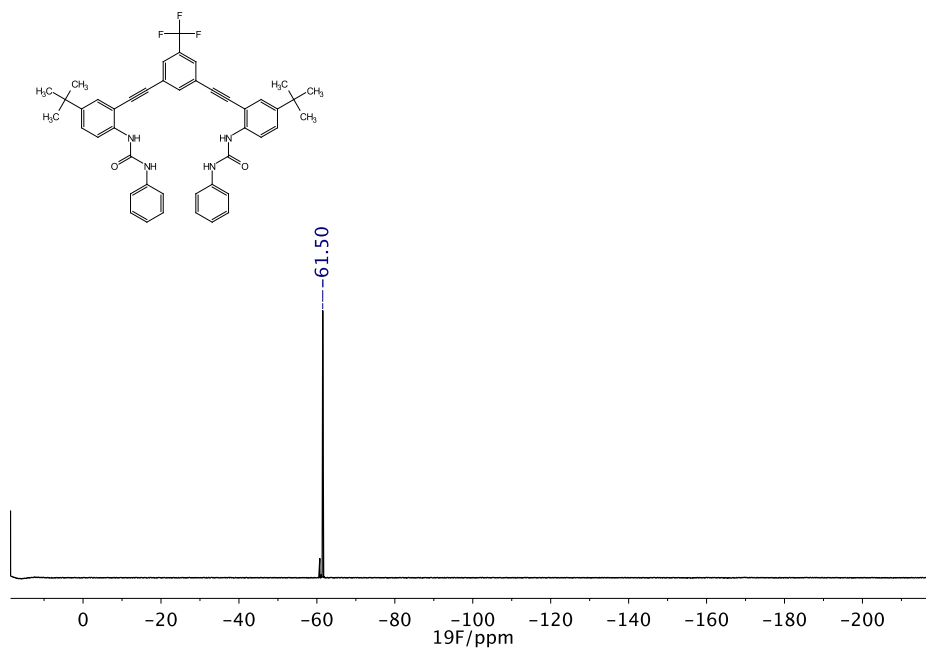
Figure 15. ^{19}F NMR of **3b** in DMSO-d_6.

Figure 16. ^{13}C NMR of **3b** in DMSO-d_6.

Figure 17. ^{1}H NMR of **3c** in DMSO-d_6.

233
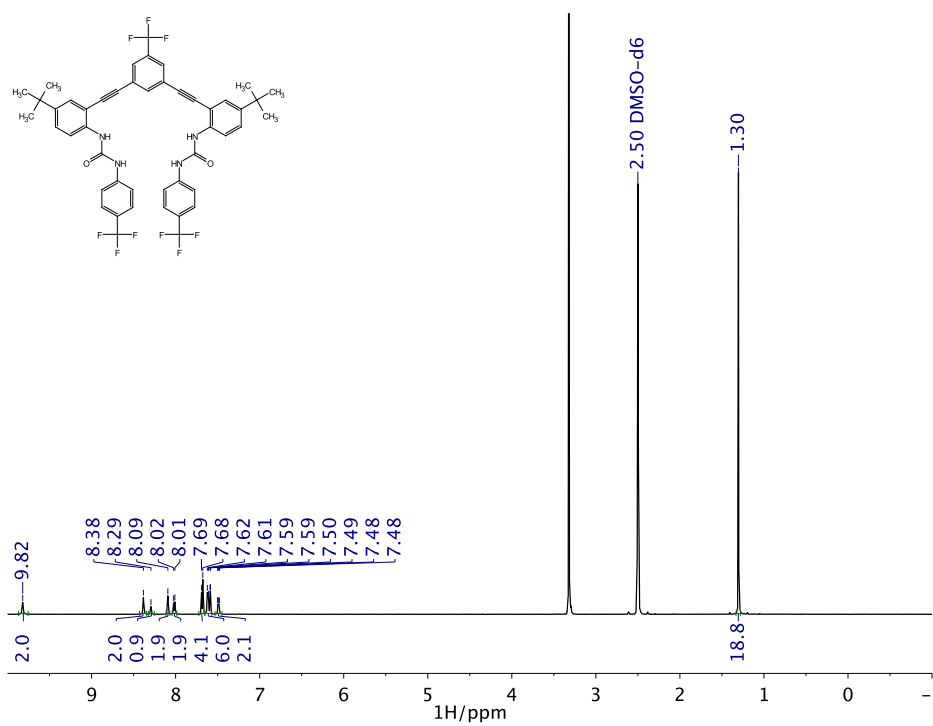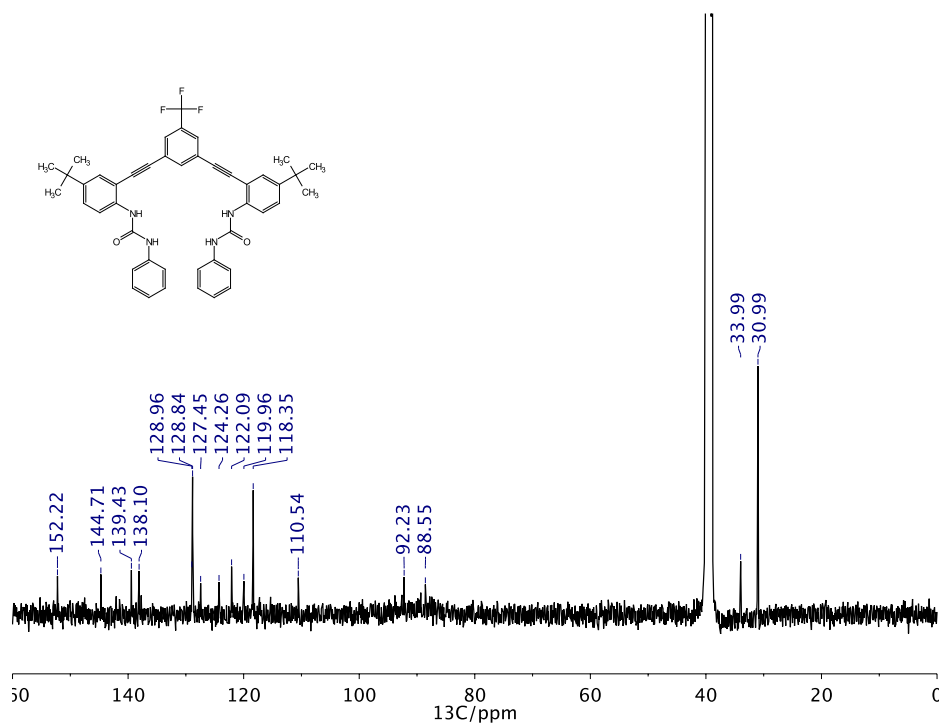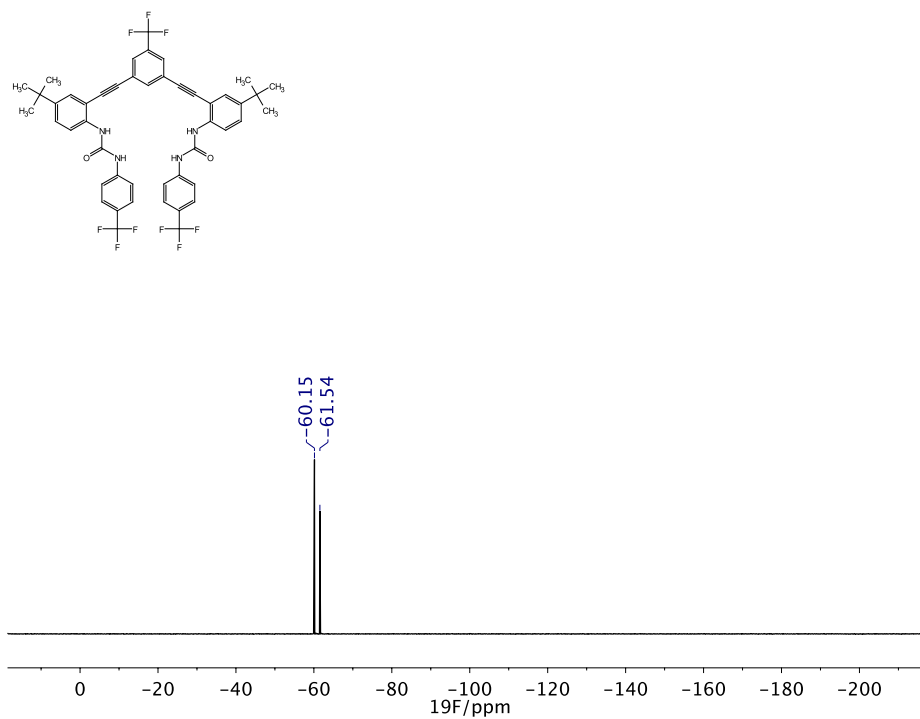
Figure 18. ^{19}F NMR of **3c** in DMSO-d_6.
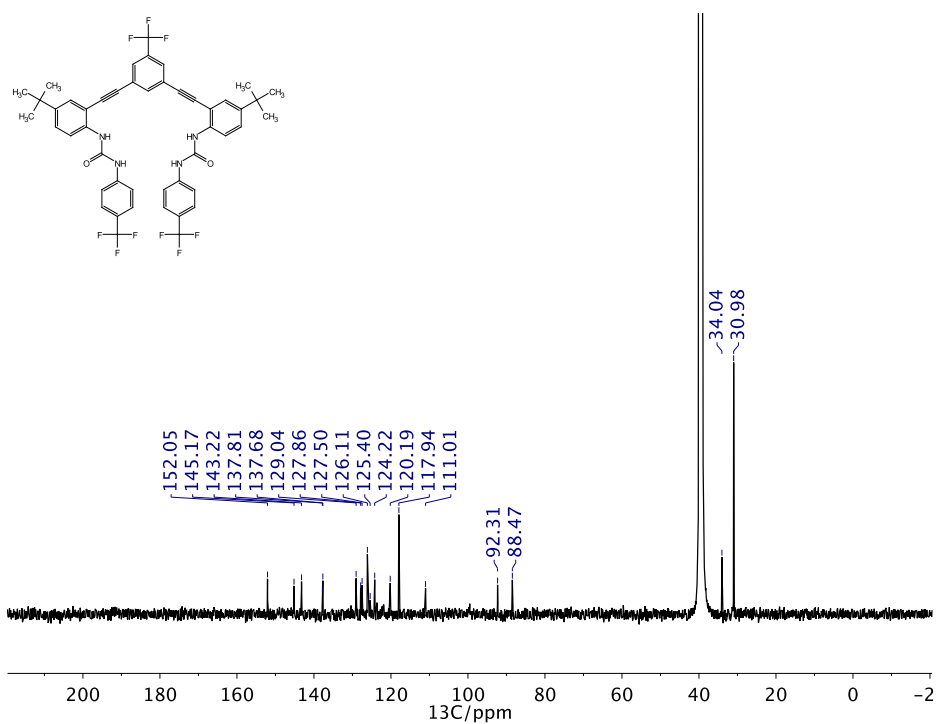
Figure 19. ^{13}C NMR of **3c** in DMSO-d_6.

234
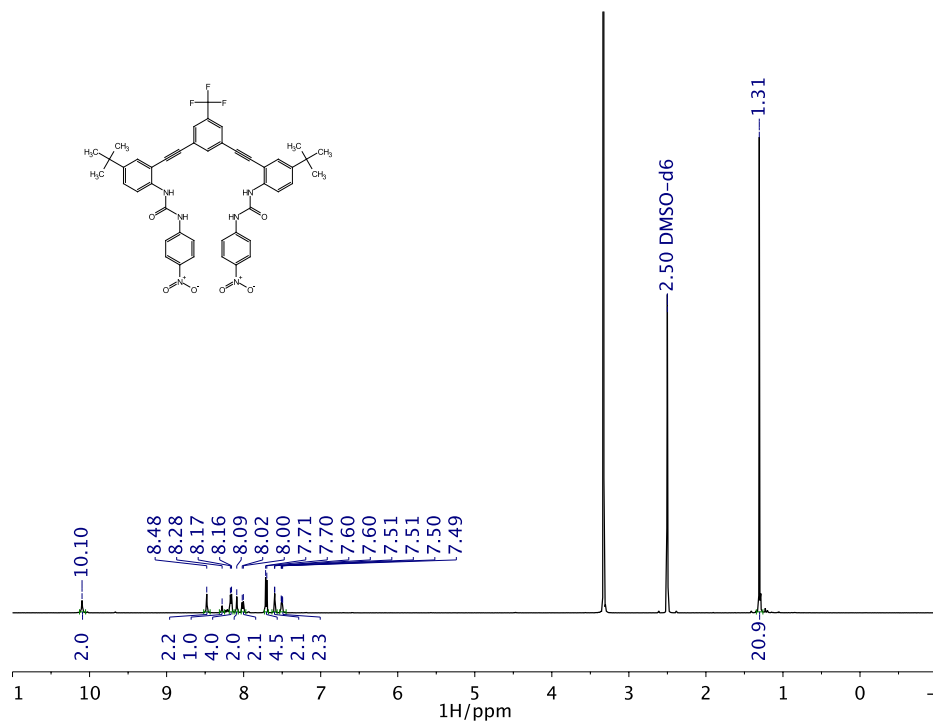
Figure 20. ^{1}H NMR of **3d** in DMSO-d_6.
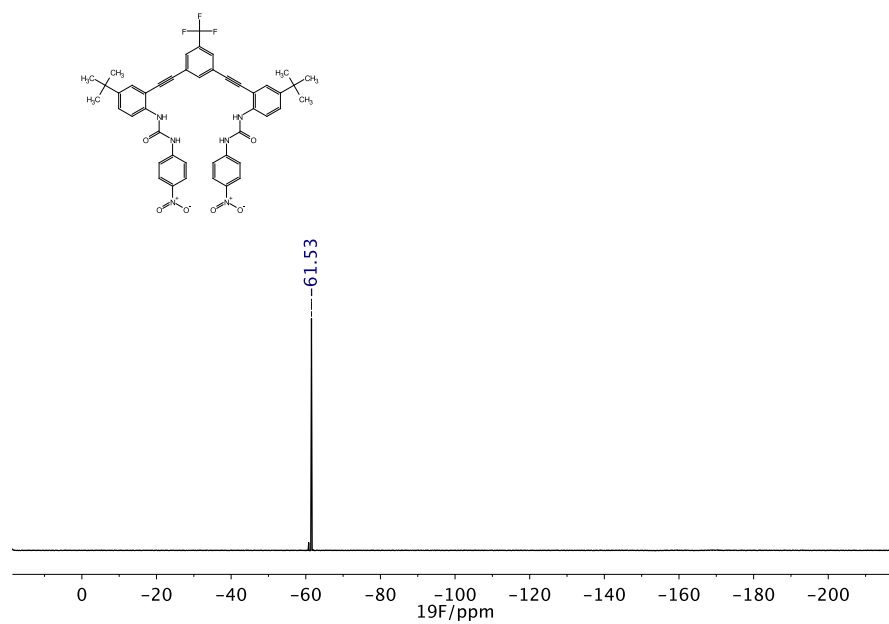
Figure 21. ^{19}F NMR of **3d** in DMSO-d_6.
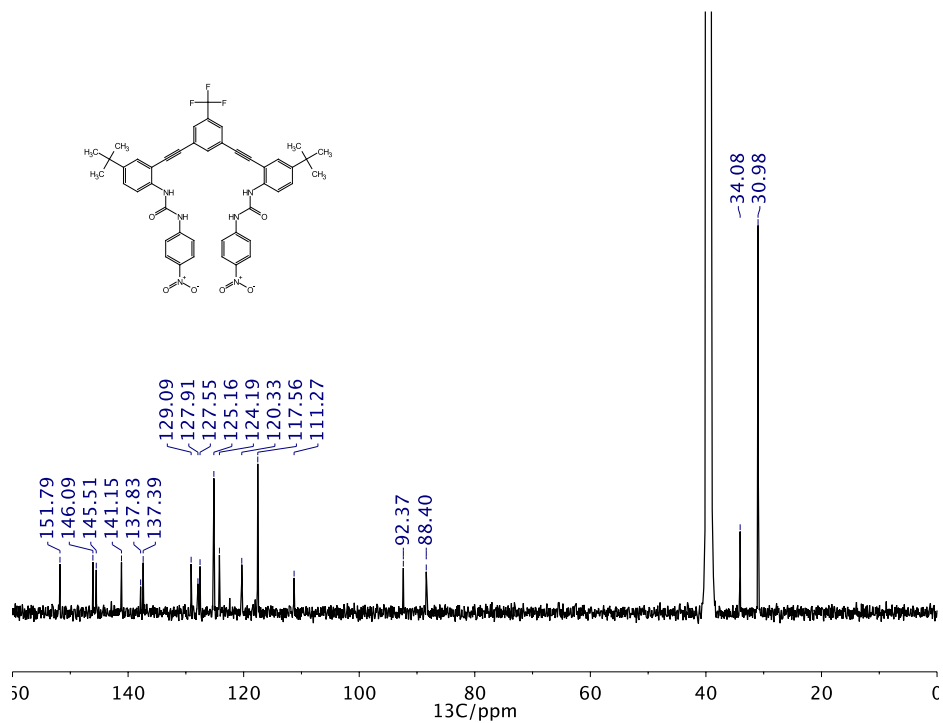
Figure 22. ^{13}C NMR of **3d** in DMSO-d_6.

Atomic Coordinates

2c

R = *t*Bu, R' = CF$_3$, E = -2667.713805 hartree

O	-7.67984	0.80479	0.24798
O	5.71604	-3.17327	-0.83811
N	-5.68478	1.96025	0.11634
H	-4.67683	1.85846	0.08684
N	-5.67167	-0.30243	0.51981
H	-4.67649	-0.15972	0.62629
N	3.78982	-1.90694	-0.96721
H	3.39200	-0.99165	-0.79120
N	5.74536	-0.94687	-0.23010
H	5.17741	-0.11284	-0.17012
C	-0.82529	1.82691	-0.70813
H	-1.58267	1.08974	-0.95166
C	-1.19753	3.14295	-0.39051
C	-0.19896	4.08782	-0.09181
H	-0.51219	5.09749	0.15109
C	1.16248	3.75282	-0.10075
C	1.50647	2.43542	-0.41629

236

H	2.54581	2.13121	-0.43833
C	0.52873	1.46476	-0.72077
C	-2.57315	3.52121	-0.36375
C	-3.73616	3.88428	-0.33636
C	-5.10930	4.26058	-0.30105
C	-6.11475	3.28066	-0.08346
C	-7.45774	3.68044	-0.06137
H	-8.22586	2.93735	0.09808
C	-7.78697	5.01952	-0.24623
H	-8.83727	5.30179	-0.22355
C	-6.81429	6.00900	-0.45751
C	-5.48202	5.60604	-0.48071
H	-4.69523	6.33692	-0.64448
C	-6.45835	0.82373	0.29019
C	-6.09087	-1.62828	0.71822
C	-7.42829	-2.04809	0.62537
H	-8.20048	-1.32730	0.39987
C	-7.74120	-3.38921	0.82831
H	-8.77563	-3.70782	0.74976
C	-6.74928	-4.32799	1.12059
C	-5.41899	-3.90994	1.21146
H	-4.63698	-4.62909	1.43161
C	-5.09370	-2.57537	1.01159
H	-4.05407	-2.26131	1.08093
C	0.90605	0.12680	-1.03891
C	1.17551	-1.02890	-1.31786
C	1.52254	-2.37361	-1.63127
C	2.85508	-2.83356	-1.45381
C	3.16079	-4.16415	-1.77037
H	4.17273	-4.51797	-1.63578
C	2.16620	-5.01083	-2.24958
H	2.43201	-6.03836	-2.48771
C	0.84213	-4.58371	-2.43445
C	0.54423	-3.26101	-2.11930
H	-0.46678	-2.88570	-2.25014
C	5.13310	-2.10868	-0.69334
C	7.08547	-0.76304	0.14880
C	8.04666	-1.78777	0.14919
H	7.76525	-2.78456	-0.15698
C	9.35000	-1.50426	0.54669
H	10.08597	-2.30177	0.55118
C	9.72183	-0.21923	0.94816
C	8.76520	0.79919	0.94907
H	9.03754	1.80069	1.26534
C	7.46171	0.52953	0.55489
H	6.72350	1.32914	0.56390
C	-0.21694	-5.52902	-2.95111
H	-1.17033	-5.01462	-3.10720

H	0.07966	-5.97935	-3.90613
H	-0.39531	-6.35317	-2.24890
C	-7.20452	7.45497	-0.65509
H	-6.32450	8.09112	-0.79245
H	-7.84621	7.58009	-1.53616
H	-7.76326	7.84065	0.20665
C	2.21313	4.82916	0.23349
C	2.10336	5.98575	-0.78843
H	2.83841	6.76619	-0.55839
H	2.29303	5.62956	-1.80728
H	1.11148	6.44903	-0.77539
C	1.95432	5.37446	1.65814
H	2.69623	6.14136	1.91048
H	0.96277	5.82981	1.74803
H	2.02416	4.57523	2.40471
C	3.65191	4.28029	0.18383
H	4.35843	5.08076	0.42857
H	3.80573	3.47326	0.91015
H	3.91260	3.90574	-0.81286
C	11.14576	0.07926	1.31619
F	11.23405	1.09377	2.20803
F	11.76297	-0.99414	1.85976
F	11.88298	0.44636	0.23920
C	-7.10968	-5.75814	1.39740
F	-6.11354	-6.60522	1.04601
F	-7.35425	-5.97516	2.71300
F	-8.22147	-6.13952	0.72891

2d

R = *t*Bu, R' = NO$_2$, E = -2402.541755 hartree

O	-7.59555	-0.29957	-0.33570
O	6.01814	3.05660	0.60954
N	-5.64706	-1.52870	-0.18966
H	-4.63608	-1.46504	-0.15128
N	-5.54511	0.73192	-0.59870
H	-4.55501	0.55212	-0.69817
N	4.00972	1.92429	0.72410
H	3.56241	1.02434	0.59237
N	5.90676	0.82290	0.03277
H	5.27621	0.03819	-0.06135
C	-0.77487	-1.58427	0.63554
H	-1.49829	-0.79531	0.81029
C	-1.20723	-2.89660	0.38600
C	-0.25221	-3.90783	0.17446
H	-0.61139	-4.91317	-0.01768

238

C	1.12432	-3.64319	0.20588
C	1.52847	-2.32862	0.45457
H	2.58154	-2.07811	0.49415
C	0.59549	-1.29228	0.66935
C	-2.59905	-3.20750	0.34209
C	-3.77623	-3.52039	0.30316
C	-5.16215	-3.84471	0.25634
C	-6.12876	-2.83174	0.01866
C	-7.48513	-3.18050	-0.01407
H	-8.22372	-2.41141	-0.18881
C	-7.86616	-4.50448	0.18093
H	-8.92584	-4.74784	0.15002
C	-6.93288	-5.52664	0.41254
C	-5.58662	-5.17337	0.44558
H	-4.82949	-5.93134	0.62470
C	-6.37644	-0.36807	-0.36940
C	-5.91289	2.06847	-0.78679
C	-7.23918	2.53422	-0.70484
H	-8.03815	1.83739	-0.49916
C	-7.50596	3.88448	-0.89478
H	-8.51986	4.26094	-0.83516
C	-6.46464	4.77126	-1.16501
C	-5.14477	4.32831	-1.25195
H	-4.35469	5.03746	-1.46530
C	-4.87578	2.98252	-1.06297
H	-3.84906	2.62935	-1.13018
C	1.03523	0.04132	0.91868
C	1.36119	1.19540	1.13746
C	1.77567	2.53549	1.38181
C	3.12740	2.91985	1.17534
C	3.50191	4.24668	1.42386
H	4.52937	4.54314	1.26909
C	2.55427	5.16458	1.86637
H	2.87285	6.18783	2.05205
C	1.21219	4.81344	2.07897
C	0.84645	3.49342	1.83023
H	-0.18085	3.17579	1.98465
C	5.36452	2.03400	0.47130
C	7.23412	0.54210	-0.30823
C	8.27292	1.49129	-0.25851
H	8.05761	2.50148	0.05665
C	9.56247	1.11736	-0.61576
H	10.37402	1.83402	-0.58344
C	9.82376	-0.19075	-1.02117
C	8.80759	-1.14475	-1.07729
H	9.03759	-2.15380	-1.39591
C	7.52100	-0.77484	-0.72123
H	6.72319	-1.51342	-0.76151

C	0.20588	5.83368	2.55657
H	-0.77464	5.37852	2.72742
H	0.52522	6.30093	3.49594
H	0.07495	6.64043	1.82455
C	-7.37830	-6.95473	0.62250
H	-6.52294	-7.62477	0.75372
H	-8.01426	-7.04915	1.51152
H	-7.96190	-7.32164	-0.23069
C	2.12580	-4.78990	-0.03192
N	11.18441	-0.57354	-1.39436
O	11.37560	-1.73884	-1.75026
O	12.06238	0.28878	-1.33201
N	-6.75666	6.19017	-1.36080
O	-5.80876	6.94473	-1.59183
O	-7.93210	6.55200	-1.28314
C	1.92733	-5.87614	1.05191
H	2.62923	-6.70317	0.89218
H	2.10396	-5.46900	2.05385
H	0.91455	-6.29149	1.03327
C	1.87854	-5.40496	-1.42993
H	2.58172	-6.22625	-1.61161
H	0.86535	-5.80823	-1.52626
H	2.01750	-4.65769	-2.21945
C	3.58942	-4.31266	0.02992
H	4.25921	-5.16103	-0.14700
H	3.80493	-3.55916	-0.73727
H	3.84260	-3.89344	1.01056

REFERENCES CITED

Chapter I

1. J. Szejtli, *Chem. Rev.* **1998**, *98*, 1743 – 1754.

2. J. F. Stoddart, *Annu. Rep. Sect. B* **1983**, *80*, 353 – 378.

3. S. Leininger, B. Olenyuk, P. J. Stang, *Chem. Rev.* **2000**, *100*, 853 – 908.

4. C. N. Carroll, J. J. Naleway, M. M. Haley, D. W. Johnson, *Chem. Soc. Rev.* **2010**, *39*, 3875 – 3888.

5. D. Habrant, V. Rauhala, A. M. P. Koskinen, *Chem. Soc. Rev.* **2010**, *39*, 2007 – 2017.

6. S. D. Zanatta, *Aust. J. Chem.* **2007**, *60*, 963 – 964.

7. R. Chinchilla, C. Nájera, *Chem. Soc. Rev.* **2011**, *40*, 5084 – 5121.

8. R. Chinchilla, C. Nájera, *Chem. Rev.* **2007**, *107*, 874 – 922.

9. J. A. Marsden, M. M. Haley in *Metal-Catalyzed Cross-Coupling Reactions, 2nd ed.* (Eds.: A. de Meijere, F. Diederich), Wiley-VCH, Weinheim, **2004**, pp. 317 – 394.

10. S. W. Thomas, G. D. Joly, T. M. Swager, *Chem. Rev.* **2007**, *107*, 1339 –1388.

11. N. M. Sangeetha, U. Maitra, *Chem. Soc. Rev.* **2005**, *34*, 821 – 836.

12. S. E. Kudaibergenov, N. Nuraje, V. V. Khutoryanskiy, *Soft Matter* **2012**, *8*, 9302 – 9321.

13. J. Hu, G. Zhang, S. Liu, *Chem. Soc. Rev.* **2012**, *41*, 5933 – 5949.

14. C. Wolf, K. W. Bentley, *Chem. Soc. Rev.* **2013**, *42*, 5408 – 5424.

15. A. P. de Silva, H. Q. N. Gunaratne, T. Gunnlaugsson, A. J. M. Huxley, C. P. McCoy, J. T. Rademacher, T. E. Rice, *Chem. Rev.* **1997**, *97*, 1515 – 1566.

16. Y. Yang, Q. Zhao, W. Feng, F. Li, *Chem. Rev.* **2013**, *113*, 192 – 270.

17. T. Terai, T. Nagano, *Pflüg. Arch. Eur. J. Physiol.* **2013**, *465*, 347 – 359.

18. Z. R. Grabowski, K. Rotkiewicz, W. Rettig, *Chem. Rev.* **2003**, *103*, 3899 –4032.

19. Y. Hong, J. W. Y. Lam, B. Z. Tang, *Chem. Commun.* **2009**, 4332 – 4353.

20. J. Wu, W. Liu, J. Ge, H. Zhang, P. Wang, *Chem. Soc. Rev.* **2011**, *40*, 3483 –3495.

21. D. Ding, K. Li, B. Liu, B. Z. Tang, *Acc. Chem. Res.* **2013**, *46*, 2441 – 2453.

22. S. Menning, M. Krmer, A. Duckworth, F. Rominger, A. Beeby, A. Dreuw, U. H. F. Bunz, *J. Org. Chem.* **2014**, *79*, 6571 – 6578.

23. E. V. Anslyn, *J. Org. Chem.* **2007**, *72*, 687 – 699.

24. K. Rurack, U. Resch-Genger, *Chem. Soc. Rev.* **2002**, *31*, 116 – 127.

25. J. M. Engle, C. N. Carroll, D. W. Johnson, M. M. Haley, *Chem. Sci.* **2012**, *3*, 1105 – 1110.

26. C. N. Carroll, O. B. Berryman, C. A. Johnson, L. N. Zakharov, M. M. Haley, D.W. Johnson, *Chem. Commun.* **2009**, 2520 – 2522.

27. J. M. Engle, P. S. Lakshminarayanan, C. N. Carroll, L. N. Zakharov, M. M. Haley, D. W. Johnson, *Cryst. Growth Des.* **2011**, *11*, 5144 – 5152.

28. C. A. Johnson, O. B. Berryman, A. C. Sather, L. N. Zakharov, M. M. Haley, D.W. Johnson, *Cryst. Growth Des.* **2009**, 9, 4247 – 4249.

29. J. V. Gavette, N. S. Mills, L. N. Zakharov, C. A. Johnson, II, D. W. John-son, M. M. Haley, *Angew. Chem. Int. Ed.* **2013**, 52, 10270 – 10274; *Angew. Chem.* **2013**, *125*, 10460 – 10464.

30. Z. Liu, W. He, Z. Guo, *Chem. Soc. Rev.* **2013**, *42*, 1568 – 1600.

31. K. P. Carter, A. M. Young, A. E. Palmer, *Chem. Rev.* **2014**, *114*, 4564 –4601.

32. G. Aragay, J. Pons, A. MerkoÅi, *Chem. Rev.* **2011**, *111*, 3433 – 3458.

33. N. Kaur, S. Kumar, *Tetrahedron* **2011**, 67, 9233 – 9264.

34. K. Kaur, R. Saini, A. Kumar, V. Luxami, N. Kaur, P. Singh, S. Kumar, *Coord. Chem. Rev.* **2012**, *256*, 1992 – 2028.

35. B. Valeur, I. Leray, *Coord. Chem. Rev.* **2000**, *205*, 3 – 40.

36. K. Deibler, P. Basu, *Eur. J. Inorg. Chem.* **2013**, 1086 – 1096.

37. M. Formica, V. Fusi, L. Giorgi, M. Micheloni, *Coord. Chem. Rev.* **2012**, *256*, 170 – 192.

38. A. de Los Rios, P. Mal, A. J. Meixner, D. Khoptyar, M. Schmittel, *Bull. Chem. Soc. Jpn.* **2011**, *84*, 620 – 622.

39. Y.-P. Zhao, L.-Z. Wu, G. Si, Y. Liu, H. Xue, L.-P. Zhang, C.-H. Tung, *J. Org. Chem.* **2007**, *72*, 3632 – 3639.

40. M. Shao, P. Dongare, L. N. Dawe, D. W. Thompson, Y. Zhao, *Org. Lett.* **2010**, *12*, 3050 – 3053.

41. A. P. de Silva, B. McCaughan, B. O. F. McKinney, M. Querol, *Dalton Trans.* **2003**, 1902 – 1913.

42. L. Li, N. She, Z. Fei, P. So, Y. Wang, L. Cao, A. Wu, Z. Yao, *J. Fluoresc.* **2011**, *21*, 1103 – 1110.

43. A. J. Zucchero, P. L. McGrier, U. H. F. Bunz, *Acc. Chem. Res.* **2010**, *43*, 397 – 408.

44. J. N. Wilson, U. H. F. Bunz, *J. Am. Chem. Soc.* **2005**, *127*, 4124 – 4125.

45. P. L. McGrier, K. M. Solntsev, A. J. Zucchero, O. R. Miranda, V. M. Rotello, L.M. Tolbert, U. H. F. Bunz, *Chem. Eur. J.* **2011**, *17*, 3112 – 3119.

46. A. J. Zucchero, J. N. Wilson, U. H. F. Bunz, *J. Am. Chem. Soc.* **2006**, *128*, 11872 – 11881.

47. A. Mangalum, R. J. G. Jr, J. M. Hanley, A. M. Parker, R. C. Smith, *Org. Biomol. Chem.* **2010**, *8*, 5620 – 5627.

48. E. L. Spitler, L. D. Shirtcliff, M. M. Haley, *J. Org. Chem.* **2007**, *72*, 86 – 96.

49. E. L. Spitler, C. A. Johnson, M. M. Haley, *Chem. Rev.* **2006**, *106*, 5344 –5386.

50. J. A. Marsden, J. J. Miller, L. D. Shirtcliff, M. M. Haley, *J. Am. Chem. Soc.* **2005**, *127*, 2464 – 2476.

51. P. N. W. Baxter, J.-P. Gisselbrecht, L. Karmazin-Brelot, A. Varnek, L. Allou-che, *Chem. Eur. J.* **2013**, *19*, 12336 – 12349.

52. A. Al Ouahabi, P. Baxter, C. Mathis, M. Bernard, B. Vileno, J.-P. Gissel-brecht, P. Turek, J.-M. Mouesca, S. Choua, *ChemPhysChem* **2013**, *14*, 958 – 969.

53. G. W. Gokel, W. M. Leevy, M. E. Weber, *Chem. Rev.* **2004**, *104*, 2723 –2750.

54. J. L. Sessler, P. A. Gale, W.-S. Cho, *Anion Receptor Chemistry*, Royal Society Of Chemistry, Cambridge, **2006**.

55. V. Amendola, M. Bonizzoni, D. Esteban-Gomez, L. Fabbrizzi, M. Licchelli, F. Sancenn, A. Taglietti, Coord. *Chem. Rev.* **2006**, *250*, 1451 – 1470.

56. O. B. Berryman, V. S. Bryantsev, D. P. Stay, D. W. Johnson, B. P. Hay, *J. Am. Chem. Soc.* **2007**, 129, 48 – 58.

57. L. E. Santos-Figueroa, M. E. Moragues, E. Climent, A. Agostini, R. Martnez, M. Çez, F. Sancenn, *Chem. Soc. Rev.* **2013**, *42*, 3489 – 3613.

58. P. A. Gale, N. Busschaert, C. J. E. Haynes, L. E. Karagiannidis, I. L. Kirby, *Chem. Soc. Rev.* **2014**, *43*, 205 – 241.

59. N. H. Evans, P. D. Beer, *Angew. Chem. Int. Ed.* **2014**, *53*, 11716 – 111754; *Angew. Chem.* **2014**, *126*, 11908 – 11948.

60. W. N. George, M. Giles, I. McCulloch, J. H. G. Steinke, J. C. deMello, *ChemPhysChem* **2011**, *12*, 765 – 768.

61. M. Cametti, K. Rissanen, Chem. Soc. Rev. 2013, 42, 2016 – 2038.

62. H. Sun, X. Dong, S. Liu, Q. Zhao, X. Mou, H. Y. Yang, W. Huang, *J. Phys. Chem. C* **2011**, *115*, 19947 – 19955.

63. R. C. Lirag, H. T. M. Le, O. Š. Miljanić, *Chem. Commun.* **2013**, *49*, 4304 –4306.

64. J. Lim, D. Nam, O. Š. Miljanić, *Chem. Sci.* **2012**, *3*, 559 – 563.

65. J. Lim, O. Š. Miljanić, *Chem. Commun.* **2012**, *48*, 10301 – 10303.

66. A. N. Swinburne, M. J. Paterson, A. Beeby, J. W. Steed, *Chem. Eur. J.* **2010**, *16*, 2714 – 2718.

67. I. M. Jones, A. D. Hamilton, *Angew. Chem. Int. Ed.* **2011**, *50*, 4597 – 4600; *Angew. Chem.* **2011**, *123*, 4693 – 4696.

68. A. B. Wolk, E. Garand, I. M. Jones, A. D. Hamilton, M. A. Johnson, *J. Phys. Chem. A* **2013**, *117*, 5962 – 5969.

69. D. M. Jessen, A. N. Wercholuk, B. Xiong, A. L. Sargent, W. E. Allen, *J. Org. Chem.* **2012**, *77*, 6615 – 6619.

70. N.-K. Kim, K.-J. Chang, D. Moon, M. S. Lah, K.-S. Jeong, *Chem. Commun.* **2007**, 3401 – 3403.

71. S. Freye, J. Hey, A. Torras-Gal n, D. Stalke, R. Herbst-Irmer, M. John, G. H. Clever, *Angew. Chem. Int. Ed.* **2012**, *51*, 2191 – 2194; *Angew. Chem.* **2012**, *124*, 2233 – 2237.

72. S. Freye, R. Michel, D. Stalke, M. Pawliczek, H. Frauendorf, G. H. Clever, *J. Am. Chem. Soc.* **2013**, *135*, 8476 – 8479.

73. M. Han, R. Michel, B. He, Y.-S. Chen, D. Stalke, M. John, G. H. Clever, *Angew. Chem. Int. Ed.* **2013**, *52*, 1319 – 1323; *Angew. Chem.* **2013**, *125*, 1358 – 1362.

74. V. Valderrey, E. C. Escudero-Adán, P. Ballester, *Angew. Chem. Int. Ed.* **2013**, *52*, 6898 – 6902; *Angew. Chem.* **2013**, *125*, 7036 – 7040.

75. V. Valderrey, E. C. Escudero-Adán, P. Ballester, *J. Am. Chem. Soc.* **2012**, *134*, 10733 – 10736.

76. H. J. Kim, J.-M. Suk, K.-S. Jeong, *Supramol. Chem.* **2013**, *25*, 46 – 53.

77. O. B. Berryman, C. A. Johnson, II, L. N. Zakharov, M. M. Haley, D. W. Johnson, *Angew. Chem. Int. Ed.* **2008**, *47*, 117 – 120; *Angew. Chem.* **2008**, *120*, 123 – 126.

78. M. M. Watt, L. N. Zakharov, M. M. Haley, D. W. Johnson, *Angew. Chem. Int. Ed.* **2013**, *52*, 10275 – 10280; *Angew. Chem.* **2013**, *125*, 10465 –10470.

79. B. W. Tresca, L. N. Zakharov, C. N. Carroll, D. W. Johnson, M. M. Haley, *Chem. Commun.* **2013**, *49*, 7240 – 7242.

80. J. V. Gavette, C. J. Evoniuk, L. N. Zakharov, M. E. Carnes, M. M. Haley, D.W. Johnson, *Chem. Sci.* **2014**, *5*, 2899 – 2905.

81. H. Maeda, K. Kitaguchi, Y. Haketa, *Chem. Commun.* **2011**, *47*, 9342 –9344.

82. G. Wei, S. Zhang, C. Dai, Y. Quan, Y. Cheng, C. Zhu, *Chem. Eur. J.* **2013**, *19*, 16066 – 16071.

83. W. Makiguchi, S. Kobayashi, Y. Furusho, E. Yashima, *Angew. Chem. Int. Ed.* **2013**, *52*, 5275 – 5279; *Angew. Chem.* **2013**, *125*, 5383 – 5387.

84. Y. Nakatani, Y. Furusho, E. Yashima, *Org. Biomol. Chem.* **2013**, *11*, 1614 –1623.

85. Y. Wu, H. Guo, X. Zhang, T. D. James, J. Zhao, *Chem. Eur. J.* **2011**, *17*, 7632 – 7644.

86. D. P. Iwaniuk, C. Wolf, *J. Am. Chem. Soc.* **2011**, *133*, 2414 – 2417.

87. D. P. Iwaniuk, C. Wolf, *Chem. Commun.* **2012**, *48*, 11226 – 11228.

88. D. P. Iwaniuk, C. Wolf, *Org. Lett.* **2011**, *13*, 2602 – 2605.

89. D. A. Kim, P. Kang, M.-G. Choi, K.-S. Jeong, *Chem. Commun.* **2013**, *49*, 9743 – 9745.

90. M. J. Kim, Y. R. Choi, H.-G. Jeon, P. Kang, M.-G. Choi, K.-S. Jeong, *Chem. Commun.* **2013**, *49*, 11412 – 11414.

91. H.-G. Jeon, M. J. Kim, K.-S. Jeong, *Org. Biomol. Chem.* **2014**, *12*, 5464 –5468.

92. Y. R. Choi, M. K. Chae, D. Kim, M. S. Lah, K.-S. Jeong, *Chem. Commun.* **2012**, *48*, 10346 – 10348.

93. T. Muraoka, T. Shima, T. Hamada, M. Morita, M. Takagi, K. V. Tabata, H. Noji, K. Kinbara, *J. Am. Chem. Soc.* **2012**, *134*, 19788 – 19794.

94. J. M. Heemstra, J. S. Moore, *J. Org. Chem.* **2004**, *69*, 9234 – 9237.

95. H. Abe, H. Machiguchi, S. Matsumoto, M. Inouye, *J. Org. Chem.* **2008**, *73*, 4650 – 4661.

96. F. Kayamori, H. Abe, M. Inouye, *Eur. J. Org. Chem.* **2013**, 1677 – 1682.

97.   H. Abe, K. Okada, H. Makida, M. Inouye, *Org. Biomol. Chem.* **2012**, *10*, 6930 – 6936.

98.   J. Dash, Z. A. E. Waller, G. D. Pantos, S. Balasubramanian, *Chem. Eur. J.* **2011**, *17*, 4571 – 4581.

99.   S. Shanmugaraju, S. A. Joshi, P. S. Mukherjee, *Inorg. Chem.* **2011**, *50*, 11736 – 11745.

100.   M. Wang, V. Vajpayee, S. Shanmugaraju, Y.-R. Zheng, Z. Zhao, H. Kim, P. S. Mukherjee, K.-W. Chi, P. J. Stang, *Inorg. Chem.* **2011**, *50*, 1506 –1512.

101.   S. Li, T. Leng, H. Zhong, C. Wang, Y. Shen, *J. Heterocycl. Chem.* **2012**, *49*, 64 – 70.

102.   A. Wild, A. Winter, M. D. Hager, U. S. Schubert, *Chem. Commun.* **2012**, *48*, 964 – 966.

103.   D. M. D'Alessandro, B. Smit, J. R. Long, *Angew. Chem. Int. Ed.* **2010**, *49*, 6058 – 6082; *Angew. Chem.* **2010**, *122*, 6194 – 6219.

104.   Y. Jin, B. A. Voss, A. Jin, H. Long, R. D. Noble, W. Zhang, *J. Am. Chem. Soc.* **2011**, *133*, 6650 – 6658.

105.   Y. Jin, B. A. Voss, R. McCaffrey, C. T. Baggett, R. D. Noble, W. Zhang, *Chem. Sci.* **2012**, *3*, 874 – 877.

Chapter II

1.   J. L. Sessler, P. A. Gale, W.-S. Cho, *Anion Receptor Chemistry*, Royal Society of Chemistry, Cambridge, 2006.

2.   P. D. Beer, P. A. Gale, *Angew. Chem. Int. Ed.* 2001, **40**, 486–516.

3.   F. G. Bordwell, *Acc. Chem. Res.* 1988, **21**, 456–463.

4.   E. V. Anslyn, D. A. Dougherty *Modern Physical Organic Chemistry*, University Science Books, Sausalito, CA, 2006, p. 280.

5.   G. R. Desiraju, T. Steiner, *The Weak Hydrogen Bond: in Structural Chemistry and Biology*, Oxford University Press, Oxford; New York, 1999.

6.   H.-J. Schneider, *Angew. Chem. Int. Ed.* 2009, **48**, 3924–3977.

7.   N. G. White, S. Carvalho, V. Felix, P. D. Beer, *Org. Biomol. Chem.* 2012, **10**, 6951–6959.

8.   Y. Li, A. H. Flood, *Angew. Chem. Int. Ed.* 2008, **47**, 2649–2652.

9.   H. Maeda, Y. Haketa, T. Nakanishi, *J. Am. Chem. Soc.* 2007, **129**, 13661–13674.

10. B. Dong, T. Sakurai, Y. Honsho, S. Seki, H. Maeda, *J. Am. Chem. Soc.* 2013, **135**, 1284–1287.

11. Y. Terashima, M. Takayama, K. Isozaki, H. Maeda, *Chem. Commun.* 2013, **49**, 2506–2508.

12. V. S. Bryantsev, B. P. Hay, *J. Am. Chem. Soc.* 2005, **127**, 8282–8283.

13. Y. Hua, A. H. Flood, *Chem. Soc. Rev.* 2010, **39**, 1262–1271.

14. K. P. McDonald, Y. Hua, A. H. Flood, *Top. Heterocycl. Chem.* 2010, **24**, 341–366.

15. Y. Hua, R. O. Ramabhadran, J. A. Karty, K. Raghavachari, A. H. Flood, *Chem. Commun.* 2011, **47**, 5979–5981.

16. V. S. Bryantsev, B. P. Hay, *Org. Lett.* 2005, **7**, 5031–5034.

17. H. Juwarker, J. M. Lenhardt, D. M. Pham, S. L. Craig, *Angew. Chem. Int. Ed.* 2008, **47**, 3740–3743.

18. C.-H. Lee, H.-K. Na, D.-W. Yoon, D.-H. Won, W.-S. Cho, V. M. Lynch, S. V. Shevchuk, J. L. Sessler, *J. Am. Chem. Soc.* 2003, **125**, 7301–7306.

19. F. Szemes, D. Hesek, Z. Chen, S. W. Dent, M. G. B. Drew, A. J. Goulden, A. R. Graydon, A. Grieve, R. J. Mortimer, T. Wear, J. S. Weightman, P. D. Beer, *Inorg. Chem.* 1996, **35**, 5868–5879.

20. C. N. Carroll, J. J. Naleway, M. M. Haley, D. W. Johnson, *Chem. Soc. Rev.* 2010, **39**, 3875–3888.

21. O. B. Berryman, C. A. Johnson II, L. N. Zakharov, M. M. Haley, D. W. Johnson, *Angew. Chem. Int. Ed.* 2008, **47**, 117–120.

22. J. M. Engle, C. N. Carroll, D. W. Johnson, M. M. Haley, *Chem. Sci.* 2012, **3**, 1105–1110.

23. C. N. Carroll, B. A. Coombs, S. P. McClintock, C. A. Johnson, O. B. Berryman, D. W. Johnson, M. M. Haley, *Chem. Commun.* 2011, **47**, 5539–5541.

24. C. N. Carroll, O. B. Berryman, C. A. Johnson, L. N. Zakharov, M. M. Haley, D. W. Johnson, *Chem. Commun.* 2009, 2520–2522.

25. J. M. Heemstra, J. S. Moore, *Org. Lett.* 2004, **6**, 659–662.

26. I. Kaljurand, A. Kütt, L. Soovali, T. Rodima, V. Mäemets, I. Leito, I. A. Koppel, *J. Org. Chem.* 2005, **70**, 1019–1028.

27. P. Thordarson, *Chem. Soc. Rev.* 2011, **40**, 1305–1323.

28. D.-W. Yoon, D. E. Gross, V. M. Lynch, J. L. Sessler, B. P. Hay, C.-H. Lee, *Angew. Chem. Int. Ed.* 2008, **47**, 5038–5042.

29. J. M. Engle, P. S. Lakshminarayanan, C. N. Carroll, L. N. Zakharov, M. M. Haley, D. W. Johnson, *Cryst. Growth Des.* 2011, **11**, 5144–5152.

30. R. Taylor, O. Kennard, *J. Am. Chem. Soc.* 1982, **104**, 5063–5070.

31. B. P. Hay, V. S. Bryantsev, *Chem. Commun.* 2008, **21**, 2417–2428.

32. P. A. Wood, F. H. Allen, E. Pidcock, *CrystEngComm.* 2009, **11**, 1563–1571.

33. P. Gans, A. Sabatini, A. Vacca, *Talanta* **1996**, *43*, 1739–1753.

34. G. M. Sheldrick, *Bruker/Siemens Area Detector Absorption Correction Program*, Bruker AXS, Madison, WI, 1998.

35. SHELXTL-6.10 "Program for Structure Solution, Refinement and Presentation" BRUKER AXS Inc., 5465 East Cheryl Parkway, Madison, WI 53711-5373 USA.

Chapter III

1.   Cai, J.; Sessler, J. L. *Chem. Soc. Rev.* **2014**, *43*, 6198–6213.

2.   Steiner, T.; Desiraju, G. R. *The Weak Hydrogen Bond in Structural Chemistry and Biology*; Oxford University Press: Oxford, 1999.

3.   Lee, S.; Flood, A. H. In *Topics in Heterocyclic Chemistry*; Gale, P.A.; Dehaen, W., Eds.; Springer: Berlin, 2012; Vol. 28, pp. 85–107.

4.   Hua, Y.; Flood, A. H. *Chem. Soc. Rev.* **2010**, *39*, 1262–1271.

5.   McDonald, K. P.; Hua, Y.; Flood, A. H. In *Topics in Heterocyclic Chemistry*; Gale, P.A.; Dehaen, W., Eds.; Springer: Berlin, 2010; Vol. 24, pp. 341–366.

6.   Johnston, R. C.; Cheong, P. H.-Y. *Org. Biomol. Chem.* **2013**, *11*, 5057–5064.

7.   Desiraju, G. R. *Acc. Chem. Res.* **1996**, *29*, 441–449.

8.   Horowitz, S.; Trievel, R. C. *J. Biol. Chem.* **2012**, *287*, 41576–41582.

9.   Lee, S.; Flood, A. H. *J. Phys. Org. Chem.* **2012**, *26*, 79–86.

10. Hua, Y.; Liu, Y.; Chen, C.-H.; Flood, A. H. *J. Am. Chem. Soc.* **2013**, *135*, 14401–14412.

11. Maeda, H.; Kitaguchi, K.; Haketa, Y. *Chem. Commun.* **2011**, *47*, 9342–9344.

12. Beckendorf, S.; Asmus, S.; Mück Lichtenfeld, C.; García Mancheño, O. *Chem.–Eur. J.* **2013**, *19*, 1581–1585.

13. Asmus, S.; Beckendorf, S.; Zurro, M.; Mück Lichtenfeld, C.; Fröhlich, R.; García Mancheño, O. *Chem.–Asian J.* **2014**, *9*, 2178–2186.

14. Lee, S.; Chen, C.-H.; Flood, A. H. *Nat. Chem.* **2013**, *5*, 704–710.

15. Hua, Y.; Ramabhadran, R. O.; Uduehi, E. O.; Karty, J. A.; Raghavachari, K.; Flood, A. H. *Chem.–Eur. J.* **2011**, *17*, 312–321.

16. Ballester, P. *Acc. Chem. Res.* **2013**, *46*, 874–884.

17. Adriaenssens, L.; Gil-Ramírez, G.; Frontera, A.; Quiñonero, D.; Escudero-Adán, E. C.; Ballester, P. *J. Am. Chem. Soc.* **2014**, *136*, 3208–3218.

18. Berryman, O. B.; Hof, F.; Hynes, M. J.; Johnson, D. W. *Chem. Commun.* **2006**, 506–508.

19. Watt, M. M.; Collins, M. S.; Johnson, D. W. *Acc. Chem. Res.* **2013**, *46*, 955–966.

20. Wang, D.-X.; Wang, M.-X. *J. Am. Chem. Soc.* **2013**, *135*, 892–897.

21. Nepal, B.; Scheiner, S. *Chem.–Eur. J.* **2015**, *21*, 1474–1481; Scheiner, S.; Grabowski, S. J.; Kar, T. *J. Phys. Chem. A* **2001**, *105*, 10607–10612.

22. Hwang, J.; Li, P.; Carroll, W. R.; Smith, M. D.; Pellechia, P. J.; Shimizu, K. D. *J. Am. Chem. Soc.* **2014**, *136* , 14060–14067.

23. Wheeler, S. E.; McNeil, A. J.; Müller, P.; Swager, T. M.; Houk, K. N. *J. Am. Chem. Soc.* **2010**, *132*, 3304–3311.

24. Zhou, Y.; Yuan, Y.; You, L.; Anslyn, E. V. *Chem.–Eur. J.* **2015**, *21*, 8207–8213.

25. Zhou, Y.; Ye, H.; You, L. *J. Org. Chem.* **2015**, *80*, 2627–2633.

26. Bryantsev, V. S.; Hay, B. P. *J. Am. Chem. Soc.* **2005**, *127*, 8282–8283.

27. Bryantsev, V. S.; Hay, B. P. *Org. Lett.* **2005**, *7*, 5031–5034.

28. Hansch, C.; Leo, A.; Taft, R. W. *Chem. Rev.* **1991**, *91*, 165–195.

29. Arunan, E.; Desiraju, G. R.; Klein, R. A.; Sadlej, J.; Scheiner, S.; Alkorta, I.; Clary, D. C.; Crabtree, R. H.; Dannenberg, J. J.; Hobza, P.; Kjaergaard, H. G.; Legon, A. C.; Mennucci, B.; Nesbitt, D. J. *Pure Appl. Chem.* **2011**, *83*, 1637–1641.

30. Tresca, B. W.; Zakharov, L. N.; Carroll, C. N.; Johnson, D. W.; Haley, M. M. *Chem. Commun.* **2013**, *49*, 7240–7242.

31. Swain, C. G.; Lupton, E. C. *J. Am. Chem. Soc.* **1968**, *90*, 4328–4337.

32.   Swain, C. G.; Unger, S. H.; Rosenquist, N. R. *J. Am. Chem. Soc.* **1983**, *105*, 492–502.

33.   Johnson, C. A., II; Berryman, O. B.; Sather, A. C.; Zakharov, L. N.; Haley, M. M.; Johnson, D. W. *Cryst. Growth Des.* **2009**, *9*, 4247–4249.

34.   Gavette, J. V.; Mills, N. S.; Zakharov, L. N.; Johnson, C. A.; Johnson, D. W.; Haley, M. M. *Angew. Chem., Int. Ed.* **2013**, *52*, 10270–10274.

35.   Gavette, J. V.; Evoniuk, C. J.; Zakharov, L. N.; Carnes, M. E.; Haley, M. M.; Johnson, D. W. *Chem. Sci.* **2014**, *5*, 2899–2905.

36.   Watt, M. M.; Engle, J. M.; Fairley, K. C.; Robitshek, T. E.; Haley, M. M.; Johnson, D.W. *Org. Biomol. Chem.* **2015**, *13*, 4266–4270.

37.   Watt, M. M.; Zakharov, L. N.; Haley, M. M.; Johnson, D. W. *Angew. Chem., Int. Ed.* **2013**, *52*, 10275–10280.

38.   Engle, J. M.; Carroll, C. N.; Johnson, D. W.; Haley, M. M. *Chem. Sci.* **2012**, *3*, 1105–1110.

39.   Vonnegut, C. L.; Tresca, B. W.; Johnson, D. W.; Haley, M. M. *Chem.–Asian J.* **2015**, *10*, 522–535.

40.   Yoon, D.-W.; Gross, D. E.; Lynch, V. M.; Sessler, J. L.; Hay, B. P.; Lee, C.-H. *Angew. Chem., Int. Ed.* **2008**, *47*, 5038–5042.

41.   McGrath, J. M.; Pluth, M. D. *J. Org. Chem.* **2014**, *79*, 11797–11801.

42.   Carroll, C. N.; Berryman, O. B.; Johnson, C. A.; Zakharov, L. N.; Haley, M. M.; Johnson, D. W. *Chem. Commun.* **2009**, 2520–2522.

43.   Carroll, C. N.; Coombs, B. A.; McClintock, S. P.; Johnson, C. A.; Berryman, O. B.; Johnson, D. W.; Haley, M. M. *Chem. Commun.* **2011**, *47*, 5539–5541.

44.   Thordarson, P. *Chem. Soc. Rev.* **2011**, *40*, 1305–1323.

45.   Salis, A.; Ninham, B. W. *Chem. Soc. Rev.* **2014**, *43*, 7358–7377.

46.   Carnegie, R. S.; Gibb, C. L. D.; Gibb, B. C. *Angew. Chem. Int. Ed.* **2014**, *53*, 11498–11500.

47.   Gans, P.; Sabatini, A.; Vacca, A. *Talanta* **1996**, *43*, 1739–1753.

48.   Busschaert, N.; Bradberry, S. J.; Wenzel, M.; Haynes, C. J. E.; Hiscock, J. R.; Kirby, I. L.; Karagiannidis, L. E.; Moore, S. J.; Wells, N. J.; Herniman, J.; Langley, G. J.; Horton, P. N.; Light, M. E.; Marques, I.; Costa, P. J.; Felix, V.; Frey, J. G.; Gale, P. A. *Chem. Sci.* **2013**, *4*, 3036–3045.

49.   Lisbjerg, M.; Valkenier, H.; Jessen, B. M.; Al-Kerdi, H.; Davis, A. P.; Pittelkow, M. *J. Am. Chem. Soc.* **2015**, *137*, 4948–4951.

50.   Hancock, L. M.; Gilday, L. C.; Carvalho, S.; Costa, P. J.; Felix, V.; Serpell, C. J.; Kilah, N. L.; Beer, P. D. *Chem.–Eur. J.* **2010**, *16*, 13082–13094.

51.   Kimball, D. B.; Weakley, T. J. R.; Haley, M. M. *J. Org. Chem.* **2002**, *67*, 6395–6405.

52.   Chanteau, S. H.; Tour, J. M. *J. Org. Chem.* **2003**, *68*, 8750–8766.

53.   Haley, M. M.; Wan, W. B. *J. Org. Chem.* **2001**, *66*, 3893–3901.

54.   Probst, G. D.; Bowers, S.; Sealy, J. M.; Stupi, B.; Dressen, D.; Jagodzinska, B. M.; Aquino, J.; Gailunas, A.; Truong, A. P.; Tso, L.; Xu, Y.-Z.; Hom, R. K.; John, V.; Tung, J. S.; Pleiss, M. A.; Tucker, J. A.; Konradi, A. W.; Sham, H. L.; Jagodzinski, J.; Toth, G.; Brecht, E.; Yao, N.; Pan, H.; Lin, M.; Artis, D. R.; Ruslim, L.; Bova, M. P.; Sinha, S.; Yednock, T. A.; Gauby, S.; Zmolek, W.; Quinn, K. P.; Sauer, J.-M. *Bioorg. Med. Chem. Lett.* **2010**, *20*, 6034–6039.

55.   Lee, G. W.; Kim, N.-K.; Jeong, K.-S. *Org. Lett.* **2010***, 12*, 2634–2637.

56.   Görl, C.; Beck, N.; Kleiber, K.; Alt, H. G. *J. Mol. Catal. A: Chem.* **2012**, *352,* 110–127.

57.   Sheldrick, G. M. *Bruker/Siemens Area Detector Absorption Correction Program*, Bruker AXS, Madison, WI, 1998.

58.   SHELXTL-6.10 "Program for Structure Solution, Refinement and Presentation" BRUKER AXS Inc., 5465 East Cheryl Parkway, Madison, WI 53711-5373 USA.

59.   Sheldrick, G. M. *Acta Cryst. A* **2008**, *64*, 112–122.

60.   Gans, P.; Sabatini, A. Vacca, A. *Talanta* **1996**, *43*, 1739–1753.

Chapter IV

1.   Wade, D. *Chem.-Biol. Interact.* **1999**, *117*, 191–217.

2.   Kohen, A.; Limbach, H.-H. *Isotope Effects In Chemistry and Biology*; CRC Press: Boca Raton, FL, 2005.

3.   Tran, C. D.; Mejac, I.; Rebek, J.; Hooley, R. J. *Anal. Chem.* **2009**, *81*, 1244–1254.

4.   Laughrey, Z. R.; Upton, T. G.; Gibb, B. C. *Chem. Commun.* **2006**, 970–972.

5.   Świderek, K.; Paneth, P. *Chem. Rev.* **2013**, *113*, 7851–7879.

6.   Wang, Z.; Singh, P.; Czekster, C. M.; Kohen, A.; Schramm, V. L. *J. Am. Chem. Soc.* **2014**, *136*, 8333–8341.

7.   Mugridge, J. S.; Bergman, R. G.; Raymond, K. N. *Angew. Chem. Int. Ed.* **2010**, *49*, 3635–3637.

8.   Mugridge, J. S.; Bergman, R. G.; Raymond, K. N. *J. Am. Chem. Soc.* **2012**, *134*, 2057–2066.

9.   Mugridge, J. S.; Bergman, R. G.; Raymond, K. N. *J. Am. Chem. Soc.* **2010**, *132*, 1182–1183.

10.   Zhao, C.; Parrish, R. M.; Smith, M. D.; Pellechia, P. J.; Sherrill, C. D.; Shimizu, K. D. *J. Am. Chem. Soc.* **2012**, *134*, 14306–14309.

11.   Perrin, C. L.; Karri, P. *J. Am. Chem. Soc.* **2010**, *132*, 12145–12149.

12.   Rechavi, D.; Scarso, A.; Rebek, J. *J. Am. Chem. Soc.* **2004**, *126*, 7738–7739.

13.   Zhao, Y. L.; Houk, K. N.; Rechavi, D.; Scarso, A. *J. Am. Chem. Soc.* **2004**, *126*, 11428–11429.

14.   Lewis, B. E.; Schramm, V. L. *J. Am. Chem. Soc.* **2001**, *123*, 1327–1336.

15.   Lewis, B. E.; Schramm, V. L. *J. Am. Chem. Soc.* **2003**, *125*, 4785–4798.

16.   Tresca, B. W.; Hansen, R. J.; Chau, C. V.; Hay, B. P.; Zakharov, L. N.; Haley, M. M.; Johnson, D. W. *J. Am. Chem. Soc.* **2015**, *137*, 14959–14967.

17.   Majek, M.; Filace, F.; Jacobi von Wangelin, A. *Chem. Eur. J.* **2015**, *21*, 4518–4522.

18.   Carroll, C. N.; Berryman, O. B.; Johnson, C. A.; Zakharov, L. N.; Haley, M. M.; Johnson, D. W. *Chem. Commun.* **2009**, 18, 2520–2522.

19.   Kimball, D. B.; Weakley, T. J. R.; Haley, M. M. *J. Org. Chem.* **2002**, *67*, 6395–6405.

20.   Perrin, C. L.; Fabian, M. A. *Anal. Chem.* **1996**, *68*, 2127–2134.

21.   Gavette, J. V.; Evoniuk, C. J.; Zakharov, L. N.; Carnes, M. E.; Haley, M. M.; Johnson, D. W. *Chem. Sci.* **2014**, *5*, 2899–2905.

22.   Gavette, J. V.; Mills, N. S.; Zakharov, L. N.; Johnson, C. A.; Johnson, D. W.; Haley, M. M. *Angew. Chem. Int. Ed.* **2013**, *52*, 10270–10274.

23.   Singh, A.; Gangopadhyay, D.; Popp, J.; Singh, R. K. *Spectrochim. Acta A* **2012**, *99*, 136–143.

24.   Lee, C.; Yang, W.; Parr, R. G. *Phys. Rev. B* **1988**, *37*, 785–789.

25.   Becke, A. D. *J. Chem. Phys.* **1993**, *98*, 5648–5652.

26.   M.J. Frisch, G.W. Trucks, H.B. Schlegel, G.E. Scuseria, M.A. Robb, J.R. Cheeseman, G. Scalmani, V. Barone, B. Mennucci, G.A. Petersson, H. Nakatsuji, M. Caricato, X. Li, H.P. Hratchian, A.F. Izmaylov, J. Bloino, G. Zheng, J.L. Sonnenberg, M. Hada, M. Ehara, K. Toyota, R. Fukuda, J. Hasegawa, M. Ishida, T. Nakajima, Y. Honda, O. Kitao, H. Nakai, T. Vreven, J.A. Montgomery, J.E. Peralta, F. Ogliaro, M. Bearpark, J.J. Heyd, E. Brothers, K.N. Kudin, V.N. Staroverov, R. Kobayashi, J. Normand, K. Raghavachari, A. Rendell, J.C. Burant, S.S. Iyengar, J. Tomasi, M. Cossi, N. Rega, J.M. Millam, M. Klene, J.E. Knox, J.B. Cross, V. Bakken, C. Adamo, J. Jaramillo, R. Gomperts, R.E. Stratmann, O. Yazyev, A.J. Austin, R. Cammi, C. Pomelli, J.W. Ochterski, R.L. Martin, K. Morokuma, V.G. Zakrzewski, G.A. Voth, P. Salvador, J.J. Dannenberg, S. Dapprich, A.D. Daniels, O. Farkas, J.B. Foresman, J.V. Ortiz, J. Cioslowski, D.J. Fox, Gaussian 09, Wallingford, CT, 2009.

Chapter V

1.   Whitesides, G.M.; Grzybowski, B. *Science* **2002**, *295*, 2418 – 2421.

2.   Yoshizawa, M.; Klosterman, J.K. *Chem. Soc. Rev.* **2014**, *43*, 1885 – 1898.

3.   Park, J.S.; Karnas, E.; Ohkubo, K.; Chen, P.; Kadish, K.M.; Fukuzumi, S.; Bielawski, C.W.; Hudnall, T.W.; Lynch, V.M.; Sessler, J.L. *Science* **2010**, *329*, 1324 – 1327.

4.   Carnes, M.E.; Collins, M.S.; Johnson, D.W. *Chem. Soc. Rev.* **2014**, *43*, 1825 – 1834.

5.   Ren, C.; Zhang, J.; Chen, M.; Yang, Z. *Chem. Soc. Rev.* **2014**, *43*, 7257 – 7266.

6.   Zhang, Z.; Kim, D.S.; Lin, C.-Y.; Zhang, H.; Lammer, A.D.; Lynch, V.M.; Popov, I.; Miljanić, O.Š.; Anslyn, E.V.; Sessler, J.L. *J. Am. Chem. Soc.* **2015**, *137*, 7769 – 7774.

7.   Knipe, P.C.; Thompson, S.; Hamilton, A.D. *Chem. Sci.* **2015**, *6*, 1630 – 1639.

8.   Spence, G.T.; Beer, P.D. *Acc. Chem. Res.* **2013**, *46*, 571 – 586.

9.   Kim, D.S.; Lynch, V.M.; Park, J.S.; Sessler, J.L. *J. Am. Chem. Soc.* **2013**, *135*, 14889 – 14894.

10.   Black, S.P.; Sanders, J.K.M.; Stefankiewicz, A.R. *Chem. Soc. Rev.* **2014**, *43*, 1861 – 1872.

11.   Park, J.S.; Yoon, K.Y.; Kim, D.S.; Lynch, V.M.; Bielawski, C.W.; Johnston, K.P.; Sessler, J.L. *Proc. Natl. Acad. Sci. USA* **2011**, *108*, 20913 – 20917.

12.   Han, M.; Michel, R.; He, B.; Chen, Y.-S.; Stalke, D.; John, M.; Clever, G.H. *Angew. Chem. Int. Ed.* **2012**, *52*, 1319 – 1323.

13.   Gong, H.-Y.; Rambo, B.M.; Nelson, C.A.; Lynch, V.M.; Zhu, X.; Sessler, J.L. *Chem. Commun.* **2012**, *48*, 10186 – 10188.

14. Gong, H.-Y.; Rambo, B.M.; Karnas, E.; Lynch, V.M.; Sessler, J.L. *Nat. Chem.* **2010**, *2*, 406 – 409.

15. Riddell, I.A.; Ronson, T.K.; Clegg, J.K.; Wood, C.S.; Bilbeisi, R.A.; Nitschke, J.R. *J. Am. Chem. Soc.* **2014**, *136*, 9491 – 9498.

16. Moyer, B.A.; Custelcean, R.; Hay, B.P.; Sessler, J.L.; Bowman-James, K.; Day, V.W.; Kang, S.O. *Inorg. Chem.* **2012**, *52*, 3473 – 3490.

17. Vonnegut, C.L.; Tresca, B.W.; Johnson, D.W.; Haley, M.M. *Chem.–Asian J.* **2015**, *10*, 522 – 535.

18. Berryman, O.B.; Johnson, C.A.; Zakharov, L.N.; Haley, M.M.; Johnson, D.W. *Angew. Chem. Int. Ed.* **2008**, *47*, 117 – 120.

19. Carroll, C.N.; Berryman, O.B.; Johnson, C.A.; Zakharov, L.N.; Haley, M.M.; Johnson, D.W. *Chem. Commun.* **2009**, 2520 – 2522.

20. Johnson, C.A., II; Berryman, O.B.; Sather, A.C.; Zakharov, L.N.; Haley, M.M.; Johnson, D.W. *Cryst. Growth Des.* **2009**, *9*, 4247 – 4249.

21. Carroll, C.N.; Coombs, B.A.; McClintock, S.P.; Johnson, C.A.; Berryman, O.B.; Johnson, D.W.; Haley, M.M. *Chem. Commun.* **2011**, *47*, 5539 – 5541.

22. Engle, J.M.; Lakshminarayanan, P.S.; Carroll, C.N.; Zakharov, L.N.; Haley, M.M.; Johnson, D.W. *Cryst. Growth Des.* **2011**, *11*, 5144 – 5152.

23. Engle, J.M.; Carroll, C.N.; Johnson, D.W.; Haley, M.M. *Chem. Sci.* **2012**, *3*, 1105.

24. Berryman, O.B.; Johnson, C.A., II; Vonnegut, C.L.; Fajardo, K.A.; Zakharov, L.N.; Johnson, D.W.; Haley, M.M. *Cryst. Growth Des.* **2015**, *15*, 1502 – 1511.

25. Watt, M.M.; Engle, J.M.; Fairley, K.C.; Robitshek, T.E.; Haley, M.M.; Johnson, D.W. *Org. Biomol. Chem.* **2015**, *13*, 4266 – 4270.

26. Gavette, J.V.; Mills, N.S.; Zakharov, L.N.; Johnson, C.A.; Johnson, D.W.; Haley, M.M. *Angew. Chem. Int. Ed.* **2013**, *52*, 10270 – 10274.

27. Gavette, J.V.; Klug, C.M.; Zakharov, L.N.; Shores, M.P.; Haley, M.M.; Johnson, D.W. *Chem. Commun.* **2014**, *50*, 7173 – 7175.

28. Gavette, J.V.; Evoniuk, C.J.; Zakharov, L.N.; Carnes, M.E.; Haley, M.M.; Johnson, D.W. *Chem. Sci.* **2014**, *5*, 2899 – 2905.

29. Tresca, B.W.; Zakharov, L.N.; Carroll, C.N.; Johnson, D.W.; Haley, M.M. *Chem. Commun.* **2013**, *49*, 7240 – 7242.

30. Watt, M.M.; Zakharov, L.N.; Haley, M.M.; Johnson, D.W. *Angew. Chem. Int. Ed.* **2013**, *52*, 10275 – 10280.

31.   Berryman, O.B.; Hof, F.; Hynes, M.J.; Johnson, D.W. *Chem. Commun.* **2006**, 506 – 508.

32.   Watt, M.M.; Collins, M.S.; Johnson, D.W. *Acc. Chem. Res.* **2013**, *46*, 955 – 966.

33.   Wheeler, S.E.; Bloom, J.W. G. *J. Phys. Chem. A* **2014**, *118*, 6133 – 6147.

34.   Adriaenssens, L.; Gil-Ramírez, G.; Frontera, A.; Quiñonero, D.; Escudero-Adán, E.C.; Ballester, P. *J. Am. Chem. Soc.* **2014**, *136*, 3208 – 3218.

35.   Adriaenssens, L.; Estarellas, C.; Vargas Jentzsch, A.; Martinez Belmonte, M.; Matile, S.; Ballester, P. *J. Am. Chem. Soc.* **2013**, *135*, 8324 – 8330.

36.   Berryman, O.B.; Sather, A.C.; Hay, B.P.; Meisner, J.S.; Johnson, D.W. *J. Am. Chem. Soc.* **2008**, *130*, 10895 – 10897.

37.   Morris, G.A. *Diffusion-Ordered Spectrocopy*; John Wiley and Sons: Chichester, UK, 2009.

38.   Lamm, J.-H.; Niermeier, P.; Mix, A.; Chmiel, J.; Neumann, B.; Stammler, H.-G.; Mitzel, N.W. *Angew. Chem. Int. Ed.* **2014**, *53*, 7938 – 7942.

39.   Sheldrick, G.M. *Bruker/Siemens Area Detector Absorption Correction Program;* Bruker AXS: Madison, WI, 1998.

40.   SHELXTL-6.10, *Program for Structure Solution, Refinement and Presentation*; Bruker AXS Inc.: Madison, WI, 2001.

Chapter VI

1.   Nguyen, B. T.; Anslyn, E. V. *Coord. Chem. Rev.* **2006**, *250*, 3118–3127.

2.   Lee, M. H.; Kim, J. S.; Sessler, J. L. *Chem. Soc. Rev.* **2015**, *44*, 4185–4191.

3.   Lim, J.; Miljanić, O. Š. *Chem. Commun.* **2012**, *48*, 10301–10303.

4.   Gale, P. A.; Caltagirone, C. *Chem. Soc. Rev.* **2015**, *44*, 4212–4227.

5.   Jo, H. H.; Gao, X.; You, L.; Anslyn, E. V.; Krische, M. J. *Chem. Sci.* **2015**, *6*, 6747–6753.

6.   Watt, M. M.; Engle, J. M.; Fairley, K. C.; Robitshek, T. E.; Haley, M. M.; Johnson, D. W. *Org. Biomol. Chem.* **2015**, *13*, 4266–4270.

7.   Steed, J. W. *Chem. Soc. Rev.* **2010**, *39*, 3686–3699.

8.   Wolfbeis, O. S. *Angew. Chem. Int. Ed.* **2013**, *52*, 9864–9865.

9.   Jimenez-Jorquera, C.; Orozco, J.; Baldi, A. *Sensors* **2009**, *10*, 61–83.

10.   Stewart, S.; Ivy, M. A.; Anslyn, E. V. *Chem. Soc. Rev.* **2013**, *43*, 70–84.

11.   Zhang, Z.; Kim, D. S.; Lin, C.-Y.; Zhang, H.; Lammer, A. D.; Lynch, V. M.; Popov, I.; Miljanić, O. Š.; Anslyn, E. V.; Sessler, J. L. *J. Am. Chem. Soc.* **2015**, *137*, 7769–7774.

12.   Lim, J.; Nam, D.; Miljanić, O. Š. *Chem. Sci.* **2012**, *3*, 559–563.

13.   Engle, J. M.; Carroll, C. N.; Johnson, D. W.; Haley, M. M. *Chem. Sci.* **2012**, *3*, 1105–1110.

14.   Carroll, C. N.; Coombs, B. A.; McClintock, S. P.; Johnson, C. A.; Berryman, O. B.; Johnson, D. W.; Haley, M. M. *Chem. Commun.* **2011**, *47*, 5539–5541.

15.   Tresca, B. W.; Hansen, R. J.; Chau, C. V.; Hay, B. P.; Zakharov, L. N.; Haley, M. M.; Johnson, D. W. *J. Am. Chem. Soc.* **2015**, *137*, 14959–14967.

16.   M.J. Frisch, G.W. Trucks, H.B. Schlegel, G.E. Scuseria, M.A. Robb, J.R. Cheeseman, G. Scalmani, V. Barone, B. Mennucci, G.A. Petersson, H. Nakatsuji, M. Caricato, X. Li, H.P. Hratchian, A.F. Izmaylov, J. Bloino, G. Zheng, J.L. Sonnenberg, M. Hada, M. Ehara, K. Toyota, R. Fukuda, J. Hasegawa, M. Ishida, T. Nakajima, Y. Honda, O. Kitao, H. Nakai, T. Vreven, J.A. Montgomery, J.E. Peralta, F. Ogliaro, M. Bearpark, J.J. Heyd, E. Brothers, K.N. Kudin, V.N. Staroverov, R. Kobayashi, J. Normand, K. Raghavachari, A. Rendell, J.C. Burant, S.S. Iyengar, J. Tomasi, M. Cossi, N. Rega, J.M. Millam, M. Klene, J.E. Knox, J.B. Cross, V. Bakken, C. Adamo, J. Jaramillo, R. Gomperts, R.E. Stratmann, O. Yazyev, A.J. Austin, R. Cammi, C. Pomelli, J.W. Ochterski, R.L. Martin, K. Morokuma, V.G. Zakrzewski, G.A. Voth, P. Salvador, J.J. Dannenberg, S. Dapprich, A.D. Daniels, O. Farkas, J.B. Foresman, J.V. Ortiz, J. Cioslowski, D.J. Fox, Gaussian 09, Wallingford, CT, 2009.

17.   Lee, C.; Yang, W.; Parr, R. G. *Phys. Rev. B* **1988**, *37*, 785–789.

18.   Becke, A. D. *J. Chem. Phys.* **1993**, *98*, 5648–5652.

19.   Watt, M. M.; Engle, J. M.; Fairley, K. C.; Robitshek, T. E.; Haley, M. M.; Johnson, D. W. *Org. Biomol. Chem.* **2015**, *13*, 4266–4270.

20.   Tobe, Y.; Sasaki, S.-I.; Mizuno, M.; Hirose, K.; Naemura, K. *J. Org. Chem.* **1998**, *63*, 7481–7489.